AN ELECTROCHEMICAL & CATALYTIC STUDY OF GRAPHITE-SUPPORTED PALLADIUM-GOLD CATALYSTS FOR VINYL ACETATE SYNTHESIS

A thesis submitted to the

University of Wales

for the degree of

Philosophiae Doctor

by

Mark Greenslade B.Sc.

School of Chemistry

Cardiff University

September 2006

UMI Number: U584912

UMI U584912

ABSTRACT

The chemistry of vinyl acetate synthesis from ethylene, acetic acid, and oxygen over palladium-gold catalysts has been investigated in a study which has concentrated on the use of cyclic voltammetry as a surface sensitive analytical technique. Three series of palladium-gold/graphite catalysts were prepared by slurry precipitation or by incipient wetness impregnation and by reduction with formaldehyde or hydrazine. These catalysts, which behaved similarly, contained metallic particles having bi-modal particle-size distributions and alloy compositions, as judged by X-ray diffraction, high resolution transmission electron microscopy, and energy dispersive X-ray analysis. Surface characterisation was achieved by cyclic voltammetry and X-ray photoelectron spectroscopy.

In experiments intended to mimic the industrial LEAP process (in which potassium acetate is added to the reaction mixture) catalysts were treated with acetic acid or potassium acetate/acetic acid mixtures. Such treatments resulted in etching of the catalysts with consequent loss of palladium; dissolution of the lost palladium as dimeric and trimeric palladium acetate complexes was confirmed by ultra-violet absorption spectroscopy. Such etching occurred at the surfaces of palladium-rich particles; gold-rich particles were resistant to etching. Thus, the role of gold as a promoter is to stabilise the optimum alloy phase against loss of palladium. Reduction of palladium acetate complexes by ethylene led to plating of metallic palladium onto the surfaces of etched catalysts. Thus, a cycle of palladium dissolution and deposition occurred under reaction conditions leading to a redistribution of palladium between the catalyst particles.

Palladium acetate forms complexes with acetic acid and water that are liquid at synthesis temperatures. Thus, even under gas-phase reaction conditions, a liquid-phase may be present in which palladium acetate complexes can facilitate the homogeneous catalysis of vinyl acetate synthesis. This investigation provides definitive evidence that the balance of heterogeneous and homogeneous synthesis is determined by the range of the palladium-gold alloy composition present at the surface of the active catalyst. Etching and dissolution would be avoided by suitably restricting this range, whereupon reaction would be confined to that achieved by heterogeneous catalysis.

ACKNOWLEDGEMENTS

DEDICATION

To my family.

CONTENTS

5 REACTIVITY OF GRAPHITE-SUPPORTED PALLADIUM-GOLD CATALYSTS

6 DISCUSSION

CHAPTER 1
INTRODUCTION

1.1 Catalysis

The term catalysis was first used in a chemical context in 1835 by Berzelius who noted that certain chemicals speeded up chemical reactions. Chemical reactions involve changes in the arrangement and bonding of atoms in molecules, changes that are characterised by a diminution in free energy, the evolution or absorption of heat, and alterations in the state and ordering of a system. Reaction rate is determined by the energy pathway for the conversion of reactants to products and, by providing an advantageous energy pathway, catalysts improve process economics both in terms of productivity and energy consumption.

A catalyst is a substance that increases the rate at which a chemical reaction approaches equilibrium without itself being consumed or undergoing any permanent chemical change in the process. Catalysts increase the rate by reducing the activation barrier between reactants and products. Catalyst concentrations, which are usually very small, do not appear in equilibrium constants and hence catalysts do not influence positions of equilibrium. A lowered activation barrier and an unperturbed position of equilibrium suggest that the reverse reaction is catalysed to the same degree as the forward reaction. Thus, a good hydrogenation catalyst will also be a good dehydrogenation catalyst (under appropriate conditions).

In cases where the presence of a catalyst increases the number of phases present the phenomenon is termed heterogeneous catalysis and in cases where the catalyst is in the same phase as one or more of the reactants in the system, the system exhibits homogeneous catalysis.

1.1.1 Homogenous Catalysis by Metal Complexes in Solution

This type of homogeneous catalysis is based on organometallic chemistry. Most such catalysts consist of a transition metal centre to which are coordinated entities known as ligands. Ligands may be charged or uncharged, and are molecules having at least one unshared electron pair (Lewis bases). Ligands are capable of coordinating to a central metal atom or ion thereby forming a complex or a complex ion. The metal atom within the complex may exist with a variable oxidation state. Mono-dentate ligands donate one electron pair, whereas bidentate, tridentate, and quadridentate ligands donate two, three,

and four electron pairs respectively and are known as chelates. Transition metals have the ability to form complexes in which their oxidation state, coordination number, and the type of ligand coordinated can be systematically varied thus, providing a pool from which suitable homogeneous catalysts can be selected.

The advantages of homogeneous catalysts include high selectivity (to single products) and very efficient utilisation of the metal i.e. all of the catalytically active metal is equally available to the reactants. However, homogenous catalysts are prone to poisoning and deactivation and homogeneous processes often require additional steps to separate the products from the catalyst and unused reactants.

Methanol carbonylation in the synthesis of acetic acid is an example of a homogeneously catalysed process of great importance to the chemicals industry [1]. Acetic acid is one of the world's most important chemicals having applications in the manufacture of foods, coatings, adhesives, and inks as well as being an important feedstock in the synthesis of acetic anhydride, vinyl acetate, ethyl acetate, and other acetate esters [2]. Annually, approximately 5 million tonnes of acetic acid is synthesised via this route [3]. The first commercial methanol carbonylation process was developed by BASF; it involved use of iodide-promoted cobalt catalysts at 573 K and 700 atm [4]. However, in 1970, the BASF process was superseded by the Monsanto process [5] which used the same reaction but a superior catalyst system. The Monsanto process operated under milder conditions (323 – 373 K and 30 – 60 atm) using an iodide-promoted rhodium catalyst system [5].

Acetic acid is also manufactured using the BP CATIVA process [6]. Like the BASF and Monsanto processes, the CATIVA process involves the carbonylation of methanol but uses an iodide-promoted iridium catalyst along with ruthenium promoters. The CATIVA catalyst is more cost effective as; (i) the cost of iridium is approximately one-tenth that of rhodium [7] and (ii) the iridium catalyst has a higher turnover number allowing many more conversions before the catalyst has to be replaced. CATIVA catalysts are more selective to acetic acid than their predecessors and CATIVA plants can produce up to 75% more acetic acid than plants operating using the Monsanto technology.

1.1.2 Heterogeneous Catalysis

Heterogeneous catalysis is at the heart of the modern chemicals industry, dominating industrial organic, inorganic, environmental, and pharmaceuticals chemistry whilst making inroads into the fine chemicals area as old-fashioned stoichiometric processes involving environmentally unfriendly reagents give way to cleaner technologies. Selected examples of modern industrial catalytic processes involving heterogeneous catalysts are shown in Table 1.1.

Table 1.1 – A selection of heterogeneously catalysed processes of industrial importance

Process	Chemical transformation[a]	Catalyst
Steam reforming	$CH_4 + H_2O \rightarrow CO + 3H_2$	Ni/Al_2O_3
	$C_nH_m + nH_2O \rightarrow nCO + (n + m/2)H_2$	$Ni/Ca/Al_2O_3$
Methanol synthesis	$CO + 2H_2 \rightarrow CH_3OH$	$Cu/ZnO/Al_2O_3$
	$CO_2 + 3H_2 \rightarrow CH_3OH + H_2O$	
Hydrocarbon (Fischer	$nCO + 3H_2 \rightarrow C_nH_{2n} + nH_2O$	Alkali-promoted Fe
Tropsch) synthesis	$nCO + (3n + 1)H_2 \rightarrow C_nH_{2n+2} + nH_2O$	Alkali-promoted Co
Low temperature water-gas shift	$CO + H_2O \rightarrow CO_2 + H_2$	Ni/Al_2O_3
Nitrogen fixation (Haber process)	$N_2 + 3H_2 \rightarrow 2NH_3$	K-promoted Fe
Ammonia oxidation	$4NH_3 + 5O_2 \rightarrow 4NO + 6H_2O$	Pt-Rh gauze

[a]for reaction conditions see Handbook of Heterogeneous Catalysis (Ertl et al. 1997)

Catalysts for heterogeneously catalysed processes are commonly solids including metals, metal oxides, and metal sulphides. In almost all cases catalysts for these processes are high area materials as large surface areas are normally required to provide a sufficient number of active sites for the achievement of acceptable reaction rates. This requirement can be demonstrated by a simple calculation. Suppose a platinum catalyst is required to produce 1 mole of products per hour in a reaction where the rate of production at the catalyst surface is 1 molecule converted (active site)$^{-1}$ s^{-1}. The number of active sites required is 1.7×10^{20}. Supposing that each surface atom of radius 0.27 nm is an active site, the area of catalyst surface required is approximately 12 m^2. The use of a platinum sheet or wire having this area would be impracticable. However, the required number of platinum atoms is contained in just 0.057 g if this amount of platinum could be distributed over a support as individual atoms. In practice, such dispersion is usually unstable, but nano-scale

metal particles, say 2 nm in diameter, exhibit considerable stability and contain about half of their metal atoms in the surface. Thus, 0.1 g distributed over a high area support would provide the catalytic activity required in this case. In practice, many heterogeneous catalysts are prepared in this manner consisting of an active phase distributed in a finely divided form over a high area inert support. These catalysts are known as supported catalysts.

Materials commonly used as catalyst supports include carbon having surface areas from $400 - 1000$ m^2 g^{-1}, alumina having surface areas from $200 - 400$ m^2 g^{-1}, and silica having surface areas from $100 - 300$ m^2 g^{-1}. Titania, zirconia, ceria, and other transition metal oxides also find applications; their reactivity is such that chemical interactions between support and active phase may occur and can sometimes beneficially modify the reactivity of the active phase. Catalyst activity is sometimes improved by incorporation of promoters which either stabilise an active phase or modify its electronic properties.

The desired reaction should leave the catalyst in such a condition that it can affect an infinite number of further conversions i.e. the surface should be regenerated after each reaction turnover so that the catalyst has an infinite lifetime. However, this requirement is nearly always compromised in practice as the rigorous conditions used in some catalytic processes and the heat flow which results may lead to irreversible changes in catalyst morphology such as particle growth which is associated with loss of surface area and the transformation of the catalyst into a less active or inactive form.

As the reaction pathway facilitated by a catalyst is conditioned by its own surface chemistry, the reaction products will be catalyst dependant. This is the origin of catalyst selectivity, e.g. under appropriate conditions the reaction between carbon monoxide and hydrogen gives entirely methane over a nickel catalyst, almost entirely methanol over a promoted copper catalyst, and hydrocarbons over ruthenium; each process is operated on an industrial scale. Selectivity can be modified by the incorporation of poisons which reduce the rates of undesired surface processes.

The metallic elements of the periodic table divide naturally into the d and f-block of transition and rare earth metals, and the s and p-block main group metals. The former dissociatively chemisorb hydrogen molecules as hydrogen atoms and the majority interact strongly with nitrogen, carbon monoxide, and many hydrocarbons. Metals of groups 3 to 7 form oxides and carbides that are irreducible at temperatures normally employed for

catalysed reactions and hence become irreversibly deactivated. At the other extreme, the main group metals either do not adsorb hydrogen, nitrogen, carbon monoxide, and hydrocarbons or do so only weakly. For these reasons the catalytically active metals that feature in Table 1.1 are mostly those of groups 8 (Fe, Ru, Os), 9 (Co, Rh, Ir), 10 (Ni, Pd, Pt), and 11 (Cu, Ag).

1.1.3 Adsorption by Catalyst Surfaces

Molecules of a reactant approaching the surface of a solid catalyst through a fluid-phase (liquid or a gas) are first subject to weak van der Waals interactions and, on closer approach, may undergo chemical combination with the surface. The overall process is termed adsorption, the weakly bound state being termed physical adsorption or physisorption, and the strongly bound state chemical adsorption or chemisorption. Where chemisorption is accompanied by a degree of molecular dissociation it is termed dissociative adsorption. The process whereby reactants or products leave the surface is termed desorption. The locations at which reactants or intermediates are chemisorbed at catalyst surfaces are referred to as active sites and are present in the surface of the active phase. Depending on the nature and morphology of the catalyst, the active sites may constitute a majority or minority of the total surface area of the catalyst.

1.1.3.1 Physisorption

Adsorbate atoms or molecules are bound to the catalyst surface by weak van der Waals interactions. These interactions have a long range but are weak. Typically the energy released when an atom or molecule is physisorbed is approximately 20 kJ mol^{-1} [8]. These very small energies can be absorbed by the lattice and dissipated as thermal motion. The molecule will move along a surface, gradually losing energy until it finally adsorbs onto it. This process is called accommodation. An enthalpy change of this magnitude is too small to lead to bond breaking; therefore a physisorbed molecule retains its identity, although it may become distorted by the presence of the surface.

1.1.3.2 Chemisorption

Adsorbate atoms or molecules are bound to the catalyst surface by the formation of a chemical (usually covalent) bond. The adsorbate usually finds sites such as steps and kinks which maximise their coordination number. Chemisorption is characterised by the transfer of electrons between the adsorbate and the surface and its enthalpy of adsorption is much greater than that observed in physisorption. Typically, enthalpies of adsorption are in the region of 200 kJ mol^{-1} [8]. To satisfy the demand of unsatisfied valencies at the surface, a chemisorbed molecule may dissociate. The existence of molecular fragments is one reason why solid surfaces catalyse chemical reactions, and may also be a reason why catalysts gradually undergo deactivation.

Thus, there are two forms of chemisorption. The first is known as associative chemisorption and in this case the adsorbate molecule remains intact. The second form is called dissociative chemisorption and in this case the adsorbate dissociates forming molecular fragments which become bonded to the catalyst surface.

Except in special cases, chemisorption must be an exothermic ($\Delta H < 0$) process because adsorption onto a surface is usually accompanied by a restriction in the translational freedom of a molecule and hence a negative entropy change ($\Delta S < 0$). However, in cases where molecules are adsorbed dissociatively by the surface the adsorption may be characterised by an increase in the translational freedom of the molecule and a positive entropy change ($\Delta S > 0$). Thus, the enthalpy change may also be positive (i.e. endothermic) for the adsorption process whilst also maintaining that $\Delta G < 0$, a requirement for a spontaneous process. Temperature also plays a role in adsorption processes. e.g. hydrogen absorption on glass. This occurs endothermically due to a large increase of translational entropy accompanying the dissociation of hydrogen molecules to hydrogen atoms which move freely over the surface. In this example the entropy change associated with the dissociative chemisorption of hydrogen is sufficiently positive to overcome the slight positive enthalpy change.

1.1.3.3 Surface coverage

The extent of adsorption is expressed as the fractional coverage of the surface and is given the symbol θ. The surface coverage is therefore defined as:

$$\theta = \frac{\text{number of adsorption sites occupied}}{\text{number of adsorption sites available}} \tag{1}$$

When θ = 1, all the adsorbate sites are filled and this adsorbate assemble is referred to as a monolayer. This allows simple quantification of surface adsorption.

1.1.4   Kinetics and Mechanisms in Heterogeneous Catalysis

Catalytic action normally depends on at least one reactant being adsorbed and modified to a form in which it readily undergoes reaction. Two general types of mechanism have been proposed to explain catalytic action at solid surfaces.

A majority of surface-catalysed reactions are thought to proceed via a mechanism known as the Langmuir-Hinshelwood (LH) mechanism. However, some surface-catalysed reactions have been identified to follow an alternative mechanism known as the Eley-Rideal (ER) mechanism.

According to the Langmuir-Hinshelwood mechanism, reaction takes place as a result of encounters between molecular fragments and atoms adsorbed on the catalyst surface. The rate equations are thus expected to be second order in surface coverage.

$$A_{(ads)} + B_{(ads)} \longrightarrow P$$
$$\upsilon = k\theta_A\theta_B \tag{2}$$
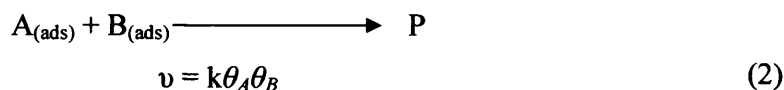
where k is the rate constant of the surface reaction and θ_A and θ_B are the surface coverages of A and B respectively.

According to the Eley-Rideal mechanism molecules from the gas-phase may react with species already adsorbed on the catalyst surface. The rate equation then involves the partial pressure P_b, of the gas-phase species B and the surface coverage θ_A of the adsorbed substance A.

$$A_{(ads)} + B_{(g)} \longrightarrow P$$

$$\upsilon = k\theta_A p_B \tag{3}$$
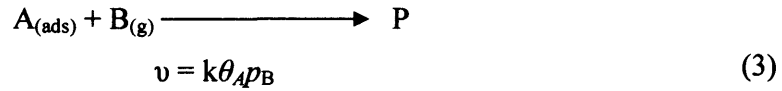
The rate constants for catalysed reactions may be much larger than those for corresponding un-catalysed reactions because surface reactions have smaller activation energy barriers and the adsorption process is often not activated. Langmuir equations are normally used to replace the unknown surface coverage terms in rate equations with known concentration or pressure terms. The Langmuir equation for a gas X which absorbs without dissociation at an energetically uniform surface is:

$$\theta_X = \frac{b_X P_X}{1 + b_X P_X} \tag{4}$$

where P_X is the pressure of the gas and b_X is the equilibrium constant for the adsorption process.

The equation for a gas Y which adsorbs with dissociation (e.g. $O_{2(g)} \rightleftharpoons 2\ O_{(ads)}$) at an energetically uniform surface is:

$$\theta_Y = \frac{(b_Y P_Y)^{0.5}}{1 + (b_Y P_Y)^{0.5}} \tag{5}$$

Thus, in the LH mechanism, if both reactants A and B are adsorbed without dissociation, the rate equation becomes:

$$\upsilon = \frac{k(b_A P_A)(b_B P_B)}{(1 + b_A P_A)(1 + b_B P_B)} \tag{6}$$

In such a process the measured orders of reaction will vary with pressure. Simpler equations arise if the reactants are strongly or weakly adsorbed. So, for example, if A is strongly adsorbed so that $b_A P_A \gg 1$, and B is weakly adsorbed so that $b_B P_B \ll 1$, then

$$\upsilon = k\ b_B P_B \tag{7}$$

i.e. the reaction is of zero order in the strongly adsorbed reactant and first order in the weakly adsorbed reactant.

If the weakly adsorbed reactant B had dissociated on adsorption, the reaction would have been half-order in B. This methodology can be similarly applied to reactions proceeding by the ER mechanism.

The use of Langmuir equations to replace surface coverage terms with expressions in pressure (or concentration) is open to the criticism that catalyst surfaces are seldom if ever energetically homogeneous. Freundlich and Tempkin equations are available which relate surface coverage to pressure for situations in which enthalpies of adsorption vary with coverage, but these are rarely used because of their analytical complexity. The value of the use of Langmuir equations is that they permit the conclusions that (i) an order of zero indicates strong adsorption of that reactant, (ii) an order of unity indicates weak adsorption of the that reactant, (iii) a fractional order tends to confirm dissociative adsorption of that reactant. Finally, it must be appreciated that these conclusions apply only to reactions in which the rate is not limited by diffusion of reactants to the surface, or by diffusion of products away from the surface (mass transfer effects) or by temperature rises at the catalyst surface due to a failure of the system to dissipate the heat of reaction (heat transfer effects).

1.2   Vinyl Acetate Monomer

Vinyl acetate (VA) is an unsaturated organic ester (Figure 1.1). It is a colourless flammable liquid with a characteristic sweet odour and a boiling point of 72.8 $^\circ$C [9].
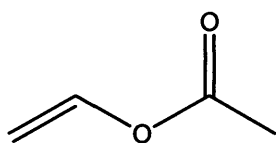
Figure 1.1 – Vinyl acetate, $C_2H_3OOCCH_3$

Vinyl acetate monomer (VAM) is readily homo-polymerised in the presence of free radicals or light to form polyvinyl acetate which can be hydrolysed to polyvinyl alcohol. VAM is used as a co-monomer with ethylene, vinyl chloride, acrylate esters, and higher vinyl esters in the manufacture of polymers which have extensive applications in the

manufacture of paints, adhesives, textiles, diesel fuel modifiers, and flexible films for packaging applications (Figure 1.2) [10]. The uses of VA are summarised in Figure 1.3.

| ▣ Polyvinyl Alcohol | ■ Polyvinyl Acetate | ▢ Co-polymers | ▢ Vinyl Acetate Ethylene | ■ Ethylene Vinyl Acetate | ▣ Polyvinyl Butyral | ■ Other |
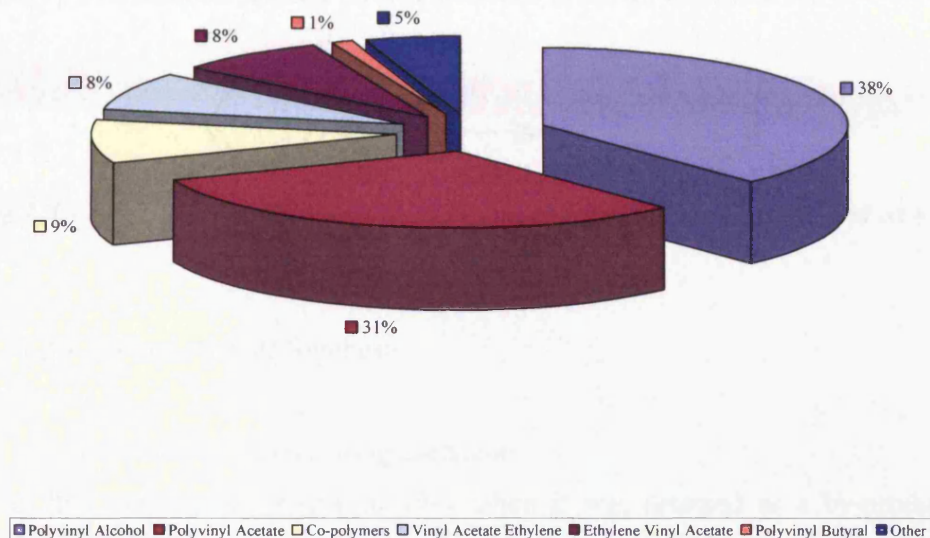
Figure 1.2 – Proportions of VAM used in the preparation of polymers in 2001
Source: BP
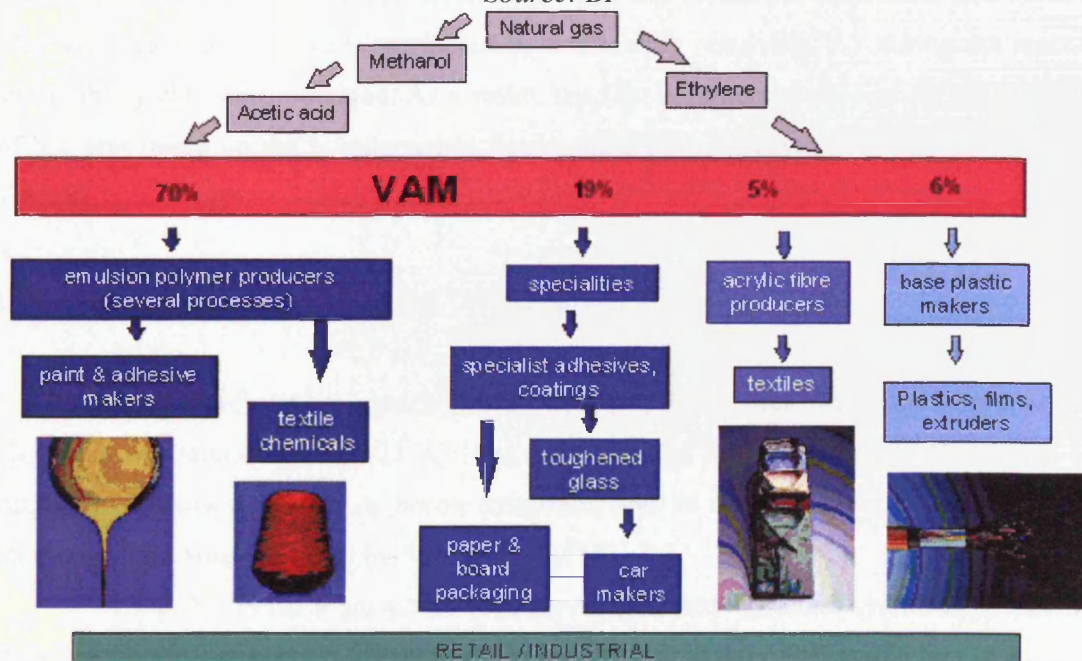
Figure 1.3 – Approximate proportions of VAM used by specific technologies
Source: BP

Due to its extensive applications VA is one of the world's most versatile and widely used petrochemical intermediates. Annually 4.5 million tonnes of VA is synthesised heterogeneously in the gas-phase via the acetoxylation of ethylene, using acetic acid, and oxygen [11]. VA synthesis is catalysed by a palladium-gold alloy supported on high surface area silica [12 – 16]. Worldwide, the main producers of VA are, BP, Celanese, DOW, and DuPont [9]. The reaction scheme for VA synthesis is shown in Figure 1.4.
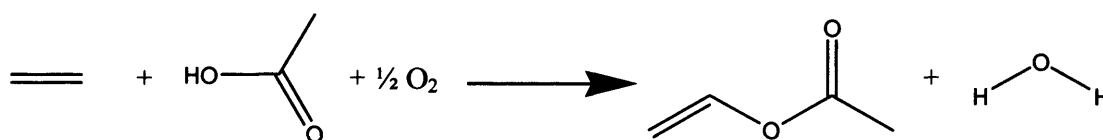
Figure 1.4 – Reaction scheme for the conversion of ethylene, acetic acid, and oxygen to VA and water

1.2.1 Vinyl Acetate Synthesis

1.2.1.1 Synthesis using acetylene

VA was first prepared by Klatte in 1912 when it was detected as a by-product in the homogeneous catalytic synthesis of ethylidene diacetate [17]. This was achieved by bubbling acetylene through a mixture of acetic acid and mercurous sulphate at 333 – 373 K. The VA yield was extremely small, but by continually removing VA during the reaction acceptable yields were obtained. As a result, the first commercial process for the synthesis of VA was based on the homogeneous liquid-phase reaction between acetylene and acetic acid (8).

$$C_2H_2 + CH_3COOH \longrightarrow CH_3COOCH=CH_2 \qquad (8)$$
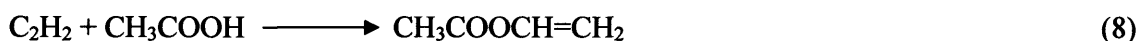
Further developments, mainly to the catalyst, meant that VA could be prepared at slightly lower temperatures (323 K) [18] and the yield was improved by the use of co-catalysts or *promoters* such as boron trifluoride and its complexes with acetic acid and ammonia. This was described by Schildknecht [18].

During the 1940s a gas-phase process for the heterogeneous synthesis of VA was developed [19]. The process, developed by Wacker, relied upon the gas-phase combination of acetylene (23% by mass) and acetic acid (77% by mass) over a carbon-supported zinc

acetate catalyst at 443 K. The best compromise between conversion, rate, and catalytic lifetime, was to adopt 60% conversion, although 98% conversion could be achieved in the laboratory. VA was separated from the product stream by distillation and unconverted acetylene/acetic acid was returned to the reactor for an additional pass. Significant by-products included acetone, acetaldehyde, and crotonaldehyde although many more were identified in small quantities [20 – 23]. The kinetics of this process were studied by Tolstikova [24] who reported that between 453 – 493 K the rate of VA formation was independent of the partial pressures of both acetic acid and VA, but directly proportional the partial pressure of acetylene. Catalytic activity was proportional to the zinc acetate surface area and to the third power of zinc acetate content [25]. This process was used to satisfy the economic demand for VA until the early 1960s.

Nowadays, only 25% or so of the VA demand is satisfied by this reaction [9]; it having been superseded by the gas-phase heterogeneous acetoxylation of ethylene which is discussed in Section 1.2.1.2.

1.2.1.2 Synthesis using ethylene

Until the 1960s VA was prepared commercially using acetylene and acetic acid (Section 1.2.1.1). Despite major developments which provided cheaper and cleaner acetylene, separate developments in the petrochemical industry provided large quantities of ethylene. By 1967 ethylene was available at around one third the price of acetylene [26]. Therefore great efforts were made to obtain VA from an ethylene feedstock.

The first homogeneous conversion of ethylene and acetic acid to VA was reported by Moiseev et al. in 1960 [27] and this process was commercialised by ICI in 1968 [28]. This process used palladium chloride as a catalyst to convert ethylene to VA. Palladium chloride formed a complex with ethylene which reacted with an acetate anion from sodium acetate to form VA (9). As a result of this oxidation of ethylene, palladium (II) was reduced to palladium metal, which was reoxidised by copper (II) (10). The copper (I) thus generated was converted back to copper (II) by air oxidation (11).

$$PdCl_2 + CH_2=CH_2 + 2\,NaOAc \longrightarrow CH_2=CHOCOCH_3 + AcOH + 2\,NaCl + Pd \qquad (9)$$

$$Pd + 2CuCl_2 \longrightarrow PdCl_2 + 2\,CuCl \qquad (10)$$

$$4\,CuCl + O_2 + 4\,HCl \longrightarrow 4\,CuCl_2 + H_2O \qquad (11)$$

The process was carried out by passing ethylene and oxygen through a slurry of acetic acid, sodium acetate, and copper (II) chloride in the presence of the palladium chloride catalyst. Typical conditions involved temperatures ranging from 353 – 423 K and superatmospheric pressures. Reaction times were 5 – 20 minutes and yields were 70 – 90% (based on ethylene) [29]. The major by-products included ethylidene diacetate and acetaldehyde [30]. Acetaldehyde was formed by the reaction of ethylene and water (Wacker reaction). Hydrolysis of VA was later inhibited by the continuous removal of water by distillation or adsorption [30]. Clement et al. showed that palladium chloride catalyses the cleavage of VA to acetaldehyde and acetic anhydride in the presence of acetic acid and sodium acetate. This is thought to be a major route to acetaldehyde formation [31]. Unfortunately, due to the presence of chloride ions, VA production plants of this type encountered serious corrosion problems. In some cases, this was countered by the construction of equipment using titanium alloys. Later, halide-free catalysts were introduced which gave faster reaction times without the corrosion problems and halogenated by-products associated with halide-containing catalysts [32].

Heterogeneous processes for the synthesis of VA in the gas-phase were developed almost immediately following the introduction of the homogeneous liquid-phase process [9]. These and related processes have been in use since the late 1960s. The first heterogeneous process was developed by National Distillers Products (now Celanese) [33]. The catalyst consisted of (0.5% palladium)/carbon. However, palladium could be used unsupported or supported on alternative materials such as silica, alumina, or other metal oxides. In contrast to the homogeneous liquid-phase process, where only palladium salts in acetic acid oxidise ethylene to VA, other metals were reported to be active for the heterogeneous gas-phase synthesis of VA. Heterogeneous catalysts including the oxides, chlorides, sulphates, benzoates, and acetates of rhodium, platinum, ruthenium, osmium, and iridium were found to be active for VA synthesis [33].

In the early heterogeneous gas-phase processes, ethylene reacted with acetic acid and oxygen over a palladium-containing catalyst at 5 – 11 bar and at 413 – 453 K to form VA and water (Figure 1.5).
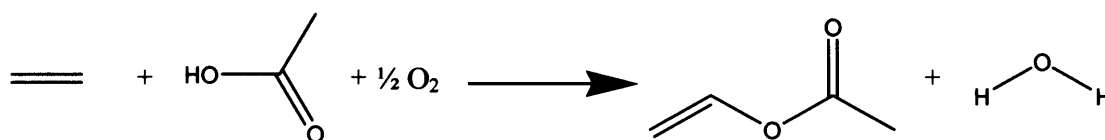
Figure 1.5 – Reaction scheme for the conversion of ethylene, acetic acid, and oxygen to vinyl acetate and water

VA synthesis is an exothermic reaction (ΔH° = -178 kJ mol^{-1}) [9]. The heterogeneous process produces fewer by-products than the homogeneous process [9], the major by-product being carbon dioxide. This is formed by the *complete combustion* of ethylene to carbon dioxide and water [34 – 37] although acetic acid has also been reported to contribute to carbon dioxide formation [34, 36]. On a small scale, the other by-products include acetaldehyde, ethyl acetate, and heavy ends [9]. Commercial catalysts for VA synthesis are promoted by alkali metal salts and they contain additional activators such as gold, cadmium, platinum, rhodium, barium, copper, manganese, or iron [33, 38, 39]. Different supports have been used, including silica [40 – 46], alumina [47, 48], aluminosilicates [49], and activated carbon [47].

Typical catalysts provide space-time yields from 200 – 800 g$_{VA}$ (dm^{-3})$_{cat}$ h^{-1} [50]. The space-time yield generally increases with reactant pressure and with temperature to a certain extent. Increases in pressure lower the flammable limits of ethylene/oxygen mixtures, which favour the formation of carbon dioxide [50], and thus sets a limit for reactor pressure. Temperature increases the extent of carbon dioxide formation. Generally, catalyst activity remains constant for several years but catalysts eventually undergo deactivation [51 – 56] for reasons unknown. Deactivation is discussed in Section 1.2.6.

The precise mechanism for the heterogeneous gas-phase synthesis of VA is a topic of much debate. The proposed mechanisms and the kinetics of VA synthesis are addressed in Sections 1.2.4 and Section 1.2.5 respectively.

1.2.2 Catalysts for the Heterogeneous Synthesis of Vinyl Acetate from Ethylene

Traditionally, two types of catalyst have been used in the gas-phase heterogeneous synthesis of VA [36], palladium-cadmium catalysts developed by Hoechst, and palladium-gold catalysts developed by Bayer. Hoechst and Bayer catalysts are not only compositionally different; they also differ in their methods of preparation [36].

1.2.2.1 Hoechst catalysts

Palladium acetate, cadmium acetate, and potassium acetate are impregnated evenly throughout a silica (bentonite or aerogenic) support in the form of 5 mm spheres. Palladium acetate is then reduced to palladium metal. The palladium content is 2.0 – 2.5 wt% whereas the contents of cadmium and of potassium vary between 1.0 – 3.0 wt%. The silica support has a surface area of 120 – 140 m^2 g^{-1} and a pore volume of 0.8 cm^3 g^{-1}

Bentonite-supported catalysts provide space-time yields between 400 – 600 g_{VA} (dm^{-3})$_{cat}$ h^{-1} and their selectivity to carbon dioxide is 8 – 10%. The space-time yields for catalysts based on aerogenic silica are 600 – 800 g_{VA} (dm^{-3})$_{cat}$ h^{-1} and their selectivity to carbon dioxide is 4 – 6% [57].

1.2.2.2 Bayer catalysts

Palladium and gold are impregnated as their chloride salts onto a spherical silica pellet and the impregnate is dried and then treated with sodium hydroxide or other bases to convert the chlorides to hydroxides. Excess chloride is then washed out and the water is removed by drying. Palladium and gold are then reduced to their metallic states with a suitable reducing agent to give a thin outer shell of metals around the spherical silica pellet [36]. In the last step, potassium acetate is impregnated evenly throughout the catalyst. A typical composition of a Bayer catalyst is 0.5 wt% palladium and 0.25 wt% gold and with approximately 2 wt% potassium [58].

Bentonite having surface areas of approximately 150 m^2 g^{-1} and a pore volume of 0.5 – 0.7 cm^3 g^{-1} is normally used as a support [40 – 46]. Alpha-alumina has also been reported to be a suitable support for the palladium-gold catalyst system since it is resistant to acetic acid under reaction conditions [59]. Other types of alumina (e.g. gamma) are not resistant to acetic acid under reaction conditions and therefore catalysts having this type of support undergo rapid deactivation [60].

1.2.3 LEAP Technology

In the 1980's BP developed new technology which led to a new generation of catalysts for the heterogeneous gas-phase synthesis of VA. The catalyst was used in a traditional fixed bed process. Fixed bed VA synthesis became dominant throughout the 1980s to the mid-1990s [61].

In the 1990s the majority of BP's VA manufacturing units were approximately 20 years old and the company decided to invest in a new process rather than to modernise old reactors and/or build new ones [62]. In their search for a new process it soon became apparent that fluid bed technology would be advantageous for VA synthesis. The advantages of fluidisation included smaller construction costs, lower operating costs, and the fact that there are fewer limitations on maximum reactor size for a fluidised bed reactor [61, 62]. Fluidisation provides more efficient heat removal/dispersion; for exothermic processes this is very useful and, unlike the case for fixed bed reactors, catalyst and promoter(s) can be added to fluidised bed reactors without disrupting the process. This can be used advantageously to adjust production rate to the economic demand for VA.

Whilst fluidised reactors are cheaper and easier to build they are difficult to scale up. The research involved a different approach to the conventional reactor scale up. Computer modelling was used and the explosive properties of ethylene/oxygen mixtures were extensively measured. The use of X-ray imaging at BP's visualisation, imaging, and process analysis centre (VIPA) was especially useful as, this permitted catalyst imaging under process conditions and allowed researchers to determine the fluid dynamics of catalyst particles in an industrial scale reactor. The combined effectiveness of these techniques eliminated the need for the construction of a very costly demonstration plant as well as many more years of research.

The chosen location for the plant was at BP's integrated petrochemical site at Hull, primarily because ethylene and acetic acid was readily available – acetic acid was already produced on site and an ethylene supply pipeline had recently been approved for construction. An industrial gas specialist was brought in to produce oxygen on site.

After several years of research BP unveiled a new process for the synthesis of VA. The process was called LEAP. LEAP utilises the advantages of fluid bed technology and is more cost effective and efficient than traditional fixed bed processes. It was seen as the most significant breakthrough in VA manufacturing technology since the 1960s and it was

a major part of BP's EuroVAM investment in 2001. The LEAP reactor has the capacity to produce up to 250,000 metric tonnes of VAM per year.

The LEAP catalyst consists of a palladium-gold alloy, supported on microspheroidal silica. The catalyst takes the form of very small spheres which are so fine they flow almost as a fluid. In LEAP, the gaseous reactants (ethylene, acetic acid, and oxygen) flow upwards through the reactor and fluidise the catalyst. This provides efficient mixing between the gases and catalyst particles and provides excellent heat dispersion within the reactor.

LEAP was the first fluidised bed process to use a supported precious metal catalyst [61]. The process won the BP Breakthrough Award in 1999, a competition held annually to celebrate innovation within the Chemicals Division. LEAP also won the 2002 AspenTech Award organised by the Institution of Chemical Engineers.

1.2.3.1 LEAP catalyst preparation

The impregnate is prepared at ambient temperature by adding solutions containing sodium chloropalladite (Na_2PdCl_4) and chloroauric acid ($HAuCl_4$) to the required mass of the silica support. The metal precursor solutions are made up to a volume corresponding to the volume of the pores of a given mass of the support particles using water although acetic acid, benzene, toluene, methanol, or ethanol can also be used as a solvent. The impregnate is dried at temperatures between 393 K and 413 K although in some cases the impregnate may be dried at ambient temperature and reduced pressure under air, nitrogen, helium, or carbon dioxide. At ambient temperature the palladium and gold precursors are immobilised onto the support by reduction with excess aqueous hydrazine. Formaldehyde, sodium formate, or sodium borohydride, are alternative reductants. The catalyst is then filtered, washed with distilled water, and dried [12 – 16].

1.2.3.2 LEAP catalyst specification

The catalyst is supported on microspheroidal silica particles, the majority of which have mean diameters less than 300 μm. By virtue of their size, the support particles can be maintained in a fluid state under reaction conditions for VA synthesis while also maintaining a high resistance to attrition. Whereas Bayer and the later Hoescht catalysts were prepared by shell-impregnation of the metals onto the support particles [36], the

support particles used in LEAP catalysts are sufficiently porous to allow reactants to diffuse into the particles and contact the catalytic sites which are located between 5 μm and 15 μm below the surface. The catalytic layer has a thickness between 0.1 μm and 25 μm and the support particles have pore volumes between 0.20 cm^3 g^{-1} and 0.70 cm^3 g^{-1}. The surface area of the microspheroidal silica particles varies between 60 m^2 g^{-1} and 125 m^2 g^{-1}. The catalysts contain between 0.2 – 5.0 wt% palladium and promoters such as gold (0.2 – 3.0 wt%), copper (0.1 – 10 wt%), or cerium (0.2 – 10 wt%). The promoter may be co-impregnated with palladium or impregnated in an additional stage. The catalyst may also be impregnated with potassium acetate (0.1 – 15 wt %) [12 – 16].

1.2.4 Mechanism for Gas-Phase Vinyl Acetate Synthesis

Although the overall reaction chemistry of the heterogeneous gas-phase synthesis of VA from ethylene, acetic acid, and oxygen was determined over 30 years ago, the precise mechanism remains a controversial issue [34, 35, 63, 64].

Two very different mechanisms have been suggested for reaction over palladium-based catalysts. The first suggests that palladium remains in the metallic state and VA formation occurs via the reaction of adsorbed intermediates on the catalyst surface [34, 63]. An alternative mechanism proposes that the reaction occurs in a similar manner to that observed in the liquid-phase. In this context, co-ordinated ethylene inserts into a Pd-OAc bond in a palladium-alkali metal acetate complex, and the complex undergoes decomposition to yield VA and palladium metal [35, 64].

1.2.4.1 Mechanism for reaction occurring heterogeneously

Nakamura and Yasui [34, 63] suggested that, in the gas-phase reaction, VA is formed via a reaction between intermediates adsorbed on the catalyst surface by a Langmuir-Hinshelwood mechanism. According to this mechanism, ethylene and acetic acid are activated as a result of hydrogen abstraction by palladium. For ethylene hydrogen abstraction occurs regardless of whether oxygen is present whereas for acetic acid hydrogen abstraction occurs only in the presence of oxygen. VA is formed as a result of the combination of dissociatively adsorbed acetic acid and dissociatively adsorbed ethylene, this being rate determining [34]. They suggested that co-catalysts such as potassium acetate

or other alkali metals promote the abstraction of hydrogen from acetic acid and weaken the palladium-oxygen bonds in the dissociatively adsorbed acetic acid species [34].

These investigators also addressed the issue of palladium (II) acetate formation at the surface of the catalyst under reaction conditions, suggesting that acetate formation occurred only at higher partial pressures of acetic acid and oxygen and at lower temperatures. They associated palladium particle aggregation with the formation of palladium (II) acetate on the surface of the catalyst, but reported that catalytic activity was maintained for prolonged periods in which palladium (II) acetate was not formed. They also reported that palladium acetate facilitates the formation of acetaldehyde as a by-product [63]. Nakamura and Yasui also investigated the effect of various different co-catalysts on the rate of VA formation [34]. They reported that acetate and propanoate provided superior catalytic activities to pentanoate, oxalate, hydroxide, carbonate, or chloride anions and also that alkali metal cations such as caesium, rubidium, and potassium were preferred over transition metal monovalent cations. Their suggested mechanism for VA formation is as follows, where Pd represents a palladium atom in a metallic surface.

$$C_2H_4 + 2\ Pd \longrightarrow Pd–CH–CH_2 + Pd–H \qquad (12)$$

$$O_2 + 2\ Pd \longrightarrow 2\ Pd–O \qquad (13)$$

$$CH_3COOH + Pd \longrightarrow Pd–CH_3COOH \qquad (14)$$

$$Pd–CH_3COOH + Pd–O \longrightarrow Pd–OCOCH_3 + Pd–OH \qquad (15)$$

$$Pd–OCOCH_3 + Pd–CH–CH_2 \longrightarrow Pd–CH_2CHOCOCH_3 + Pd \qquad (16)$$

$$Pd–CH_2CHOCOCH_3 \longrightarrow CH_2=CHOCOCH_{3\ (g)} + Pd \qquad (17)$$
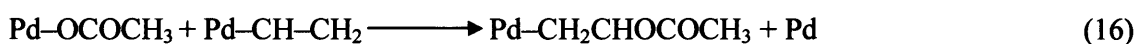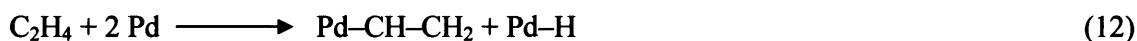
$$VA$$

The catalyst surface is then regenerated by:

$$Pd–OH + Pd–H \longrightarrow Pd–H_2O + Pd \qquad (18)$$

$$Pd–H_2O \longrightarrow Pd + H_2O \qquad (19)$$

Kinetics studies by Goodman and co-workers also reported that VA is formed by a Langmuir-Hinshelwood mechanism involving the combination of adsorbed intermediates

over supported and unsupported palladium and palladium-gold catalyst systems [65 – 67]. Kinetic data was supplied to support this conclusion (Section 1.2.5).

1.2.4.2 Mechanism for reaction occurring homogeneously

van Helden et al. have proposed the following mechanism for the homogeneous liquid-phase synthesis of VA from ethylene and acetic acid using a palladium chloride catalyst in the presence of sodium acetate [68]. Palladium acetate is considered to form a complex with an additional acetate anion (20) with which ethylene then reacts (21). The ethylene ligand is then considered to insert into one of the palladium acetate bonds of the complex, whereupon decomposition occurs to form VA, palladium metal, acetic acid, and acetate anions, in a rate limiting step (22).

$$Pd(OAc)_2 + AcO^- \longrightarrow Pd(OAc)_3^- \tag{20}$$

$$Pd(OAc)_3^- + C_2H_4 \longrightarrow C_2H_4Pd(OAc)_3^- \tag{21}$$

$$C_2H_4Pd(OAc)_3^- \longrightarrow \underset{VA}{CH_2=CHOCOCH_3} + Pd + AcOH + AcO^- \tag{22}$$
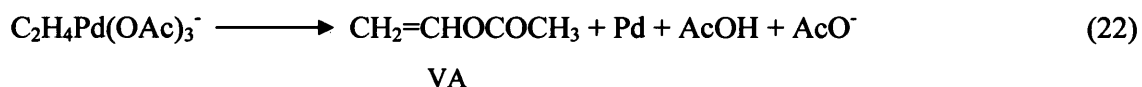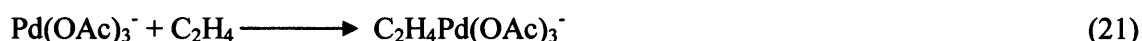
The catalyst is then regenerated by:

$$Pd + 2CuCl_2 \longrightarrow PdCl_2 + 2\,CuCl \tag{23}$$

$$4\,CuCl + O_2 + 4\,HCl \longrightarrow 4\,CuCl_2 + H_2O \tag{24}$$
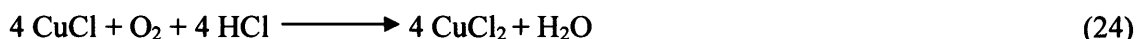
Results presented in Chapter 4 show that when palladium acetate is treated with ethylene, metallic palladium is formed. Thus, the mechanism suggested by van Helden et al. [68] may also include a heterogeneous component as the presence of metallic palladium (possibly colloidal) particles can not be excluded.

Samanos et al. [35] examined the kinetics of VA synthesis over (palladium)/silica and (palladium)/alumina by varying the partial pressures of acetic acid, ethylene, oxygen, and water vapour. They also studied the role of alkali metal acetates and concluded that VA synthesis, in the gas-phase, occurs via a similar mechanism to that which occurs in the liquid-phase (i.e. the mechanism proposed by van Helden et al.) except that palladium acetate is formed via oxidation of palladium at metal sites at the catalyst surface (25).

$$Pd + \tfrac{1}{2} O_2 + 2\, AcOH \longrightarrow Pd(OAc)_2 + H_2O \tag{25}$$

In this connection, Crathorne et al. employed isotopic transient kinetics to establish that, under reaction conditions, heterogeneous VA catalysts are covered by a liquid-layer of acetic acid with some water [36]. This layer was estimated to consist of 2 to 3 monolayers of adsorbed molecules and the majority of the acetic acid was thought to be adsorbed on the support [36]. They also suggested that potassium acetate aids the retention of acetic acid in the liquid-layer under reaction conditions by adduct formation and that there were no significant interactions detected between ethylene, oxygen, and the catalyst [36]. Complimentary results reported by Samanos et al. showed significant interactions between acetic acid and the catalyst support (silica and alumina) and little or no interactions between the catalyst and ethylene or oxygen [35]. Samanos also reported that the rate of VA formation is proportional to ethylene and oxygen partial pressures and is independent of the acetic acid partial pressure [35]. The kinetics of VA synthesis are discussed in Section 1.2.5.

Since metallic palladium is converted to palladium acetate under oxidising conditions [69] the homogeneous route to VA synthesis under the conditions of the heterogeneous gas-phase process is possible. Thus, Kragten et al. [70] studied the interaction of palladium and potassium acetates which are used in the homogeneous acetoxylation of ethylene. Raman spectroscopy showed that palladium acetate in glacial acetic acid attained a trimeric structure and upon addition of potassium acetate the trimeric palladium acetate decomposed to dimeric palladium acetate. In the presence of ethylene, dimeric palladium acetate was formed by the decomposition of the trimers. They proposed that dimeric palladium acetate is catalytically active for the homogeneous synthesis of VA. The equilibria which exist between potassium acetate and trimeric, dimeric, and monomeric palladium acetate are shown in equations (26) and (27).

$$2\, Pd_3(OAc)_6 + 6\, KOAc \rightleftharpoons 6\, K^+ + 3\, [Pd_2(OAc)_6]^{2-} \tag{26}$$

trimer   dimer

$$2\, K^+ + [Pd_2(OAc)_6]^{2-} + 2\, KOAc \rightleftharpoons 4\, K^+ + 2\, [Pd(OAc)_4]^{2-} \tag{27}$$

dimer   monomer
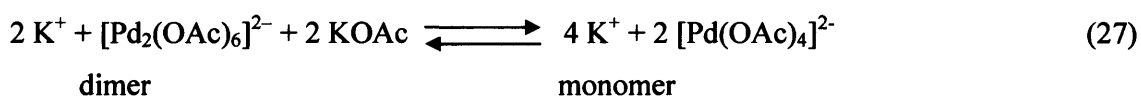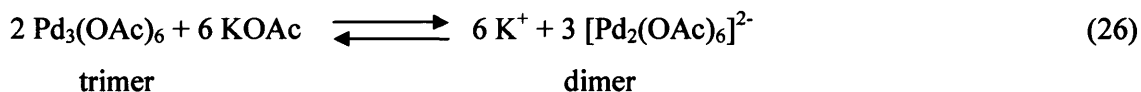
These forms of palladium acetate can be detected by ultra-violet absorption spectroscopy, and spectral transitions due to trimers and dimers were found to occur at ~ 400 nm and ~ 350 nm respectively [70].

1.2.5 Kinetics of Vinyl Acetate Synthesis

The power-rate law has been used to express the dependence of synthesis rate, r, on pressure and temperature, thus:

$$r = k \, (P_{C2H4})^{\alpha} \, (P_{O2})^{\beta} \, (P_X)^{\gamma} \tag{28}$$

where α and β are orders or reaction in ethylene and oxygen respectively and γ is the order in some other component (such as acetic acid) that may influence the rate. The rate coefficient, k, varies with temperature according to the Arhenius equation $k = A\exp(-E/RT)$ where A is a pre-exponential factor, E is the observed activation energy, and T is the temperature.

1.2.5.1 Orders of reaction

The orders of reaction in ethylene and oxygen have been reported by Han et al. for vinyl acetate formation over silica-supported catalysts (Table 1.2) [65]. Over (1 wt% palladium)/

Table 1.2 – Kinetic parameters for the synthesis of VA over palladium-based catalysts

Catalyst /SiO$_2$	Temperature / K	Rate constant (k) x10^{-2} s^{-1}	Order in ethylene (α)	Order in oxygen (β)	r_{VA}[a] * 10^{-3} s^{-1}
(Pd-Au)	393	2.45	0.38 ± 0.04	0.20 ± 0.02	3.48
(Pd-Au)	413	4.03	0.35 ± 0.01	0.20 ± 0.03	6.47
(Pd-Au)	433	4.70	0.35 ± 0.03	0.21 ± 0.03	7.54
(Pd)	413	0.03	-0.34 ± 0.02	0.18 ± 0.01	0.21

[a]*rates obtained with P_{C2H4} = 5.0 kPa, P_{O2} = 1.0 kPa, and P_{ACOH} = 2.0 kPa*

silica the order in ethylene was negative and that in oxygen fractionally positive whereas, over (1.0 wt% palladium, 0.5 wt% gold)/silica the order in ethylene was fractionally positive and that in oxygen was unchanged. The authors proposed that, on palladium, ethylene was more strongly adsorbed than oxygen, such that dissociative oxygen adsorption

was rate-determining and inhibited by the competitive adsorption of ethylene. On the palladium-gold surface, where the concentration of palladium-palladium ensembles was reduced, ethylene adsorption was weaker (so that the order became positive) and the inhibition of oxygen adsorption was consequently less severe, leading to a rate enhancement by a factor of 30 at 413 K.

Goodman and co-workers [66] studied VA synthesis over (1 wt% palladium)/silica, (5 wt% palladium)/silica, and Pd(100) (Table 1.3). Over all three surfaces, reaction was of negative order in ethylene and positive order in oxygen, consistent with the results of Han

Table 1.3 – Kinetic parameters for VA synthesis over palladium substrates

Substrate	Rate constant (k) $\times 10^{-3}$ s^{-1}	Order in ethylene (α)	Order in oxygen (β)	E_a (kJ mol^{-1})
Pd (100)[a]	0.4 – 0.8	-0.40 ± 0.04	0.50 ± 0.05	23.0 ± 3.0
(5 wt% Pd)/SiO$_2$[b]	0.8 – 1.4	-0.60 ± 0.02	0.12 ± 0.01	17.3 ± 2.0
(1 wt% Pd)/SiO$_2$[b]	2.4 – 5.1	-0.34 ± 0.02	0.18 ± 0.01	39.0 ± 2.0

et al. [65]. The mean palladium particle-size in (1% palladium)/silica was 2.5 nm and in (5% palladium)/silica was 4.2 nm. The former was 3.5 times more active than the latter (Table 1.3) which, at first sight, suggests that the reaction was mildly structure sensitive. However, true structure sensitivity requires that, when a change in catalyst structure brings about a change in activity (strictly in rate coefficient) the reaction should give *the same products*. In Goodman's study, selectivity to VA was higher over the catalyst containing the smaller particles, i.e. there was less deep oxidation to carbon oxides. Thus, catalyst structure controls both the activity and the products of reaction, but it is technically incorrect to say that VA synthesis is a structure sensitive reaction. It is the balance between VA synthesis and deep oxidation that is controlled by particle-size.

1.2.5.2 Activation energies

Activation energies are sensitive both to catalyst formulation and reaction conditions. Goodman has reported recently that the addition of gold to a palladium surface causes a reduction in the activation energy and an associated increase in rate by a factor of 30 [65]. His earlier work (Table 1.3), showed that the activation energy was reduced as palladium particle-size was increased and the reaction moved towards more extensive deep oxidation.

1.2.5.3 Effect of acetic acid on rate

Augustine and Blitz have addressed the role of acetic acid in VA synthesis [71]. The presence of potassium acetate lowers the activation energy for VA formation, which the authors attributed to the formation of islands of potassium acetate-like species adsorbed on the palladium surface. The order of reaction in acetic acid was zero, a value also reported by Goodman [65 – 67] and Samanos et al. [35]. However, values of 0.5 [72] and 1.0 [34] have been reported by others. Such variability suggests that the strength of acetic acid adsorption can vary significantly with reaction conditions.

1.2.5.4 Summary

The kinetics of the reaction are consistent with a situation in which ethylene and oxygen competitively adsorb at palladium sites on the surface, the former more strongly than the latter. VA synthesis competes with deep oxidation to carbon dioxide, the former being favoured by reduced palladium particle-size and modest temperatures. One effect of gold can be to reduce palladium ensemble size, so enhancing VA synthesis at the expense of deep oxidation. Whether gold also reduces the strength of adsorption of species adsorbed to palladium, thereby facilitating faster reaction is not clear.

1.2.6   Deactivation of Vinyl Acetate Synthesis Catalysts

The reasons for deactivation probably include reduction in metal surface area by sintering, poisoning of the surface, or palladium-gold surface segregation.

Fresh and aged (palladium-gold-potassium)/silica catalysts have been compared by Lambert and co-workers [73]. They found that the fresh catalyst contained palladium in two forms: palladium-gold alloy particles, 4 – 5 nm in size, containing 59 atom% gold, and a very highly dispersed palladium metal component. The aged catalyst contained three separate palladium components: palladium-gold alloy particles, 12 nm in size, palladium acetate, a highly dispersed palladium component. They concluded that usage resulted in pronounced sintering of the palladium-gold alloy phase but that this change occurred without significant variation in alloy composition. The gold composition of the alloy rose from 59 atom% to 62 atom% gold, which may interpret the constant selectivity during catalyst lifetime. The palladium acetate was considered to have been formed from the highly dispersed palladium phase and was not thought to have contributed greatly to the

sintering mechanism. The study also revealed the presence of acetic acid and silyl ester species on the surface of the aged catalyst, as well as a monodentate ester-like palladium acetate species which is postulated as a key intermediate for VA formation.

Goodman and co-workers have suggested that catalyst deactivation may occur as a result of carbide poisoning of the active phase of the catalyst [74]. The formation of carbides over palladium catalysts was first reported in 1970 [34] and the species were fully defined as palladium carbide some ten years later. It is also known that interstitial carbon can significantly alter the bulk and surface structure of palladium and lead to catalytic deactivation in reactions involving hydrocarbons [75 – 83]. Independently, Bowker has shown that acetic acid and ethylene decompose over palladium single crystal surfaces leading to the deposition of carbon and at elevated temperatures carbon is lost from the surface to the bulk [84, 85]. He concluded that palladium is capable of acting as a sponge for carbon. Due to carbon deposition, the formation of palladium carbide on the surface of palladium-containing catalysts is possible and deactivation via palladium carbide poisoning is plausible. Goodman and co-workers have investigated the possibility of palladium carbide formation occurring over silica supported palladium and palladium-gold catalysts during VA synthesis [74]. They report the formation of palladium carbide on palladium catalysts after VA synthesis but also report that smaller palladium particles were more resistant to palladium carbide formation. i.e. ease of palladium carbide formation varied inversely with particle-size. However, there was no evidence for the formation of palladium carbide over palladium-gold catalysts following VA synthesis. Thus, alloying of gold with palladium is very effective in preventing palladium carbide formation over palladium-based catalysts under the conditions of VA synthesis.

Catalyst deactivation may also occur as a result of surface segregation i.e. the formation of separate palladium and gold particles from the original palladium-gold alloy. Samanos et al. [35] and Zaidi et al. [64] proposed mechanisms in which palladium is oxidised from the catalyst surface and forms a palladium acetate complex. The coordination and subsequent oxidation of ethylene to VA completes a cycle in which palladium (II) is reduced to palladium metal over the catalyst surface. It is conceivable that this mechanism could operate within the liquid-layer associated with the catalyst particles under reaction conditions [36] and it is likely that palladium, which is subjected to a series of

oxidation/reduction cycles during the catalyst lifetime, may be re-deposited in a different form, one which may be inactive or less active for VA synthesis.

For a catalyst operating in this manner it is easy to envisage substantial time-dependant surface changes which may lead to the loss of palladium-gold phases and the formation of separate palladium and gold particles. Palladium oxidation/reduction cycles are also likely to play a significant role in the formation of palladium acetate at the surface of working catalysts and in particle sintering [73].

1.2.7 Deep Oxidation in Vinyl Acetate Synthesis

Carbon dioxide is the major deep oxidation product in the heterogeneous VA process. It is well known that, in VA synthesis, carbon dioxide can be formed by the combustion of ethylene and/or acetic acid and this lowers selectivity. However, the source of carbon dioxide is a topic of much debate. Selectivity to VA is known to vary with many parameters and values as low as 80% and as high as 94% have been recorded for (palladium)/silica and (palladium-gold)/silica catalysts respectively [86].

1.2.7.1 Carbon dioxide formation from ethylene

Nakamura and Yasui have suggested that, in VA synthesis, carbon dioxide could be derived from both ethylene and acetic acid following their adsorption [34]. However, they concluded that carbon dioxide was mainly formed from ethylene, based on the observations that (i) the selectivity to VA increases with an increase in the ratio of acetic acid to ethylene and (ii) ethylene is more easily oxidised than acetic acid over palladium. Samanos et al. also concluded from a kinetics study that carbon dioxide was formed solely from ethylene [35] but Crathorne et al. showed, by use of isotopic tracers, that carbon dioxide was derived equally from ethylene and acetic acid under reaction conditions [36]. Provine et al. have studied the roles of acetic acid and ethylene in carbon dioxide formation over palladium and palladium-gold catalysts in the presence and absence of potassium acetate [37]. This study, which also included isotopic tracer experiments, concluded that carbon dioxide was formed from ethylene and that potassium acetate suppressed ethylene combustion. There is, therefore, a conflict of evidence. It appears certain that carbon dioxide is formed from ethylene, but its formation from acetic acid may also occur under some conditions.

1.2.7.2 Kinetics of ethylene combustion

Goodman and co-workers have investigated the kinetic parameters of ethylene combustion in the presence and absence of acetic acid (2.0 kPa) and VA (2.0 – 3.5 kPa) over unpromoted palladium catalysts supported on high surface area silica (600 m^2 g^{-1}) [86]. The experiments were carried out at 413 – 453 K with partial pressures of ethylene of 5.0 – 15.0 kPa and of oxygen pressures of 1.0 – 10.0 kPa. Ethylene and oxygen exhibited negative and positive reaction orders respectively (Table 1.4). These measurements were essentially the same in the presence and absence of acetic acid and are consistent with ethylene combustion being the major route to carbon dioxide formation in VA synthesis over unpromoted palladium within the pressure regime investigated.

Table 1.4 – Kinetic parameters for ethylene combustion in the absence and presence of acetic acid (Goodman and co-workers [86])

Kinetic parameter	Absence of AcOH			Presence of AcOH		
	413 K	433 K	453 K	413 K	433 K	453 K
Rate constant (x 10^{-3} s^{-1})	1.66	1.66	1.78	0.38	0.42	0.71
Order in ethylene (α)	-0.15	-0.17	-0.19	-0.27	-0.31	-0.27
Order in oxygen (β)	1.22	1.18	1.16	0.88	0.82	0.89

Guo et al. suggested two possible pathways for the catalytic combustion of ethylene over palladium [87]. The first involved indirect combustion, in which ethylene was considered to be dissociatively adsorbed on palladium giving $C_{(ads)}$ and $H_{(ads)}$, the absorbed species reacting with adsorbed oxygen to give carbon monoxide, carbon dioxide, and water. The alternative proposed pathway was oxygen-activated combustion in which adsorbed oxygen assists the removal of hydrogen from ethylene via the formation of O–H and/or O–C bonds, again yielding carbon monoxide, carbon dioxide, and water.

The orders with respect to ethylene and oxygen (Table 1.4) show that ethylene combustion can be fitted by a Langmuir-Hinshelwood mechanism where the adsorption or dissociation of oxygen is the rate-determining step. The model explains these kinetics as well as previous data for ethylene combustion over a palladium single-crystal surface [66].

Goodman and co-workers [65] studied the kinetics of carbon monoxide oxidation over (palladium)/silica and (palladium-gold)/silica catalysts. A negative order for carbon monoxide and a positive order for oxygen were reported. These results are in agreement

with previous studies [88 – 90] and they concluded that CO oxidation also proceeds via a Langmuir-Hinshelwood mechanism.

1.2.7.3 Carbon dioxide formation from acetic acid

Almost all authors have reported that the majority of the carbon dioxide formed during VA synthesis is a result of ethylene combustion [34 – 37]. Crathorne et al. provided positive evidence for the substantial conversion of acetic acid to carbon dioxide [36] whereas only Samanos et al. have proposed that carbon dioxide in VA synthesis does not involve acetic acid combustion [35].

Acetic acid adsorption and decomposition over palladium (110) has been studied by Bowker et al. [84]. Using a molecular beam reactor and temperature programmed desorption they deduced that the sticking probability of acetic acid is very high and that it results in hydrogen evolution and acetate formation at room temperature. Adsorbed acetate (which was assumed to be bonded in a bidentate fashion) decomposed between 320 K and 440 K producing carbon dioxide and hydrogen. Acetic acid (acetate) decomposition leaves carbon on the palladium (110) surface which has implications for catalyst deactivation pathways (Section 1.2.6). At temperatures above 450 K acetate was unstable [84].

The interaction between palladium and acetic acid over palladium single crystals has also been studied by Lambert and co-workers [91]. At low temperature (170 K) the adsorbed monolayer contained dissociated and non-dissociated acetic acid molecules. The dissociated molecules consisted of a mixture of bidentate and monodentate species. Monodentate acetate was formed at high coverages, consistent with its reduced coordination at the surface. These species closely resembled the acetate species observed at the surface of a working VA synthesis catalyst under reaction conditions [73]. Thermal decomposition of adsorbed acetic acid yielded carbon dioxide, water, carbon monoxide, hydrogen, and carbon.

1.2.8   Alternative Processes for Vinyl Acetate Synthesis

VA can be synthesised using reactants other than acetylene, ethylene, acetic acid, and oxygen.

1.2.8.1 Synthesis from CO/H_2 mixtures

Tustin et al. have investigated two routes for the manufacture of VA from synthesis gas (CO/H_2 mixtures) [92]. The first of which synthesises VA from acetic acid (formed by the carbonylation of methanol (30) which was synthesised from CO/H_2 (29)) via ketene which is formed by acetic acid dehydration (31). Ketene is hydrogenated to acetaldehyde (32), which is subsequently reacted with ketene to produce VA (33).

$$2\,CO + 4\,H_2 \longrightarrow 2\,CH_3OH \tag{29}$$

$$CH_3OH + CO \longrightarrow CH_3COOH \tag{30}$$

$$CH_3COOH \longrightarrow H_2C=C=O + H_2O \tag{31}$$

$$H_2C=C=O + H_2 \longrightarrow CH_3CHO \tag{32}$$

$$CH_3CHO + H_2C=C=O \longrightarrow \underset{VA}{CH_2=CHOCOCH_3} \tag{33}$$

The second route investigated the conversion of dimethyl ether to acetic anhydride (34) and the reaction of acetic anhydride with acetaldehyde (35) in a reactive distillation column to produce VA and acetic acid.

$$CH_3OCH_3 + 2\,CO \longrightarrow CH_3COOOCCH_3 \tag{34}$$

$$CH_3COOOCCH_3 + CH_3CHO \longrightarrow \underset{VA}{CH_2=CHOCOCH_3} + CH_3COOH \tag{35}$$
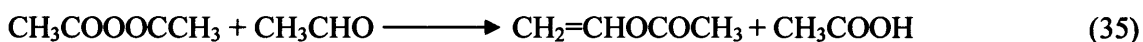
The acetic acid produced is hydrogenated to form acetaldehyde which is required in the reactive distillation stage (36).

$$CH_3COOH + H_2 \longrightarrow CH_3CHO + H_2O \tag{36}$$

1.2.8.2 Synthesis from methanol and acetic acid

In 1981 Halcon international developed a unique process for the synthesis of VA using ethylidene diacetate as an intermediate [93]. The process involves the formation of methyl acetate from methanol and acetic acid (37), followed by carbonylation and hydrogenation (38) of the ester to give ethylidene diacetate. The carbonylation stage is catalysed by

rhodium (III) chloride and modified by the presence of β-picoline and methyl iodide [93]. VA is produced by the pyrolysis of ethylidene diacetate in which acetic acid is a by-product (39).

$$CH_3OH + CH_3COOH \longrightarrow CH_3OCOCH_3 + H_2O \tag{37}$$

$$2\ CH_3OCOCH_3 + 2\ CO + H_2 \longrightarrow CH_3CH(COOCH_3)_2 + CH_3COOH \tag{38}$$

$$CH_3CH(COOCH_3)_2 \longrightarrow CH_2=CHOCOCH_3 + CH_3COOH \tag{39}$$
$$\text{VA}$$

Overall:

$$2\ CH_3OH + 2\ CO + H_2 \longrightarrow CH_2=CHOCOCH_3 + 2\ H_2O \tag{40}$$

1.2.8.3 Synthesis from ethylene glycol diacetate

The ethylene glycol diacetate process was developed by Halcon international. This compound (like ethylidene diacetate) provides VA and acetic acid on pyrolysis (41) [94].

$$CH_3COOCH_2CH_2OOCCH_3 \longrightarrow CH_2=CHOCOCH_3 + CH_3COOH \tag{41}$$
$$\text{VA}$$
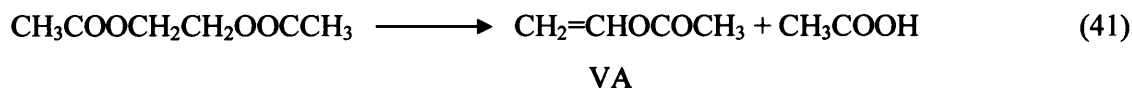
1.2.8.4 Synthesis from acetic anhydride

The acetic anhydride process was developed by the Mitsubishi Gas Chemical Company. The process is one of oxidative reduction by hydrogen (42) [94].

$$CH_3COOCOCH_3 + H_2 \longrightarrow CH_2=CHOCOCH_3 + H_2O \tag{42}$$
$$\text{VA}$$

1.2.9 Physical Properties of Vinyl Acetate

VA is a colourless liquid with a sweet odour [9]. Its physical properties are shown in Table 1.5 (data supplied by BP).

Table 1.5 – Physical properties of VA

Molecular mass	86.09
Density at 20°C	0.9312 kg dm^{-3}
Coefficient of expansion at 20°C	1.32 x 10^{-3} /°C
Boiling point at 1.013 bar	72.5°C
Vapour pressure at 20°C	118.1 mbar
Critical pressure	36 bar
Flash point (tag open cup)	-8°C
Explosive limits of vapour with air upper	13.4% volume
lower	2.6% volume
Melting point	-100.2°C
Refractive index nD20	1.395
Absolute viscosity at 20°C	0.432 cP
Specific heat at 25°C	1.95 kJ kg^{-1} deg^{-1}
Latent heat of vaporisation	379 kJ kg^{-1}
Heat of polymerisation	89.3 kJ mol^{-1}
Permittivity at 25°C	5.8

1.2.10 BP Sales Specification for Vinyl Acetate

The following is the standard sales specification for VA supplied by BP.

Table 1.6 – BP sales specification for VA monomer

Property	Value
Appearance	Clear, free from suspended matter
Colour	5 Hazen units max.
Density at 20°C	0.931 – 0.933 kg dm^{-3}
Assay	99.9% mass min.
Acidity	0.005% mass max.
Acetaldehyde	0.01% mass max.
Water	0.04% mass max.
Hydroquinone	8 – 12 ppm
Distillation range at 1.013 bar	72.3 – 73.3 °C

1.3   Probes Used in the Present Study

Characterisation of supported catalysts, before and after exposure to reactants at high pressures and elevated temperatures is very important as it provides information which may be used to improve catalyst performance.

Traditionally, palladium-gold catalysts used in VA synthesis have been characterised using techniques such as X-ray diffraction and high resolution transmission electron microscopy which provide information on particle composition (and thus the extent of alloying), particle-size, and particle location.

In this study the characterisation is concerned mainly with the surfaces of graphite-supported palladium-gold catalysts. This has been achieved using cyclic voltammetry and X-ray photoelectron spectroscopy. The benefits of techniques such as X-ray fluorescence, X-ray diffraction, high resolution transmission electron microscopy, and energy dispersive X-ray analysis have been utilised to determine; bulk compositions, particle-size, alloy compositions, and morphology of supported metal particles. Chemisorption of CO has been used to determine relative palladium surface areas (CO is not adsorbed by gold) and ultra-violet absorption spectroscopy has been used to determine the relative concentrations of palladium (II) acetate species in the solution-phase. The latter technique provided quantitative information concerning the extent of palladium dissolution which occurs when palladium is treated with acetic acid-based solutions under oxidising conditions.

The following sub-sections indicate the merits and limitations of these techniques.

1.3.1   X-Ray Florescence

X-ray fluorescence has been used to measure the emissions characteristics of palladium K and gold L lines and thus calculate the relative amounts of palladium and of gold present in a sample of catalyst. This has allowed determination of palladium and of gold loadings and hence the calculation of bulk palladium/gold atom ratios. X-ray fluorescence has also been used to examine whether a catalyst contains the desired amount of palladium and gold thus, to provide a check on the success of metal precursor reduction in catalyst preparations.

1.3.2 X-Ray Diffraction

As the wavelengths of X-rays are comparable to interatomic distances, X-ray diffraction can be used to determine interatomic spacing, *d*, by use of the Bragg equation: $n\lambda$ = *2dsinθ*; where λ is the X-ray wavelength, and θ is the angle of the diffracted beam. Where a diffractogram is provided by a number of phases deconvolution (curve-fitting) can be used to identify the individual phases.

For large particles, diffraction peaks are sharp. For particles of 5 nm diameter or less, the diffraction peaks show a broadening, and the mean particle-size can be estimated from the extent of the broadening by use of the Scherrer equation (43).

$$S_c = \frac{K\lambda}{\beta \cos 2\theta} \tag{43}$$

In this equation S_c is the mean crystallite size, K is a constant known as a shape factor (it is usually set to 0.9 for spherical particles but can be up to 1.1 for various common geometries), λ is the X-ray wavelength, and β is the full-width half-maximum (FWHM) of the diffraction peak in radians.

Alloy composition can be determined on the assumption that the lattice constant of the alloy is given by a linear variation of the lattice constant with the concentrations of the constituent metals at a given temperature (Vergard's Law).

1.3.3 High Resolution Transmission Electron Microscopy

This method has allowed detailed accurate measurement of a large number of particle diameters in given catalysts and thus the generation of detailed particle-size distributions. In favourable cases it has also permitted particle morphology and metal location in segregated alloys to be investigated.

1.3.4 Energy Dispersive X-Ray Analysis

Energy dispersive X-ray analysis has been used to determine the palladium and gold compositions of individual metal particles. It has been used to determine the palladium and gold compositions of a large number of particles of various sizes, allowing the correlation

of (i) bulk composition with the existence of alloy particles, and (ii) individual particle composition with particle-size.

1.3.5   X-Ray Photoelectron Spectroscopy

X-ray photoelectron spectroscopy has been used to gather information about the surface phases existing in palladium-gold catalysts. This has been achieved by measuring binding energies of palladium (3d) and gold (4f) photoelectrons and deconvolution of the palladium (3d) and gold (4f) regions. The relative surface areas of palladium and of gold have been determined by integration of intensity with respect to binding energy.

1.3.6   CO Chemisorption

Chemisorption has been used to determine palladium surface area in palladium-gold catalysts. This has been achieved by measuring the number of CO molecules required to form a monolayer. By use of this quantity, along with an assumed Pd:CO stoichiometry, the number of palladium atoms in the surface of the catalyst has been determined. The palladium surface area is then calculated from knowledge of the diameter of the palladium atom. In the present work, an adsorption stoichiometry of Pd:CO of 1:1 has been assumed. CO may bridge-bond to palladium (Pd:CO = 2:1) and the stoichiometry may vary with alloy composition. Thus, values of surface area determined by this method should be treated with caution; they are of value as a means of comparing trends in a series of related catalysts.

1.3.7   Ultra-Violet Absorption Spectroscopy

In the heterogeneous gas-phase synthesis of VA over supported palladium-gold catalysts it is likely that the synthesis occurs via a homogeneous mechanism within a thin film of acetic acid and potassium adducts [35] (Section 1.2.4.2). In this situation, a palladium complex may be generated at the catalyst surface via palladium dissolution and complexation with acetate anions. In this context, ultra-violet absorption spectroscopy has been used to measure the relative concentrations of palladium acetate in a solution-phase and thereby to probe the matter of model dissolution. Spectroscopic measurements have been used to quantify the extent of palladium dissolution from palladium and palladium-gold catalysts of various compositions when treated with acetic acid and potassium acetate.

1.4   Voltammetric Techniques

Voltammetry provides information concerning the behaviour of electrode currents as a function of varying voltage [95]. Examples of voltammetric techniques are linear sweep voltammetry and cyclic voltammetry. These techniques each involve sweeping the potential of an electrode, V, between two set points at a fixed rate (ranging from 1 mV s^{-1} to 1000 mV s^{-1}) and measuring the electrode current, i, generated. The resulting i-V curve, or CV, usually exhibits peaks and troughs that can be used to interpret redox processes occurring at the interface [96].

1.4.1   Linear Sweep Voltammetry

The simplest of the voltammetric techniques, linear sweep voltammetry (LSV) involves the ramping of the electrode potential between two extremes in a stationary solution. As such, mass transport (the rate of diffusion of a species from the bulk of the solution to the electrode surface) is an important factor. The mass transport of a species, A, can be calculated using the equation:

$$\frac{\delta [A]}{\delta t} = D_A \frac{\delta^2 [A]}{\delta x^2} \qquad (44)$$

where [A] is the concentration of the redox species A, D_A is the diffusion coefficient of A, dt is the time taken to diffuse and dx is the diffusion distance.

The sweep rate, v, can be expressed as:

$$v = \frac{dE}{dt} \qquad (45)$$

where dE is the difference in potential between the limits V_1 and V_2, and dt is the time taken to complete the modulation. As v is constant it is possible to calculate the electrode potential at any time during the experiment using the equation:

$$E_t = E_i \pm \nu t \tag{46}$$

where E_i is the initial potential.

Figure 1.6 shows the potential waveform along with a schematic of the resultant i-V curve obtained in linear sweep voltammetry for a redox active solution component.
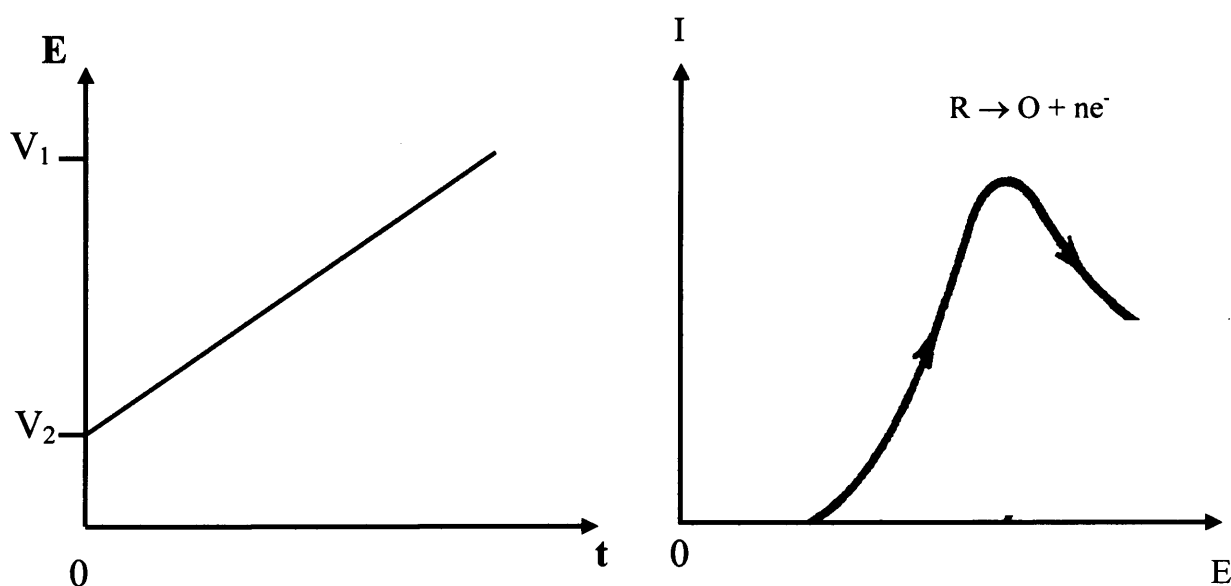
Figure 1.6 – Potential ramp and resultant voltammogram for LSV

1.4.2   Cyclic Voltammetry

In cyclic voltammetry a saw-tooth potential wave is applied to the electrode between the limits V_1 and V_2 (Figure 1.7). A typical CV for a redox couple in solution is shown in the same Figure.

In both cyclic and linear sweep voltammetry, current flow is measured between the electrode of interest (the working electrode – an electrode whose potential is monitored against a reference electrode) and a counter electrode under the control of a potentiostat. The peaks on the resulting voltammetric curve can be used to determine the potentials at which electrochemical processes occur. Peak width and height is dependant on sweep rate, electrolyte concentration, and electrode material, while the overall area under the peak is directly proportional to the charge transferred at the surface.
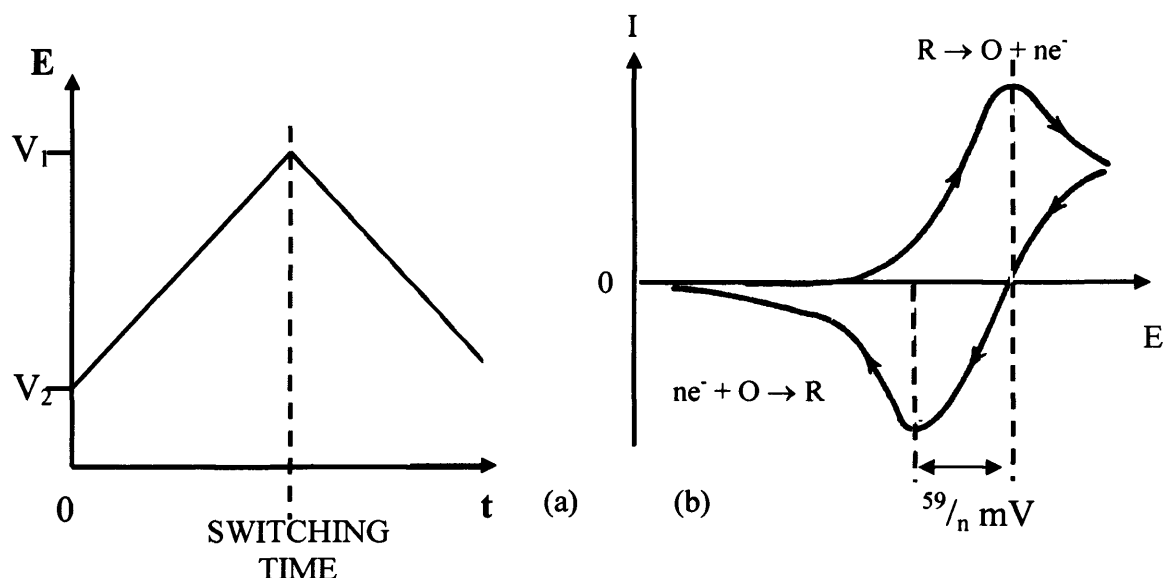
Figure 1.7 – (a) 'Sawtooth' potential pattern (potential cycle) and (b) the resulting CV for a reversible redox process

1.4.3 Electrochemical Processes

The current generated from the reaction of a species in solution with the electrode surface is the sum of two different processes termed Faradaic and non-Faradaic [97].

1.4.3.1 Faradaic processes

Faradaic processes are non-adsorptive processes that arise from charge transfer across the electrode/electrolyte interface. The redox reaction taking place can be expressed as:

$$Oxidant + ne^- \rightarrow Reductant \tag{47}$$

where the oxidant and reductant form a redox couple, and n is the number of electrons transferred. If the transfer rate of the electrons for both the forward and reverse direction is high the reaction being studied is described as being reversible. In such a case the heights of the forward and reverse peaks should be similar and the peak maximas should be separated by a potential of:

$$\left| E_P^{Ox} - E_P^{Red} \right| = 2.218 \frac{RT}{nF} \tag{48}$$

where E_p^{ox} and E_p^{red} are the potentials at which oxidation and reduction occurs, R is the universal gas constant, T is the temperature, n is the number of electrons transferred in equation 47, and F is the Faraday constant. This difference between oxidation and reduction potentials is equal to approximately 59/n mV at 298 K (see Figure 1.6) and is independent of the scan rate. Under the same reversible conditions the peak current density, I_p, can be expressed as:

$$I_P = 2.75 \times 10^5 \cdot n^{3/2} \cdot v^{1/2} \cdot Co \cdot D^{1/2} \tag{49}$$

where I_p is the current density in cm^{-2}, n is the number of electrons involved in the redox process, v is the sweep rate in $V\ s^{-1}$, Co is the concentration of the bulk solution in mol cm^{-3}, and D is the diffusion coefficient in $cm^2\ s^{-1}$. From equation 49 it can be seen that the peak height will increase with sweep rate since the peak current is proportional to the square root of the sweep rate.

1.4.3.2 Non-Faradaic processes

Non-faradaic processes are those that involve the adsorption and desorption of ions from the electrode surface. The adsorption of such ions is considered in the following equation:

$$M^{Z+}_{(aq)} + ne^- \rightarrow M_{(ads)} \tag{50}$$

For a first order reaction, the rate of the forward reaction (v_F) may be expressed as:

$$v_F = k_F\ [M^{Z+}](1-\theta) \tag{51}$$

where k_F is the rate constant of the forward reaction, θ is the fraction of sites covered with the adsorbate M and $[M^{Z+}]$ is the surface concentration of the metal ion.

The rate for the reverse reaction (v_R) is expressed as:

$$v_R = k_R\theta \tag{52}$$

where k_R is the rate constant for the reverse reaction. When the system is in equilibrium the forward and reverse reaction rates are equal:

$$|\nu_R| = |\nu_F| \tag{53}$$

Therefore by combining equations 51 and 52 and rearranging, a Langmuir-type adsorption equation is obtained:

$$\frac{\theta}{(1-\theta)} = \frac{k_F}{k_R} [M^{Z+}] \tag{54}$$

Also, for a reaction where complete charge transfer takes place the Gibbs energy of adsorption (ΔG_{ads}) is given as:

$$\Delta G_{(ads)} = \Delta G^o_{(ads)} + nFE \tag{55}$$

Where ΔG^o_{ads} represents the standard Gibbs free energy of adsorption of M, i.e. in the absence of an electric field, and nFE is the electrochemical contribution of the free energy of adsorption of M^{Z+}, where n is the number of electrons transferred, F is the Faraday constant, and E is the electrode potential. The equilibrium constant may then be expressed as:

$$K = \frac{k_F}{k_R} = \exp\left(\frac{-\Delta G_{ads}}{RT}\right) \tag{56}$$

and, from equation 55:

$$K = \frac{k_F}{k_R} = \exp\left(\frac{-\Delta G^o_{ads} - nFE}{RT}\right) \tag{57}$$

At constant temperature:

$$\exp\left(\frac{-\Delta G^o_{(ads)}}{RT}\right) = \text{constant} = \text{K'} \tag{58}$$

so that, by substitution of equation 58 into equation 57, then into equation 54 the adsorption equation becomes:

$$\frac{\theta}{(1-\theta)} = K' \exp\left(\frac{-nFE}{RT}\right)[M^{Z+}] \tag{59}$$

If lateral interactions are included, the so-called Frumkin isotherm is obtained [98]:

$$\frac{\theta}{(1-\theta)} \exp\left(A\left(\theta-\frac{1}{2}\right)\right) = K' \exp\left(\frac{-nFE}{RT}\right)[M^{Z+}] \tag{60}$$

where $\exp\left(A\left(\theta-\frac{1}{2}\right)\right)$ is the van der Waals term for adlayer interactions with A representing the magnitude of attractive and repulsive interactions included by Frumkin [98].

1.4.4 Under-potential Deposition

Under-potential deposition (UPD) is the adsorption of submonolayer quantities of metals (or protons) onto an electrode at potentials positive of its Nernst potential (E_b), i.e. before bulk deposition occurs. Adsorption at these potentials using low potential sweep rates usually results in submonolayer, monolayer, or second monolayer adsorption [99]. The first reported observation of under-potential deposition was made by Hevesy in 1912 [100].

The formation of surface alloys during under-potential deposition has also been reported [101]. This is a slow process relative to monolayer formation due to the atomic rearrangements necessary for place exchange to occur. Alloy formation results in a modification of the surface electronic structure and consequently a shift in the potential required to deposit further adatoms.

1.5   Objectives of the Investigation

The overall objective of this investigation was to use electrochemical methods to characterise (palladium-gold)/graphite catalysts and to explore their surface chemistry under conditions related to the gas-phase synthesis of vinyl acetate from ethylene, acetic acid, and oxygen over palladium-gold surfaces.

The intermediate objectives have been:

- to prepare Batches of (palladium-gold)/graphite catalysts using a variety of methods;

- to characterise the prepared catalysts using cyclic voltammetry together with a range of traditional techniques;

- to determine whether particle-size distributions and surface compositions of these palladium-gold catalysts were influenced by the preparation method or by subsequent heat treatments;

- to screen catalysts for activity using a standard hydrogenation test and examining selected catalysts for vinyl acetate synthesis activity using a high throughput testing rig in an industrial laboratory;

- to examine the effects of the presence of aqueous acetic acid/potassium acetate mixtures on catalyst composition;

- to refine the present understanding of the role of gold as a promoter of palladium in vinyl acetate synthesis;

- to contribute to the current debate as to whether the gas-phase heterogeneously-catalysed reaction is accompanied by a homogeneously catalysed component.

1.6 References

[1] A. Haynes, B. E. Mann, D. J. Gulliver, G. E. Morris, P. M. Maitlis, J. Am. Chem. Soc. 113 (1991) 8567.

[2] M. J. Cunnington, Personal Communication, BP Chemicals, 2002.

[3] A. Haynes, B. E. Mann, G. E. Morris, P. M. Maitlis, J. Am. Chem. Soc. 115 (1993) 4093.

[4] H. Hohenschutz, N. von Kutepow, W. Himmle, Hydrocarbon Process. 45 (1966) 141; N. von Kutepow, W. Himmle, H. Hohenschutz, Chem. Ing. Tech. 37 (1965) 383.

[5] F. E. Paulik, J. F. Roth, J. Chem. Soc., Chem. Commun. (1968) 1578; J. F. Roth, J. H. Craddock, A. Hershman, F. E. Paulik, Chem. Tech. (1971) 600.

[6] G. J. Sunley, D. J. Watson, Catal. Today 58 (2000) 293.

[7] Unattributed, Platinum 2006, Johnson Matthey, 2006.

[8] P. W. Atkins, *in* "Physical Chemistry", 6th ed, p. 857, Oxford University Press, Oxford, 1997.

[9] R. Abel, P. Colling, K. Eichler, D. Peters, *in* "Handbook of Heterogeneous Catalysis Vol 5" (eds. G. Ertl, H. Knozlnger, J. Weitkamp), p. 2296, Wiley-VCH, Weinheim, 1997.

[10] M. J. Cunnington, Personal Communication, BP Chemicals, 2004.

[11] M. J. Cunnington, Personal Communication, BP Chemicals, 2003.

[12] European Patent No. 1175939.

[13] US Patent No. 144544.

[14] US Patent No. 6534438.

[15] European Patent No. 1467814.

[16] US Patent No. 032638.

[17] US Patent No. 1084581.

[18] C. Schildknecht, *in* "Vinyl and Related Polymers", Wiley, New York, 1952.

[19] E. C. Leonard, *in* "Vinyl and Diene Monomers", Wiley Interscience, New York, 1970.

[20] US Patent No. 2770650.

[21] US Patent No. 2411962.

[22]   US Patent No. 2485044.

[23]   US Patent No. 2750410.

[24]   I. B. Vasil'eva, A. I. Gel'bschtein, I. N. Tolstikova, W. T. Tao, Kinet. Catal. 5 (1964) 144.

[25]   N. Yameda, Kogyo Kagaku Zasshi, 62 (1959) 1458.

[26]   Chem. Week 101 (1967) 73.

[27]   I. I. Moiseev, M. N. Vargaftik, Y. K. Syrkin, Dokl. Akad. SSSR 133 (1960) 377.

[28]   UK Patent Nos. 964001, 969162, 975683, 975709, 1026594, 1061788.

[29]   US Patent Nos. 3260739, 3253020.

[30]   Belgian Patent No. 635425.

[31]   W. H. Clement, C. M. Selwitz, Tetrahedron Lett. 1081 (1962).

[32]   US Patent No. 3221045.

[33]   US Patent No. 3190912.

[34]   S. Nakamura, T. Yasui, J. Catal. 17 (1970) 366.

[35]   B. Samanos, P. Boutry, R. Montarnal, J. Catal. 23 (1971) 19.

[36]   E. A. Crathorne, D. MacGowan, S. R. Morris, A. P. Rawlinson, J. Catal. 149 (1994) 254.

[37]   W. D. Provine, P. L. Mills, J. J. Lerou, Stud. Surf. Sci. Catal. 101 (1996) 191.

[38]   DAS 1191366, DOS 2315037, European Patent No. 519436.

[39]   DAS 1568645, DT 1185604.

[40]   US Patent No 4048096.

[41]   US Patent No. 4087622, European Patent No. 464633.

[42]   US Patent Nos. 5179056, 51790857.

[43]   US Patent Nos. 5185308, 5274181.

[44]   US Patent Nos. 5314858, 5332710.

[45]   US Patent No. 5347046.

[46]   US Patent No. 4762498.

[47]   UK Patent No. 976613.

[48]   US Patent No. 5336802.

[49]   Belgian Patent No. 627888, US Patent No. 3275680.

[50] G. Rosher, E. Hoffmann, K. A. Adey, W. Jeblick, H - J. Klimisch, H. Kieczka, Ullmann's Encyclopaedia Ind. Chem. 4th ed. Vol 23, p. 597, 1983.

[51] W. Schwerdtel, Chem. Ing. Tech. 40 (1968) 781.

[52] S. Nakamura, T. Yasui, J. Catal. 23 (1971) 315; T. Yasui, S. Nakamura, Shokubai. 14 (1972) 187; S. Nakamura, T. Yasui, Yuki Gosei Kagaku Kyokai Shi 34 (1976) 969.

[53] T. Sirasaki, I. Furuoya, Shokubai. 9 (1967) 114; T. Sirasaki, M. Okada, Shokubai. 9 (1967) 267.

[54] R. Abel, PhD Thesis, TU Munchen, 1992.

[55] R. Abel, G. Prauser, H. Tiltscher, Chem. Eng. Technol. 17 (1994) 112.

[56] S. A. H. Zaidi, J. Catal. 68 (1981) 255.

[57] European Patent Nos. 330853, 403950, 431478, 519435.

[58] UK Patent No. 1521652.

[59] US Patent No. 5336802.

[60] R. Abel, P. Colling, K. Eichler, D. Peters, *in* "Handbook of Heterogeneous Catalysis Vol 5" (eds. G. Ertl, H. Knozlnger, J. Weitkamp), p. 2298, Wiley-VCH, Weinheim, 1997.

[61] BP Technology Brochure Announcing the LEAP Process.

[62] M. Johnson, "Leaps of Innovation", BP Frontiers, BP, 2002.

[63] S. Nakamura, T. Yasui, J. Catal. 23 (1971) 315.

[64] S. A. H. Zaidi, Appl. Catal. 38 (1988) 353.

[65] Y - F. Han, J - H. Wang, D. Kumar, Z. Yan, D. W. Goodman, J. Catal. 232 (2005) 467.

[66] D. Kumar, Y - F. Han, M. S. Chen, D. W. Goodman, Catal. Lett. 106 (2006) 1.

[67] Y - F. Han, D. Kumar, D. W. Goodman, J. Catal. 230 (2005) 362.

[68] R. van Helden, C. F. Kohll, D. Medema, G. Verberg, T. Jonkhoff, Recueil 87 (1968) 961.

[69] R. G. Brown, J. M. Davidson, C. Triggs, C. Am. Chem. Soc., Div. Petrol. Chem. Preprint 14 (1969); French Patent No. 1403398 (1965).

[70] D. A. Kragten, R. A. van Santen, M. K. Crawford, W. D. Provine, J. J. Lerou, Inorg. Chem. 38 (1999) 331.

[71] S. M. Augustine, J. P. Blitz, J. Catal. 142 (1993) 312.

[72]   J. H. Wieland, G. Prauser, K. Dialer, Chem. Ing. Tech. 54 (1982) 605.

[73]   N. Macleod, J. M. Keel, R. M. Lambert, Appl. Catal., A 261 (2004) 37.

[74]   Y - F. Han, D. Kumar, C. Sivadinarayana, A. Clearfield, D. W. Goodman, Catal. Lett. 94 (2004) 131.

[75]   S. A. H. Zaidi, Appl. Catal. 30 (1987) 131; S. A. H. Zaidi, Appl. Catal. 33 (1987) 273.

[76]   R. K. Nandi, R. Pitchai, S. S. Wong, J. B. Cohen, R. L. Burwell Jr., J. B. Butt, J. Catal. 70 (1981) 298.

[77]   S. B. Ziemecki, G. A. Jones, D. G. Swartzfger, R. L. Harlow, J. Faber Jr., J. Am. Chem. Soc. 107 (1985) 4547.

[78]   T. Yamamoto, M. Adachi, K. Kawabata, K. Kimura, H. W. Hahn, Appl. Phys. Lett. 63 (1993) 3020.

[79]   J. A. McCaulley, Phys. Rev. B, 47 (1993) 4873; J. A. McCaulley, J. Phys. Chem. 97 (1993) 10372.

[80]   K. Okitsn, Y. Mizukoshi, H. Bandow, T. A. Yamamoto, Y. Nagata, Y. Maeda, J. Phys. Chem. B 101 (1997) 5470.

[81]   A. Sarkany, Appl. Catal., A 175 (1998) 245.

[82]   Z. Kaszkur, J. Stachurski, J. Pielaszek, J. Phys. Chem. Solids 47 (1986) 795.

[83]   M. Bonarowska, J. Pielaszek, V. A. Semikolenov, Z. Karpinski, J. Catal. 209 (2002) 528; M. Bonarowska, A. Malinowski, W. Juszczy, Z. Karpinski, Appl. Catal., B 30 (2001) 187.

[84]   M. Bowker, C. Morgan, J. W. Couves, Surf. Sci. 555 (2004) 145.

[85]   M. Bowker, C. Morgan, N. Perkins, R. Holroyd, E. Fourre, F. Grillo, A. MacDowall, J. Phys. Chem. B 109 (2005) 2377.

[86]   Y - F. Han, D. Kumar, C. Sivadinarayana, D. W. Goodman, J. Catal. 224 (2004) 60.

[87]   X - C. Guo, R. J. Madix, J. Am. Chem. Soc. 117 (1995) 5523.

[88]   J. Szanyi, W. K. Kuhn, D. W. Goodman, J. Phys. Chem. 98 (1994) 2972.

[89]   J. Szanyi, W. K. Kuhn, D. W. Goodman, J. Phys. Chem. 98 (1994) 2978.

[90]   N. W. Cant, P. C. Hicks, B. S. Lennon, J. Catal. 54 (1978) 372.

[91]   R. D. Haley, M. S. Tikhov, R. M. Lambert, Catal. Lett. 76 (2001) 125.

[92]   G. C. Tustin, R. D. Colberg, J. R. Zoeller, Catal. Today, 58 (2000) 281.

[93]   UK Patent Application No. 2013184 A, US Patent Nos. 4002677, 4002678.

[94]   A. Amieiro Fonseca, PhD Thesis UMIST, 2001.

[95]   A. C. Fisher, *in* "Electrode Dynamics", p. 27, Oxford University Press, Oxford, 1996.

[96]   A. Wieckowski, M. Dekker, *in* "Interfacial Electrochemistry, Theory, Experiment and Applications", New York, 1999.

[97]   M. Faraday, Phil. Trans. Roy. Soc. A 124 (1834) 77.

[98]   A. Slygin, A. Frumkin, Acta Physiochim. URSS 3 (1935) 791.

[99]   E. Herrero, L. J. Buller, H. D. Abruna, Chem. Rev. 101 (2001) 1897.

[100]   G. Hevesy, Physik. Z. 13 (1912) 715.

[101]   G. Inzelt, G. Horanyi, J. Electroanal. Chem. 491 (2000) 111.

CHAPTER 2
EXPERIMENTAL

2.1 Catalyst Preparations

Traditionally, fixed bed catalysts used in the gas-phase synthesis of vinyl acetate monomer (VAM) from ethylene, acetic acid, and oxygen have consisted of palladium-based alloys supported on high surface area silica [1]. Recently BP has developed a new generation catalyst, which is a silica-supported palladium-gold alloy [2]. The materials used and a new preparative method produce very fine particles suitable for use as a fluidised bed catalyst [3 – 7]. LEAP catalysts have revolutionised VAM synthesis. The low conductivity of silica means that real LEAP catalysts could not be analysed in this electrochemical study. Therefore, palladium-gold catalysts supported on graphite were prepared.

Catalyst nomenclature

All catalysts used in this investigation were given both a reference number, and a conventional description.

Catalyst reference numbers were allocated at the time that the materials were prepared, and the descriptions indicate the catalyst composition which became known after X-ray fluorescence analysis. Thus, the reference numbers are numerical: e.g. 3182, 4270, and 006 whereas catalyst descriptions are of the type: (Y% Pd, Z% Au)[R]/G{X}. This description conveys the following information: the active phase of the catalyst consisted of Y% palladium by mass and Z% gold by mass. The active phase was supported on graphite (abbreviated, G). [R] denotes the numerical value of the palladium/gold atom ratio. {X} denotes the Batch number, and has the values 1, 2, or 3.

Thus, as shown in Chapter 3, the catalyst having the reference number 3184 is (1.0% Pd, 0.4% Au)[4.7]/G{1}; i.e. it is a palladium-gold bimetallic catalyst supported on graphite containing 1.0% by weight of palladium and 0.4% by weight of gold. The palladium/gold atom ratio was 4.7, and it was prepared under Batch 1 conditions.

Where catalysts were prepared by plating palladium onto (0% Pd, 20% Au)/G catalyst, the appropriate catalyst description is of the form: Pd/(0% Pd, 20% Au)[0.02]/G{T}. Thus, the description indicates that palladium was plated onto 20% gold/graphite catalyst to the point where the palladium/gold atom ratio was 0.02. {T} denotes the Batch number, and has the values of 4 or 5 depending on the reduction conditions.

2.1.1 Preparation of Graphite-Supported Palladium-Gold Catalysts

Three series of palladium-gold catalysts were prepared utilising low surface area (KS15) graphite (15 m^2 g^{-1}) as a conducting support.

The catalysts were prepared at Johnson Matthey's laboratories at Royston, which permitted the use of specialised preparative equipment and analytical techniques. These included metal surface area measurement by CO chemisorption, measurement of bulk composition by X-ray fluorescence (XRF), and activity measurements by use of nitrobenzene hydrogenation.

Each Batch of palladium-gold catalysts was prepared using a specific preparative method and reducing agent and is comprised of nine samples of varied composition ranging from palladium-rich to gold-rich systems. The metal precursors were sodium chloropalladite (Na$_2$PdCl$_4$) and tetrachloroauric acid (HAuCl$_4$). Catalysts were prepared on the 100 g scale with metal loadings ranging from 0.4 to 3.6%.

Table 2.1 – Combinations of preparative method and reducing agent used in the preparation of palladium-gold catalysts

Batch	Preparative method	Reducing agent
1	slurry precipitation	alkaline formaldehyde
2	slurry precipitation	hydrazine
3	incipient wetness impregnation	hydrazine

2.1.1.1 Slurry precipitation method

Slurry precipitation preparations were carried out in glass vessels (volume 3.5 dm^3), using standard Fisher overhead mechanical stirrers (impeller shaft diameter 10 mm, 30 mm baffled PTFE blades at 90°). The baffles were immersed in the liquor. Stirrer speeds of 400 – 600 rpm were used. The blades were located close to the edge of the vessel, ensuring efficient mixing of particles and solution. Palladium and gold from premixed solutions of sodium chloropalladite and tetrachloroauric acid were precipitated as mixed hydroxides onto the graphite support suspended in an aqueous alkaline slurry. The metal hydroxides were reduced by the action of alkaline formaldehyde or hydrazine. The required mass of

graphite was measured into a vessel. Demineralised water was added and a slurry was formed by mechanical stirring. Sodium hydroxide solution (750 (mg NaOH)(g metal)$^{-1}$ dissolved in 20 cm^3 water) was added to the graphite slurry and the mixture stirred.

The required masses of the palladium and gold precursor salts (Tables 2.2 and 2.3) were mixed and dissolved in demineralised water. The solution containing the metal precursors was then added to the alkaline graphite slurry and the mixture was stirred for approximately 0.5 h to allow the mixed metal hydroxide to precipitate.

$$Na_2PdCl_4 + 2\ NaOH \longrightarrow Pd(OH)_2\downarrow + 4\ NaCl \tag{1}$$

$$HAuCl_4 + 3\ NaOH \longrightarrow Au(OH)_3\downarrow + 3\ NaCl + HCl \tag{2}$$
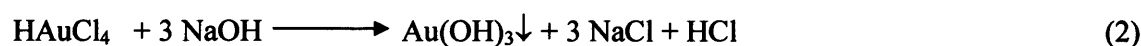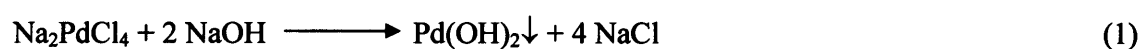
Formaldehyde reductions

This reducing agent was prepared by adding sodium hydroxide (1.2 g dissolved in 40 cm^3 water) to a 23% solution of formaldehyde (2 cm^3 (g metal)$^{-1}$). This solution was then diluted to 60 cm^3 and added to the slurry. The reaction mixture was heated and on attaining the required temperature the heat was switched off, the vessel was filled with demineralised water, and the reduced catalyst was allowed to cool. (The reduction of palladium hydroxide and gold hydroxide using alkaline formaldehyde is generally considered to proceed as shown below. There may, in addition be side reactions or auto-catalysis which make the overall process more complicated).

$$2\ HCHO + NaOH \longrightarrow HCO_2Na + CH_3OH \tag{3}$$

$$2\ Pd(OH)_2 + 2\ HCO_2Na \longrightarrow 2\ Pd + Na_2CO_3 + 3\ H_2O + CO_2 \tag{4}$$

$$2\ Au(OH)_3 + 3\ HCO_2Na \longrightarrow 2\ Au + 3\ NaOH + 3\ H_2O + 3\ CO_2 \tag{5}$$
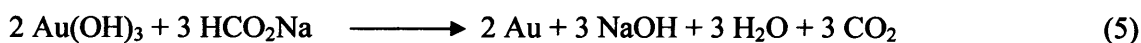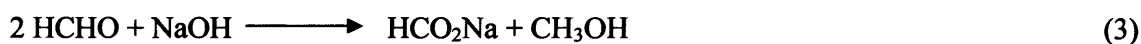
Hydrazine reductions

Hydrazine hydrate solution (24%) was added (10 cm^3 (g metal)$^{-1}$) to the alkaline slurry and stirred for 0.5 h. When the reduction was complete, the vessel was filled with demineralised water. Reduction of palladium hydroxide and gold hydroxide using hydrazine may be formally expressed using the following equations.

$$2\ Pd(OH)_2 + N_2H_4 \longrightarrow 2\ Pd + N_2 + 4\ H_2O \tag{6}$$

$$4\ Au(OH)_3 + 3\ N_2H_4 \longrightarrow 4\ Au + 3\ N_2 + 12\ H_2O \tag{7}$$
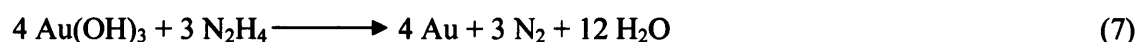
Catalyst work-up

After reduction, the catalyst was allowed to settle and the clear liquor decanted to remove excess reducing agent. The preparation vessel was refilled with water, the solution was stirred, and the catalyst allowed to settle again. The catalyst was then filtered, washed thoroughly, and dried in an oven for 16 h.

Samples were submitted to Johnson Matthey analytical services for metal assay (XRF), metal surface area (CO chemisorption), moisture content, and for measurements of activity (nitrobenzene hydrogenation).

2.1.1.2 Incipient wetness method

This synthetic route was important because commercial LEAP catalysts are manufactured by this method.

An empirical estimate of the pore volume of the graphite was made by observing the quantity of water required to convert a given mass of powder to a crumble. This quantity was found to be $\sim 1.5\ cm^3\ g^{-1}$. Catalyst preparation was comprised of three stages (I) impregnation of the metals evenly throughout the support, (II) drying, and (III) reduction.

Stages (I) and (II). The required mass of graphite was measured into a vessel. The required masses of the palladium and gold precursor salts (Table 2.4) were mixed and dissolved in that volume of demineralised water required to achieve incipient wetness for the chosen mass of support. The aqueous solution of palladium and gold precursor salts was added to the vessel containing the support with stirring until all the graphite had been wetted. The wet impregnate was stirred periodically for 0.5 h or until it acquired the properties of a crumble. It was then transferred to a tray and placed in an oven for 12 h.

Stage (III). The dried impregnate was removed from the oven and crushed using a pestle and mortar until the particles were fine enough to flow freely. The impregnate was added to a beaker containing a 24% solution of hydrazine (10 cm^3 (g metal)$^{-1}$ dissolved in 100 cm^3 water) and stirred occasionally for 1 h. The reducing agent was used in excess. The beaker was then filled with demineralised water, stirred, and the catalyst was allowed to

settle. The clear liquor was decanted and the catalyst was filtered off, washed with demineralised water, and dried in an oven for 16 h.

Samples were submitted to Johnson Matthey analytical services for metal assay (XRF), metal surface area (CO chemisorption), moisture content, and for measurements of activity (nitrobenzene hydrogenation).

Table 2.2 – Amounts of graphite and of palladium and gold precursors used in the preparation of 100 g samples of Batch 1 catalysts by the slurry precipitation method and using formaldehyde reduction

Mass of graphite / g	Mass of Na_2PdCl_4[a] / g	Mass of $HAuCl_4$[b] / g	Nominal Pd loading / %	Nominal Au loading / %	Nominal Pd/Au atom ratio[c]	ref no
99.0	8.097	0	1.0	0.0	–	3182
98.6	8.097	0.956	1.0	0.4	5:1[d]	3184
97.7	13.36	1.553	1.65	0.65	5:1[d]	3185
98.0	8.097	2.390	1.0	1.0	2:1	3186
97.2	8.097	4.302	1.0	1.8	1:1[e]	3187
97.2	8.097	4.302	1.0	1.8	1:1[e]	3200
96.4	8.097	6.214	1.0	2.6	2:3	3188
97.7	4.049	4.301	0.5	1.8	1:2	4266
98.0	1.619	4.301	0.2	1.8	1:5	4265
99.6	0	0.956	0.0	0.4	–	3183

[a] Na_2PdCl_4 contained 12.35% Pd by weight (JM Assay)
[b] $HAuCl_4$ contained 41.84% Au by weight (JM Assay)
[c] for actual Pd/Au atom ratios see Table 3.1
[d] 3184 and 3185 differed in respect of total metal loading
[e] 3187 and 3200 were duplicate preparations having the same total metal loading

Table 2.3 – Amounts of graphite and of palladium and gold precursors used in the preparation of 100 g samples of Batch 2 catalysts by the slurry precipitation method and using hydrazine reduction

Mass of graphite / g	Mass of Na₂PdCl₄[a] / g	Mass of HAuCl₄[b] / g	Nominal Pd loading / %	Nominal Au loading / %	Nominal Pd/Au atom ratio[c]	ref no
99.0	8.149	0	1.0	0.0	–	3329
98.6	8.149	0.954	1.0	0.4	5:1[d]	3331
97.7	13.44	1.550	1.65	0.65	5:1[d]	3332
98.0	8.149	2.385	1.0	1.0	2:1	3333
97.2	8.149	4.294	1.0	1.8	1:1	3334
96.4	8.149	6.202	1.0	2.6	2:3	3335
97.7	4.075	4.294	0.5	1.8	1:2	4268
98.0	1.630	4.294	0.2	1.8	1:5	4267
99.6	0	0.954	0.0	0.4	–	3330

[a] *Na₂PdCl₄ contained 12.27% Pd by weight (JM Assay)*
[b] *HAuCl₄ contained 41.92% Au by weight (JM Assay)*
[c] *for actual Pd/Au atom ratios see Table 3.2*
[d] *3331 and 3332 differed in respect of total metal loading*

Table 2.4 – Amounts of graphite and of palladium and gold precursors used in the preparation of 100 g samples of Batch 3 catalysts by the incipient wetness method and using hydrazine reduction

Mass of graphite / g	Mass of Na₂PdCl₄[a] / g	Mass of HAuCl₄[b] / g	Nominal Pd loading / %	Nominal Au loading / %	Nominal Pd/Au atom ratio[c]	ref no
99.0	8.149	0	1.0	0.0	–	3336
98.6	8.149	0.954	1.0	0.4	5:1[d]	3338
97.7	13.44	1.550	1.65	0.65	5:1[d]	3339
98.0	8.149	2.385	1.0	1.0	2:1	3340
97.2	8.149	4.294	1.0	1.8	1:1	3341
96.4	8.149	6.202	1.0	2.6	2:3	3342
97.7	4.075	4.294	0.5	1.8	1:2	4270
98.0	1.630	4.294	0.2	1.8	1:5	4269
99.6	0	0.954	0.0	0.4	–	3337

[a] *Na₂PdCl₄ contained 12.27% Pd by weight (JM Assay)*
[b] *HAuCl₄ contained 41.92% Au by weight (JM Assay)*
[c] *for actual Pd/Au atom ratios see Table 3.3*
[d] *3338 and 3339 differed in respect of total metal loading*

2.1.2 Preparation of a 20% Graphite-Supported Gold Catalyst

8 g graphite was transferred to a beaker (250 cm^3), ultra pure water (100 cm^3) added, and the contents stirred to form a slurry. 1.5 g NaOH dissolved in 20 cm^3 ultra pure water were added and the stirring continued for 0.25 h. 4.843 g HAuCl$_4$ (41.29 % w/w) dissolved in ultra pure water (40 cm^3) was then added to the slurry, and the stirring continued for 0.5 h to allow the precipitation of gold hydroxide. The pH of the slurry was measured using universal indicator paper and was found to be 10. The reducing agent, 20cm^3 hydrazine hydrate solution (24%), was then added to the gold hydroxide/graphite slurry and the stirring continued for a further 0.5 h to allow reduction to occur. The catalyst was then allowed to settle, the liquor was decanted, and the catalyst was filtered off, washed, and dried for 16 h. This preparation provided nearly 10 g of 20% gold/graphite catalyst (ref no: 006; description: (0% Pd, 20% Au)/G).

2.1.3 Palladium Plating of Supported Gold Catalysts

Palladium, as Pd(NO$_3$)$_2$ in aqueous solution, was reduced in the presence of graphite-supported gold catalysts using a range of reducing agents.

Hydrazine reductions

Various amounts of palladium were reduced in the presence of samples of (0% Pd, 20% Au)/G. The preparative method was identical to that used to prepare the Batch 2 catalyst 3329 except that (0% Pd, 20% Au)/G was used in place of clean graphite. 100 mg samples of (0% Pd, 20% Au)/G were plated with palladium by the reduction of Pd(NO$_3$)$_2$ so that the quantity of the palladium present corresponded to palladium/gold atom ratios of 1.39, 0.93, 0.46, 0.19, 0.09, 0.04, and 0.02 (Table 2.5). Due to the very small amounts of palladium being reduced in these preparations an excess of sodium hydroxide and of hydrazine was used in the precipitation and reduction stages respectively.

$$Pd(NO_3)_2 + 2\,NaOH \longrightarrow Pd(OH)_2\!\downarrow + 2\,NaNO_3 \tag{8}$$

$$Pd(OH)_2 + N_2H_4 \longrightarrow 2\,Pd + 4\,H_2O + N_2 \tag{9}$$
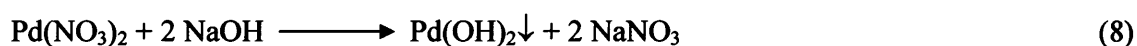
Table 2.5 – Amounts of Pd(NO₃)₂ required to produce palladium-plated gold catalysts with specified Pd/Au atom ratios by hydrazine reduction

[a] Mass of Pd(NO₃)₂ / g	Catalyst	
	ref no	description
0.1030	007	Pd/(0%Pd, 20%Au)[1.39]/G{4}
0.0675	008	Pd/(0%Pd, 20%Au)[0.93]/G{4}
0.0338	009	Pd/(0%Pd, 20%Au)[0.46]/G{4}
0.0135	010	Pd/(0%Pd, 20%Au)[0.19]/G{4}
0.0068	011	Pd/(0%Pd, 20%Au)[0.09]/G{4}
0.0027	012	Pd/(0%Pd, 20%Au)[0.04]/G{4}
0.0014	013	Pd/(0%Pd, 20%Au)[0.02]/G{4}

[a]Pd(NO₃)₂ contained 14.18% Pd by weight (JM Assay)
mass of (0% Pd, 20% Au)/G = 100 mg

Hydrogen reductions

A further range of catalysts (Table 2.6) were prepared using the same methodology except that reduction was achieved by bubbling gaseous H_2 through the alkaline slurry containing the gold catalyst and palladium nitrate.

Sodium hydroxide (50 mg) was dissolved in ultra pure water (50 cm³) and the solution added to 100 mg (0% Pd, 20% Au)/G in a vessel. The required mass of palladium nitrate was then dissolved in the solution and, with caution, H_2 was slowly passed through the slurry for about ten minutes. After reduction, the catalyst was allowed to settle, was filtered, washed with ultra pure water, and dried in air. Due to the very small amounts of palladium being reduced in these preparations an excess of sodium hydroxide and of hydrazine was used in the precipitation and reduction stages respectively.

$$Pd(NO_3)_2 + 2\ NaOH \longrightarrow Pd(OH)_2\downarrow + 2\ NaNO_3 \qquad (10)$$

$$Pd(OH)_2 + H_2 \longrightarrow Pd + 2\ H_2O \qquad (11)$$
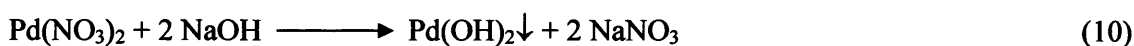
Table 2.6 – Amounts of Pd(NO₃)₂ required to produce palladium-plated gold catalysts with specified Pd/Au atom ratios by hydrogen reduction

[a] Mass of Pd(NO₃)₂ / g	Catalyst	
	ref no	description
0.0135	014	Pd/(0%Pd, 20%Au)[0.19]/G{5}
0.0068	015	Pd/(0%Pd, 20%Au)[0.09]/G{5}
0.0027	016	Pd/(0%Pd, 20%Au)[0.04]/G{5}
0.0014	017	Pd/(0%Pd, 20%Au)[0.02]/G{5}

[a]$Pd(NO_3)_2$ contained 14.18% Pd by weight (JM Assay)
mass of (0% Pd, 20% Au)/G = 100 mg

2.1.4 Measurement of Palladium and Gold Loadings

Total metal loadings were measured at Johnson Matthey using X-ray fluorescence spectroscopy. The instrument used was a Philips PW1404 computer-controlled wavelength-dispersive spectrometer equipped with a Philips PW1500/15 automatic sample holder and sample changer.

Catalyst samples were ground, dried at 303 K, pressed into pellets, and analysed using the spectrometer, which had been calibrated against known standards. The intensity of the resultant radiation characteristic of palladium K and gold L lines was measured and thus the concentrations of palladium and of gold calculated.

2.1.5 Measurements of Catalytic Activity

2.1.5.1 Nitrobenzene hydrogenation

The standard reaction used by Johnson Matthey to determine catalytic activity is the hydrogenation of nitrobenzene to (mostly) aniline at 2 bar and 313 K. Hydrogenations were carried out in sealed autoclaves i.e. under constant volume conditions, with constant pressure maintained by instrumentation that detected hydrogen uptake and compensated by regularly topping up the hydrogen pressure. The reaction is then described in terms of a hydrogen uptake verses time curve, a typical example of which is shown in Figure 2.1. The initial rate of hydrogen uptake is constant, and hence the activity recorded is measured by determining the initial gradient of the uptake/time curve. The units of the activity measurements are: μmol H_2 consumed per unit time per unit mass of catalyst.
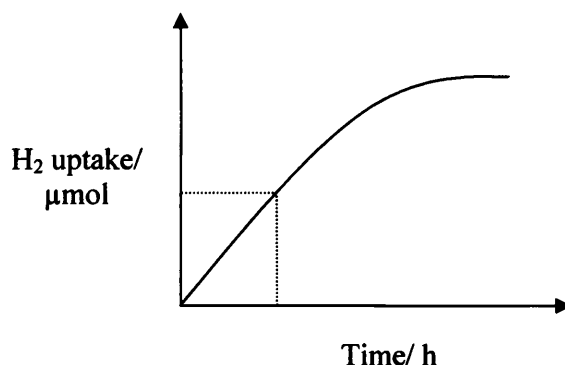
Figure 2.1 – *A typical hydrogen uptake curve obtained during nitrobenzene hydrogenation.*

2.1.5.2 Ethylene acetoxylation

One untreated, one etched, and one plated sample of graphite-supported palladium-gold catalysts were tested on a high throughput testing rig (HTTR) at BP HRTC. The catalysts tested (Table 2.7) were selected on the basis of their similarity to commercial catalysts.

Table 2.7 – *Composition and state of catalysts tested on the HTTR*

ref no	Composition	State
3331	1% Pd, 0.4% Au	untreated
3332	1.65% Pd, 0.65 % Au	etched
3332	1.65% Pd, 0.65 % Au	plated

The HTTR was a flexible testing unit, used for high throughput experimentation on materials potentially useful as catalysts for heterogeneously catalysed processes. The rig consisted of 16 independent reactors each having a common gas feed composition and pressure but for which reactant flow rate, temperature, and liquid/gas ratio could be independently varied. The rig could be operated at temperatures up to 773 K and at pressures up to 20 bar, and was equipped with both on-line micro-GC and mass spectrometric analysis of the exit stream.

Catalyst samples were pressed, ground, and sieved to produce granules 250 – 500 μm in size. Approximately 300 – 400 mg of catalyst was placed in a reactor tube and held in position by a wire gauze. The HTTR was then operated in fixed-bed mode under realistic process conditions (temperature, pressure, and reactant composition) for approximately 40 h. A temperature programme was then initiated to study the variation of catalyst activity and product selectivity as a function of temperature. Temperature was raised from 423 K to 433 K, and then to 443 K, and was then lowered to 413 K; it was held at each temperature

for 5 – 12 h before being allowed to return to 423 K. Catalyst activity and product selectivity was measured at each temperature and the first and last measurements (at 423 K) were taken to indicate the extent of catalyst deactivation. Catalyst activity, was measured in the units of grams vinyl acetate formed $(kg_{cat})^{-1}$ h^{-1} and selectivity was calculated based on the amounts of vinyl acetate and carbon dioxide formed as shown in equation (12).

$$\text{Selectivity (\%)} = \frac{N_{VA}}{N_{VA} + N_{CO2}} * 100 \qquad (12)$$

where N_{VA} is the amount of vinyl acetate and N_{CO2} is the amount of carbon dioxide formed.

2.1.6   Catalyst Summary

Table 2.8 – Summary of catalyst reference numbers and methods of preparation

ref no	Section	Preparative method
3182	2.1.1.1	slurry precipitation & formaldehyde reduction
3184	2.1.1.1	slurry precipitation & formaldehyde reduction
3185	2.1.1.1	slurry precipitation & formaldehyde reduction
3186	2.1.1.1	slurry precipitation & formaldehyde reduction
3187	2.1.1.1	slurry precipitation & formaldehyde reduction
3200	2.1.1.1	slurry precipitation & formaldehyde reduction
3188	2.1.1.1	slurry precipitation & formaldehyde reduction
4266	2.1.1.1	slurry precipitation & formaldehyde reduction
4265	2.1.1.1	slurry precipitation & formaldehyde reduction
3183	2.1.1.1	slurry precipitation & formaldehyde reduction
3329	2.1.1.1	slurry precipitation & hydrazine reduction
3331	2.1.1.1	slurry precipitation & hydrazine reduction
3332	2.1.1.1	slurry precipitation & hydrazine reduction
3333	2.1.1.1	slurry precipitation & hydrazine reduction
3334	2.1.1.1	slurry precipitation & hydrazine reduction
3335	2.1.1.1	slurry precipitation & hydrazine reduction
4268	2.1.1.1	slurry precipitation & hydrazine reduction
4267	2.1.1.1	slurry precipitation & hydrazine reduction
3330	2.1.1.2	incipient wetness & hydrazine reduction
3336	2.1.1.2	incipient wetness & hydrazine reduction
3338	2.1.1.2	incipient wetness & hydrazine reduction
3339	2.1.1.2	incipient wetness & hydrazine reduction
3340	2.1.1.2	incipient wetness & hydrazine reduction
3341	2.1.1.2	incipient wetness & hydrazine reduction
3342	2.1.1.2	incipient wetness & hydrazine reduction
4270	2.1.1.2	incipient wetness & hydrazine reduction
4269	2.1.1.2	incipient wetness & hydrazine reduction
3337	2.1.1.2	incipient wetness & hydrazine reduction
006	2.1.2	slurry precipitation & hydrazine reduction
007	2.1.3	slurry precipitation & hydrazine reduction
008	2.1.3	slurry precipitation & hydrazine reduction
009	2.1.3	slurry precipitation & hydrazine reduction
010	2.1.3	slurry precipitation & hydrazine reduction
011	2.1.3	slurry precipitation & hydrazine reduction
012	2.1.3	slurry precipitation & hydrazine reduction
013	2.1.3	slurry precipitation & hydrazine reduction
014	2.1.3	slurry precipitation & hydrogen reduction
015	2.1.3	slurry precipitation & hydrogen reduction
016	2.1.3	slurry precipitation & hydrogen reduction
017	2.1.3	slurry precipitation & hydrogen reduction

2.2   Electrochemical Characterisation of Graphite-Supported Catalysts

Cyclic voltammetry has been used to characterise surface composition and the extent of alloying in a series of palladium-gold catalysts. Catalysts were analysed in their initially prepared states.

2.2.1   The Electrochemical Cell

A two-compartment electrochemical cell (Figure 2.2) constructed of Pyrex glass contained a working electrode, a reference electrode, and a counter electrode.

CATALYST HOLDER

REFERENCE ELECTRODE

(c)

(a)   (b)

FILL LINE

WORKING ELECTRODE (Pt MESH AND ATTACHED CATALYST)

COUNTER ELECTRODE IN LUGGIN CAPILLIARY
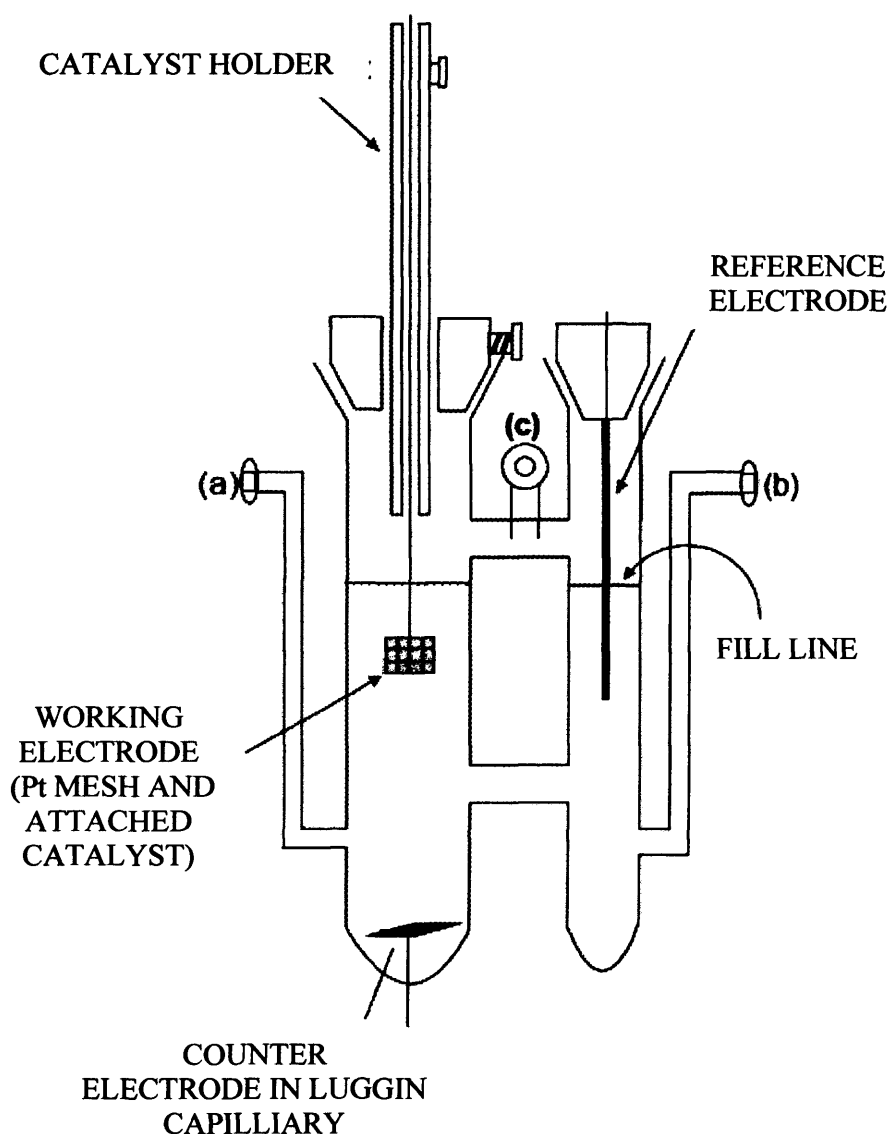
Figure 2.2 – The electrochemical cell

The larger compartment of the cell housed the working and counter electrodes and the smaller compartment housed the reference electrode. The working electrode, which held the catalyst, was comprised of a platinum mesh attached to a platinum wire approximately 20 cm in length and 0.5 mm in diameter. 1.2 mg of the catalyst under test was pressed onto the mesh. The catalyst holder consisted of a teflon stopper and a glass rod with a hole bored through the middle. During the experiment, the working electrode was threaded through this capillary. The reference electrode was a saturated palladium/hydrogen (Pd/H) electrode manufactured in-house from 0.5 mm palladium wire spot-welded to a short length of platinum wire and embedded into a quick-fit stopper. The Pd/H electrode exhibited a stable potential (50 mV versus standard hydrogen electrode) for 8 h in sulphuric acid electrolytes of concentration $0.1 - 0.5$ mol dm^{-3}; it was simple to charge and contaminations inherent in the use of other reference sources were avoided. The counter electrode was made from a platinum mesh and was housed beneath the working electrode in a Luggin capillary.

Two bridges connected each half of the cell, one above and one below the fill-level. The submerged bridge provided effective transport of the electrolyte between the two compartments; the upper bridge allowed for gas flow through the cell. There were three gas inlets: inlet (a) allowed N_2 gas into the main compartment in order to deoxygenate the electrolyte; inlet (b) allowed H_2 gas into the smaller compartment to charge the Pd/H reference electrode, and inlet (c) allowed N_2 gas into the head-space above both cell compartments to prevent diffusion of oxygen into the electrolyte.

2.2.2 Collection of Cyclic Voltammograms
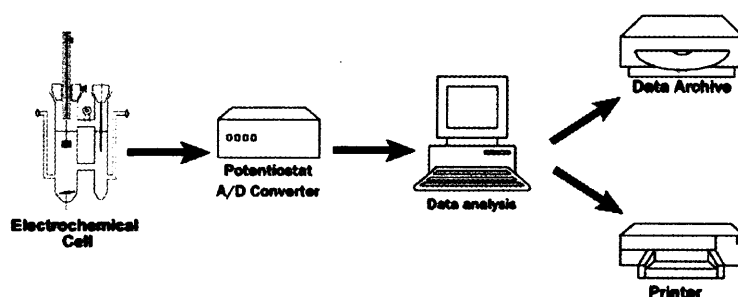
Figure 2.3 – Schematic representation of the cyclic voltammetry system

The cell was connected to a potentiostat (CH Instruments) which was controlled by a computer (Research Machines, Windows 98) loaded with CHI software. Electrochemical data were collected by a computer and stored in the form of .bin and .txt files on the hard disk. The data were analysed using CHI software and Microsoft Excel allowing analysis of peak heights, peak potentials, and peak areas as well as the compilation of multiple plots. The raw and analysed data were archived on CD/DVD and backed up on an additional computer.

2.2.3 The Millipore Water Purification System

Water used for electrolyte preparation and for cleaning purposes was obtained from a Millipore water purification system. The system delivered research grade ultra pure water with a resistivity of 18.2 MΩ cm^{-1} and a total organics content of less than 10 ppb; it was capable of supplying ultra pure water at a rate of 25 cm^3 s^{-1}.

First, laboratory mains water was passed through a 5 μm filter (Water Filtration, Cardiff). Next, a Milli-RO 10 plus system provided purification of the filtered tap water through a series of semi-permeable reverse-osmosis membranes and activated carbon filters. This water was stored in a 60 dm^3 tank ready for the next stage of purification (Milli-Q system) which involved cycling the water in a closed loop though a mixed resin purification pack until water of the desired resistivity was produced. Finally, the water was passed through a pre-sterilised microporous filter to remove particulate matter larger than 0.22 μm. The resistivity of the water was continuously measured using a sensor located at the outlet of the purification pack and this value was shown on an alphanumeric display.

2.2.4 Cleaning Procedures

New glassware was cleaned with concentrated nitric acid to remove any residual metallic contaminants and then rinsed with ultra pure water to remove all traces of acid. Vessels were then washed with permanganic acid; potassium permanganate at low concentration in concentrated sulphuric acid.

$$2\ KMnO_4 + H_2SO_4 \longrightarrow 2\ HMnO_4 + K_2SO_4 \qquad (13)$$

Regular cleaning of the cell was achieved by filling it completely with permanganic acid and leaving it to stand overnight. Associated glassware, such as quick-fit stoppers, the palladium reference electrode, inlet caps, and the catalyst holder including the teflon stopper were also cleaned by soaking in permanganic acid. For other glassware such as beakers and volumetric flasks it was sufficient to use a smaller volume of permanganic acid by making sure that a thin film of the acid was maintained over the internal walls of the glassware. After the permanganic acid treatment, all glassware was rinsed thoroughly with ultra pure water and was then ready for use.

2.2.5 Electrolytes

Electrolyte solutions were prepared using clean glassware and high quality reagents (Section 2.7). All electrolyte solutions were prepared using ultra pure water (Section 2.2.3). Sulphuric acid electrolyte solutions (0.5 mol dm^{-3}) were prepared from Fisher concentrated sulphuric acid.

2.2.6 Preparation of the Electrochemical Cell

The cell fitted with an appropriate stopper on the main compartment and with caps on gas inlets (a) and (c) (Figure 2.2) was filled with ultra pure water and H_2 was allowed, via inlet (b) to flow through the cell. The Pd/H reference electrode (which had previously been (i) cleaned overnight in permanganic acid, (ii) rinsed with plenty of ultra pure water, (iii) heated in the hottest region of a Bunsen flame to remove any contaminants) was inserted into the cell which had a steady flow of hydrogen passing through it. The electrode was then allowed to charge for approximately 0.5 h. The cell was then emptied by removing the stopper and inverting it. It was then rinsed with ultra pure water and filled to the fill level ($\sim$ 100 cm^3) with a solution containing the electrolyte of choice. Unless otherwise stated, the electrolyte used was 0.5 mol dm^{-3} sulphuric acid. The stopper was replaced in the main compartment of the cell. The arrangement of the caps was altered and an oxygen-free N_2 supply connected to gas inlet (a). N_2 gas was then allowed to bubble through the cell for approximately 0.5 h to deoxygenate the electrolyte solution. Just prior the commencement of an experiment, the N_2 supply was transferred to gas inlet (c) and the gas pressure slightly increased; this maintained an inert atmosphere inside the cell.

2.2.7 Procedure Used During a Typical Electrochemical Experiment

When the reference electrode had been charged and the electrolyte was deoxygenated, the reference and counter electrodes were connected to the potentiostat. The potentiostat and computer were switched on and the CHI software was activated.

Unless otherwise stated the potential was swept upwards from 0.0 V at 10 mV s^{-1}. The upper potential limit depended upon the region under investigation. Typical cyclic voltammograms contain two regions. The first is known as the hydrogen under-potential deposition (HUPD) region, and analysis extends from 0.0 V to 0.8 V. Two cycles were collected for each catalyst and the voltammograms were stored; the second cycle was accepted as the stable voltammogram as the first cycle may have been erroneous due to the possible presence of organic species pre-absorbed on the catalyst surface. The second region is known as the oxide region. Analysis of this region was achieved by increasing the upper potential limit to 1.4 V. Two cycles (0.0 V to 1.4 V) were collected using the same catalyst sample as that used for the collection of the HUPD data. This was deemed acceptable, as cycling between limits of 0.0 V and 0.8 V is considered to be a non-destructive process. Therefore, the first sweep into the oxide region was accepted as the stable voltammogram.

2.2.8 Corrosive Etching of Palladium-Gold Catalysts

5 g samples of catalysts from Batch 1, Batch 2, and Batch 3 were weighed into glass vessels and glacial acetic acid (50 cm^3) was added. A small magnetic stirrer bar was introduced and the vessel was placed on a stirrer/hotplate. Temperature was raised to approximately 373 K and the slurry was maintained at this temperature for about 10 minutes. The solutions were then allowed to cool to room temperature and the vessels were filled to a common volume with glacial acetic acid to compensate for the volume lost by evaporation during heating. The vessels were sealed. The slurries were stirred and exposed to air regularly over a period of three weeks, during which the etching process occurred.

The etched catalysts were filtered under suction and the acetic acid solutions were retained for subsequent catalyst preparations. The catalysts were allowed to dry at room temperature in air. The dried catalyst was weighed and separated into two portions of equal mass. One portion was examined as an etched catalyst whilst the other portion was retained for use in palladium plating preparations (Section 2.2.9).

This whole procedure was repeated using a solution consisting of 0.5 mol dm^{-3} potassium acetate dissolved in glacial acetic acid.

2.2.9 Procedures for Palladium Plating of Etched Catalyst Surfaces

A quantity of etched catalyst *half the mass of the etched catalyst* and the corresponding palladium acetate solution *half the volume of the solution recovered after etching* were mixed in a beaker and the slurry thus formed was transferred to a gas bubbler fitted with a hydrogen supply. Hydrogen was introduced into the bubbler for about 10 minutes to reduce the palladium over the etched catalyst. After reduction, the solution had lost its yellow colour and was clear. The plated catalyst was allowed to settle, was filtered under suction, and then allowed to dry in air. Catalysts from Batch 1, Batch 2, and Batch 3 which had been etched in (i) glacial acetic acid and (ii) 0.5 mol dm^{-3} potassium acetate in glacial acetic acid, were plated, in this manner, using the palladium acetate solutions formed as a result of palladium dissolution.

$$Pd(OAc)_2 + H_2 \longrightarrow Pd + 2\,HOAc \qquad (14)$$
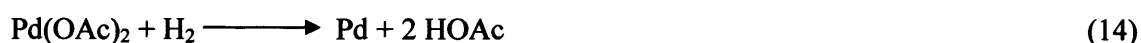
In a further series of plating preparations, ethylene was used as the reductant. These preparations followed an almost identical procedure except the duration of the reduction by ethylene was 20 minutes.

$$6\,Pd(OAc)_2 + CH_2{=}CH_2 + 4\,H_2O \longrightarrow 6\,Pd + 12\,HOAc + 2\,CO_2 \qquad (15)$$
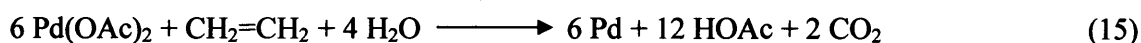
2.2.10 Normalisation of Cyclic Voltammograms

Normalisation was used extensively in the preparation of Figures throughout Chapters 3 and 4, in those cases where it was difficult or impossible to measure the mass of the catalyst mounted on the working electrode prior to the collection of a cyclic voltammogram. In these cases, a normalisation procedure was applied to the data after collection using Microsoft Excel software. This procedure involved calculating the difference between the charges associated with the forward and reverse sweeps at 400 mV (300 mV in Section 3.5.2) and then calculating a scaling factor which allowed the difference between the forward and reverse sweeps to equal 100 μA at 400 mV. Finally, an addition or subtraction

was applied on the current axis (the ordinate) to allow the forward sweep to have the point 400 mV, 50 μA and the reverse sweep to have the point 400 mV, -50 μA. i.e. 100 μA.

The validity of this procedure was based on the assumption that, at 400 mV, the charges associated with both the forward and reverse sweeps in the CV were independent of the metal and were due to the capacitance of the graphite support. This assumed that the graphite support remained unaffected by procedures such as palladium etching and plating.

2.3   Electrochemical Determination of the Extent of Ethylene Adsorption

Certain palladium-gold catalysts were exposed to ethylene and the extent of adsorption determined by use of cyclic voltammetry. 1.2 mg of catalyst were mounted onto the working electrode and placed in the electrochemical cell. The first cycle was from 0.3 V to 0.0 V, then to 1.4 V, and back to 0.0 V. The working electrode was then removed from the cell and placed in a gas bubbler which contained a small amount of ultra pure water and was receiving a steady flow of ethylene. The catalyst was exposed to ethylene for about five minutes. After this exposure, the working electrode was replaced in the cell and six cycles were recorded using the potential limits indicated above.

Comparison of the first and second cycles provided an estimate of the extent of ethylene adsorption. Comparison of the third, fourth, fifth, and sixth cycles provided an estimate of the ease of ethylene oxidation under these electrochemical conditions. Catalysts from Batch 1, Batch 2, and Batch 3 were used in these adsorption investigations.

2.4   Catalyst Heat Treatments

To investigate the effect of annealing on surface composition, 1 g samples of catalysts were heated in an argon flow in a Carbolite CFT 12/50 furnace. Temperature was raised at 10 K min^{-1} to either 673 K or 923 K and maintained for 3 h. Heating was then discontinued, and samples were allowed to cool naturally in the furnace in the argon flow from 673 K or 923 K to ambient temperature. Catalysts treated in this way were Batch 1 catalysts: 3184, 3185, 3186, 3187, 3188, and 3200 (Table 2.2).

2.5 Catalyst Characterisation by use of Physical Methods

2.5.1 X-Ray Diffraction

Analysis by X-ray diffraction was performed at BP's Hull Research & Technology Centre (HRTC) using two instruments. The first, a Bruker D5000, was operated at 40 kV and 40 mA and the data collection time was 12 h. The second, a Bruker D8, utilised a turbo X-ray source (TXS) or rotating anode, and was operated at 35 kV and 300 mA; the data collection time was typically 1 h.

Instrument calibration was achieved by mixing the catalyst with a silicon standard. Accurate calibration (to ~ 0.1 picometers) allowed accurate determination of peak positions. Data were collected over the range 35 – 50 degrees and were analysed by use of Standard Bruker EVA and TOPAS software.

Untreated samples analysed were: 3184, 3185, 3186, 3188, 3200, 4265, 4266, 3331, 3332, 3333, 3334, 3335, 4267, 4268 3338, 3339, 3340, 3341, 3342, 4269, and 4270. Etched and plated versions of catalysts analysed were those derived from 3184, 3185, 3186, 3331, 3332, 3333, 3338, 3339, and 3340.

2.5.2 X-Ray Photoelectron Spectroscopy

Palladium-gold catalysts were characterised using X-ray photoelectron spectroscopy. The ESCA300 spectrometer was calibrated using the Ag $3d^{5/2}$, M4VV lines, and the Fermi edge provided by a sample of Ag foil that had been cleaned by sputtering. These measured binding energies were correct to within 0.1 eV of the literature values (368.26 eV, 1128.78 eV, and 0.00 eV respectively).

The operating voltage and current of the X-ray source were 14 kV and 200 mA respectively and the X-ray energy (monochromatic Al K alpha) was measured at 1486.6 eV. The pressure in the analysis chamber was approximately 10^{-9} mbar. Samples were prepared for analysis by creating a thin coating of the catalyst on double-sided adhesive tape which was fixed to a standard stainless steel stub. The slit width varied depending on the region under investigation. Survey scans were measured using a width of 1.9 mm whereas high resolution scans were measured using a width of 0.8 mm. The photoelectric current was detected at an angle of 45° relative to the sample surface and a low energy electron flood gun provided charge compensation. Catalysts 3182, 3183, 3186, 3188, 3200

(Table 2.2), 3331, 3332, 3333, 3334, 3335 (Table 2.3), 3341, and 3342 (Table 2.4) were analysed.

2.5.3 Electron Microscopy

2.5.3.1 Metal particle-size distributions

High resolution transmission electron microscopy was used to analyse metal particle-size and morphology in supported palladium-gold catalysts at Johnson Matthey Technology Centre (JMTC). Images were collected using an FEI microscope (F20 S-TWIN), fitted with a Schottky field emission electron source; it was operated at accelerating voltages of up to 200 kV.

A small amount of the catalyst was crushed between two glass plates and dusted onto a copper TEM grid, which had previously been coated with a holey carbon film. Information obtained included metal particle-size distributions, provided by the instrument software, and information concerning catalyst morphology (particle shape). Catalysts investigated were: 3184, 3185, 3188, and 4265 from Batch 1 (Table 2.2), untreated, etched, and plated versions of 3331, 3332, and 3333 as well as 3334, 4267, and 4268 from Batch 2 (Table 2.3), and 3341, 3342, 4269, and 4270 from Batch 3 (Table 2.4). (0% Pd, 20% Au)/G (006), 010, 012, and 014 (Table 2.5) were also analysed.

2.5.3.2 Energy dispersive X-ray analysis

The compositions of individual metallic particles were determined by use of energy dispersive X-ray (EDX) analysis. This was accomplished using an EDAX analyzer (R-TEM CM200 Si (Li) detector) attached to the microscope described in Section 2.5.3.1. Samples were prepared using a procedure identical to that used for the preparation of samples for analysis by HRTEM.

2.5.4 Ultra-Violet Absorption Spectroscopy

To investigate the possibility of palladium dissolution during vinyl acetate synthesis the absorption of palladium-containing solutions (derived by treating catalysts with acetate-containing solutions) were measured using a Perkin Elmer Lambda 900 UV/VIS/NIR spectrometer.

10 cm³ glacial acetic acid or 10 cm³ of 0.5 mol dm⁻³ potassium acetate dissolved in glacial acetic acid were added to 100 mg samples of each catalyst contained in a sample vial. The vials were heated to 373 K with stirring, and maintained at that temperature for about ten minutes using a stirrer hotplate. The vials were then allowed to cool to ambient temperature, were filled to compensate for evaporation of glacial acetic acid (boiling point = 391 K), and sealed to prevent further evaporation. The catalysts were stirred and exposed to air regularly over a period of a few weeks.

Ultra-violet absorption spectra were recorded using plastic cells with a path length of 1 cm. Instrument calibration was not required as absolute concentrations were not measured. The instrument was prepared by first selecting the experimental parameters, such as wavelength limits (800 nm and 300 nm), the increment of measurement (1 nm), and the intensity range. A cell containing a reference solution (glacial acetic acid or 0.5 mol dm⁻³ potassium acetate in glacial acetic acid) was then inserted into the appropriate holder and a background measurement of the region of interest was recorded. Using a pipette, samples of the palladium-containing solutions were then transferred from their vials to the cells, taking care not to extract the catalyst (which was at the bottom of the vial). The absorption of each solution was then measured using the experimental parameters described above and peaks for the absorption of radiation by palladium acetate dimers and trimers were detected at approximately 350 nm and 400 nm respectively [8]. The intensities of peaks in the spectra for solutions derived from catalysts of Batch 1 (Table 2.2), Batch 2 (Table 2.3), and Batch 3 (Table 2.4) were compared (Section 4.1.3).

2.6 Metal Surface Area Measurement of Palladium-Gold Catalysts

CO pulse chemisorption was performed to determine the palladium surface area of the catalysts.

Typically, 500 mg of catalyst was used for each measurement. The catalysts (Tables 2.2 – 2.4) were first dried under vacuum at 323 K and then reduced in a flow of H_2 (60 cm³ min⁻¹) at 348 K for 0.5 h. The volume of CO adsorbed was measured at room temperature (Micromeritics Flowsorb II 2300) and hence the number of moles of CO adsorbed onto the palladium surface was determined. The metal surface area (units: m^2 $(g_{cat})^{-1}$) was calculated assuming a 1:1 Pd:CO stoichiometry.

2.7 Chemicals

Unless otherwise indicated the materials listed in Table 2.9 were used in their as-received state.

Table 2.9 – List of materials used

Reagent	Supplier	Purity
Argon	BOC Gasses	> 99.998%
Ethylene	BOC Gasses	100%
Formaldehyde	Lansdowne Chemicals	–
Glacial acetic acid	Fisher Chemicals	99.8%
Hydrazine monohydrate	Aldrich	98%
Hydrogen	BOC Gasses	> 99.995%
Nitrogen	BOC Gasses	> 99.998%
Palladium nitrate[a]	Johnson Matthey	–
Potassium acetate	Fisher Chemicals	99%
Propan-2-ol	Aldrich	99.5%
Sodium chloropalladite[a]	Johnson Matthey	–
Sodium hydroxide	Fisher Chemicals	> 97%
Sulphuric acid	Fisher Chemicals	98%
Tetrachloroauric acid[a]	Johnson Matthey	–
Timrex graphite (KS15)	Timcal Graphite & Carbon	> 99.9%

[a]*for assays, see Tables 2.4 – 2.6*

2.8 References

[1] R. Abel, P. Colling, K. Eichler, D. Peters, *in* "Handbook of Heterogeneous Catalysis Vol 5" (eds. G. Ertl, H. Knozlnger, J. Weitkamp), p. 2298, Wiley-VCH, Weinheim, 1997.

[2] M. Johnson, "Leaps of Innovation", BP Frontiers, BP, 2002.

[3] European Patent No. 1175939.

[4] US Patent No. 144544.

[5] US Patent No. 6534438.

[6] European Patent No. 1467814.

[7] US Patent No. 032638.

[8] D. A. Kragten, R. A. van Santen, M. K. Crawford, W. D. Provine, J. J. Lerou, Inorg. Chem. 38 (1999) 331.

CHAPTER 3
CHARACTERISTION OF
GRAPHITE-SUPPORTED
PALLADIUM-GOLD CATALYSTS

3.1 Characterisation of Batch 1, Batch 2, and Batch 3 Catalysts by use of Physical Methods

Information concerning the bulk and surface compositions and properties of Batch 1, Batch 2, and Batch 3 catalysts were obtained by use of X-ray fluorescence (XRF), X-ray diffraction (XRD), high resolution transmission electron microscopy (HRTEM), energy dispersive X-ray analysis (EDX), and X-ray photoelectron spectroscopy (XPS).

3.1.1 X-Ray Fluorescence

Absolute amounts of palladium and of gold were measured using X-ray fluorescence and metal loadings, atom compositions, and palladium/gold atom ratios were calculated (Tables 3.1 – 3.3).

Table 3.1 – Batch 1 catalysts: palladium and gold loadings measured by XRF together with the resulting overall atom compositions and palladium/gold atom ratios [intended values shown in parenthesis]

ref no	Palladium loading		Gold loading		Atom composition		Pd/Au atom ratio
	mg^a	%	mg^b	%	Pd/%	Au/%	
3182	2.00	1.00 (1.0)	0.00	0.00 (0.0)	100.0	0.0	∞
3184	1.96	0.98 (1.0)	0.78	0.39 (0.4)	82.4	17.6	4.7 (4.6)
3185	3.26	1.63 (1.65)	1.26	0.63 (0.65)	82.8	17.2	4.8 (4.7)
3186	2.02	1.01 (1.0)	1.92	0.96 (1.0)	66.2	33.8	2.0 (1.9)
3187^c	1.96	0.98 (1.0)	3.46	1.73 (1.8)	51.3	48.7	1.1 (1.0)
3188	2.02	1.01 (1.0)	5.04	2.52 (2.6)	42.7	57.3	0.7 (0.7)
3200^c	1.94	0.97 (1.0)	1.88	0.94 (1.8)	65.7	34.3	1.9 (1.0)
4266	1.04	0.52 (0.5)	3.56	1.78 (1.8)	35.2	64.8	0.5 (0.5)
4265	0.42	0.21 (0.2)	3.48	1.74 (1.8)	18.3	81.7	0.2 (0.2)
3183	0.00	0.00 (0.0)	0.76	0.38 (0.4)	0.0	100.0	0.0 (0.0)

^{a}mass Pd per 200 mg catalyst
^{b}mass Au per 200 mg catalyst
^{c}3187 and 3200 were intended to have identical metal loadings

Generally the measured and intended metal loadings are in good agreement as are the actual and intended palladium/gold atom ratios. Catalyst 3187 was found to have 0.07% less gold than intended but this result is consistent with a yellow colouration of the solution post-reduction. Catalyst 3200 was also intended to contain 1.8% gold. The reasons for this major discrepancy are uncertain; this catalyst was found to have different but interesting properties when examined using X-ray diffraction (Section 3.1.2).

Table 3.2 – Batch 2 catalysts: palladium and gold loadings measured by XRF together with the resulting overall atom compositions and palladium/gold atom ratios [intended values shown in parenthesis]

ref no	Palladium loading		Gold loading		Atom composition		Pd/Au atom ratio
	mg[a]	%	mg[b]	%	Pd/%	Au/%	
3329	1.98	0.99 (1.0)	0.00	0.00 (0.0)	100.0	0.0	∞
3331	2.02	1.01 (1.0)	0.78	0.39 (0.4)	82.8	17.2	4.8 (4.6)
3332	3.32	1.66 (1.65)	1.28	0.64 (0.65)	82.8	17.2	4.8 (4.7)
3333	2.02	1.01 (1.0)	1.96	0.98 (1.0)	65.7	34.3	1.9 (1.9)
3334	2.00	1.00 (1.0)	3.62	1.81 (1.8)	50.7	49.3	1.0 (1.0)
3335	1.98	0.99 (1.0)	5.38	2.69 (2.6)	40.6	59.4	0.7 (0.7)
4268	1.06	0.53 (0.5)	3.56	1.78 (1.8)	35.6	64.4	0.6 (0.5)
4267	0.42	0.21 (0.2)	3.58	1.79 (1.8)	17.9	82.1	0.2 (0.2)
3330	0.00	0.00 (0.0)	0.76	0.38 (0.4)	0.0	100.0	0.0 (0.0)

[a] *mass Pd per 200 mg catalyst*
[b] *mass Au per 200 mg catalyst*

Table 3.3 – Batch 3 catalysts: palladium and gold loadings measured by XRF together with the resulting overall atom compositions and palladium/gold atom ratios [intended values shown in parenthesis]

ref no	Palladium loading		Gold loading		Atom composition		Pd/Au atom ratio
	mg[a]	%	mg[b]	%	Pd/%	Au/%	
3336	2.02	1.01 (1.0)	0.00	0.00 (0.0)	100.0	0.0	∞
3338	2.00	1.00 (1.0)	0.76	0.38 (0.4)	83.0	17.0	4.9 (4.6)
3339	3.32	1.66 (1.65)	1.14	0.57 (0.65)	84.4	15.6	5.4 (4.7)
3340	2.00	1.00 (1.0)	1.80	0.90 (1.0)	67.4	32.6	2.1 (1.9)
3341	1.98	0.99 (1.0)	3.38	1.69 (1.65)	52.1	47.9	1.1 (1.0)
3342	1.98	0.99 (1.0)	5.18	2.59 (2.6)	41.5	58.5	0.7 (0.7)
4270	1.04	0.52 (0.5)	3.58	1.79 (1.8)	35.1	64.9	0.5 (0.5)
4269	0.42	0.21 (0.2)	3.54	1.77 (1.8)	18.1	81.9	0.2 (0.2)
3337	0.00	0.00 (0.0)	0.78	0.39 (0.4)	0.0	100.0	0.0 (0.0)

[a] *mass Pd per 200 mg catalyst*
[b] *mass Au per 200 mg catalyst*

For Batch 2 catalysts the intended and measured loadings and palladium/gold atom ratios are in agreement throughout. For Batch 3 catalysts at high palladium loadings (catalysts 3338 – 3341) the measured palladium/gold atom ratios slightly exceeded their intended values.

Catalyst descriptions are shown in Table 3.4, based on the actual loadings determined by X-ray fluorescence.

Table 3.4 – Catalyst descriptions based on X-ray fluorescence analysis

Batch	ref no	Catalyst description
1	3182	(1.0% Pd, 0.0% Au)[∞]/G{1}
1	3185	(1.6% Pd, 0.6% Au)[4.8]/G{1}
1	3184	(1.0% Pd, 0.4% Au)[4.7]/G{1}
1	3186	(1.0% Pd, 1.0% Au)[2.0]/G{1}
1	3200	(1.0% Pd, 0.9% Au)[1.9]/G{1}
1	3187	(1.0% Pd, 1.7% Au)[1.1]/G{1}
1	3188	(1.0% Pd, 2.5% Au)[0.7]/G{1}
1	4266	(0.5% Pd, 1.8% Au)[0.5]/G{1}
1	4265	(0.2% Pd, 1.7% Au)[0.2]/G{1}
1	3183	(0.0% Pd, 0.4% Au)[0.0]/G{1}
2	3329	(1.0% Pd, 0.0% Au)[∞]/G{2}
2	3331	(1.0% Pd, 0.4% Au)[4.8]/G{2}
2	3332	(1.7% Pd, 0.6% Au)[4.8]/G{2}
2	3333	(1.0% Pd, 1.0% Au)[1.9]/G{2}
2	3334	(1.0% Pd, 1.8% Au)[1.0]/G{2}
2	3335	(1.0% Pd, 2.7% Au)[0.7]/G{2}
2	4268	(0.5% Pd, 1.8% Au)[0.6]/G{2}
2	4267	(0.2% Pd, 1.8% Au)[0.2]/G{2}
2	3330	(0.0% Pd, 0.4% Au)[0.0]/G{2}
3	3336	(1.0% Pd, 0.0% Au)[∞]/G{3}
3	3339	(1.7% Pd, 0.6% Au)[5.4]/G{3}
3	3338	(1.0% Pd, 0.4% Au)[4.9]/G{3}
3	3340	(1.0% Pd, 0.9% Au)[2.1]/G{3}
3	3341	(1.0% Pd, 1.7% Au)[1.1]/G{3}
3	3342	(1.0% Pd, 2.6% Au)[0.7]/G{3}
3	4270	(0.5% Pd, 1.8% Au)[0.5]/G{3}
3	4269	(0.2% Pd, 1.8% Au)[0.2]/G{3}
3	3337	(0.0% Pd, 0.4% Au)[0.0]/G{3}

3.1.2 X-Ray Diffraction

Diffractograms for palladium-gold catalysts from Batches 1, 2, and 3 are shown in Figures 3.1, 3.2, and 3.3. Each diffractogram contained two peaks, one having its maximum at a value of 2θ slightly greater than 38.2° (the value for pure gold) and one at a value of 2θ slightly less than 40.1° (the value for pure palladium). For any given peak, the value of 2θ is determined by the atom composition of the palladium-gold phase giving rise to the

diffraction line, and the peak width at half height is a measure of the mean size of the crystallites having that phase composition. A computer programme (TOPAS) was used to extract from each diffractogram the alloy composition (by application of Vergard's Law) and the mean particle-size (by use of the Scherer equation). The results so obtained are shown in Tables 3.5 – 3.11.

Batch 1 catalysts (Figure 3.1) contained a distribution of large particles, all of which were gold-rich (Table 3.5) and a distribution of smaller particles most of which were palladium-rich (Table 3.6). The large particles had mean crystallite sizes in the range 8.5 – 21.2 nm and contained 94 – 99 atom% gold [exception: catalyst 3200]. By contrast the small particles had mean crystallite sizes in the range 2.3 – 4.0 nm and contained 46 – 88 atom% palladium [exception catalyst 3185].

In the cases of the exceptional catalysts, 3200 contained gold-rich (80 atom% gold) particles having a mean size of 5.5 nm, only slightly larger than the palladium-rich (80 atom% palladium) particles which had a mean size of 2.9 nm and 3185 contained distributions of gold-rich (95 atom% gold) and palladium-rich (93 atom% palladium) particles of comparable mean size (10.8 nm and 12.4 nm respectively).

	Catalysts
3185	(1.6% Pd, 0.6% Au)[4.8]/G{1}
3184	(1.0% Pd, 0.4% Au)[4.7]/G{1}
3186	(1.0% Pd, 1.0% Au)[2.0]/G{1}
3200	(1.0% Pd, 0.9% Au)[1.9]/G{1}
3188	(1.0% Pd, 2.5% Au)[0.7]/G{1}
4266	(0.5% Pd, 1.8% Au)[0.5]/G{1}
4265	(0.2% Pd, 1.7% Au)[0.2]/G{1}

2-Theta - Scale

Figure 3.1 – Diffractograms for selected Batch 1 catalysts

73

Table 3.5 – TOPAS analysis of gold-rich alloys detected in Batch 1 catalysts

ref no	Catalyst description	Atom% Au	Atom% Pd	Atom Pd/Au ratio	Weight% Au	Weight% Pd	Mean crystallite size /nm
3185	(1.6% Pd, 0.6% Au)[4.8]/G{1}	95	5	0.05	97	3	10.8
3184	(1.0% Pd, 0.4% Au)[4.7]/G{1}	94	6	0.06	97	3	8.5
3186	(1.0% Pd, 1.0% Au)[2.0]/G{1}	97	3	0.03	98	2	12.7
3188	(1.0% Pd, 2.5% Au)[0.7]/G{1}	99	1	0.01	99	1	11.7
3200	(1.0% Pd, 0.9% Au)[1.9]/G{1}	80	20	0.25	88	12	5.5
4266	(0.5% Pd, 1.8% Au)[0.5]/G{1}	98	2	0.02	99	1	16.3
4265	(0.2% Pd, 1.7% Au)[0.2]/G{1}	96	4	0.04	98	2	21.2

Table 3.6 – TOPAS analysis of palladium-rich alloys detected in Batch 1 catalysts

ref no	Catalyst description	Atom% Au	Atom% Pd	Atom Pd/Au ratio	Weight% Au	Weight% Pd	Mean crystallite size /nm
3185	(1.6% Pd, 0.6% Au)[4.8]/G{1}	7	93	13.29	12	88	12.4
3184	(1.0% Pd, 0.4% Au)[4.7]/G{1}	12	88	7.33	20	80	2.7
3186	(1.0% Pd, 1.0% Au)[2.0]/G{1}	40	60	1.50	55	45	4.0
3188	(1.0% Pd, 2.5% Au)[0.7]/G{1}	52	48	0.92	67	33	3.2
3200	(1.0% Pd, 0.9% Au)[1.9]/G{1}	20	80	4.00	32	68	2.9
4266	(0.5% Pd, 1.8% Au)[0.5]/G{1}	44	56	1.27	59	41	2.7
4265	(0.2% Pd, 1.7% Au)[0.2]/G{1}	54	46	0.85	68	32	2.3

Batch 2 catalysts (Figure 3.2, Tables 3.7 – 3.8) all contained a distribution of large gold-rich particles (mean sizes: 10.0 – 21.9 nm; 92 – 98 atom% gold) and a distribution of small particles (mean sizes: 2.9 – 4.0 nm) which were mostly palladium-rich (42 – 88 atom% palladium).

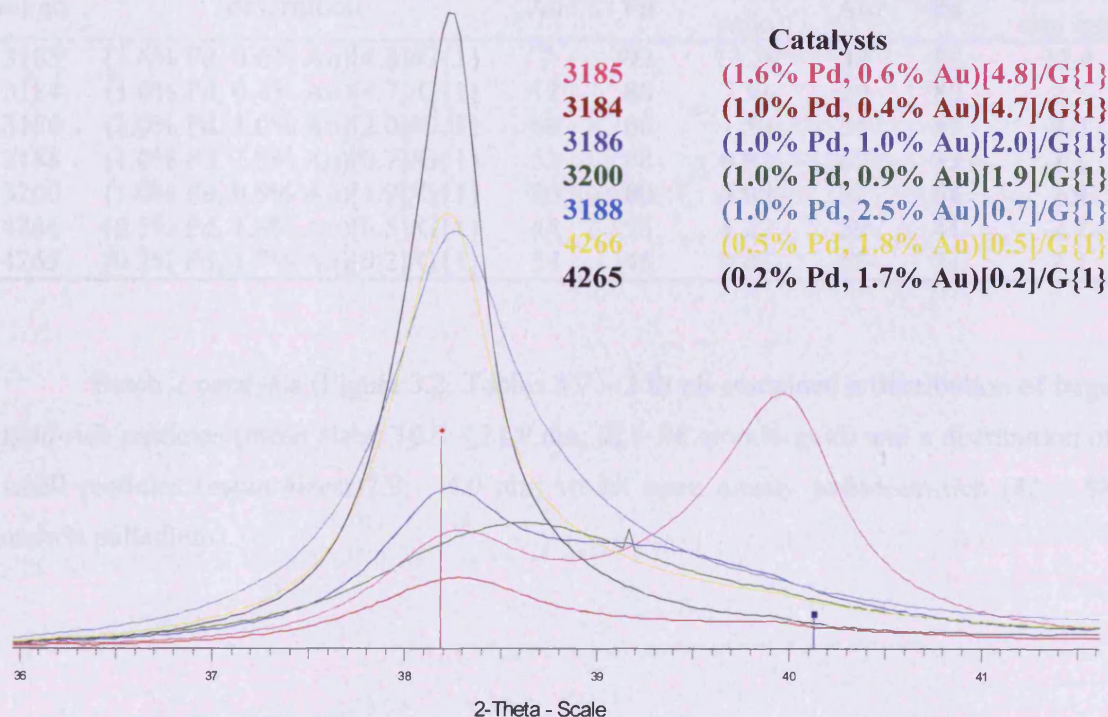|	Catalysts
3331	**(1.0% Pd, 0.4% Au)[4.8]/G{2}**
3332	**(1.7% Pd, 0.6% Au)[4.8]/G{2}**
3333	**(1.0% Pd, 1.0% Au)[1.9]/G{2}**
3334	**(1.0% Pd, 1.8% Au)[1.0]/G{2}**
3335	**(1.0% Pd, 2.7% Au)[0.7]/G{2}**
4268	**(0.5% Pd, 1.8% Au)[0.6]/G{2}**
4267	**(0.2% Pd, 1.8% Au)[0.2]/G{2}**
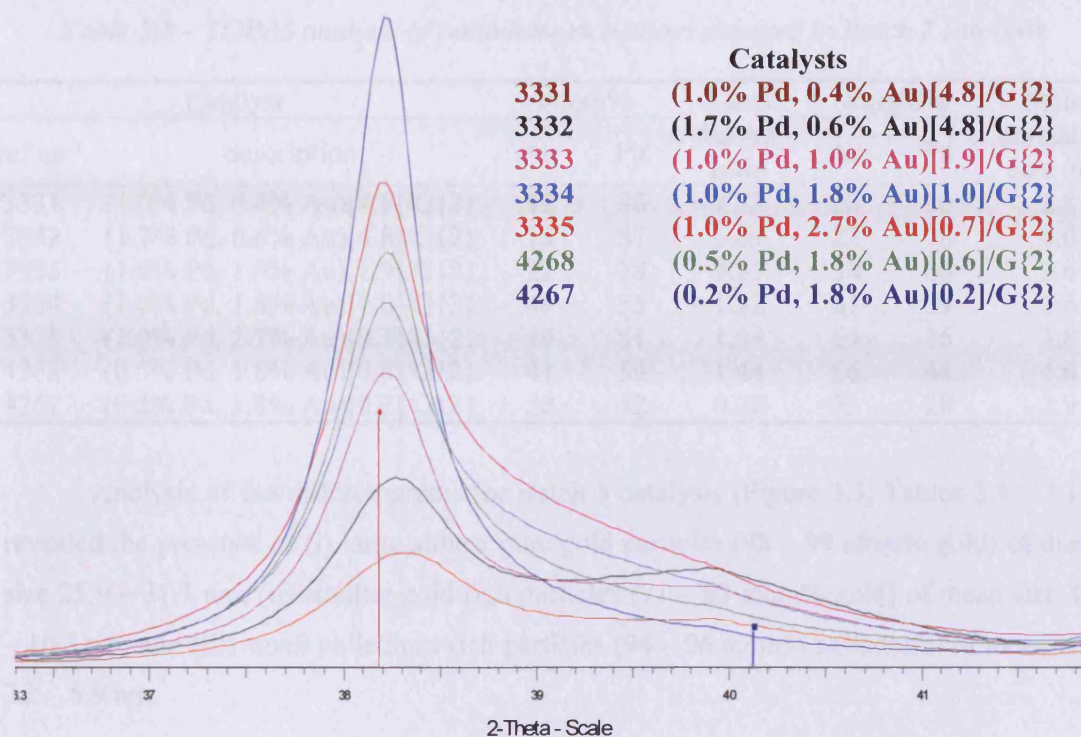
Figure 3.2 – Diffractograms for Batch 2 catalysts

Table 3.7 – TOPAS analysis of gold-rich alloys detected in Batch 2 catalysts

Catalyst		Atom%		Atom Pd/Au ratio	Weight%		Mean crystallite size /nm
ref no	description	Au	Pd		Au	Pd	
3331	(1.0% Pd, 0.4% Au)[4.8]/G{2}	92	8	0.09	96	4	10.0
3332	(1.7% Pd, 0.6% Au)[4.8]/G{2}	95	5	0.05	97	3	12.0
3333	(1.0% Pd, 1.0% Au)[1.9]/G{2}	98	2	0.02	99	1	15.4
3334	(1.0% Pd, 1.8% Au)[1.0]/G{2}	97	3	0.03	99	1	15.9
3335	(1.0% Pd, 2.7% Au)[0.7]/G{2}	98	2	0.02	99	1	17.5
4268	(0.5% Pd, 1.8% Au)[0.6]/G{2}	97	3	0.03	98	2	15.8
4267	(0.2% Pd, 1.8% Au)[0.2]/G{2}	97	3	0.03	98	2	21.9

Table 3.8 – TOPAS analysis of palladium-rich alloys detected in Batch 2 catalysts

Catalyst		Atom%		Atom Pd/Au ratio	Weight%		Mean crystallite size /nm
ref no	description	Au	Pd		Au	Pd	
3331	(1.0% Pd, 0.4% Au)[4.8]/G{2}	12	88	7.33	20	80	3.8
3332	(1.7% Pd, 0.6% Au)[4.8]/G{2}	13	87	6.69	22	78	4.0
3333	(1.0% Pd, 1.0% Au)[1.9]/G{2}	22	78	3.55	34	66	3.6
3334	(1.0% Pd, 1.8% Au)[1.0]/G{2}	45	55	1.22	61	39	3.6
3335	(1.0% Pd, 2.7% Au)[0.7]/G{2}	49	51	1.04	64	36	3.8
4268	(0.5% Pd, 1.8% Au)[0.6]/G{2}	41	59	1.44	56	44	4.0
4267	(0.2% Pd, 1.8% Au)[0.2]/G{2}	58	42	0.72	72	28	2.9

Analysis of the diffractograms for Batch 3 catalysts (Figure 3.3, Tables 3.9 – 3.11) revealed the presence of (i) large almost pure gold particles (98 – 99 atom% gold) of mean size 25.9 – 31.1 nm, (ii) smaller gold-rich particles (71 – 83 atom% gold) of mean size 4.0 – 10.3 nm, and (iii) small palladium-rich particles (94 – 96 atom% palladium) of mean size 2.2 – 5.9 nm.

Catalysts

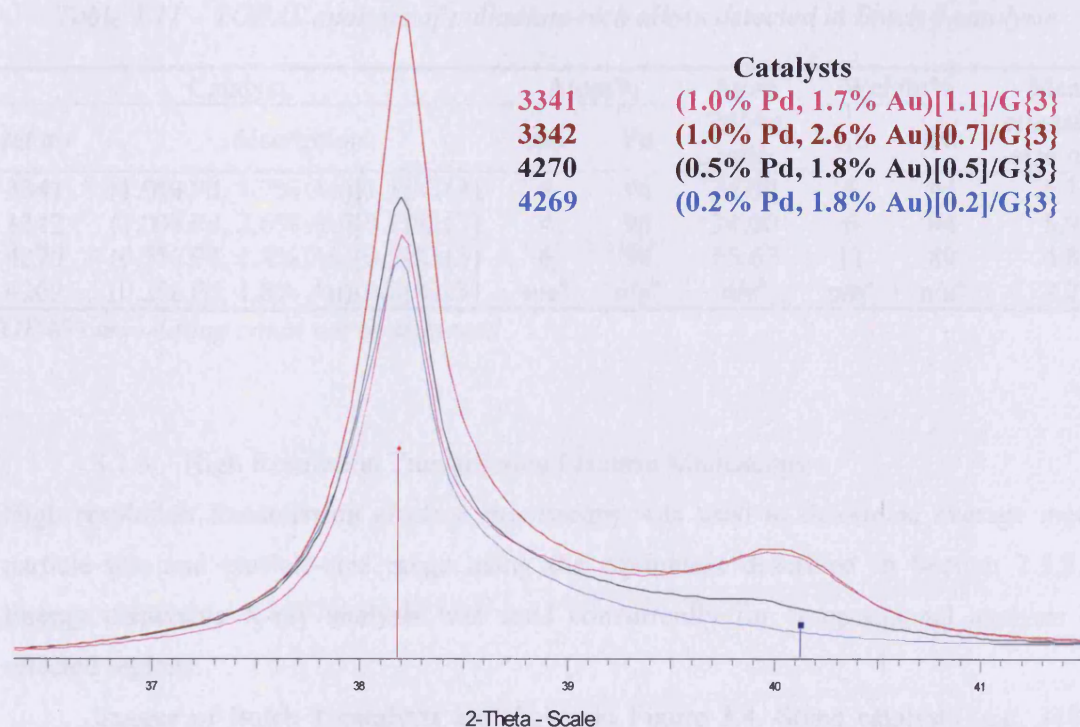|	
3341	**(1.0% Pd, 1.7% Au)[1.1]/G{3}**
3342	**(1.0% Pd, 2.6% Au)[0.7]/G{3}**
4270	**(0.5% Pd, 1.8% Au)[0.5]/G{3}**
4269	**(0.2% Pd, 1.8% Au)[0.2]/G{3}**

2-Theta - Scale

Figure 3.3 – Diffractograms for selected Batch 3 catalysts

Table 3.9 – TOPAS analysis of large gold-rich alloys detected in Batch 3 catalysts

| Catalyst | | Atom% | | Atom | Weight% | | Mean |
ref no	description	Au	Pd	Pd/Au ratio	Au	Pd	crystallite size /nm
3341	(1.0% Pd, 1.7% Au)[1.1]/G{3}	99	1	0.01	99	1	29.0
3342	(1.0% Pd, 2.6% Au)[0.7]/G{3}	98	2	0.02	99	1	31.1
4270	(0.5% Pd, 1.8% Au)[0.5]/G{3}	99	1	0.01	99	1	28.4
4269	(0.2% Pd, 1.8% Au)[0.2]/G{3}	99	1	0.01	99	1	25.9

Table 3.10 – TOPAS analysis of smaller gold-rich alloys detected in Batch 3 catalysts

| Catalyst | | Atom% | | Atom | Weight% | | Mean |
ref no	description	Au	Pd	Pd/Au ratio	Au	Pd	crystallite size /nm
3341	(1.0% Pd, 1.7% Au)[1.1]/G{3}	71	29	0.41	82	18	9.8
3342	(1.0% Pd, 2.6% Au)[0.7]/G{3}	77	23	0.30	86	14	10.3
4270	(0.5% Pd, 1.8% Au)[0.5]/G{3}	79	21	0.27	87	13	5.8
4269	(0.2% Pd, 1.8% Au)[0.2]/G{3}	83	17	0.20	90	10	4.0

Table 3.11 – TOPAS analysis of palladium-rich alloys detected in Batch 3 catalysts

| Catalyst | | Atom% | | Atom | Weight% | | Mean |
ref no	description	Au	Pd	Pd/Au ratio	Au	Pd	crystallite size /nm
3341	(1.0% Pd, 1.7% Au)[1.1]/G{3}	4	96	24.00	6	94	5.1
3342	(1.0% Pd, 2.6% Au)[0.7]/G{3}	4	96	24.00	6	94	5.9
4270	(0.5% Pd, 1.8% Au)[0.5]/G{3}	6	94	15.67	11	89	4.8
4269	(0.2% Pd, 1.8% Au)[0.2]/G{3}	n/a[a]	n/a[a]	n/a[a]	n/a[a]	n/a[a]	2.2

[a]*TOPAS curve-fitting could not be achieved*

3.1.3 High Resolution Transmission Electron Microscopy

High resolution transmission electron microscopy was used to determine average metal particle-size and particle-size range using the equipment described in Section 2.5.3.1. Energy dispersive X-ray analysis was used concurrently for compositional analysis of selected regions.

Images of Batch 1 catalysts are shown in Figure 3.4. Some catalysts (e.g. 3184, image (a)) showed well dispersed metal particles whereas others (e.g. 3188, image (d)) showed the elementary particles to be present as aggregates. Particle-size distributions were

obtained using the microscope software by counting approximately 100 particles, i.e. aggregated clusters were ignored, and the mean particle-sizes were determined from these distributions (Table 3.12). As the palladium/gold atom ratio decreased, so the mean particle-size tended to increase.

*Table 3.12 – Particle-size ranges and mean particle-sizes for Batch 1 catalysts*

| Catalyst		Image[a]	Particle-size range /nm	Mean particle-size /nm
ref no	description			
3185	(1.6% Pd, 0.6% Au)[4.8]/G{1}	b	2 – 10	4
3184	(1.0% Pd, 0.4% Au)[4.7]/G{1}	a	2 – 4.5	2.5
3186	(1.0% Pd, 1.0% Au)[2.0]/G{1}	c	5 – 15	5
3188	(1.0% Pd, 2.5% Au)[0.7]/G{1}	d	2 – 10	5
3200	(1.0% Pd, 0.9% Au)[1.9]/G{1}	e	5 – 10	5
4266	(0.5% Pd, 1.8% Au)[0.5]/G{1}	f	4 – 18	8
4265	(0.2% Pd, 1.7% Au)[0.2]/G{1}	g	5 – 15	5

[a] *see Figure 3.4*

Figure 3.4 – HRTEM images of catalysts identified in Table 3.12.
Image (g) overpage. (The marker bar in each micrograph represents 50 nm)
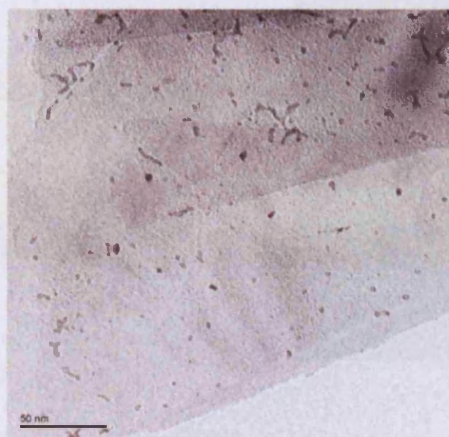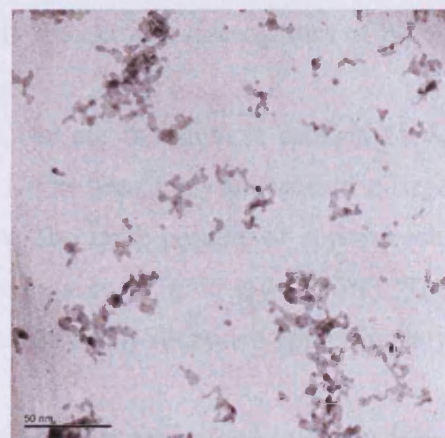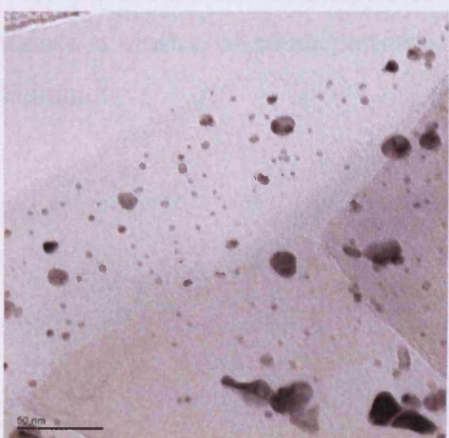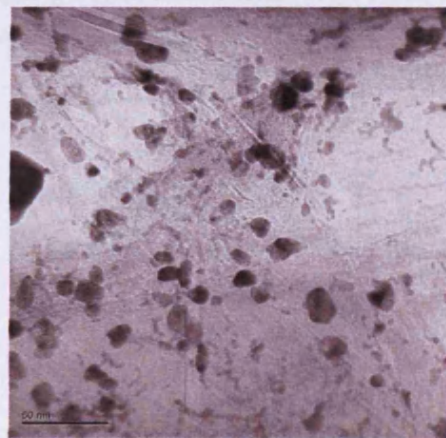

(a)
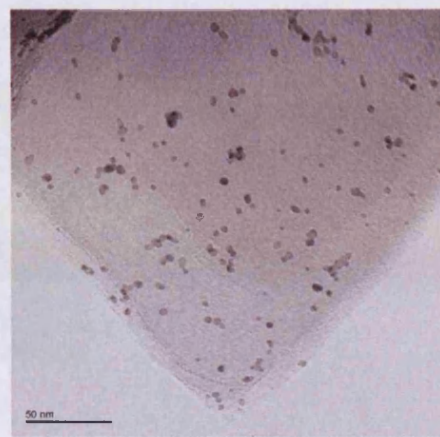
(b)
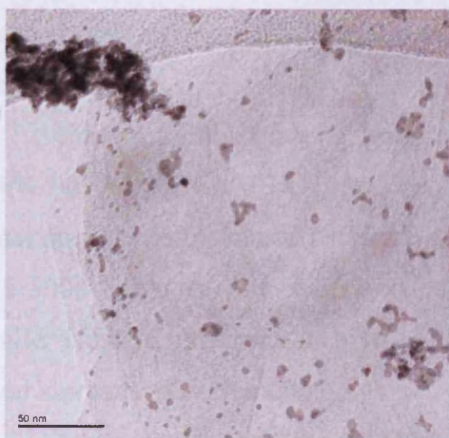
(c)

(d)

(e)

(f)
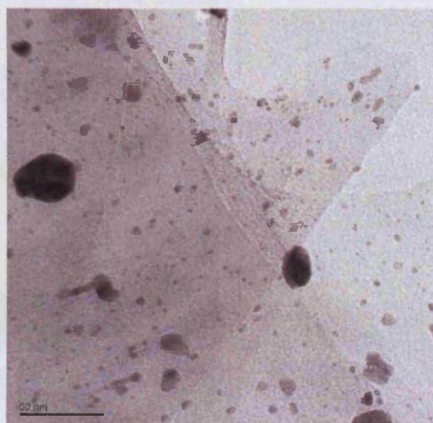
(g)

3.1.4   Energy Dispersive X-Ray Analysis

This technique allowed the determination of the atom compositions of selected regions (some containing individual metal particles) observed in the electron micrographs of Batch 1 catalysts.

Compositional analysis along a linear element 100 nm in length in catalyst 3188, (1.0% Pd, 2.5% Au)[0.7]/G{1}, is shown in Figure 3.5. The area analysed crossed a large metal particle and a cluster of small metallic particles. The large particle of approximate area 5000 nm^2 (100 nm x 50 nm) contained a predominance of gold (50 – 80%). The smaller clusters present in an area of 2000 nm^2 (40 nm x 50 nm) contained approximately equal amounts of each metal.

Areas analysed in the micrograph shown in Figure 3.6 (also catalyst 3188) were approximately 2500 nm^2 (50 nm x 50 nm). Area 1 appeared to represent a single large particle and the elemental analysis showed it to contain gold, almost exclusively. Area 2 contained a cluster of small particles for which the analysis showed a predominance of palladium.
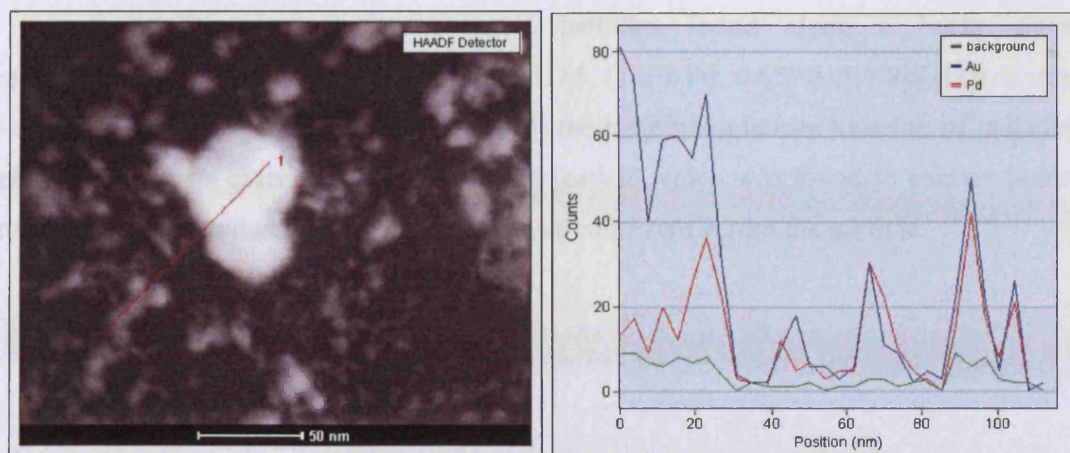
Figure 3.5 – Particle gradient analysis in catalyst 3188, (1.0% Pd, 2.5% Au)[0.7]/G{1}
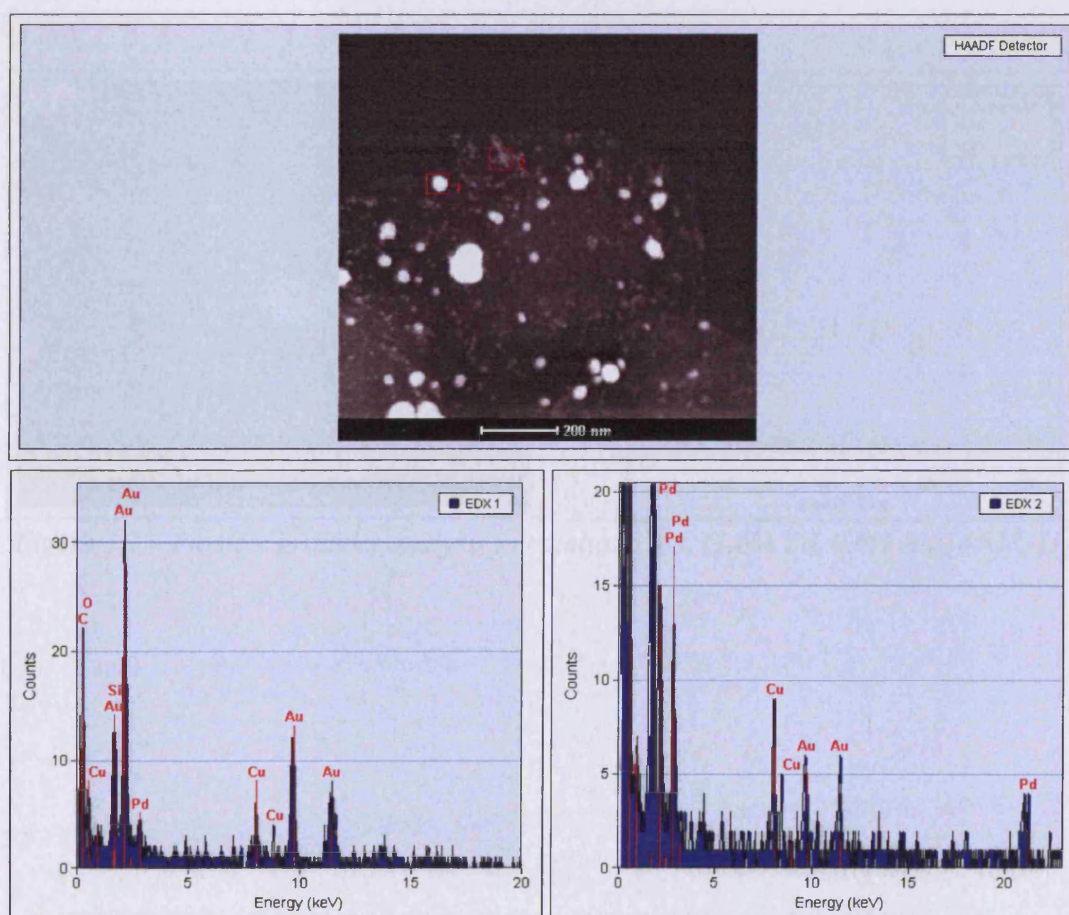
Figure 3.6 – Particle analysis in catalyst 3188, (1.0% Pd, 2.5% Au)[0.7]/G{1}

Compositional analysis of metal particles found along a linear element approximately 100 nm in length in catalyst 3185, (1.6% Pd, 0.6% Au)[4.8]/G{1}, is shown in Figure 3.7. The small metallic cluster near the large particle was found to be palladium-rich. The analysis extended across the large particle which was found to contain twice as much gold as palladium. This composition was consistent across the particle.
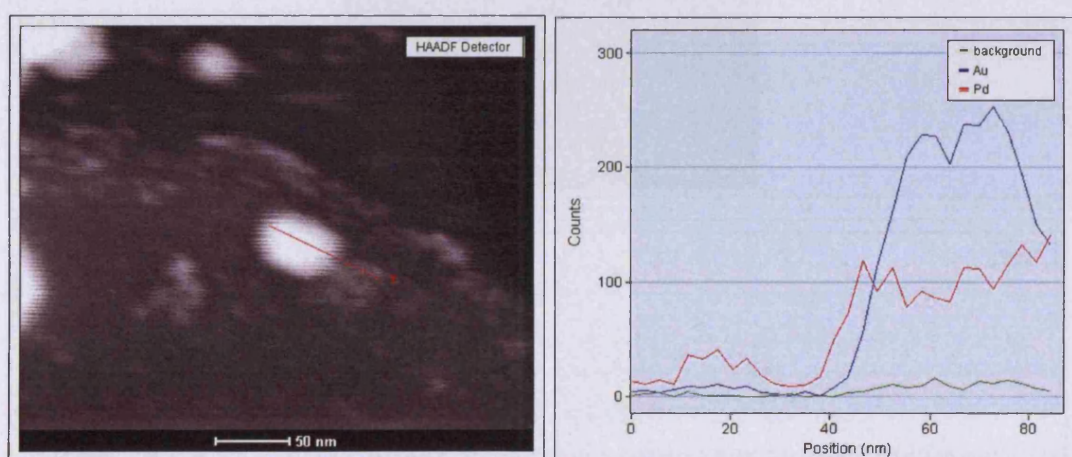
Figure 3.7 – Particle gradient analysis in catalyst 3185, (1.6% Pd, 0.6% Au)[4.8]/G{1}

Figure 3.8 shows elemental analysis of metallic particles in catalyst 3185, (1.6% Pd, 0.6% Au)[4.8]/G{1}. The region analysed, which was approximately 400 nm^2 (20 nm x 20 nm), was found to contain a large amount of palladium and a small amount of gold.
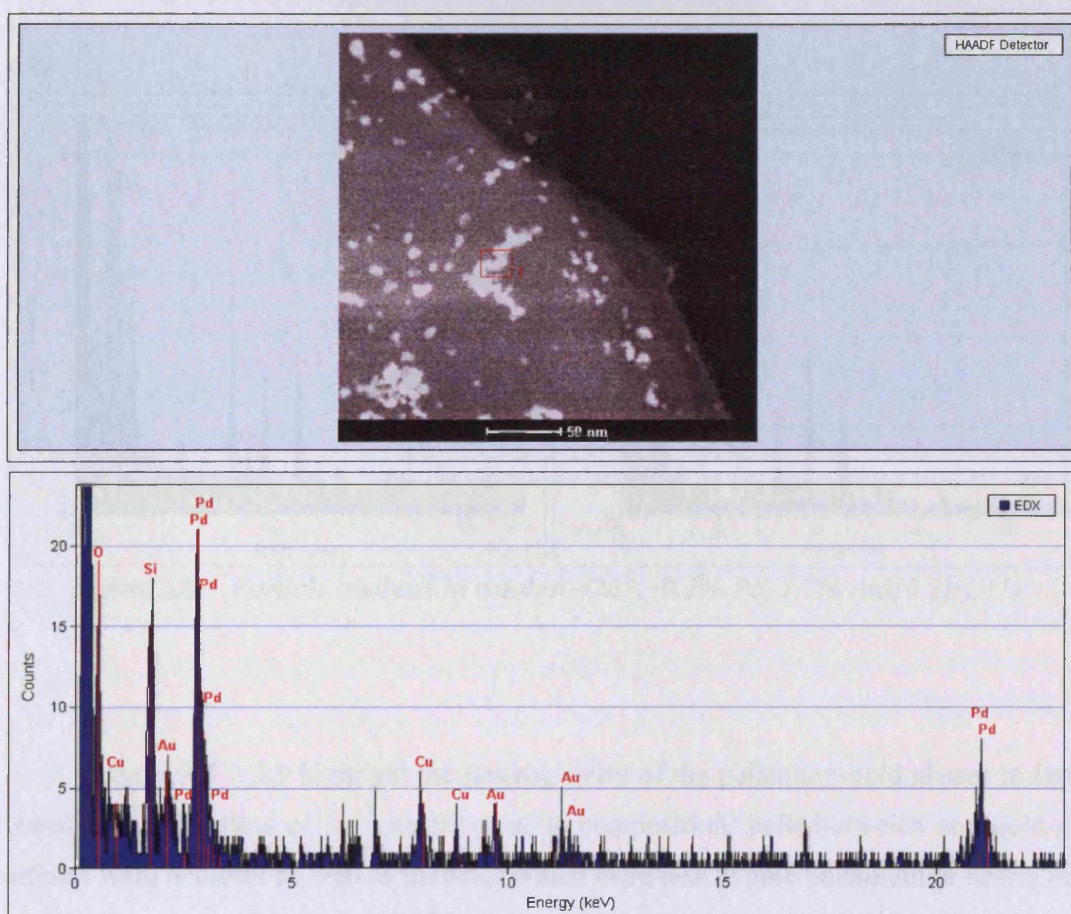
Figure 3.8 – Particle analysis in catalyst 3185, (1.6% Pd, 0.6% Au)[4.8]/G{1}

Figure 3.9 shows elemental analysis of two areas of approximately 400 nm^2 (20 nm x 20 nm) in catalyst 4265, (0.2% Pd, 1.7% Au)[0.2]/G{1}. Area 1 shows a cluster of small particles containing slightly more gold than palladium. In close proximity (150 nm), area 2 shows an individual metal particle which contained an overwhelming predominance of gold and only a trace of palladium.
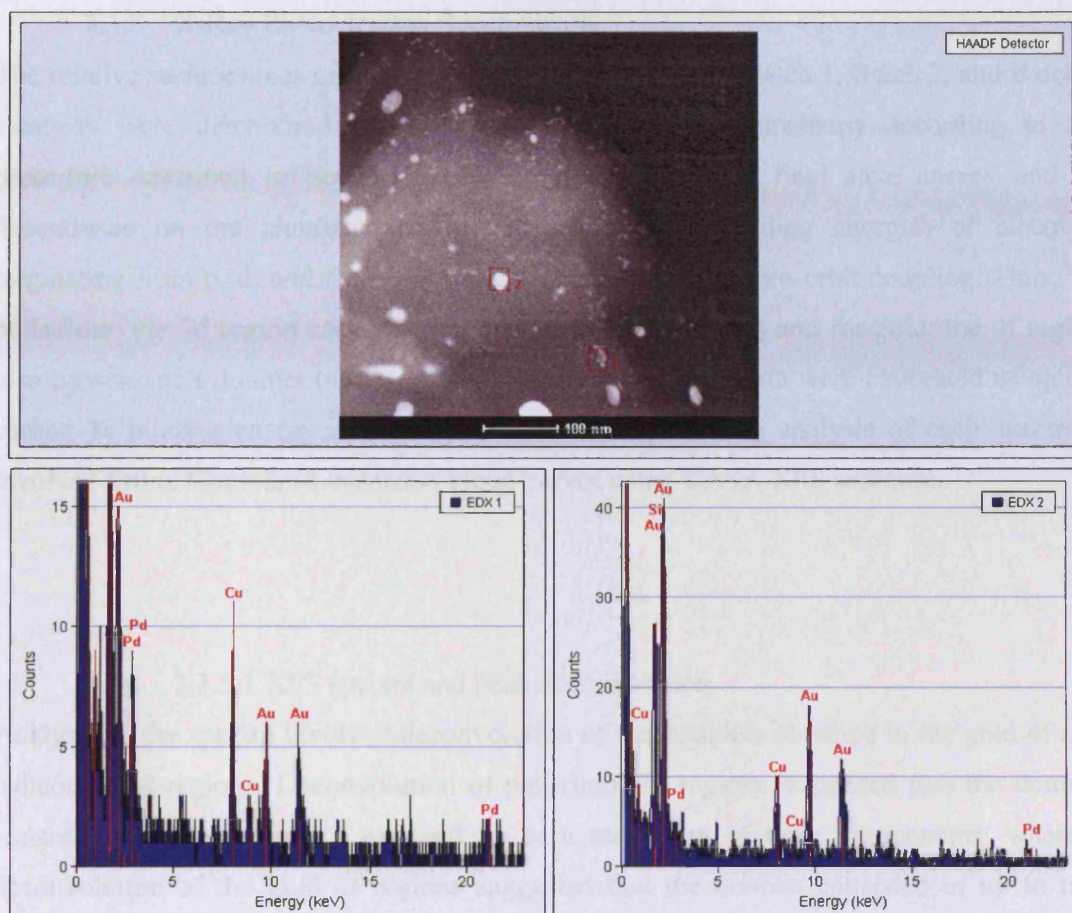
Figure 3.9 – Particle analysis in catalyst 4265, (0.2% Pd, 1.7% Au)[0.2]/G{1}

Figures 3.5 – 3.9 highlight the heterogeneity of the palladium-gold phases in Batch 1 catalysts. Regardless of the overall metallic composition, palladium-rich and gold-rich particles were detected as well as particles which were nearly pure palladium or nearly pure gold. Particles of different composition were found in close proximity and composition gradients were observed across single metal particles. Catalysts from Batches 2 and 3 provided results which showed similar trends in terms of compositional heterogeneity.

3.1.5   X-Ray Photoelectron Spectroscopy

The relative surface areas of palladium and of gold in certain Batch 1, Batch 2, and Batch 3 catalysts were determined using X-ray photoelectron spectroscopy according to the procedure described in Section 2.5.2. Due to the variable final state energy and its dependence on the photoelectron binding energy, the binding energies of electrons originating from p, d, and f orbitals vary. This is a result of spin-orbit coupling. Thus, for palladium; the 3d region consists of a doublet ($3d^{5/2}$ and $3d^{3/2}$) and for gold; the 4f region also consists of a doublet ($4f^{7/2}$ and $4f^{5/2}$). The experimental data were calibrated using the carbon 1s binding energy as a reference (284.5 eV) and the analysis of each spectrum involved fitting Gaussian-Lorentzian blend curves using CASA XPS software.

3.1.5.1 XPS spectra and peak deconvolution

Analysis of the spectra involved deconvolution of the doublets obtained in the gold 4f and palladium 3d regions. Deconvolution of palladium 3d regions suggested that the doublet consisted of a minimum of two and up to a maximum of three components, whereas deconvolution of the gold 4f regions suggested that the doublet consisted of up to two components.

The gold 4f and palladium 3d regions in the spectrum for catalyst 3186, (1.0% Pd, 1.0% Au)[2.0]/G{1}, are shown in Figures 3.10 and 3.11 respectively. Deconvolution (dashed lines) of the doublet for the gold 4f region shows that each peak can be fitted with a single component. This almost certainly indicates the existence of metallic gold at the catalyst surface.

Figure 3.10 – Gold 4f region: XPS spectrum and deconvolution for catalyst 3186, (1.0% Pd, 1.0% Au)[2.0]/G{1}

Deconvolution of the doublet in the palladium 3d region suggested that each peak consisted of two components. This indicates the existence of two types of palladium, one metallic palladium and the other, at higher binding energy, palladium-oxide. The palladium-oxide component had a greater full-width half-maximum (FWHM) than the metallic palladium component, which is well known [1]. Deconvolution of the gold 4f and of the palladium 3d doublets in the spectrum for catalyst 3188, (1.0% Pd, 2.5% Au)[0.7]/G{1}, suggested that it was similar to catalyst 3186.
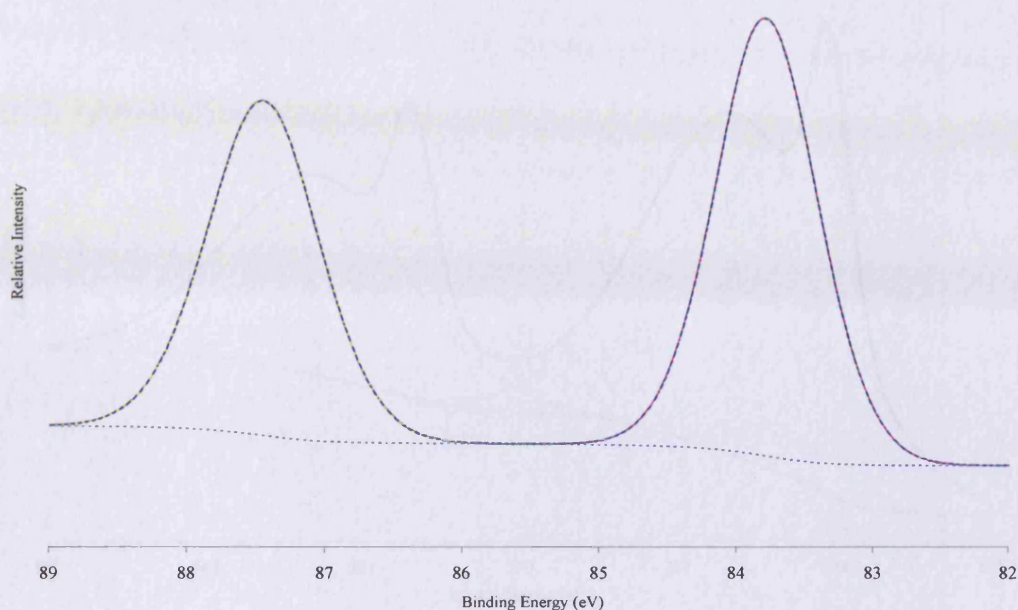
86
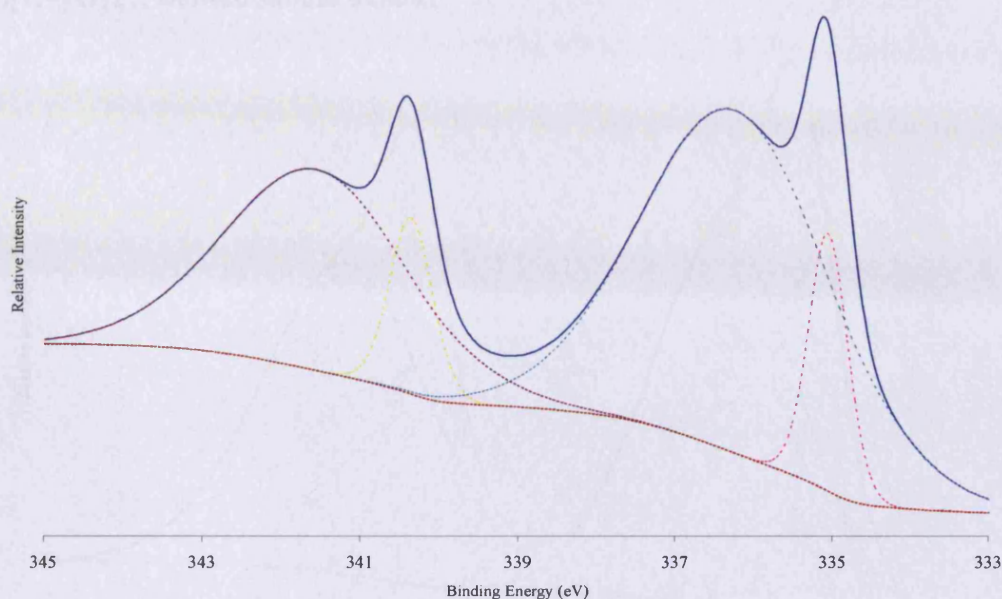
Figure 3.11 – Palladium 3d region: XPS spectrum and deconvolution for catalyst 3186, (1.0% Pd, 1.0% Au)[2.0]/G{1}

Deconvolution of the peaks in the spectrum for catalyst 3334, (1.0% Pd, 1.8% Au)[1.0]/G{2}, suggested that each gold 4f doublet peak (Figure 3.12) consisted of two components. This indicates the co-existence of gold and at a higher binding energy, alloyed gold. [The second component at the higher binding energy could be interpreted as being due to gold existing in a positive oxidation state, but this is thought unlikely because the 4f doublet in a gold-only catalyst showed that it could be fitted with a single component i.e. no gold-oxide existed].

Deconvolution of the doublet in the palladium 3d region for catalyst 3334, (1.0% Pd, 1.8% Au)[1.0]/G{2}, (Figure 3.13) suggested that each peak consisted of two components showing the co-existence of metallic palladium and at higher binding energy, palladium-oxide. The FWHM of the component occurring with a higher binding energy is greater than the FWHM of the component occurring with the lower binding energy and this is consistent with it being palladium-oxide. Deconvolution of the doublets in the spectra for

catalyst 3200, (1.0% Pd, 0.9% Au)[1.9]/G{1}, and catalyst 3333, (1.0% Pd, 1.0% Au)[1.9]/G{2}, showed similar trends.

Figure 3.12 – Gold 4f region: XPS spectrum and deconvolution for catalyst 3334, (1.0% Pd, 1.8% Au)[1.0]/G{2}

Figure 3.13 – Palladium 3d region: XPS spectrum and deconvolution for catalyst 3334, (1.0% Pd, 1.8% Au)[1.0]/G{2}

The gold 4f region for catalyst 3341, (1.0% Pd, 1.7% Au)[1.1]/G{3}, is shown in Figure 3.14. Deconvolution shows that each peak in the doublet consisted of a single component due to metallic gold at the catalyst surface.
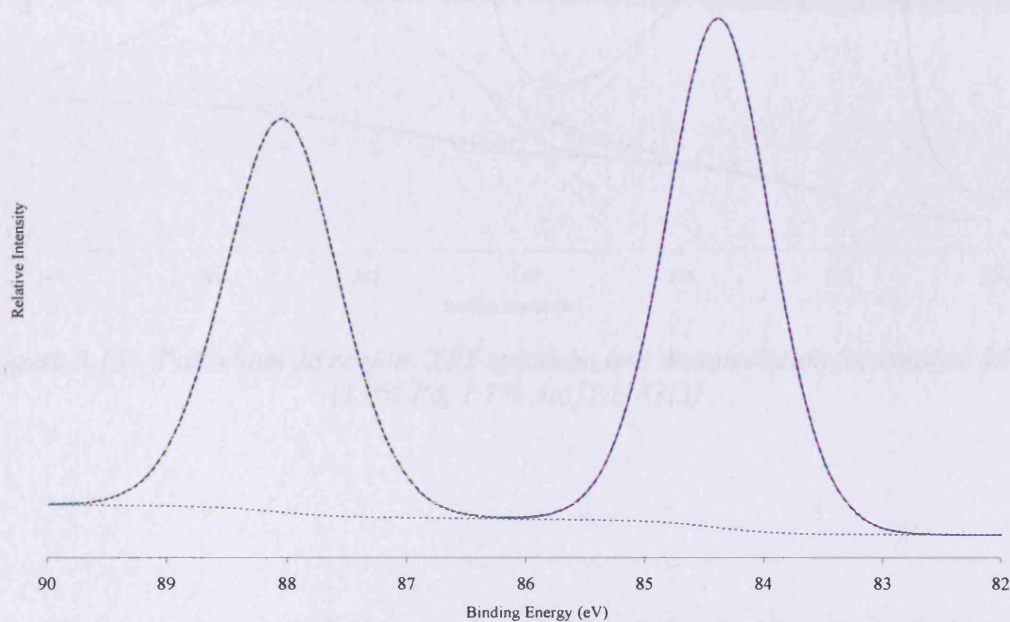
Figure 3.14 – Gold 4f region: XPS spectrum and deconvolution for catalyst 3341, (1.0% Pd, 1.7% Au)[1.1]/G{3}

However, deconvolution of the doublet in the palladium 3d region for catalyst 3341, (1.0% Pd, 1.7% Au)[1.1]/G{3}, suggested that each peak consisted of three components. This is interpreted as the co-existence of (i) metallic palladium with, at increasing binding energies, (ii) palladium in an alloy phase, and (iii) palladium-oxide. This is consistent with the palladium-oxide component having the greatest FWHM. Catalyst 3342, (1.0% Pd, 2.6% Au)[0.7]/G{3}, showed similar behaviour.

Figure 3.15 – Palladium 3d region: XPS spectrum and deconvolution for catalyst 3341, (1.0% Pd, 1.7% Au)[1.1]/G{3}

Figures 3.16 and 3.17 show deconvolution of the doublets in the gold 4f and palladium 3d regions for catalyst 3331, (1.0% Pd, 0.4% Au)[4.8]/G{2}. Each peak in the gold 4f doublet (Figure 3.16) consisted of two components and once again, this is attributed to metallic gold and gold existing in an alloy phase [although the possibility of gold existing in a higher oxidation state as gold-oxide cannot be eliminated].

Deconvolution of the doublet in the palladium 3d region for catalyst 3331, (1.0% Pd, 0.4% Au)[4.8]/G{2}, suggested that each peak in the doublet consisted of three components arising from the co-existence of metallic palladium, palladium in an alloyed phase, and palladium-oxide. Catalysts 3332, (1.7% Pd, 0.6% Au)[4.8]/G{2}, and 3335, (1.0% Pd, 2.7% Au)[0.7]/G{2}, showed similar results.
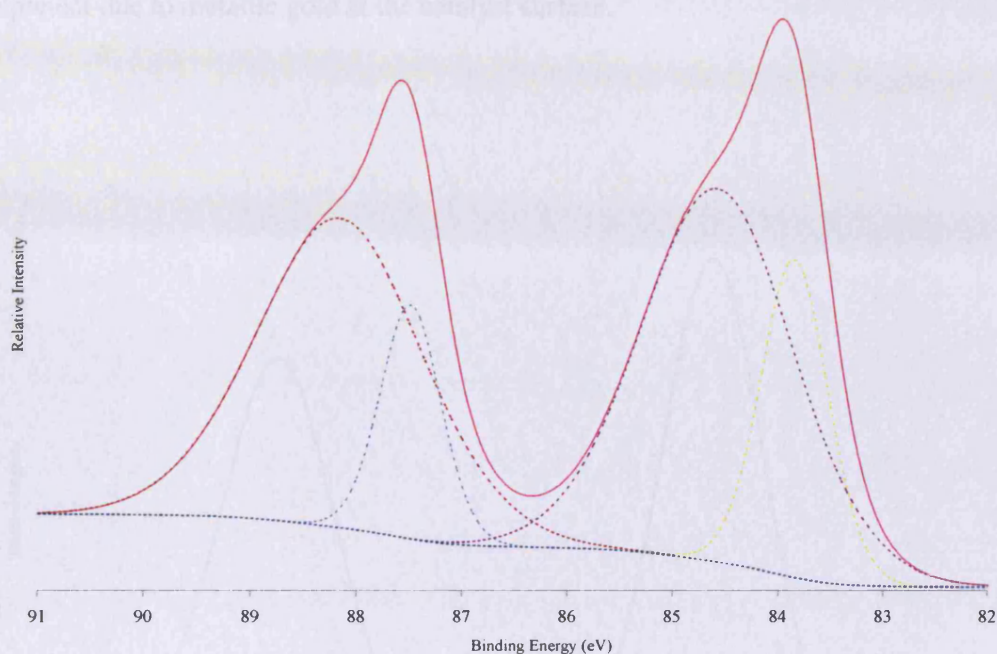
Figure 3.16 – Gold 4f region: XPS spectrum and deconvolution for catalyst 3331, (1.0% Pd, 0.4% Au)[4.8]/G{2}
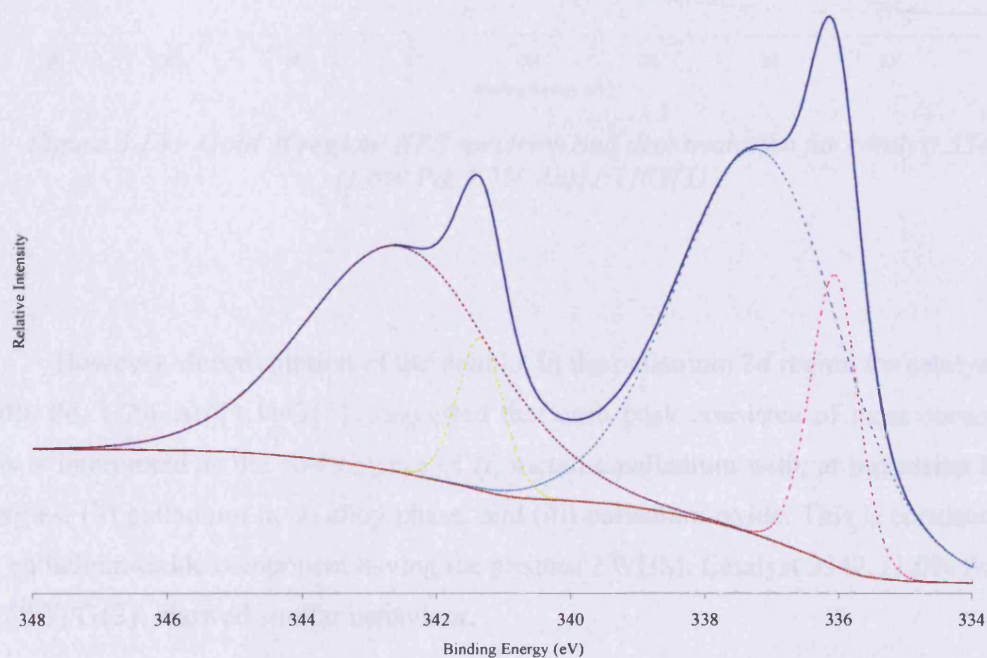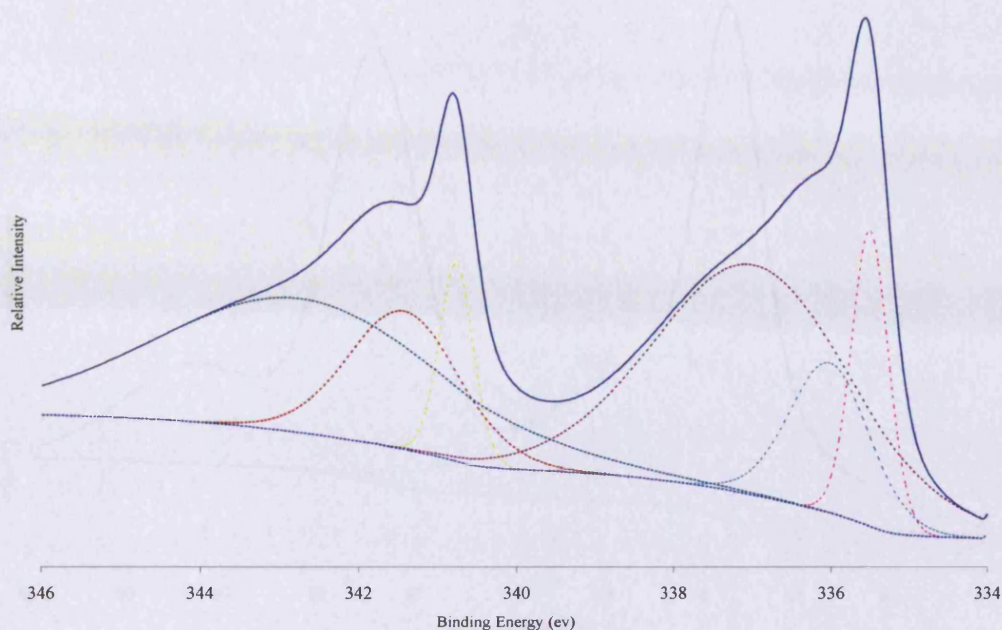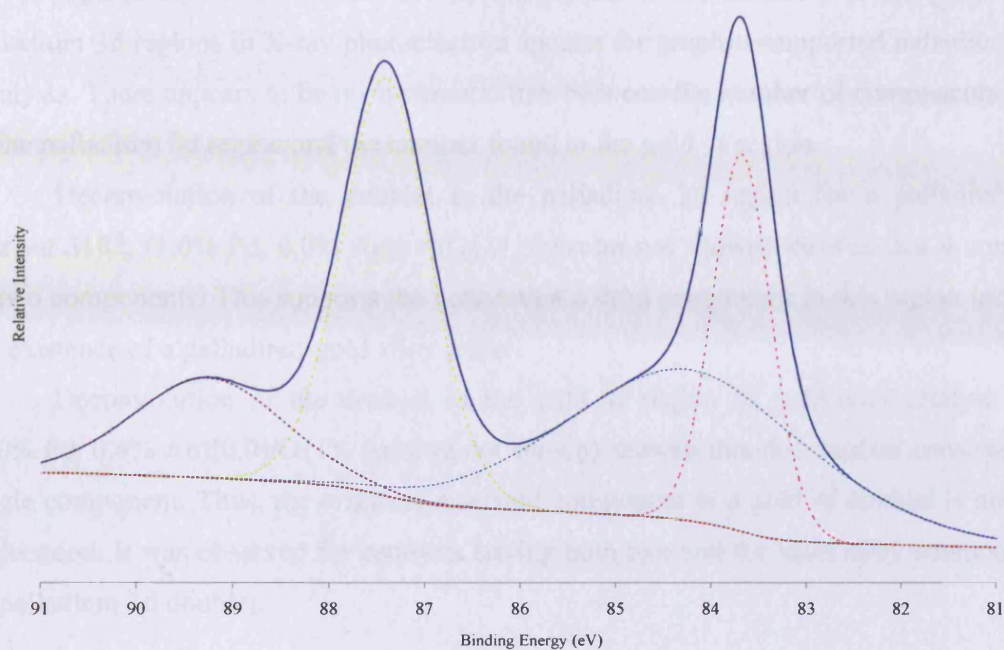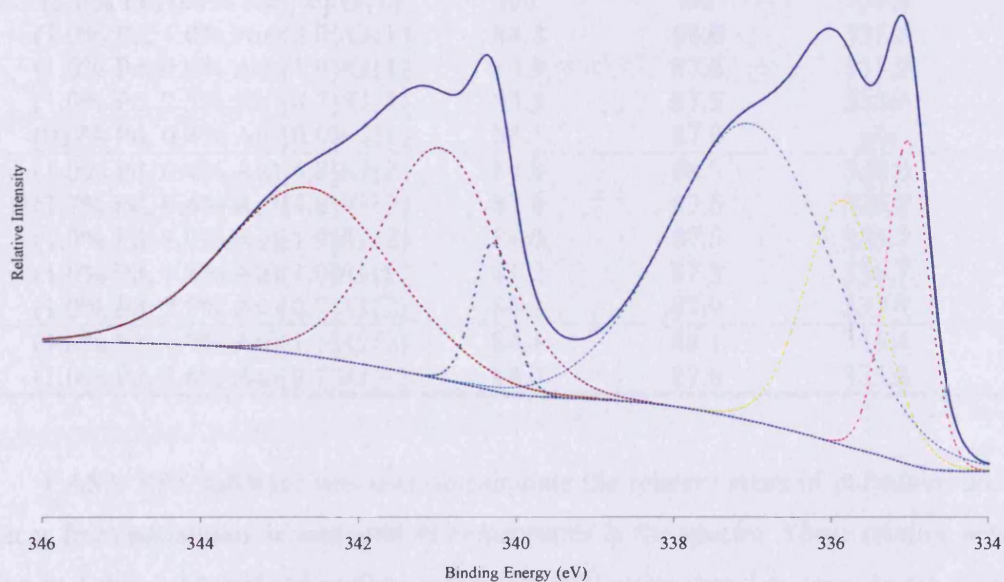

Figure 3.17 – Palladium region: XPS spectrum and deconvolution for catalyst 3331, (1.0% Pd, 0.4% Au)[4.8]/G{2}

Figures 3.10 – 3.17 show the deconvolution of the doublets in the gold 4f and palladium 3d regions in X-ray photoelectron spectra for graphite-supported palladium-gold catalysts. There appears to be no systematic link between the number of components found in the palladium 3d region and the number found in the gold 4f region.

Deconvolution of the doublet in the palladium 3d region for a palladium-only catalyst 3182, (1.0% Pd, 0.0% Au)[∞]/G{1}, (spectra not shown) showed that it consisted of two components. This supports the notion that a third component in this region indicates the existence of a palladium-gold alloy phase.

Deconvolution of the doublet in the gold 4f region of gold-only catalyst 3183, (0.0% Pd, 0.4% Au)[0.0]/G{1}, (spectra not shown) showed that this doublet consisted of a single component. Thus, the origin of a second component in a gold 4f doublet is not fully understood. It was observed for catalysts having both two and the third *alloy* component in its palladium 3d doublet.

Table 3.13 – Approximate binding energies for the gold 4f and palladium 3d regions in the X-ray photoelectron spectra for palladium-gold catalysts

Catalyst		Binding energy (eV)			
		Gold region		Palladium region	
ref no	description	$4f^{7/2}$	$4f^{5/2}$	$3d^{5/2}$	$3d^{3/2}$
3182	(1.0% Pd, 0.0% Au)[∞]/G{1}	n/a	n/a	335.5	340.7
3186	(1.0% Pd, 1.0% Au)[2.0]/G{1}	84.2	88.0	335.8	341.1
3200	(1.0% Pd, 0.9% Au)[1.9]/G{1}	83.9	87.6	335.8	341.1
3188	(1.0% Pd, 2.5% Au)[0.7]/G{1}	83.8	87.5	335.6	341.0
3183	(0.0% Pd, 0.4% Au)[0.0]/G{1}	84.1	87.8	n/a	n/a
3331	(1.0% Pd, 0.4% Au)[4.8]/G{2}	84.0	88.3	336.0	341.3
3332	(1.7% Pd, 0.6% Au)[4.8]/G{2}	83.8	87.6	335.7	341.2
3333	(1.0% Pd, 1.0% Au)[1.9]/G{2}	84.0	87.5	335.7	341.0
3334	(1.0% Pd, 1.8% Au)[1.0]/G{2}	84.2	87.8	336.7	342.0
3335	(1.0% Pd, 2.7% Au)[0.7]/G{2}	84.2	87.9	335.7	341.3
3341	(1.0% Pd, 1.7% Au)[1.1]/G{3}	84.4	88.1	336.4	341.3
3342	(1.0% Pd, 2.6% Au)[0.7]/G{3}	84.0	87.6	335.8	341.0

CASA XPS software was used to calculate the relative areas of palladium and gold surfaces from palladium 3d and gold 4f components in the spectra. These relative areas are shown in Table 3.14, and the surface palladium/gold ratios that they provide are compared with the bulk values obtained by X-ray fluorescence (Table 3.15).

Table 3.14 – Corrected areas for the gold 4f and palladium 3d regions found for palladium-gold catalysts

Catalyst		Gold 4f area[a]	Palladium 3d area[a]
ref no	description		
3182	(1.0% Pd, 0.0% Au)[∞]/G{1}	0	1159
3186	(1.0% Pd, 1.0% Au)[2.0]/G{1}	299	1220
3200	(1.0% Pd, 0.9% Au)[1.9]/G{1}	347	718
3188	(1.0% Pd, 2.5% Au)[0.7]/G{1}	835	938
3183	(0.0% Pd, 0.4% Au)[0.0]/G{1}	114	0
3331	(1.0% Pd, 0.4% Au)[4.8]/G{2}	116	1402
3332	(1.7% Pd, 0.6% Au)[4.8]/G{2}	173	1706
3333	(1.0% Pd, 1.0% Au)[1.9]/G{2}	308	1221
3334	(1.0% Pd, 1.8% Au)[1.0]/G{2}	589	1252
3335	(1.0% Pd, 2.7% Au)[0.7]/G{2}	997	1855
3341	(1.0% Pd, 1.7% Au)[1.1]/G{3}	178	436
3342	(1.0% Pd, 2.6% Au)[0.7]/G{3}	190	451

[a]corrected using Scofield's cross sections

Table 3.15 – A comparison of palladium/gold ratios determined from measurement of bulk properties (by XRF) and of surface properties (by XPS)

Catalyst		Bulk Pd/Au ratio[a]	Surface Pd/Au ratio[b]
ref no	description		
3182	(1.0% Pd, 0.0% Au)[∞]/G{1}	∞	∞
3186	(1.0% Pd, 1.0% Au)[2.0]/G{1}	2.0	4.08
3200	(1.0% Pd, 0.9% Au)[1.9]/G{1}	1.9	2.07
3188	(1.0% Pd, 2.5% Au)[0.7]/G{1}	0.7	1.12
3183	(0.0% Pd, 0.4% Au)[0.0]/G{1}	0.0	0.00
3331	(1.0% Pd, 0.4% Au)[4.8]/G{2}	4.8	12.11
3332	(1.7% Pd, 0.6% Au)[4.8]/G{2}	4.8	9.86
3333	(1.0% Pd, 1.0% Au)[1.9]/G{2}	1.9	3.97
3334	(1.0% Pd, 1.8% Au)[1.0]/G{2}	1.0	2.13
3335	(1.0% Pd, 2.7% Au)[0.7]/G{2}	0.7	1.86
3341	(1.0% Pd, 1.7% Au)[1.1]/G{3}	1.1	2.45
3342	(1.0% Pd, 2.6% Au)[0.7]/G{3}	0.7	2.38

[a]determined by X-ray fluorescence
[b]determined by X-ray photoelectron spectroscopy

The palladium/gold ratio in the surface was found to be approximately twice that of the ratio in the bulk; in extreme cases it was about three times the bulk ratio. It is likely that surface palladium enrichment is a particle-size effect. Analysis of the X-ray diffractograms (Section 3.1.2) showed that smaller particles predominantly contained palladium (i.e. palladium-rich alloys) whereas larger particles predominantly contained gold (i.e. gold-rich alloys). Energy dispersive X-ray analysis (Section 3.1.4) also showed this trend. Thus, the surface areas of palladium in these bimetallic catalysts always exceeded that of gold irrespective of the nominal composition. A plot of palladium/gold atom (bulk) ratio against surface palladium/gold ratio (Figure 3.18) shows linear behaviour; the gradient is 2.2.
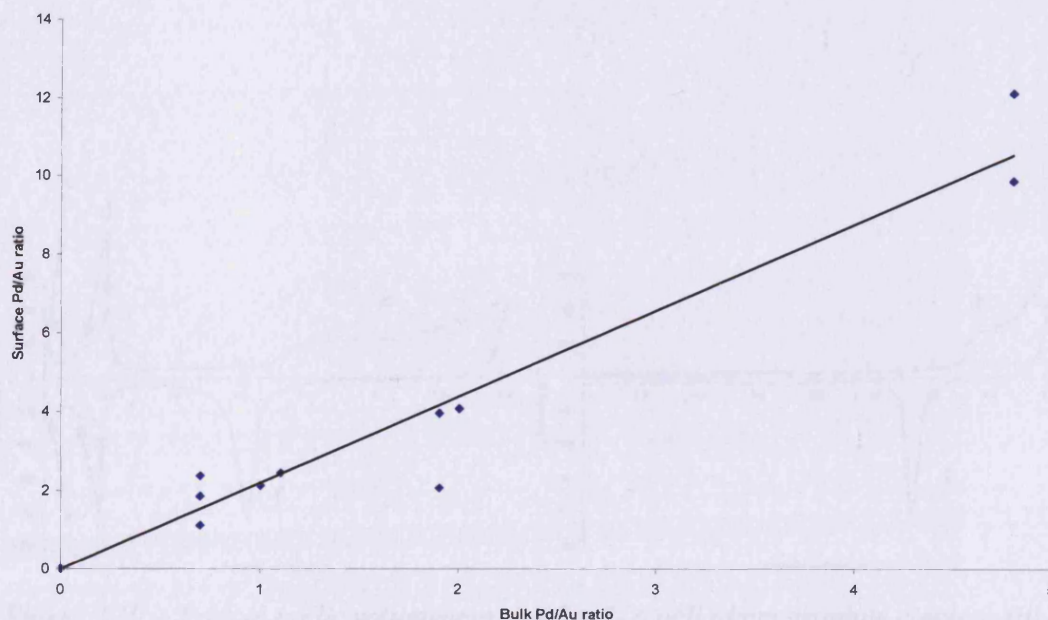
Figure 3.18 – Correlation between surface palladium/gold ratios and bulk palladium/gold ratios for palladium-gold catalysts

3.2 Characterisation of Batch 1, Batch 2, and Batch 3 Catalysts by Cyclic Voltammetry

Surface characterisation of Batch 1, Batch 2, and Batch 3 catalysts, involving estimations of palladium/gold composition, metal area, and extent of alloying was preformed using cyclic voltammetry (procedure described in Section 2.2.7).

Typical CVs of palladium/graphite and of gold/graphite catalysts are shown in Figure 3.19. The CV for the palladium catalyst shows a hydrogen under-potential deposition region, where hydrogen adsorption (a) and desorption (d) occurs. Hydrogen absorption into the bulk of the metal occurs at (b) and hydrogen evolution is observed at (c). At more positive potentials, palladium-oxide formation occurs in region (e) and palladium-oxide stripping is observed in region (f).

The CV for the gold catalyst is distinguished by the absence of a hydrogen under-potential deposition region, but gold-oxide is formed in region (g) and is stripped off in region (h).
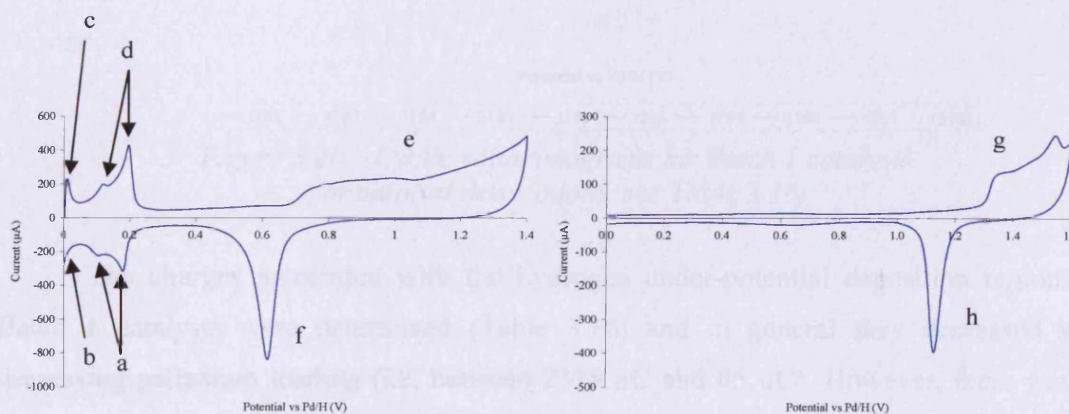
Figure 3.19 – Typical cyclic voltammograms for (i) a palladium/graphite catalyst, (ii) a gold/graphite catalyst

3.2.1 Catalysts Prepared at Ambient Temperature

CVs for Batch 1 catalysts are shown in Figure 3.20. The CVs contain many common features which include; peaks for hydrogen absorption/evolution in palladium which occurred at potentials between 0.00 V and ~ 0.05 V, hydrogen adsorption/desorption on palladium at potentials between ~ 0.05 V and 0.25 V (hydrogen under-potential deposition, HUPD) and the formation/removal of surface oxides of palladium and gold. As the contribution of gold to the overall composition increased, so the HUPD and palladium-oxide stripping regions became attenuated.
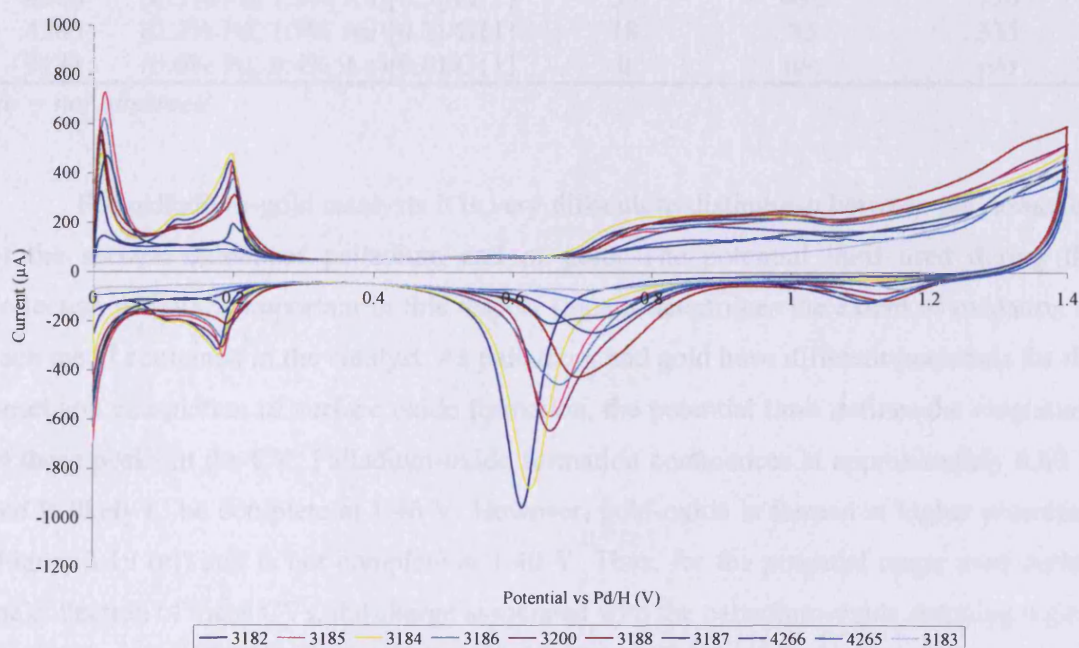
Figure 3.20 – Cyclic voltammograms for Batch 1 catalysts
(for catalyst descriptions, see Table 3.16)

The charges associated with the hydrogen under-potential deposition regions of Batch 1 catalysts were determined (Table 3.16) and in general they decreased with decreasing palladium loading (i.e. between 2375 µC and 85 µC). However, there was an exceptional result: catalyst 3182 (1.0% palladium) was found to have a hydrogen under-potential deposition charge of 2220 µC whilst the charge associated with the hydrogen under-potential region of catalyst 3187 (1.0% palladium) was only 405 µC.

Table 3.16 – Batch 1 catalysts: catalyst reference numbers, descriptions, and the charges associated with the hydrogen under-potential deposition regions

Catalyst		Palladium content / atom%	HUPD charge / μC	HUPD charge $(10\ \mu g\ Pd)^{-1}$ / μC
ref no	description			
3182	(1.0% Pd, 0.0% Au)[∞]/G{1}	100	2220	1850
3185	(1.6% Pd, 0.6% Au)[4.8]/G{1}	83	1080	555
3184	(1.0% Pd, 0.4% Au)[4.7]/G{1}	82	2375	2020
3186	(1.0% Pd, 1.0% Au)[2.0]/G{1}	66	1565	1290
3200	(1.0% Pd, 0.9% Au)[1.9]/G{1}	66	1440	1235
3188	(1.0% Pd, 2.5% Au)[0.7]/G{1}	43	1030	850
3187	(1.0% Pd, 1.7% Au)[1.1]/G{1}	51	405	345
4266	(0.5% Pd, 1.8% Au)[0.5]/G{1}	35	480	770
4265	(0.2% Pd, 1.7% Au)[0.2]/G{1}	18	85	335
3183	(0.0% Pd, 0.4% Au)[0.0]/G{1}	0	n/o	n/o

n/o = not observed

For palladium-gold catalysts it is very difficult to distinguish between the *formation* of the surface oxides of palladium and of gold. The potential limit used during the collection of CVs is important in this respect since it determines the extent of oxidation of each metal contained in the catalyst. As palladium and gold have different potentials for the onset and completion of surface oxide formation, the potential limit defines the magnitude of these peaks in the CV. Palladium-oxide formation commences at approximately 0.60 V and is likely to be complete at 1.40 V. However, gold-oxide is formed at higher potentials (Figure 3.19 (e)) and is not complete at 1.40 V. Thus, for the potential range used during the collection of these CVs, the charge associated with the palladium-oxide stripping region may be used as a quantitative measure of palladium surface area, whereas that associated with the gold-oxide stripping region is not significant (due to under-oxidation). However, *potentials* (i.e. peak minima) for the palladium-oxide and gold-oxide stripping regions may be compared, between catalysts, regardless of the extent of gold oxidation.

The potentials required to strip the surface oxides of palladium and of gold, along with the charges associated with the palladium-oxide stripping regions, for Batch 1 catalysts are shown in Table 3.17.

The potential required to remove the palladium-oxide phase varied from 0.61V to 0.74 V. With two exceptions [catalysts 3187 and 3200] the palladium-oxide stripping potential (i.e. the ease of oxide removal) increased with increasing gold composition

(Figure 3.20, Table 3.17) and, where detected, the potential of the gold-oxide stripping peak (Figure 3.20, Table 3.17) varied in the opposite manner between 1.16 V and 1.10 V. The perturbation of the gold-oxide stripping peak was found to occur with increasing palladium composition, although gold-oxide stripping in catalyst 3188 was found to occur at a more positive potential than expected.

The charges associated with the removal of palladium-oxide from the surfaces of Batch 1 catalysts were calculated (via integration of the current measured with respect to time) using CHI software. Stripping charges ranged from 220 – 3285 µC as shown in Table 3.17.

Table 3.17 – Batch 1 catalysts: catalyst reference numbers, descriptions, oxide stripping potentials, and the charges associated with the palladium-oxide stripping regions

Catalyst		Pd-O stripping potential / V	Au-O stripping potential / V	Pd-O stripping region charge / µC
ref no	description			
3182	(1.0% Pd, 0.0% Au)[∞]/G{1}	0.61	n/o	2905
3185	(1.6% Pd, 0.6% Au)[4.8]/G{1}	0.65	n/o	1670
3184	(1.0% Pd, 0.4% Au)[4.7]/G{1}	0.63	n/o	3285
3186	(1.0% Pd, 1.0% Au)[2.0]/G{1}	0.67	n/o	2105
3200	(1.0% Pd, 0.9% Au)[1.9]/G{1}	0.65	n/o	2765
3187	(1.0% Pd, 1.7% Au)[1.1]/G{1}	0.66	n/o	1110
3188	(1.0% Pd, 2.5% Au)[0.7]/G{1}	0.69	1.11	1680
4266	(0.5% Pd, 1.8% Au)[0.5]/G{1}	0.72	1.10	1420
4265	(0.2% Pd, 1.7% Au)[0.2]/G{1}	0.74	1.11	220
3183	(0.0% Pd, 0.4% Au)[0.0]/G{1}	n/o	1.16	n/o

n/o = not observed

Since the HUPD regions and palladium-oxide stripping regions are each providing a measure of palladium surface area, it is to be expected that the values obtained show a linear correlation for a given catalyst. This is shown in Figure 3.21. The points show scatter about a straight line which shows a natural extrapolation to the origin as expected. The gradient was observed to be 1.5. A value of 2.0 would have been expected for the simple case where only surface oxide of palladium (Pd-O) was formed and the charge associated with the CV in the ~ 0.05 V to ~ 0.25 V range was purely a measure of the charge associated with hydrogen under-potential deposition. However, due to the adsorption/desorption of anions also occurring in this region, the charge associated with the

CV in this range is slightly greater than expected [2 – 4]. Thus, the gradient of this line is less than 2.0.
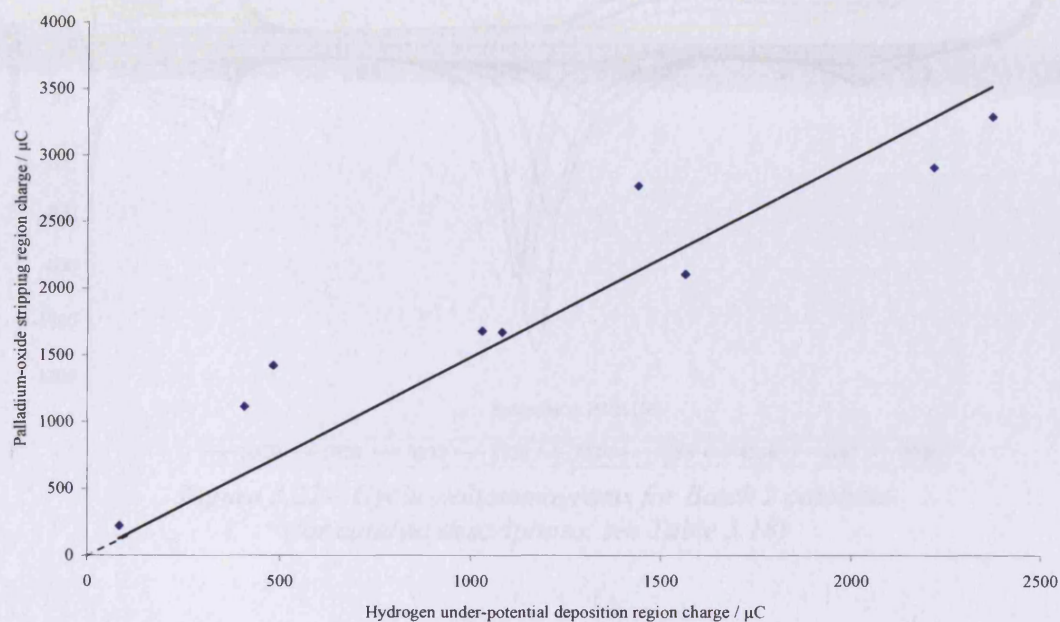
Figure 3.21 – Batch 1: charge associated with the hydrogen under-potential deposition region verses the charge associated with the stripping of palladium-oxide

CVs for Batch 2 catalysts (Figure 3.22) have similar features to those recorded for Batch 1 catalysts. Measurement of the charges associated with the hydrogen under-potential deposition regions yielded values ranging from 5 – 3165 µC (Table 3.18).

The materials required to remove palladium oxide (Figure 3.22) from Batch 2 catalysts decreased, with increasing gold substitution (exception: catalyst 3268), it varied between... to 0.77... The potential required for the removal of gold oxide varied between 1.15 V and 1.35 V, depending on the palladium composition of the catalyst. The characteristic silver palladium oxide reduction regions present in... to ... μC for catalyst...
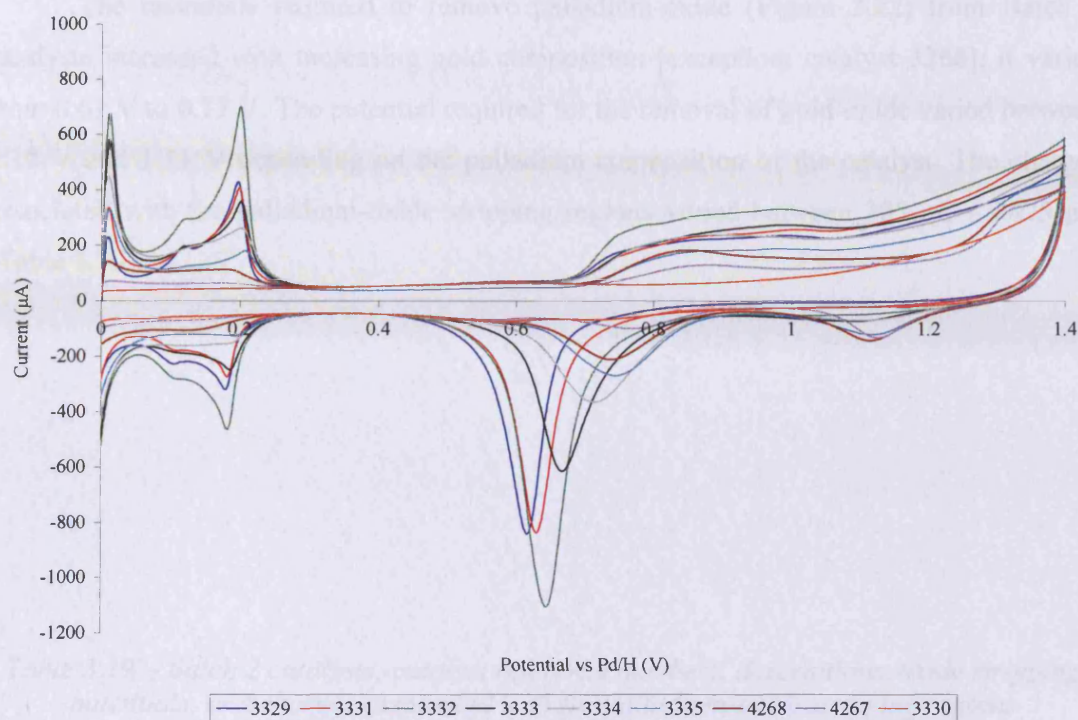
Figure 3.22 – Cyclic voltammograms for Batch 2 catalysts
(for catalyst descriptions, see Table 3.18)

Table 3.18 – Batch 2 catalysts: catalyst reference numbers, descriptions, and the charges associated with the hydrogen under-potential deposition regions

Catalyst		Palladium content / atom%	HUPD charge / μC	HUPD charge $(10\ \mu g\ Pd)^{-1}$ / μC
ref no	description			
3329	(1.0% Pd, 0.0% Au)[∞]/G{2}	100	2160	1820
3331	(1.0% Pd, 0.4% Au)[4.8]/G{2}	83	2365	1950
3332	(1.7% Pd, 0.6% Au)[4.8]/G{2}	83	3165	1590
3333	(1.0% Pd, 1.0% Au)[1.9]/G{2}	66	1870	1545
3334	(1.0% Pd, 1.8% Au)[1.0]/G{2}	51	1350	1125
3335	(1.0% Pd, 2.7% Au)[0.7]/G{2}	41	1420	1195
4268	(0.5% Pd, 1.8% Au)[0.6]/G{2}	36	235	370
4267	(0.2% Pd, 1.8% Au)[0.2]/G{2}	18	5	10
3330	(0.0% Pd, 0.4% Au)[0.0]/G{2}	0	n/o	n/o

n/o = not observed

The potentials required to remove palladium-oxide (Figure 3.22) from Batch 2 catalysts increased with increasing gold composition [exception: catalyst 3268]; it varied from 0.61 V to 0.77 V. The potential required for the removal of gold-oxide varied between 1.12 V and 1.11 V depending on the palladium composition of the catalyst. The charges associated with the palladium-oxide stripping regions varied between 305 µC – 3625 µC (Table 3.19).

Table 3.19 – Batch 2 catalysts: catalyst reference numbers, descriptions, oxide stripping potentials, and charges associated with the palladium-oxide stripping regions

Catalyst		Pd-O stripping potential / V	Au-O stripping potential / V	Pd-O stripping region charge / µC
ref no	description			
3329	(1.0% Pd, 0.0% Au)[∞]/G{2}	0.61	n/o	2605
3331	(1.0% Pd, 0.4% Au)[4.8]/G{2}	0.63	n/o	3095
3332	(1.7% Pd, 0.6% Au)[4.8]/G{2}	0.64	n/o	3625
3333	(1.0% Pd, 1.0% Au)[1.9]/G{2}	0.67	n/o	2555
3334	(1.0% Pd, 1.8% Au)[1.0]/G{2}	0.71	n/o	1265
3335	(1.0% Pd, 2.7% Au)[0.7]/G{2}	0.74	1.12	1585
4268	(0.5% Pd, 1.8% Au)[0.6]/G{2}	0.74	1.11	595
4267	(0.2% Pd, 1.8% Au)[0.2]/G{2}	0.77	1.12	305
3330	(0.0% Pd, 0.4% Au)[0.0]/G{2}	n/o	n/o	n/o

n/o = not observed

The relationship between the charges associated with the hydrogen under-potential deposition regions and the palladium-oxide stripping regions for Batch 2 catalysts is shown in Figure 3.23. Once again, the points show scatter about a straight line which shows a natural extrapolation to the origin. In this case the gradient was observed to be 1.2.
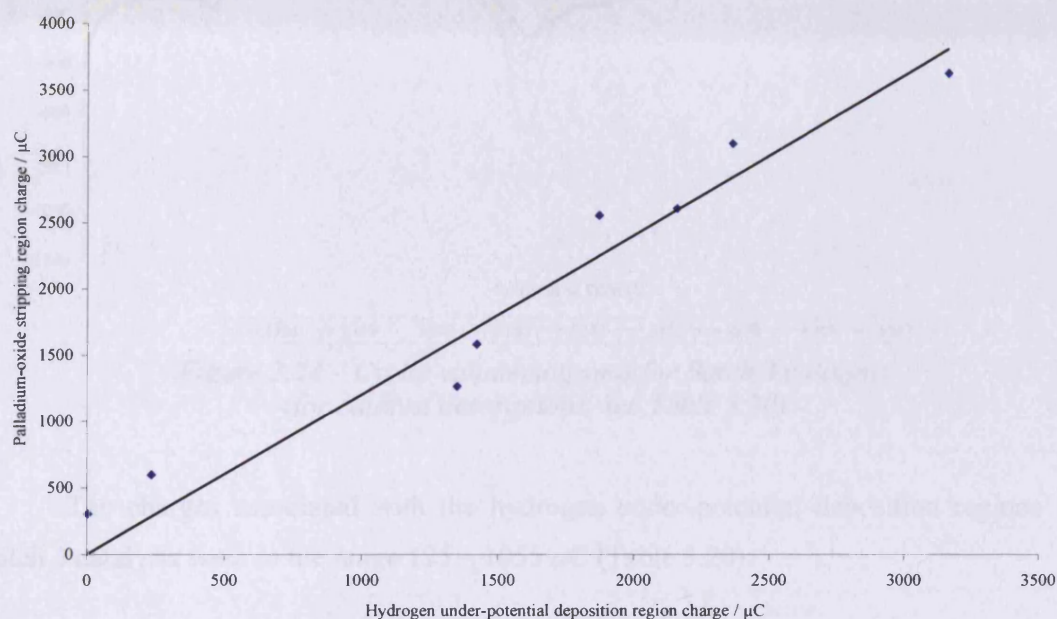
Figure 3.23 – Batch 2: charge associated with the hydrogen under-potential deposition region verses the charge associated with the stripping of palladium-oxide

CVs for Batch 3 catalysts (Figure 3.24) contained the same features as those of Batches 1 and 2. At high palladium/gold atom ratios, CVs resemble palladium (sharp peaks in the hydrogen under-potential deposition regions and little variation in potentials required for palladium-oxide stripping). At low palladium/gold atom ratios, (i) the peaks in the hydrogen under-potential deposition region were again attenuated, (ii) greater perturbation in the potential required to strip palladium-oxide was observed, and (iii) the appearance of a gold-oxide stripping region indicated the presence of gold at the surface.
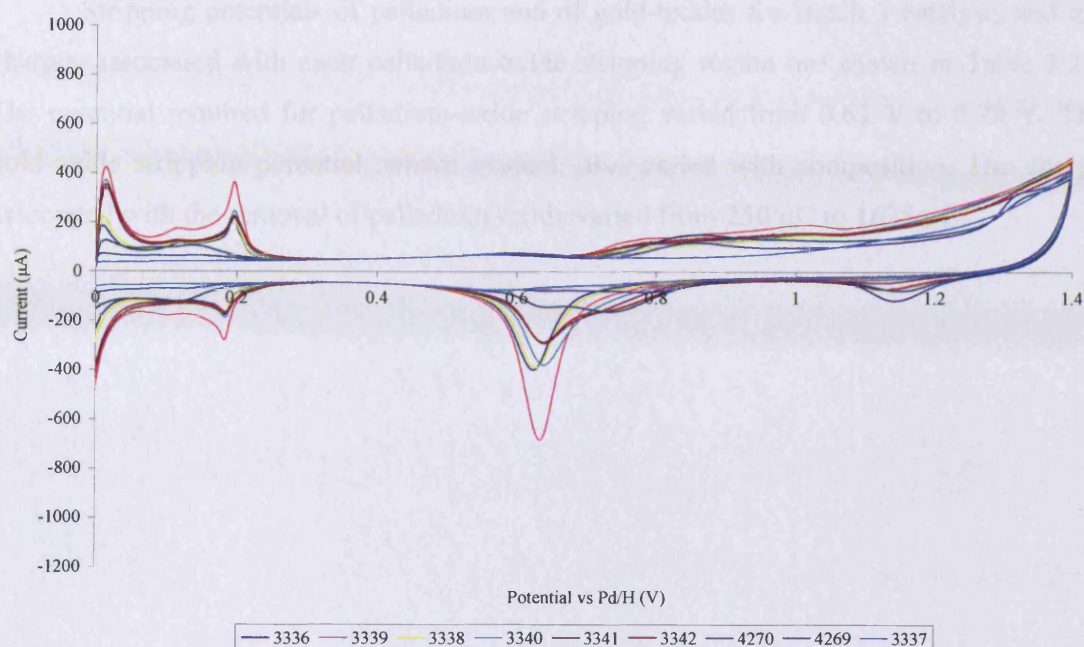
*Figure 3.24 – Cyclic voltammograms for Batch 3 catalysts
(for catalyst descriptions, see Table 3.20)*

The charges associated with the hydrogen under-potential deposition regions for Batch 3 catalysts were in the range 125 – 1055 µC (Table 3.20).

Table 3.20 – Batch 3 catalysts: catalyst reference numbers, descriptions, and the charges associated with the hydrogen under-potential deposition regions

Catalyst		Palladium content / atom%	HUPD charge / µC	HUPD charge $(10 \text{ µg Pd})^{-1}$ / µC
ref no	description			
3336	(1.0% Pd, 0.0% Au)[∞]/G{3}	100	840	695
3339	(1.7% Pd, 0.6% Au)[5.4]/G{3}	85	1055	530
3338	(1.0% Pd, 0.4% Au)[4.9]/G{3}	83	645	535
3340	(1.0% Pd, 0.9% Au)[2.1]/G{3}	67	735	615
3341	(1.0% Pd, 1.7% Au)[1.1]/G{3}	52	725	610
3342	(1.0% Pd, 2.6% Au)[0.7]/G{3}	42	610	515
4270	(0.5% Pd, 1.8% Au)[0.5]/G{3}	35	680	1090
4269	(0.2% Pd, 1.8% Au)[0.2]/G{3}	18	125	495
3337	(0.0% Pd, 0.4% Au)[0.0]/G{3}	0	n/o	n/o

n/o = not observed

Stripping potentials of palladium and of gold-oxides for Batch 3 catalysts and the charges associated with each palladium-oxide stripping region are shown in Table 3.21. The potential required for palladium-oxide stripping varied from 0.62 V to 0.78 V. The gold-oxide stripping potential, where evident, also varied with composition. The charge associated with the removal of palladium-oxide varied from 250 μC to 1625 μC.

Table 3.21 – Batch 3 catalysts: catalyst reference numbers, descriptions, oxide stripping potentials, and the charges associated with the palladium-oxide stripping regions

Catalyst		Pd-O stripping potential / V	Au-O stripping potential / V	Pd-O stripping region charge / μC
ref no	description			
3336	(1.0% Pd, 0.0% Au)[∞]/G{3}	0.62	n/o	1520
3339	(1.7% Pd, 0.6% Au)[5.4]/G{3}	0.63	n/o	1625
3338	(1.0% Pd, 0.4% Au)[4.9]/G{3}	0.63	n/o	1115
3340	(1.0% Pd, 0.9% Au)[2.1]/G{3}	0.64	n/o	1395
3341	(1.0% Pd, 1.7% Au)[1.1]/G{3}	0.64	n/o	1530
3342	(1.0% Pd, 2.6% Au)[0.7]/G{3}	0.70	1.13	1345
4270	(0.5% Pd, 1.8% Au)[0.5]/G{3}	0.73	1.15	1420
4269	(0.2% Pd, 1.8% Au)[0.2]/G{3}	0.78	1.14	250
3337	(0.0% Pd, 0.4% Au)[0.0]/G{3}	n/o	n/o	n/o

n/o = not observed

The relationship between the charges associated with the hydrogen under-potential deposition regions and the palladium-oxide stripping regions for Batch 3 catalysts is shown in Figure 3.25. Once again, the points show scatter about a straight line which again shows a natural extrapolation to the origin. The gradient was observed to be 1.8.
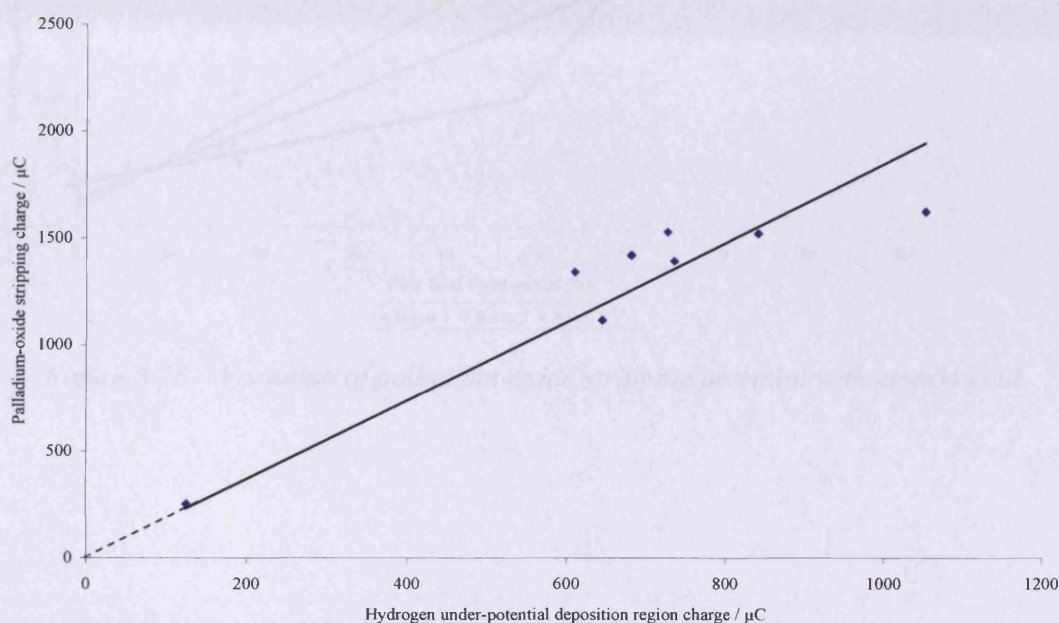
Figure 3.25 – Batch 3: charge associated with the hydrogen under-potential deposition region versus the charge associated with the stripping of palladium-oxide

The potentials required to remove palladium-oxide from Batch 1, Batch 2, and Batch 3 catalysts (Tables 3.17, 3.19, and, 3.21) are plotted as a function of atom% gold in Figure 3.26. The Figure shows the effect of gold composition on the potentials required to remove palladium-oxide from the surfaces of Batch 1, Batch 2, and Batch 3 catalysts. The results fall into three groups. Catalysts of Batches 1 and 2 show similar linear behaviour, which is interpreted as showing that systematic alloying occurred at these surfaces. The extent of alloying in Batch 2 catalysts was greater and more systematic than in Batch 1 catalysts.

105
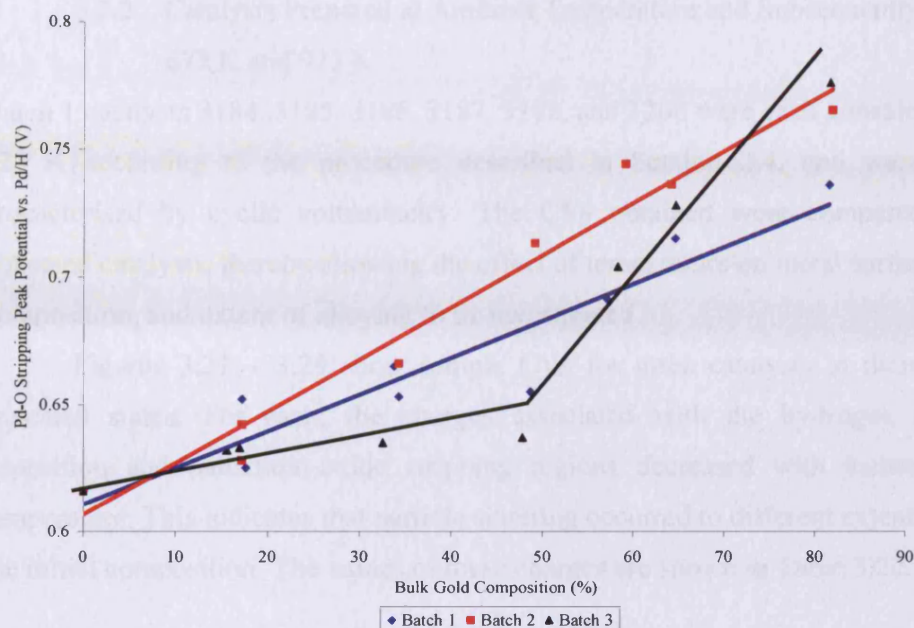
Figure 3.26 – Variation of palladium-oxide stripping potential with atom% gold

The interaction between palladium and gold in Batch 3 catalysts appears to be different. For the palladium-rich catalysts (50 – 80 atom% palladium) very little perturbation in the potential required for palladium-oxide stripping was observed, suggesting little surface alloy formation. However, for gold-rich catalysts, (> 50 atom% gold) significant variation in the potential required for palladium-oxide stripping was observed, suggesting the presence of palladium-gold surface alloys. Indeed, there is little or no distinction between catalysts of Batch 3 and those of Batches 1 and 2 in respect of the palladium-oxide stripping potentials observed at high bulk gold composition.

3.2.2 Catalysts Prepared at Ambient Temperature and Subsequently Annealed at 673 K and 923 K

Batch 1 catalysts 3184, 3185, 3186, 3187, 3188, and 3200 were each annealed at 673 K and 923 K according to the procedure described in Section 2.4, and were subsequently characterised by cyclic voltammetry. The CVs obtained were compared to those for unheated catalysts, thereby allowing the effect of temperature on metal surface area, surface composition, and extent of alloying to be investigated.

Figures 3.27 – 3.29 show sample CVs for three catalysts in their unheated and annealed states. For each, the charges associated with the hydrogen under-potential deposition and palladium-oxide stripping regions decreased with increasing treatment temperature. This indicates that particle sintering occurred to different extents depending on the initial composition. The values of these charges are shown in Table 3.22.
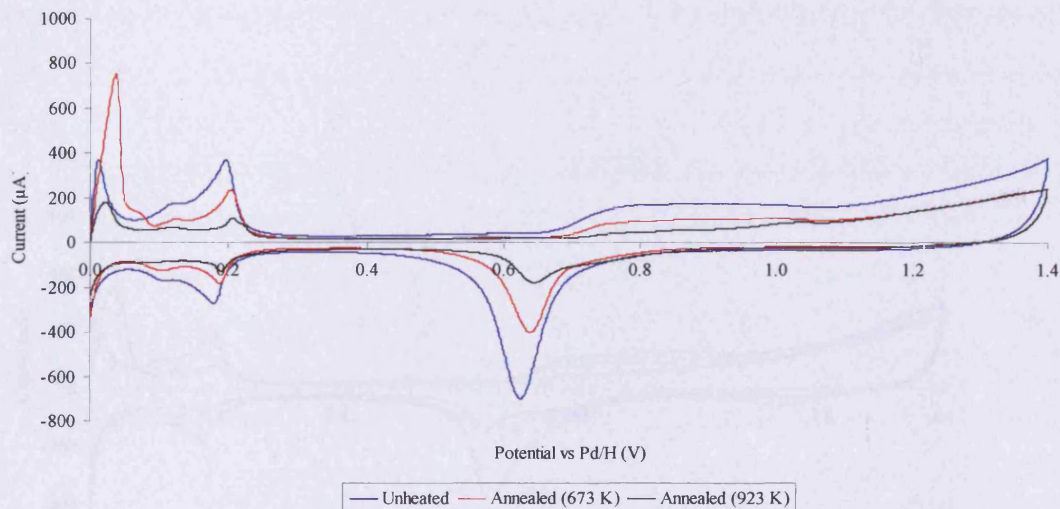

Figure 3.27 – Catalyst 3184, (1.0% Pd, 0.4% Au)[4.7]/G{1}: cyclic voltammograms of unheated and annealed catalysts
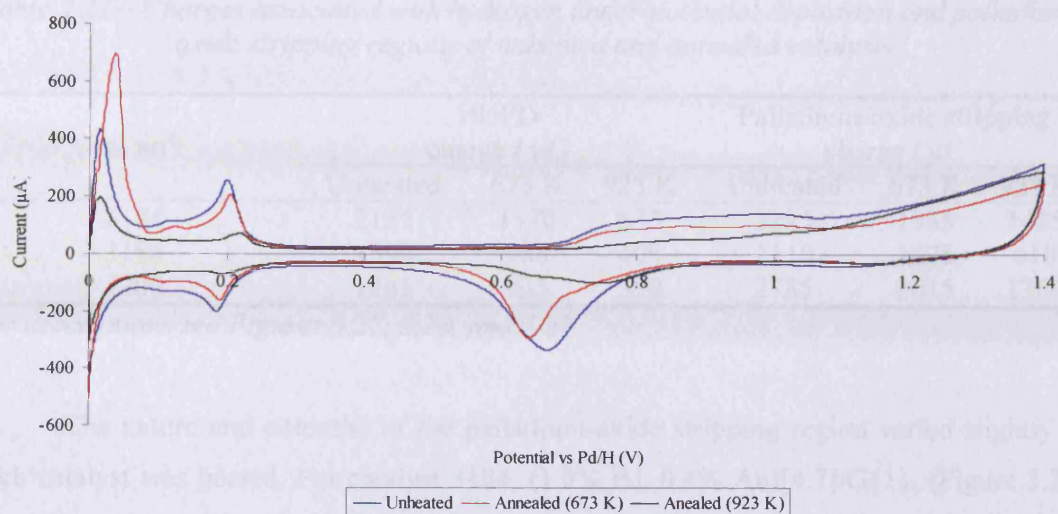
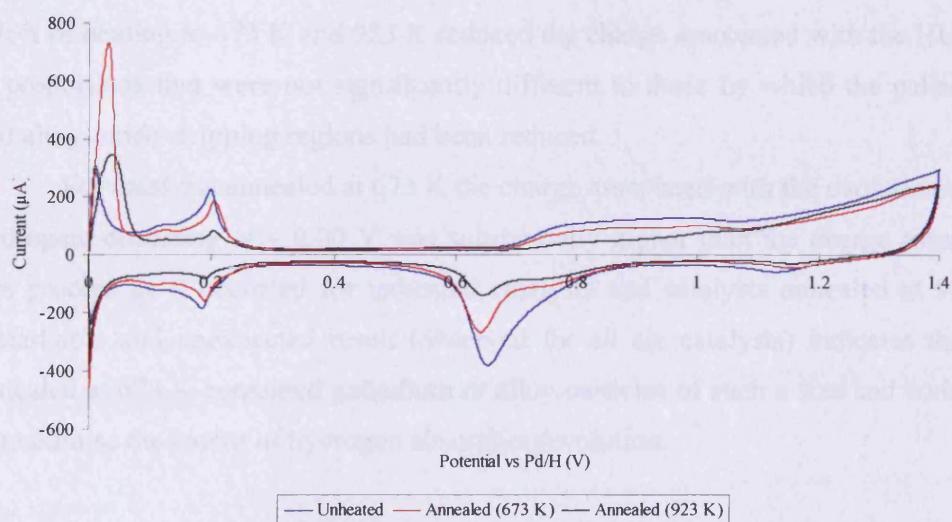*Figure 3.28 – Catalyst 3186, (1.0% Pd, 1.0% Au)[2.0]/G{1}: cyclic voltammograms of unheated and annealed catalysts*

Figure 3.29 – Catalyst 3200, (1.0% Pd, 0.9% Au)[1.9]/G{1}: cyclic voltammograms of unheated and annealed catalysts

108

Table 3.22 – Charges associated with hydrogen under-potential deposition and palladium-oxide stripping regions of unheated and annealed catalysts

ref no[a]	HUPD charge / μC			Palladium-oxide stripping charge / μC		
	Unheated	673 K	923 K	Unheated	673 K	923 K
3184	2125	1170	635	3285	1935	1435
3186	1390	980	400	2110	1975	610
3200	1265	935	350	2785	2015	1300

[a]*for descriptions see Figures 3.27, 3.28, and 3.29*

The nature and potential of the palladium-oxide stripping region varied slightly as each catalyst was heated. For catalyst 3184, (1.0% Pd, 0.4% Au)[4.7]/G{1}, (Figure 3.27) the palladium-oxide stripping potential increased after annealing at 673 K and increased further after annealing at 923 K. This indicates the formation of a greater concentration of surface alloyed phases during exposure to high temperatures.

For catalysts 3186, (1.0% Pd, 1.0% Au)[2.0]/G{1}, and 3200, (1.0% Pd, 0.9% Au)[1.9]/G{1}, (Figures 3.28 and 3.29 respectively) the unheated materials showed peaks representing both palladium-oxide stripping and alloy-oxide stripping. The alloy phases underwent preferential sintering at 673 K, leaving catalysts containing a relatively large fraction of palladium surface. Heating to 923 K caused major loss of palladium and alloy surface area, the situations being different in detail for each of the three catalysts. The effect of heating to 673 K and 923 K reduced the charge associated with the HUPD region, in proportions that were not significantly different to those by which the palladium-oxide and alloy-oxide stripping regions had been reduced.

For catalysts annealed at 673 K the charge associated with the evolution of absorbed hydrogen, occurring at ~ 0.00 V was substantially higher than the charge associated with this process as it occurred for unheated catalysts and catalysts annealed at 923 K. This remarkable and unexpected result (observed for all six catalysts) indicates that catalysts annealed at 673 K contained palladium or alloy particles of such a size and composition as to maximise the extent of hydrogen absorption/evolution.

3.3 Characterisation of Batch 1, Batch 2, and Batch 3 Catalysts: Palladium Surface Areas Determined by CO Chemisorption

Palladium surface areas of Batch 1, Batch 2, and Batch 3 catalysts were measured by CO chemisorption using the procedure set out in Section 2.6 (Table 3.23). Gold surface areas could not be measured as CO is only weakly adsorbed by gold under these conditions [5].

Table 3.23 – Palladium surface areas determined by CO chemisorption

Catalyst		Palladium surface area / $m^2\,g^{-1}$
ref no	description	
3182	(1.0% Pd, 0.0% Au)[∞]/G{1}	1.9
3185	(1.6% Pd, 0.6% Au)[4.8]/G{1}	1.3
3184	(1.0% Pd, 0.4% Au)[4.7]/G{1}	2.0
3186	(1.0% Pd, 1.0% Au)[2.0]/G{1}	1.9
3200	(1.0% Pd, 0.9% Au)[1.9]/G{1}	1.8
3187	(1.0% Pd, 1.7% Au)[1.1]/G{1}	0.7
3188	(1.0% Pd, 2.5% Au)[0.7]/G{1}	2.1
4266	(0.5% Pd, 1.8% Au)[0.5]/G{1}	1.1
4265	(0.2% Pd, 1.7% Au)[0.2]/G{1}	0.5
3183	(0.0% Pd, 0.4% Au)[0.0]/G{1}	0.0
3329	(1.0% Pd, 0.0% Au)[∞]/G{2}	2.2
3331	(1.0% Pd, 0.4% Au)[4.8]/G{2}	1.3
3332	(1.7% Pd, 0.6% Au)[4.8]/G{2}	2.6
3333	(1.0% Pd, 1.0% Au)[1.9]/G{2}	1.5
3334	(1.0% Pd, 1.8% Au)[1.0]/G{2}	1.9
3335	(1.0% Pd, 2.7% Au)[0.7]/G{2}	1.3
4268	(0.5% Pd, 1.8% Au)[0.6]/G{2}	1.0
4267	(0.2% Pd, 1.8% Au)[0.2]/G{2}	0.4
3330	(0.0% Pd, 0.4% Au)[0.0]/G{2}	0.0
3336	(1.0% Pd, 0.0% Au)[∞]/G{3}	0.5
3339	(1.7% Pd, 0.6% Au)[5.4]/G{3}	0.5
3338	(1.0% Pd, 0.4% Au)[4.9]/G{3}	0.5
3340	(1.0% Pd, 0.9% Au)[2.1]/G{3}	0.8
3341	(1.0% Pd, 1.7% Au)[1.1]/G{3}	0.7
3342	(1.0% Pd, 2.6% Au)[0.7]/G{3}	0.8
4270	(0.5% Pd, 1.8% Au)[0.5]/G{3}	0.6
4269	(0.2% Pd, 1.8% Au)[0.2]/G{3}	0.2
3337	(0.0% Pd, 0.4% Au)[0.0]/G{3}	0.0

These chemisorption measurements (Table 3.23) show that palladium surface area was not simply proportional to palladium loading. For example, catalysts 3184 and 3185 have palladium loadings of 1.0% and 1.6% respectively but palladium surface areas of 2.0 m^2 g^{-1} and 1.3 m^2 g^{-1}. In contrast, catalysts 3331 and 3332 have palladium loadings of 1.0% and 1.7% respectively but palladium surface areas of 1.3 m^2 g^{-1} and 2.6 m^2 g^{-1}. This effect may be due to the extent of mixing or alloying between palladium and gold at the catalyst surface.

3.4 Characterisation of Batch 1, Batch 2, and Batch 3 Catalysts: Propan-2-ol Electrooxidation

Propan-2-ol electrooxidation in an electrochemical cell, under basic conditions, was used as a probe to estimate metal surface area, palladium/gold composition, and extent of alloying. This was achieved by mounting a catalyst onto a working electrode and recording a CV between the potential limits of 0.00 V and 1.40 V, using an electrolyte consisting of 0.5 mol dm^{-3} propan-2-ol and 0.5 mol dm^{-3} sodium hydroxide.

Propan-2-ol electrooxidation was preformed over Batch 1, Batch 2, and Batch 3 catalysts. Distinct anodic peaks for oxidation on palladium and on gold were detected in the forward sweep of the CV. Potentials for peak maxima varied depending on palladium/gold composition.

3.4.1 Propan-2-ol Electrooxidation over Batch 1, Batch 2, and Batch 3 Catalysts

Figure 3.30 shows profiles for propan-2-ol electrooxidation over Batch 1 catalysts. The profiles (for palladium and palladium-gold catalysts) are characterised by a single peak for the electrooxidation of propan-2-ol over palladium. The charges generated during these electrooxidations ranged from 55 – 515 mC (Table 3.24). The absence of a peak for propan-2-ol electrooxidation of over gold indicated that the surface area of gold was very small in these catalysts. The electrooxidation profile for catalyst 3183, (0.0% Pd, 0.4% Au)[0.0]/G{1}, possessed a single peak for propan-2-ol electrooxidation of over gold for which the corresponding charge was 25 mC (Table 3.24).

Figure 3.30 – Propan-2-ol electrooxidation profiles over Batch 1 catalysts
(for catalyst descriptions, see Table 3.24)

Table 3.24 – Batch 1 catalysts: charges associated with the electrooxidation of propan-2-ol over palladium and gold

Catalyst		Charge: oxidation over palladium / mC	Charge: oxidation over gold / mC
ref no	description		
3182	(1.0% Pd, 0.0% Au)[∞]/G{1}	230	n/o
3185	(1.6% Pd, 0.6% Au)[4.8]/G{1}	120	n/o
3184	(1.0% Pd, 0.4% Au)[4.7]/G{1}	330	n/o
3186	(1.0% Pd, 1.0% Au)[2.0]/G{1}	300	n/o
3200	(1.0% Pd, 0.9% Au)[1.9]/G{1}	515	n/o
3187	(1.0% Pd, 1.7% Au)[1.1]/G{1}	55	n/o
3188	(1.0% Pd, 2.5% Au)[0.7]/G{1}	440	n/o
3183	(0.0% Pd, 0.4% Au)[0.0]/G{1}	n/o	25

n/o = not observed

Profiles for the electrooxidation of propan-2-ol over Batch 2 catalysts are shown in Figure 3.31. Each profile is characterised by a single peak for the electrooxidation of propan-2-ol over palladium. The associated charges varied between 185 mC and 535 mC (Table 3.25). No peak for propan-2-ol electrooxidation over gold was observed.
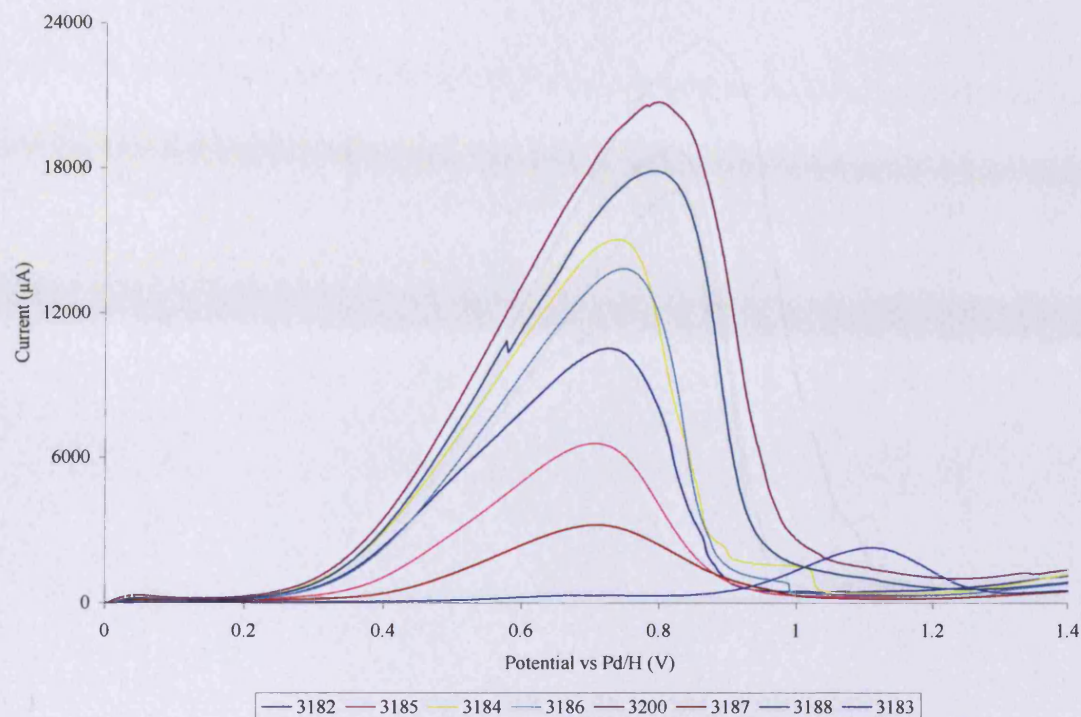
*Figure 3.31 – Propan-2-ol electrooxidation profiles over Batch 2 catalysts
(for catalyst descriptions, see Table 3.25)*

*Table 3.25 – Batch 2 catalysts: charges associated with the electrooxidation of propan-2-ol
over palladium and gold*

Catalyst		Charge: oxidation over palladium / mC	Charge: oxidation over gold / mC
ref no	description		
3329	(1.0% Pd, 0.0% Au)[∞]/G{2}	340	n/o
3331	(1.0% Pd, 0.4% Au)[4.8]/G{2}	185	n/o
3332	(1.7% Pd, 0.6% Au)[4.8]/G{2}	460	n/o
3333	(1.0% Pd, 1.0% Au)[1.9]/G{2}	365	n/o
3334	(1.0% Pd, 1.8% Au)[1.0]/G{2}	390	n/o
3335	(1.0% Pd, 2.7% Au)[0.7]/G{2}	535	n/o
3330	(0.0% Pd, 0.4% Au)[0.0]/G{2}	n/o	n/o

n/o = not observed

Profiles for propan-2-ol electrooxidation over Batch 3 catalysts are shown in Figure 3.32. Each profile is characterised by a single peak for the electrooxidation of propan-2-ol over palladium and the charges generated during each electrooxidation are shown in Table 3.26. Again, no peak was detected for the electrooxidation of propan-2-ol over gold.
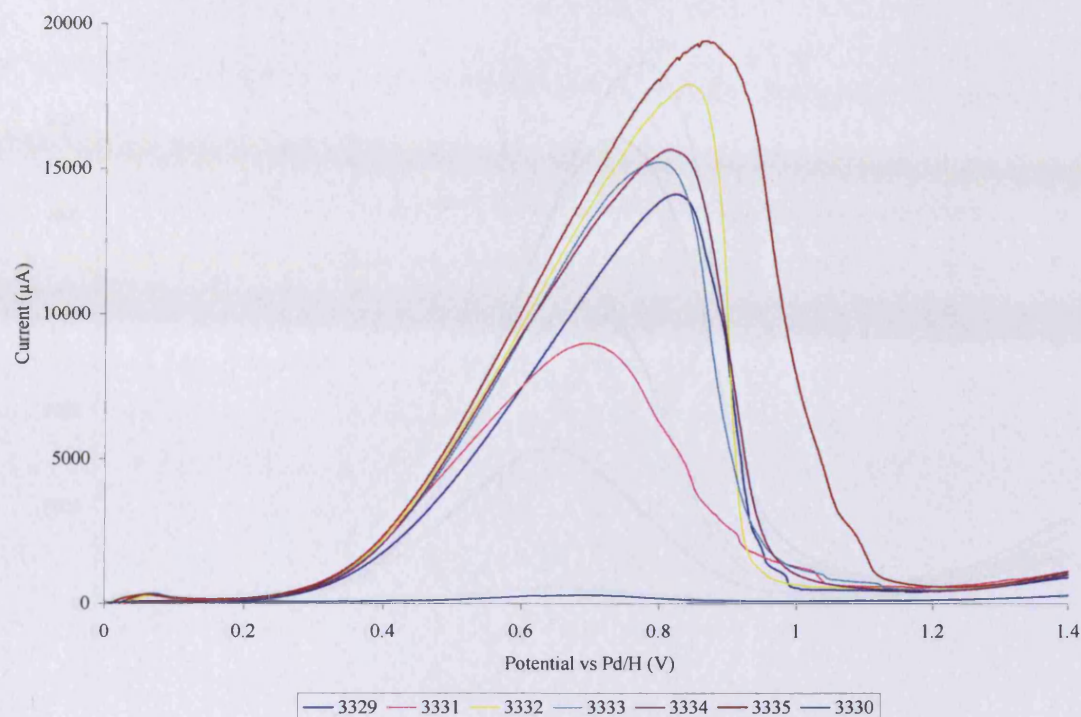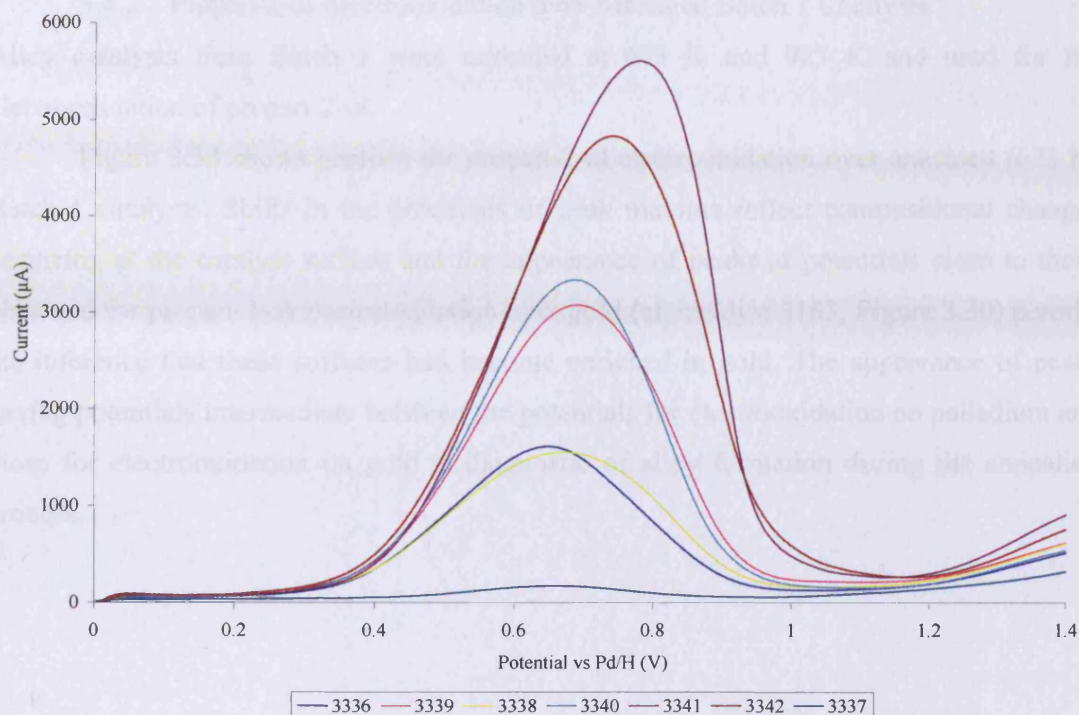
*Figure 3.32 – Propan-2-ol electrooxidation profiles over Batch 3 catalysts
(for catalyst descriptions, see Table 3.26)*

*Table 3.26 – Batch 3 catalysts: charges associated with the electrooxidation of propan-2-ol
over palladium and gold*

Catalyst		Charge: oxidation over palladium / mC	Charge: oxidation over gold / mC
ref no	description		
3336	(1.0% Pd, 0.0% Au)[∞]/G{3}	25	n/o
3339	(1.7% Pd, 0.6% Au)[5.4]/G{3}	50	n/o
3338	(1.0% Pd, 0.4% Au)[4.9]/G{3}	25	n/o
3340	(1.0% Pd, 0.9% Au)[2.1]/G{3}	55	n/o
3341	(1.0% Pd, 1.7% Au)[1.1]/G{3}	110	n/o
3342	(1.0% Pd, 2.6% Au)[0.7]/G{3}	90	n/o
3337	(0.0% Pd, 0.4% Au)[0.0]/G{3}	n/o	n/o

n/o = not observed

114

3.4.2 Propan-2-ol Electrooxidation over Annealed Batch 1 Catalysts

Alloy catalysts from Batch 1 were annealed at 673 K and 923 K and used for the electrooxidation of propan-2-ol.

Figure 3.33 shows profiles for propan-2-ol electrooxidation over annealed (673 K) Batch 1 catalysts. Shifts in the potentials of peak maxima reflect compositional changes occurring at the catalyst surface and the appearance of peaks at potentials close to those observed for propan-2-ol electrooxidation over gold (cf. catalyst 3183, Figure 3.30) permits the inference that these surfaces had become enriched in gold. The appearance of peaks having potentials intermediate between the potentials for electrooxidation on palladium and those for electrooxidation on gold is diagnostic of alloy formation during the annealing process.

Figure 3.33 – Propan-2-ol electrooxidation profiles over Batch 1 catalysts annealed at 673 K (for catalyst descriptions, see Table 3.24)

Figure 3.34 shows profiles for propan-2-ol over annealed (923 K) Batch 1 catalysts. Further compositional changes were detected by the appearance of peaks at potentials intermediate between those for oxidation over palladium and over gold. The profile for catalyst 3188 shows the clear presence of palladium, palladium-gold alloy, and gold surfaces, the first two in comparable proportions.

Thus, it is clear that the process of annealing, especially at 923 K, resulted in substantial changes to surface composition, and possibly also to the selectivity of the reaction (which was not investigated).
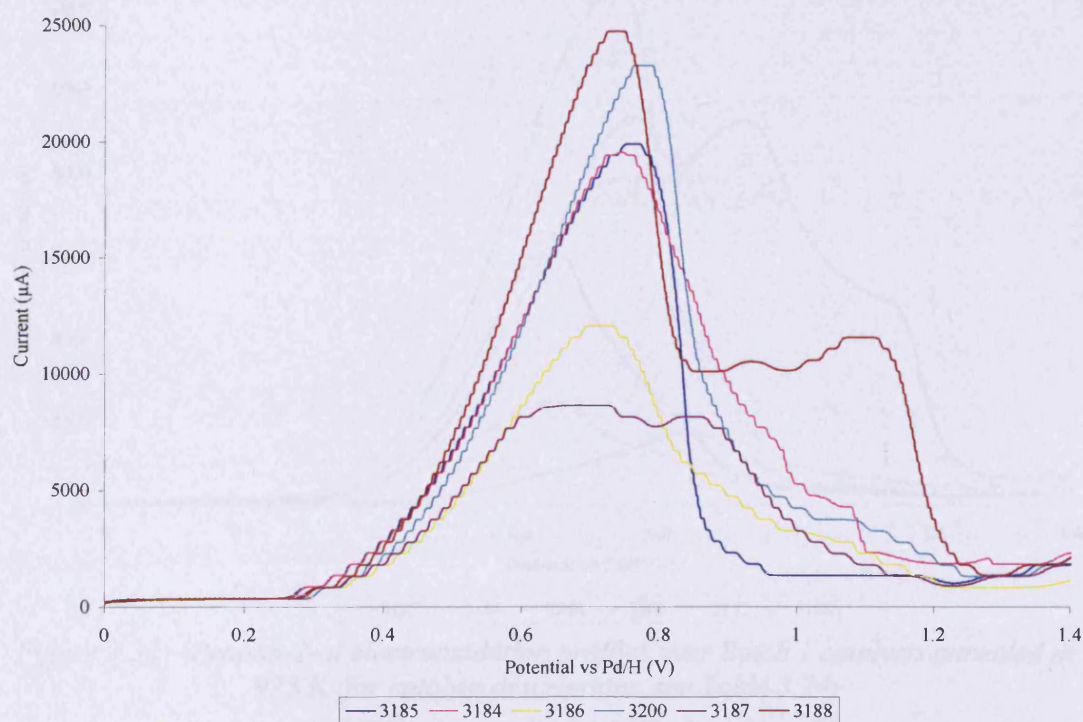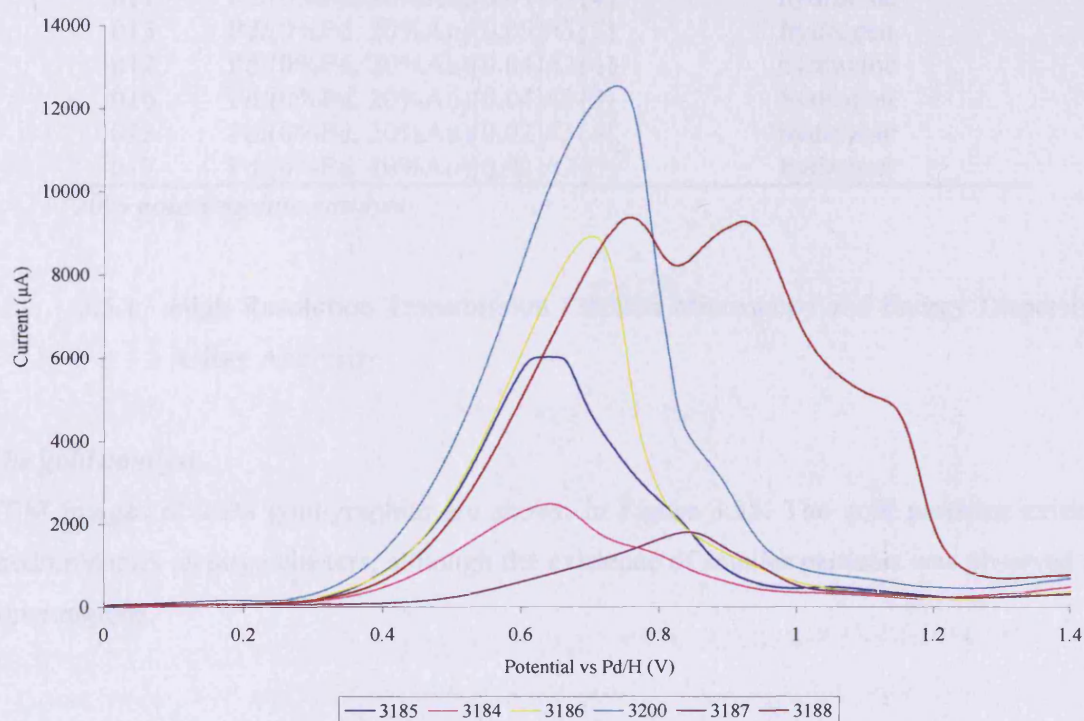

Figure 3.34 – Propan-2-ol electrooxidation profiles over Batch 1 catalysts annealed at 923 K (for catalyst descriptions, see Table 3.24)

3.5   Modification of a 20% Gold/graphite Catalyst by Palladisation

The preparation of 20% gold/graphite catalyst was described in Section 2.1.2, and of its palladised derivatives in Section 2.1.3. Catalyst reference numbers, descriptions, and palladium reduction methods are re-iterated in Table 3.27 for convenience.

Table 3.27 – Catalyst reference numbers, descriptions, and the method of palladium precursor reduction

Catalyst		Palladium reduction method
ref no	description	
006[a]	(0% Pd, 20%Au)/G	–
007	Pd/(0%Pd, 20%Au)[1.39]/G{4}	hydrazine
008	Pd/(0%Pd, 20%Au)[0.93]/G{4}	hydrazine
009	Pd/(0%Pd, 20%Au)[0.46]/G{4}	hydrazine
010	Pd/(0%Pd, 20%Au)[0.19]/G{4}	hydrazine
014	Pd/(0%Pd, 20%Au)[0.19]/G{5}	hydrogen
011	Pd/(0%Pd, 20%Au)[0.09]/G{4}	hydrazine
015	Pd/(0%Pd, 20%Au)[0.09]/G{5}	hydrogen
012	Pd/(0%Pd, 20%Au)[0.04]/G{4}	hydrazine
016	Pd/(0%Pd, 20%Au)[0.04]/G{5}	hydrogen
013	Pd/(0%Pd, 20%Au)[0.02]/G{4}	hydrazine
017	Pd/(0%Pd, 20%Au)[0.02]/G{5}	hydrogen

[a]20% gold/graphite catalyst

3.5.1   High Resolution Transmission Electron Microscopy and Energy Dispersive X-Ray Analysis

The gold catalyst

TEM images of 20% gold/graphite are shown in Figure 3.35. The gold particles existed predominantly as large clusters, although the existence of smaller particles was observed in some regions.
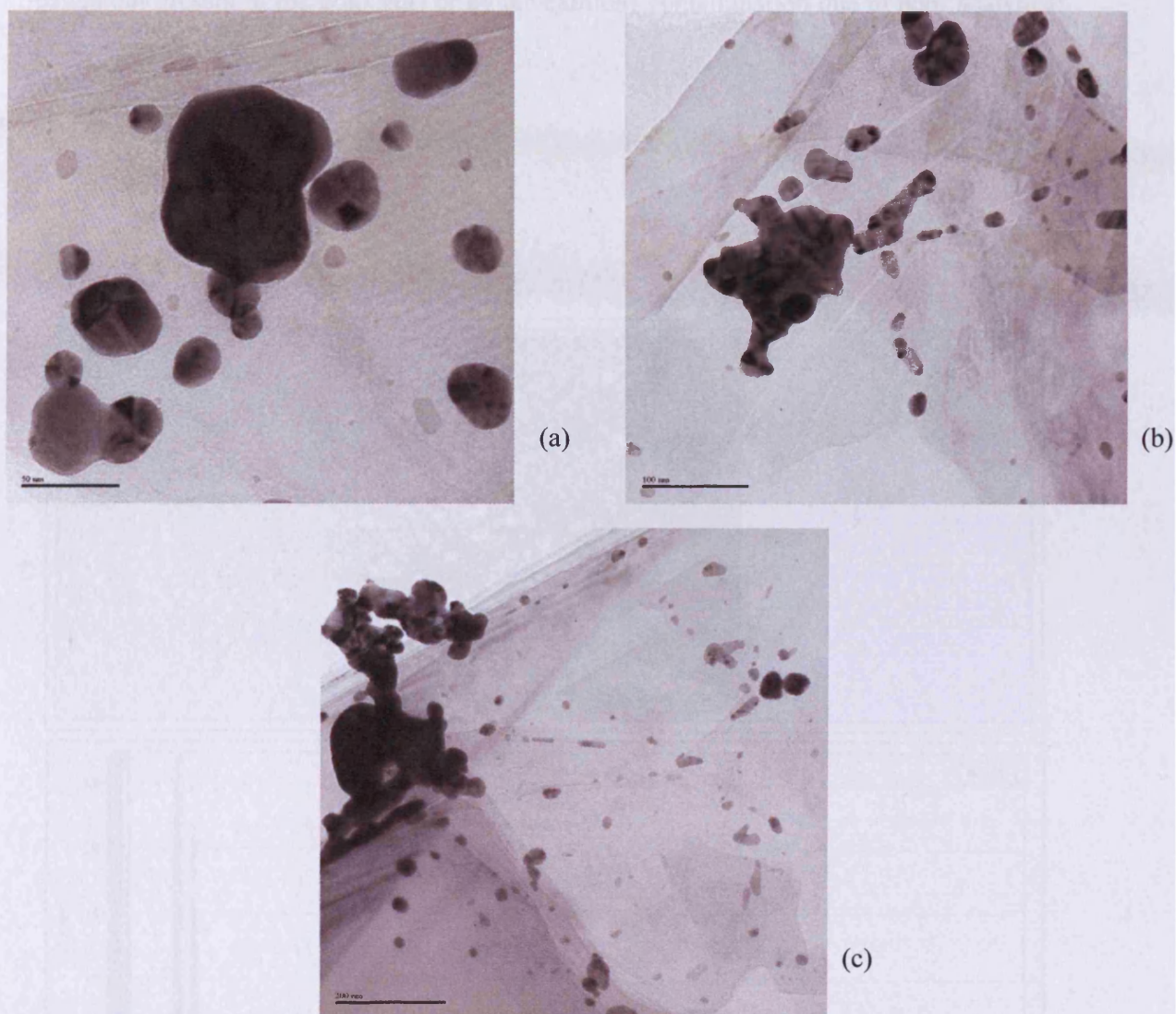
*Figure 3.35 – TEM images of catalyst 006, (0% Pd, 20%Au)/G.
(The marker bar represents 50, 100, and 200 nm in (a), (b), and, (c) respectively)*

Energy dispersive X-ray analysis of a region and an individual particle contained in (0% Pd, 20%Au)/G are shown in Figures 3.36 and 3.37 respectively. In each case the intensity of the lines attributable to gold transitions confirmed the presence of gold. Lines are present in both Figure 3.36 and 3.37 attributable to copper and palladium. The catalysts were mounted on a copper grid and the detection of copper is assigned to the presence of the grid. The existence of traces of palladium can only be explained as indicating a small degree of contamination which occurred either in the catalyst preparation stage (i.e.

118

palladium present in the gold salt) or by adventitious contamination due to poor analytical procedures.
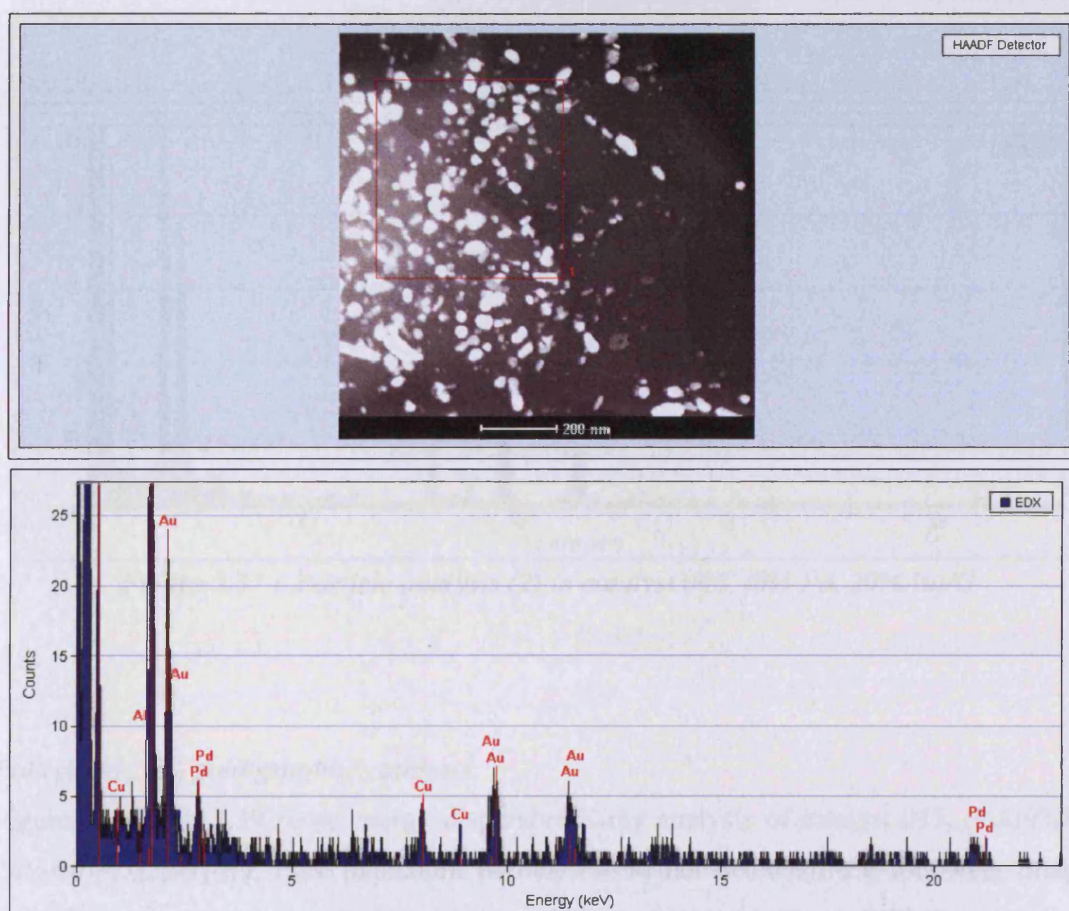
Figure 3.36 – Particle analysis (1) in catalyst 006, (0% Pd, 20%Au)/G
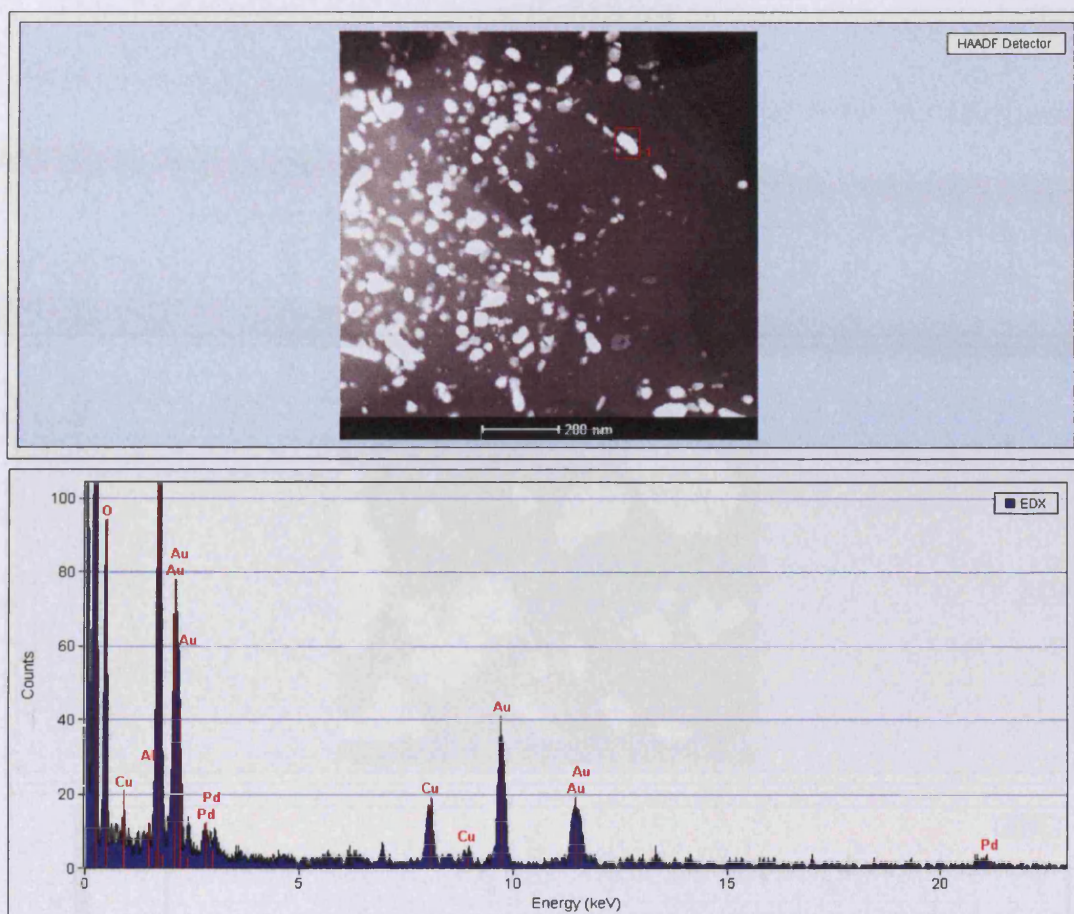
Figure 3.37 – Particle analysis (2) in catalyst 006, (0% Pd, 20%Au)/G

Palladised 20% gold/graphite catalysts

Figures 3.28 and 3.39 show energy dispersive X-ray analysis of catalyst 013, (Pd/(0%Pd, 20%Au)[0.02]/G{4}). Pure palladium particles were not detected; the following images show that palladium was only found in co-existence with gold. Figure 3.38 shows a single particle having an approximate area of 900 nm^2 (30 nm x 30 nm). The particle contained a predominance of gold with only a trace of palladium. Figure 3.39 shows an area of 250000 nm^2 (500 nm x 500 nm) which contained particles composed mostly of gold with only very small traces of palladium.
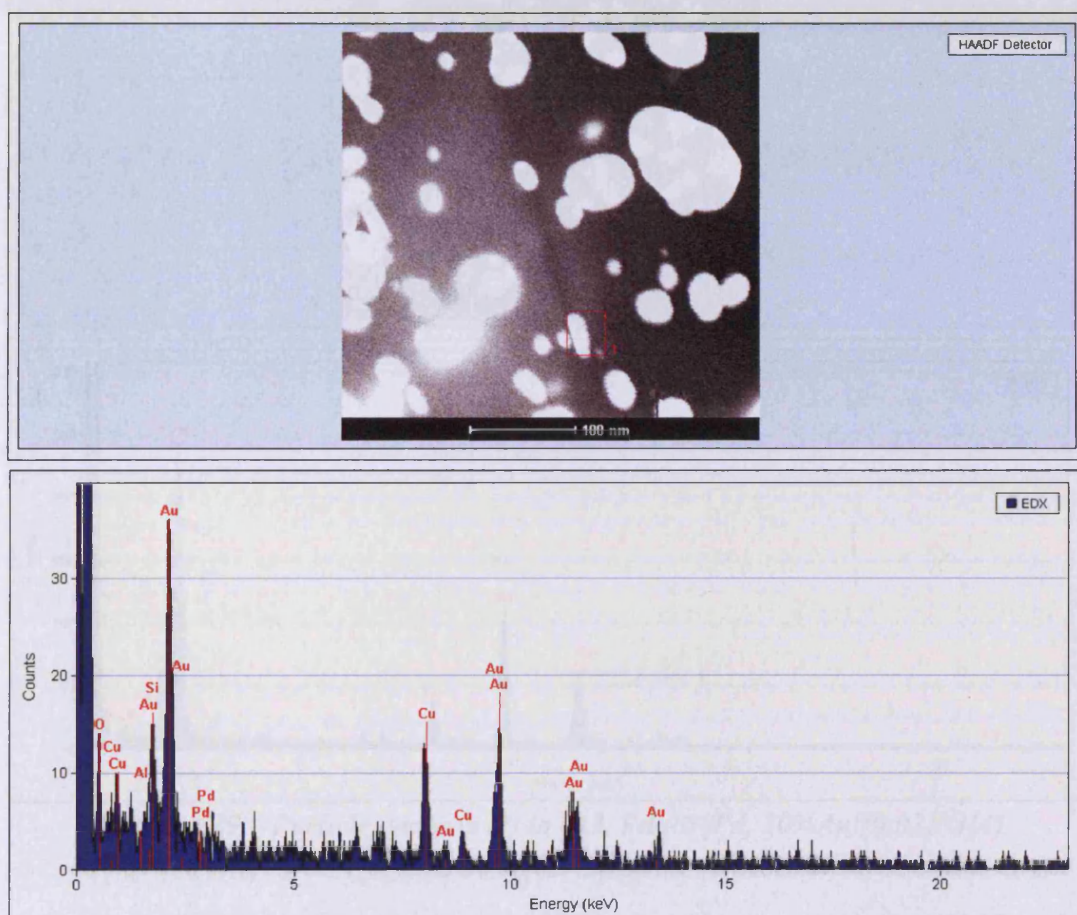
Figure 3.38 – Particle analysis (1) in catalyst 013, Pd/(0%Pd, 20%Au)[0.02]/G{4}
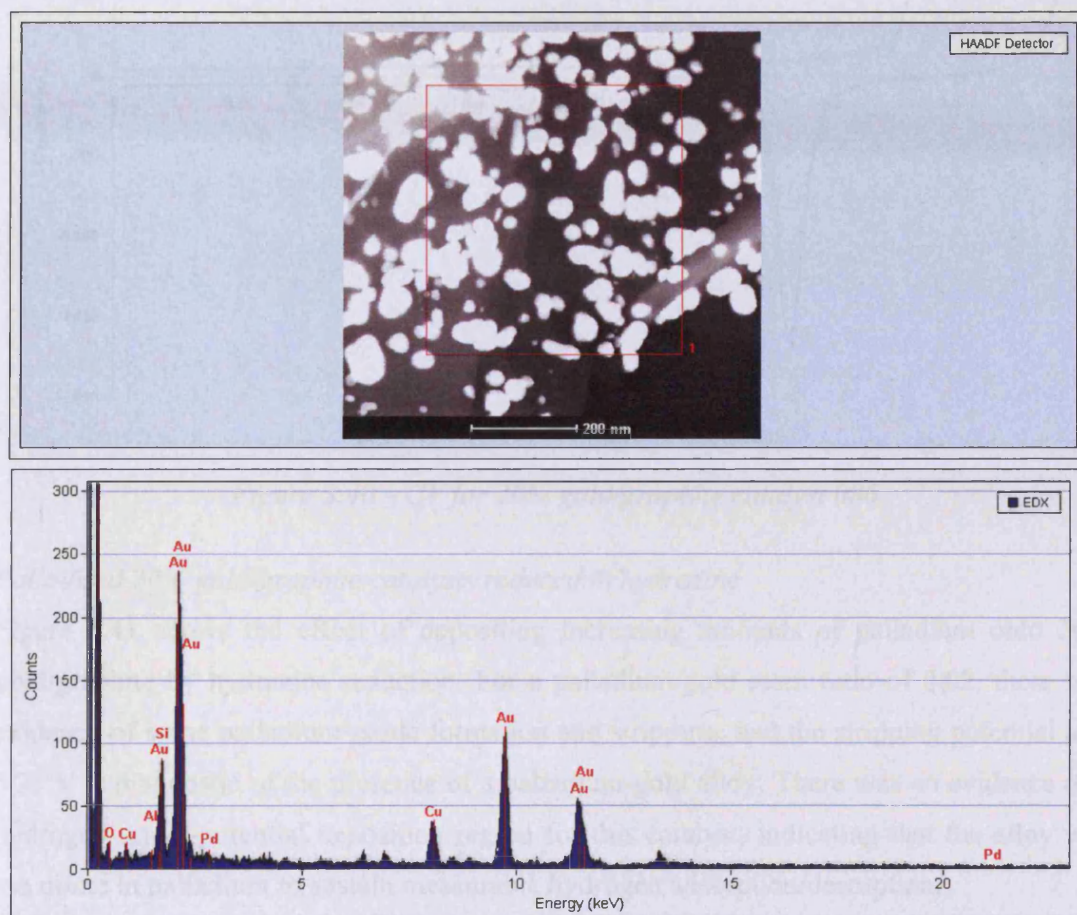
Figure 3.39 – Particle analysis (2) in 013, Pd/(0%Pd, 20%Au)[0.02]/G{4}

3.5.2   Cyclic Voltammetry

CVs for these catalysts are shown in Figures 3.40 – 3.42. 20% gold/graphite (Figure 3.40) showed features associated with gold-oxide formation during the forward sweep and gold-oxide stripping during the reverse sweep. The absence of a hydrogen under-potential deposition region was a reminder that hydrogen is not adsorbed by gold.
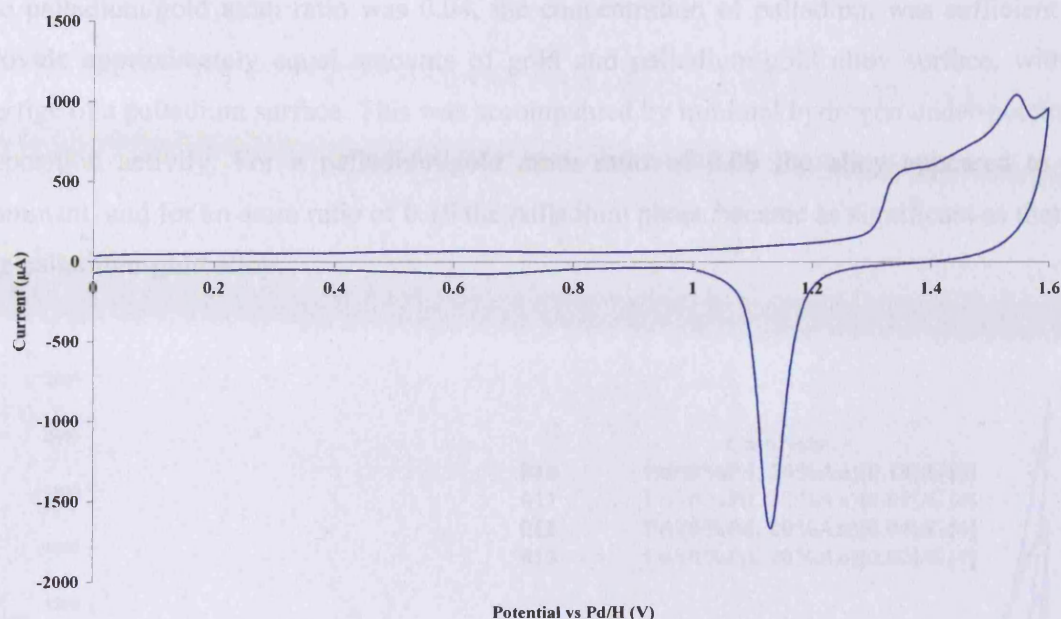
Figure 3.40 – CV for 20% gold/graphite catalyst 006

Palladised 20% gold/graphite catalysts reduced in hydrazine

Figure 3.41 shows the effect of depositing increasing amounts of palladium onto 20% gold/graphite by hydrazine reduction. For a palladium/gold atom ratio of 0.02, there was evidence of some palladium-oxide formation and stripping, and the stripping potential at ~ 0.75 V is diagnostic of the presence of a palladium-gold alloy. There was no evidence of a hydrogen under-potential deposition region for this catalyst, indicating that the alloy was too dilute in palladium to sustain measurable hydrogen adsorption/desorption.

For catalysts having palladium/gold atom ratios of 0.04, 0.09, and 0.19 the CVs showed a decreasing intensity for the gold-oxide stripping peak and increasing intensities for the palladium-oxide and alloy-oxide stripping peaks at ~ 0.58 V and ~ 0.75 V respectively. Values for the charges associated with these regions are given in Table 3.28; a deconvolution method was used to arrive at values for the palladium-oxide and alloy-oxide stripping regions, and the values are to be regarded as approximate. These results are consistent with the formation, in the first instance, of a palladium-gold alloy, and later, as the palladium/gold ratio increased, the formation of a pure palladium phase. The very small contributions attributable to hydrogen absorption/evolution and adsorption/desorption indicates that these alloy surfaces showed low reactivity with respect to hydrogen. When

the palladium/gold atom ratio was 0.04, the concentration of palladium was sufficient to provide approximately equal amounts of gold and palladium-gold alloy surface, with a vestige of a palladium surface. This was accompanied by minimal hydrogen under-potential deposition activity. For a palladium/gold atom ratio of 0.09 the alloy appeared to be dominant, and for an atom ratio of 0.19 the palladium phase became as significant as that of the palladium-gold alloy.

Figure 3.41 – CVs for palladised catalyst 006, (0%Pd, 20%Au)/G, in which the palladium precursor had been reduced by hydrazine

Three catalysts were prepared having palladium/gold atom ratios of 0.46, 0.93, and 1.39. The CVs, shown in Figure 3.42, contained a hydrogen under-potential deposition region and an oxide formation region in the forward sweep. In the reverse sweep there was a vestige of a gold-oxide stripping region, a modest alloy-oxide stripping region, and a strong palladium-oxide stripping region. These catalysts predominantly contained palladium in the surface with some palladium-gold alloy; the extent of any gold surface was minimal.

Catalysts
007 Pd/(0%Pd, 20%Au)[1.39]/G{4}
008 Pd/(0%Pd, 20%Au)[0.93]/G{4}
009 Pd/(0%Pd, 20%Au)[0.46]/G{4}

Potential vs Pd/H (V)

Figure 3.42 – CVs for heavily-palladised catalyst 006, (0%Pd, 20%Au)/G, in which the palladium precursor had been reduced by hydrazine

Table 3.28 – Palladised 20% gold/graphite catalysts prepared by hydrazine reduction; charges associated with various stripping regions

Catalyst		Charges associated with stripping regions /µC		
ref no	description	Au-O[a]	alloy-O[b]	Pd-O[c]
007	Pd/(0%Pd, 20%Au)[1.39]/G{4}	n/o	5200	6860
008	Pd/(0%Pd, 20%Au)[0.93]/G{4}	680	5330	4015
009	Pd/(0%Pd, 20%Au)[0.46]/G{4}	n/o	5570	4155
010	Pd/(0%Pd, 20%Au)[0.19]/G{4}	880	3340	3270
011	Pd/(0%Pd, 20%Au)[0.09]/G{4}	695	3205	85
012	Pd/(0%Pd, 20%Au)[0.04]/G{4}	1550	2160	120
013	Pd/(0%Pd, 20%Au)[0.02]/G{4}	4900	500	v. small

[a]*peak located at ~ 1.10 V*
[b]*peak located at ~ 0.75 V*
[c]*peak located at ~ 0.58 V*
n/o = not observed

Palladised 20% gold/graphite reduced with hydrogen

Figure 3.43 shows the effect of palladium deposition over 20% gold/graphite by hydrogen reduction. At all palladium/gold atom ratios there was evidence for the formation of surface oxides and for the stripping of gold, alloy, and palladium-oxides at ~ 1.15 V, ~ 0.75 V, and

~ 0.58 V respectively. A reduction in the charge associated with gold-oxide stripping was also observed as the palladium/gold atom ratio increased. There was no evidence of a hydrogen under-potential deposition region, again suggesting that even the alloy having a palladium/gold atom ratio = 0.19 did not sustain measurable hydrogen sorption.

For catalysts having higher palladium/gold atom ratios, gold-oxide, alloy-oxide, and palladium-oxide were detected in the reverse sweeps. Variations in charges associated with the stripping of these were observed (Table 3.29); they did not vary systematically with palladium/gold atom ratio. It therefore appears that hydrazine reduction provided catalysts with better graded properties than was evident with hydrogen reduction. Hydrazine may therefore be regarded as the better reductant for the purpose of forming alloy catalysts.
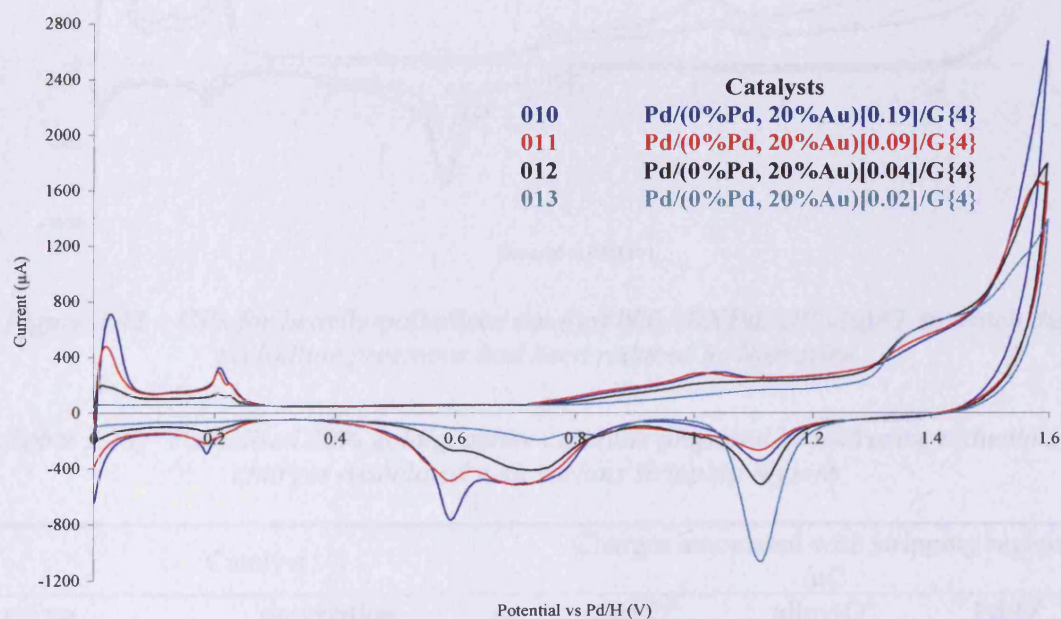

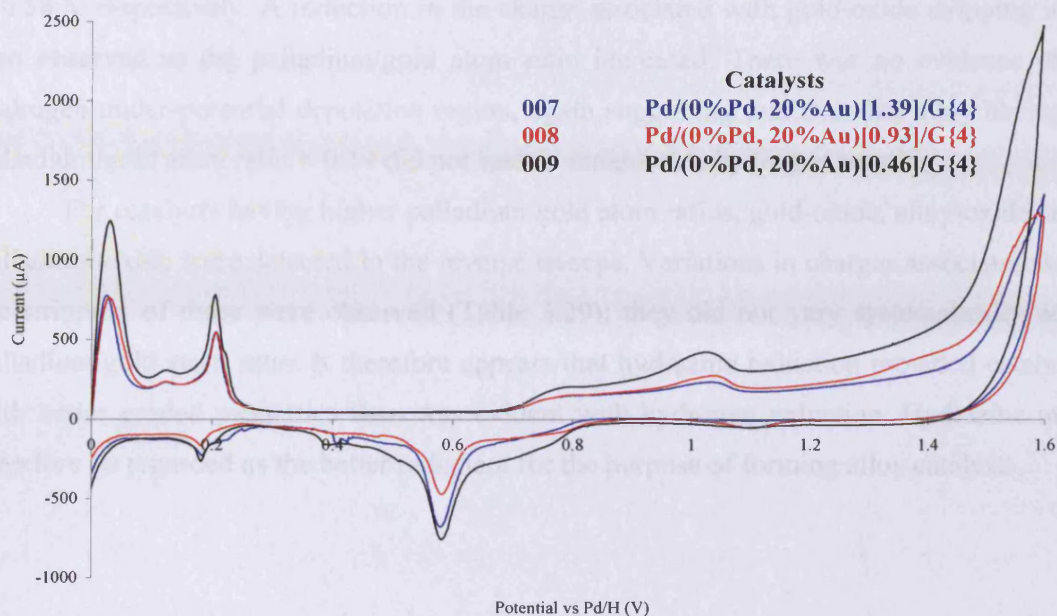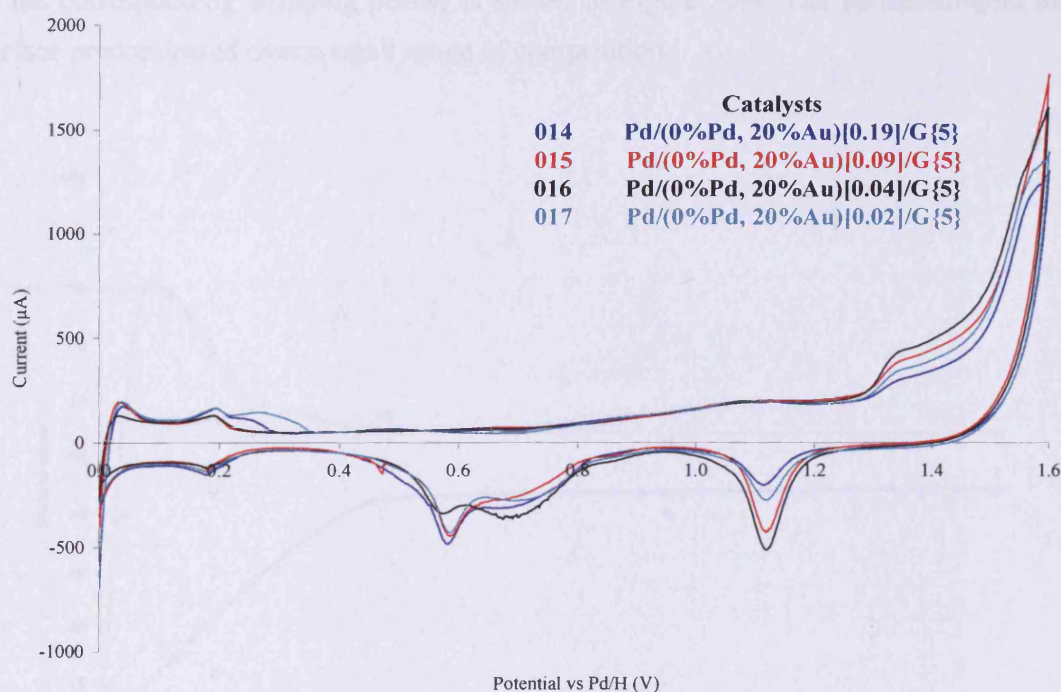*Figure 3.43 – CVs for palladised catalyst 006, (0%Pd, 20%Au)/G, in which the palladium precursor had been reduced by hydrogen*

*Table 3.29 – Palladised 20% gold/graphite catalysts prepared by hydrogen reduction;
charges associated with various stripping regions*

Catalyst		Charges associated with stripping regions /µC		
ref no	description	Au-O[a]	alloy-O[b]	Pd-O[c]
014	Pd/(0%Pd, 20%Au)[0.19]/G{5}	1055	3650	1800
015	Pd/(0%Pd, 20%Au)[0.09]/G{5}	1150	3090	680
016	Pd/(0%Pd, 20%Au)[0.04]/G{5}	1655	2550	480
017	Pd/(0%Pd, 20%Au)[0.02]/G{5}	985	3580	1920

[a]*peak located at ~ 1.10 V*
[b]*peak located at ~ 0.75 V*
[c]*peak located at ~ 0.58 V*

The manner in which the extents of the gold, palladium-gold, and palladium
surfaces varied with composition over the full range of catalysts (as judged from the areas
of the corresponding stripping peaks) is shown in Figure 3.44. The palladium-gold alloy
surface predominated over a small range of composition.
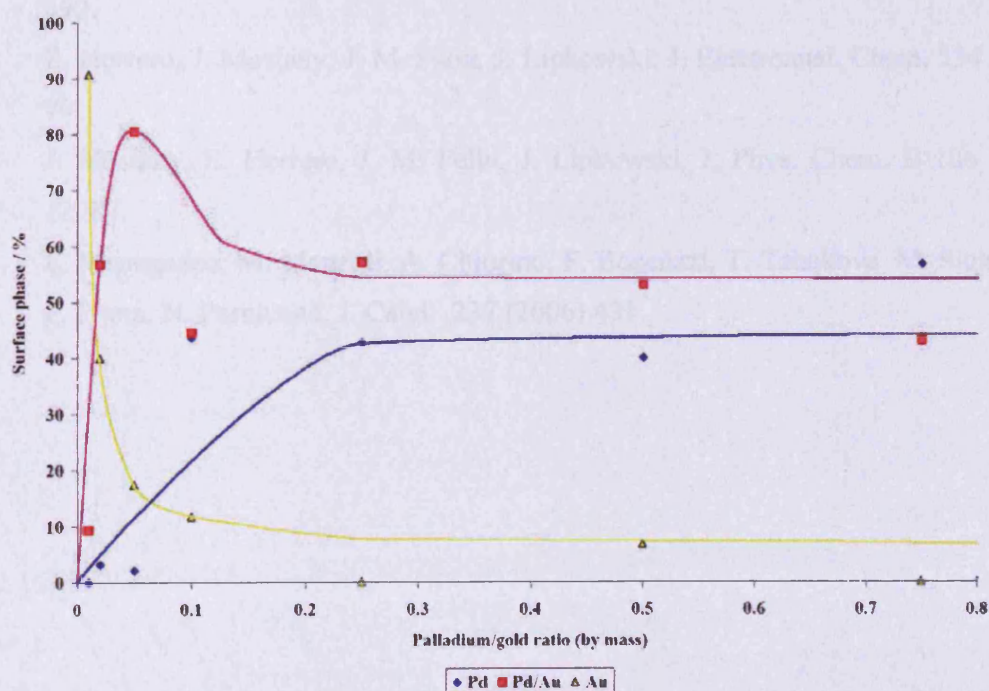
*Figure 3.44 – Variation of the abundance of surface phases with palladium/gold ratio, as
determined from the charges associated with the stripping regions presented in Table 3.28*

3.5.3 Conclusions

The results obtained by cyclic voltammetry and energy dispersive X-ray analysis show that the phases formed when palladium is reduced over a supported-gold catalyst are dependant upon the reducing agent used. In each case palladium, and palladium-gold particles were formed, and cyclic voltammetry suggests that palladium reduction by hydrazine favours surface-alloy formation and minimises the formation of pure palladium particles. When surface alloy formation was maximised, the reduction of further amounts of palladium contributed to the formation of pure palladium particles. The reduction of palladium with hydrogen led to the simultaneous formation of palladium and palladium-gold alloy particles.

3.6   References

[1]   A. F. Carley, Personal Communication, Cardiff University, 2006.

[2]   M. C. Santos, D. W. Miwa, S. A. S. Machado, Electrochem. Commun. 2 (2000) 692.

[3]   E. Herrero, J. Mostany, J. M. Feliu, J. Lipkowski, J. Electroanal. Chem. 534 (2002) 79.

[4]   J. Mostany, E. Herrero, J. M. Feliu, J. Lipkowski, J. Phys. Chem. B 106 (2002) 12787.

[5]   F. Menegazzo, M. Manzoli, A. Chiorino, F. Boccuzzi, T. Tabakova, M. Signoretto, F. Pinna, N. Pernicone, J. Catal. 237 (2006) 431.

CHAPTER 4
ETCHING AND PLATING OF
GRAPHITE-SUPPORTED
PALLADIUM-GOLD CATALYSTS

4.1 Etching by Exposure of Supported Palladium-Gold Catalysts to Solutions Containing Acetic Acid

Vinyl acetate is synthesised by the reaction between ethylene, acetic acid, and oxygen over palladium-gold catalysts in the presence of potassium acetate as a promoter. Therefore, palladium-gold catalysts were treated with solutions containing acetic acid and the resulting states of the catalyst surfaces were analysed using cyclic voltammetry.

4.1.1 Corrosive Etching of Palladium-Gold Catalysts

The mechanism of the gas-phase synthesis of vinyl acetate is not fully understood. Conflicting research (Chapter 1) suggests that it may be formed via (i) heterogeneous processes (surface reactions) and (ii) homogeneous processes occurring within a liquid-layer of acetic acid/potassium acetate adducts. In order for the latter process to occur within a heterogeneous system palladium acetate complexes must be formed under reaction conditions. To investigate this further, palladium-gold catalysts were treated with solutions of acetic acid and of acetic acid/potassium acetate and (i) the state of the catalyst surfaces were re-examined by cyclic voltammetry and (ii) the resulting solutions were analysed by ultra-violet absorption spectroscopy for the presence of palladium acetate complexes (Section 4.1.3).

In the presentation that follows, the effects of etching on nine Batch 1 catalysts are described in sequence and interpreted. As the behaviour shown by Batch 2 and Batch 3 catalysts was similar, the experimental information is presented in full but discussed more briefly.

Figures 4.1 – 4.9 show CVs for untreated Batch 1 catalysts and for catalysts exposed to solutions of acetic acid and of acetic acid/potassium acetate. In almost all cases palladium surface area losses occurred as observed by a reduction in the charges associated with the HUPD and the palladium-oxide stripping regions. Generally, greater surface area losses were observed in the presence of potassium acetate i.e. catalysts treated with 0.5 mol dm^{-3} potassium acetate in acetic acid were etched to a greater extent than those etched in acetic acid alone. For catalysts which contained significant amounts of gold, surfaces after etching showed enhanced gold compositions; this was diagnosed by (i) attenuation of the hydrogen under-potential deposition region, (ii) positive shifts in the potential required to

remove palladium-oxide, and (iii) the appearance of a peak for the stripping of gold-oxide. The charges associated with the HUPD, palladium-oxide, and gold-oxide stripping regions are shown in Table 4.1.

Figure 4.1 shows CVs for untreated and etched catalyst 3182, (1.0% Pd, 0.0% Au)[∞]/G{1}. After exposure to acetic acid-containing solutions, small palladium surface area reductions were observed from small changes in the charges associated with the HUPD and palladium-oxide stripping regions.

Figure 4.1 – CVs for untreated and etched catalyst 3182, (1.0% Pd, 0.0% Au)[∞]/G{1}

Figure 4.2 shows CVs for untreated and etched catalyst 3185, (1.6% Pd, 0.6% Au)[4.8]/G{1}. Etching is once again evident from a reduction in the charges associated with the regions which provide a measure of palladium surface area. Positive shifts in the potentials required to remove palladium-oxide were observed and the appearance of a peak for the stripping of gold-oxide (at ~ 1.10 V) was also observed for the catalyst etched in the presence of potassium acetate – both features indicate an enhanced presence of gold at the catalyst surfaces.

Figure 4.2 – CVs for untreated and etched catalyst 3185, (1.6% Pd, 0.6% Au)[4.8]/G{1}

Figure 4.3 shows CVs for untreated and etched catalyst 3184, (1.0% Pd, 0.4% Au)[4.7]/G{1}. Palladium etching is inferred from the reduction in the charges (and hence palladium surface areas) associated with the HUPD and palladium-oxide stripping regions. No gold-oxide stripping region was observed; although a slight increase in the potential required to remove palladium-oxide from the etched catalyst surfaces indicated that these surfaces had become slightly enriched with gold. The effect of the presence of this low concentration of gold in the original catalyst was substantial.

CVs for untreated and etched catalyst 3186, (1.0% Pd, 1.0% Au)[2.0]/G{1}, are shown in Figure 4.4. The charges associated with the hydrogen under-potential deposition regions decreased slightly after etching in acetic acid and decreased further after etching in acetic acid/potassium acetate. The potential required to remove palladium-oxide varied on etching and the charges associated with it *increased* after etching with acetic acid, possibly due to bulk oxidation. For the catalyst treated with acetic acid/potassium acetate, the charge associated with the palladium-oxide stripping region decreased from 2965 μC to 1890 μC. The charges associated with the gold-oxide stripping regions increased after etching.
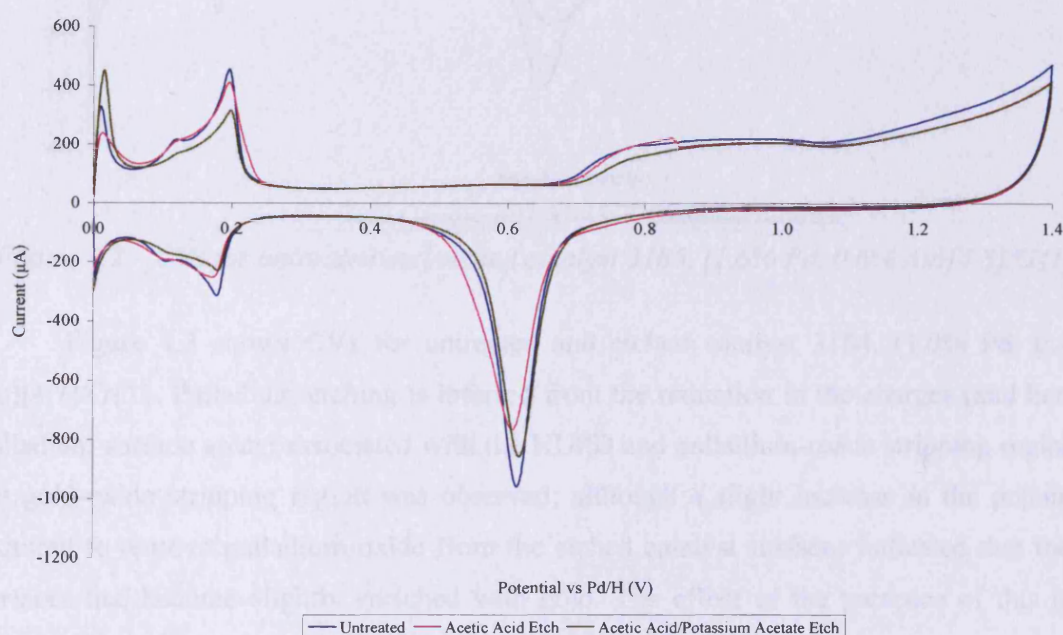
Figure 4.3 – CVs for untreated and etched catalyst 3184, (1.0% Pd, 0.4% Au)[4.7]/G{1}

Figure 4.4 – CVs for untreated and etched catalyst 3186, (1.0% Pd, 1.0% Au)[2.0]/G{1}

CVs for untreated and etched catalyst 3200, (1.0% Pd, 0.9% Au)[1.9]/G{1}, are shown in Figure 4.5. The charges associated with the HUPD and palladium-oxide stripping regions decreased spectacularly after treatment with the acetic acid-containing solutions, and the potential of the palladium-oxide stripping peak showed the surface to be that of the palladium-gold alloy. The charges associated with the gold-oxide stripping regions increased which is diagnostic of a surface enriched in gold.

Figure 4.5 – CVs for untreated and etched catalyst 3200, (1.0% Pd, 0.9% Au)[1.9]/G{1}

CVs for untreated and etched catalyst 3187, (1.0% Pd, 1.7% Au)[1.1]/G{1}, are shown in Figure 4.6. The charges associated with the HUPD region decreased after treatment with acetic acid-based solutions. After treatment, reductions in the charges associated with the palladium-oxide stripping regions were also observed. This was accompanied by the appearance of a peak having a stripping potential slightly more positive than that expected for palladium-oxide. The surface area of gold increased after exposure with charges of 70 µC, 315 µC, and 410 µC being associated with the gold-oxide stripping feature for untreated, etched (acetic acid), and etched (acetic acid/potassium acetate) catalysts respectively.
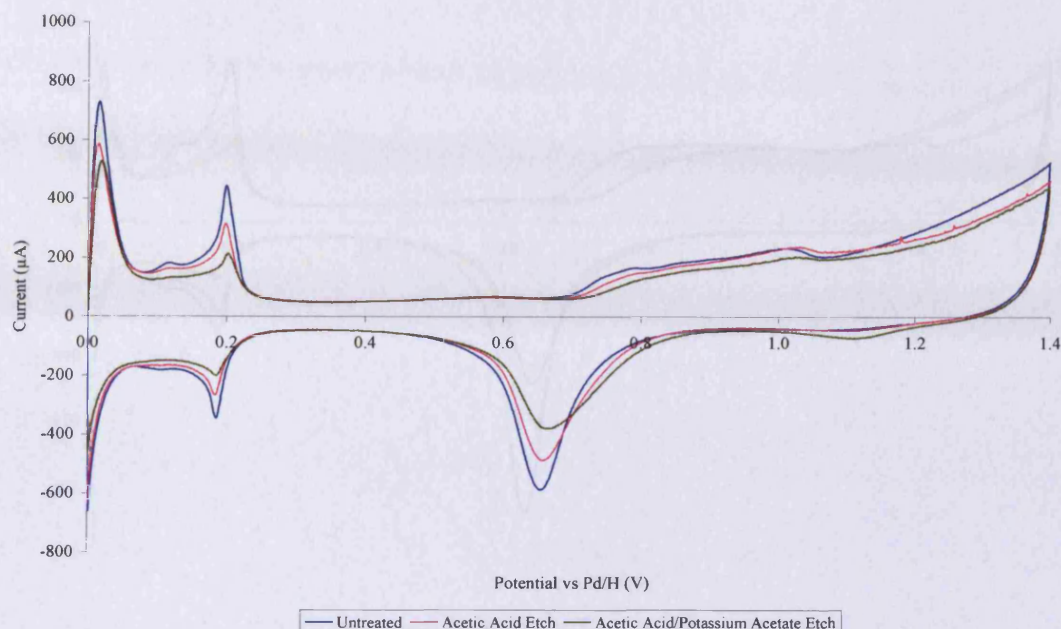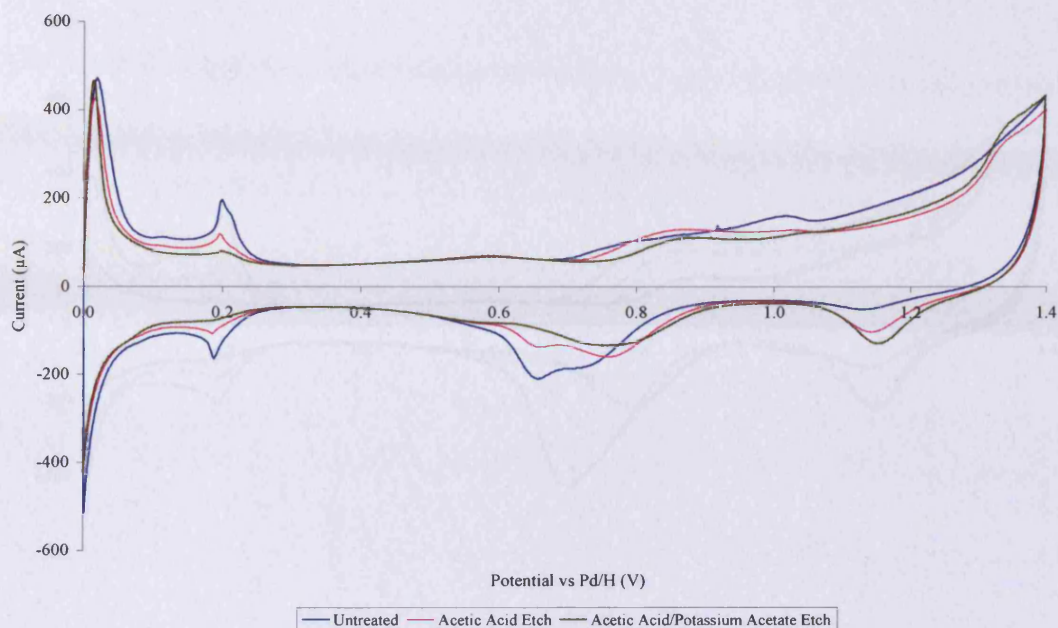
Figure 4.6 – CVs for untreated and etched catalyst 3187, (1.0% Pd, 1.7% Au)[1.1]/G{1}

Figure 4.7 shows CVs for untreated and etched catalyst 3188, (1.0% Pd, 2.5% Au)[0.7]/G{1}. After treatment with acetic acid and acetic acid/potassium acetate solutions, the surface areas of palladium were again found to decrease and surface enrichment in gold was detected by (i) an increased potential required to remove palladium-oxide and (ii) increased charges associated with the gold-oxide stripping regions.
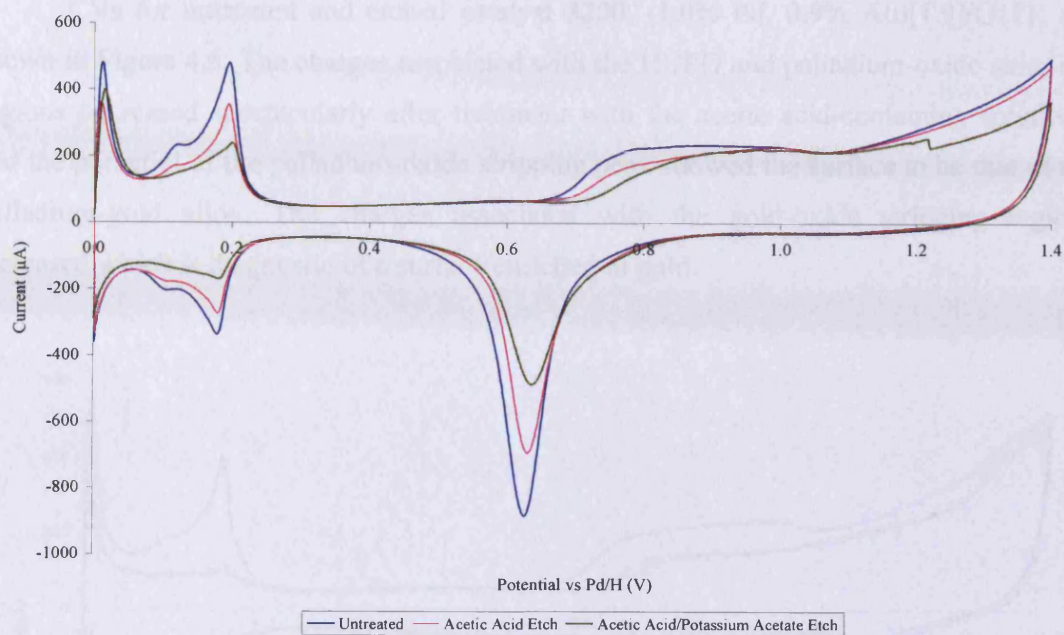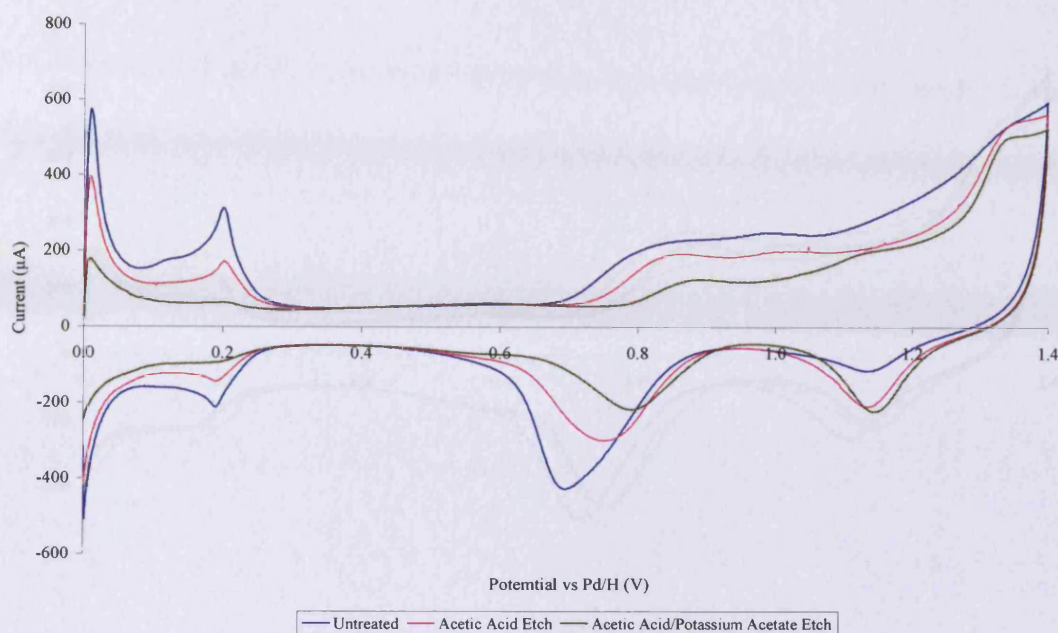
Figure 4.7 – CVs for untreated and etched catalyst 3188, (1.0% Pd, 2.5% Au)[0.7]/G{1}

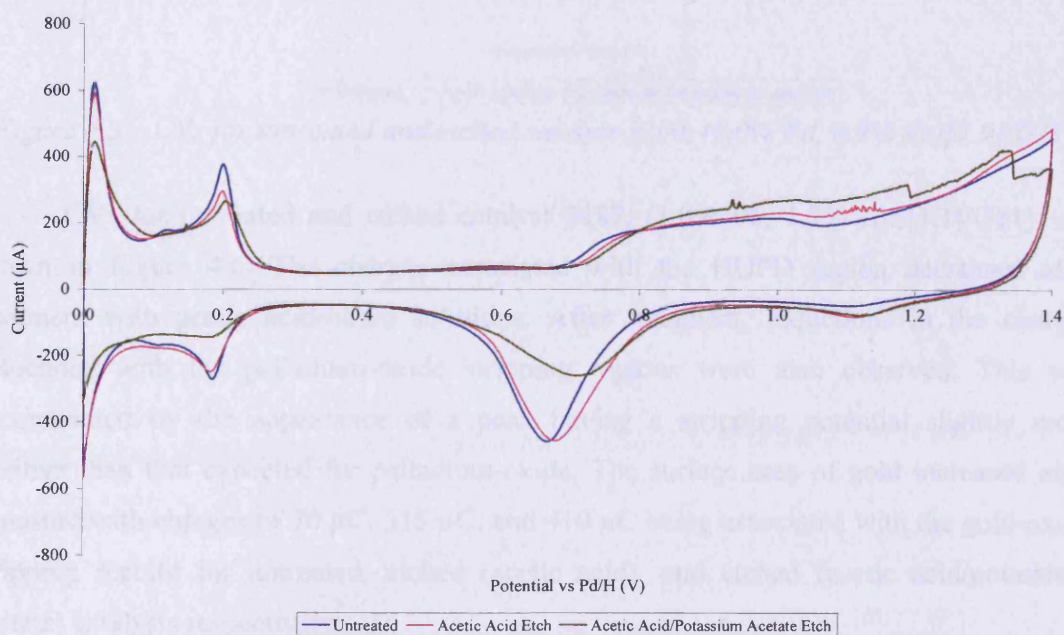Figure 4.8 shows CVs for untreated and etched catalyst 4266, (0.5% Pd, 1.8% Au)[0.5]/G{1}. Smaller changes in the charges associated with the HUPD and palladium-oxide stripping regions were detected which is consistent with the small amounts of palladium contained in this catalyst (palladium loading = 0.5%). However, smaller charges associated with the HUPD and palladium-oxide stripping regions after treatment with acetic acid-containing solutions imply that the palladium surface areas were further reduced whilst the positive shift in the potential required to remove palladium-oxide coupled with positive shift in the potential required to strip gold-oxide indicated that the surfaces became enriched with gold relative to their untreated states. The charges associated with the gold-oxide stripping regions indicated that the surface area of gold also increased as a result of these treatments.
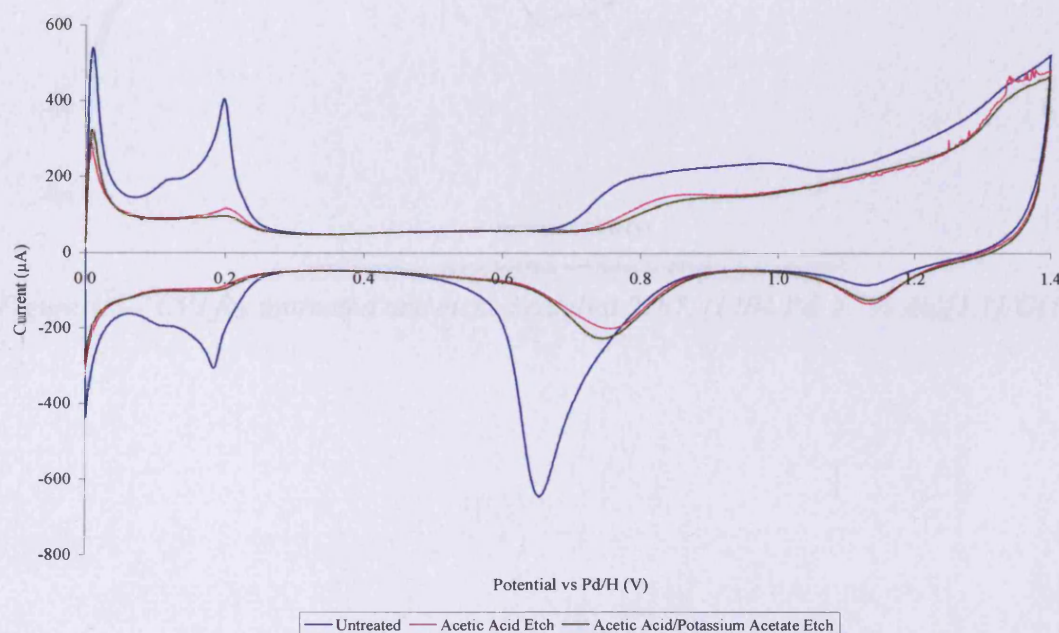
Figure 4.8 – CVs for untreated and etched catalyst 4266, (0.5% Pd, 1.8% Au)[0.5]/G{1}

The CVs for untreated and etched catalyst 4265, (0.2% Pd, 1.7% Au)[0.2]/G{1}, are shown in Figure 4.9. Once again, due to the low level of palladium in this catalyst (palladium loading = 0.2%), the changes which occurred on etching were modest. Minimal changes in the charges associated with the hydrogen under-potential deposition regions were observed, together with more substantial changes in the palladium-oxide stripping regions. Shifts in the potentials required to strip gold-oxide were detected which together with the shifts in the palladium-oxide stripping potentials imply the generation of etched surfaces having a lower palladium/gold ratio.

Figure 4.9 – CVs for untreated and etched catalyst 4265, (0.2% Pd, 1.7% Au)[0.2]/G{1}

Table 4.1 – Batch 1 catalysts: charges (normalised ^{z}) associated with the HUPD, palladium-oxide, and gold-oxide regions before and after exposure to solutions of acetic acid and of acetic acid/potassium acetate

Catalyst		HUPD region charge / μC			Pd-O stripping region charge / μC			Au-O stripping region charge / μC		
			Etched			Etched			Etched	
ref no	description	Untreated	HOAc^a	HOAc^a + KOAc^b	Untreated	HOAc^a	HOAc^a + KOAc^b	Untreated	HOAc^a	HOAc^a + KOAc^b
3182	(1.0% Pd, 0.0% Au)[∞]/G{1}	2405	2455	1855	3545	3450	3375	n/o	n/o	n/o
3185	(1.6% Pd, 0.6% Au)[4.8]/G{1}	1935	1575	1085	3345	3385	3095	n/o	35	85
3184	(1.0% Pd, 0.4% Au)[4.7]/G{1}	2875	1840	1535	4380	3765	3095	n/o	n/o	n/o
3186	(1.0% Pd, 1.0% Au)[2.0]/G{1}	1860	1695	1550	2965	3285	1890	55	130	85
3200	(1.0% Pd, 0.9% Au)[1.9]/G{1}	2215	580	465	4800	1060	1335	130	390	350
3187	(1.0% Pd, 1.7% Au)[1.1]/G{1}	770	435	210	2155	910	920	70	315	410
3188	(1.0% Pd, 2.5% Au)[0.7]/G{1}	1900	860	5	3645	1915	1190	225	740	920
3266	(0.5% Pd, 1.8% Au)[0.5]/G{1}	760	480	5	1610	1580	1575	440	285	385
3265	(0.2% Pd, 1.7% Au)[0.2]/G{1}	215	255	345	315	795	830	205	320	240

^{a}acetic acid ^{z}for procedure see Section 2.2.10

^{b}potassium acetate

n/o = not observed

138

Figures 4.10 – 4.17 show CVs for untreated and etched Batch 2 catalysts. Similar trends in terms of reductions in the charges associated with the HUPD and palladium-oxide stripping regions were observed after exposure as well as shifts in the potentials required to strip to oxides of palladium and of gold. The charges associated with the hydrogen under-potential deposition region, palladium-oxide stripping region, and gold-oxide stripping region are shown in Table 4.2.

Figure 4.10 – CVs for untreated and etched catalyst 3329, (1.0% Pd, 0.0% Au)[∞]/G{2}

Figure 4.11 – CVs for untreated and etched catalyst 3331, (1.0% Pd, 0.4% Au)[4.8]/G{2}

Figure 4.12 – CVs for untreated and etched catalyst 3332, (1.7% Pd, 0.6% Au)[4.8]/G{2}

Figure 4.13 – CVs for untreated and etched catalyst 3333, (1.0% Pd, 1.0% Au)[1.9]/G{2}

Figure 4.14 – CVs for untreated and etched catalyst 3334, (1.0%Pd, 1.8% Au)[1.0]/G{2}

Figure 4.15 – CVs for untreated and etched catalyst 3335, (1.0% Pd, 2.7% Au)[0.7]/G{2}
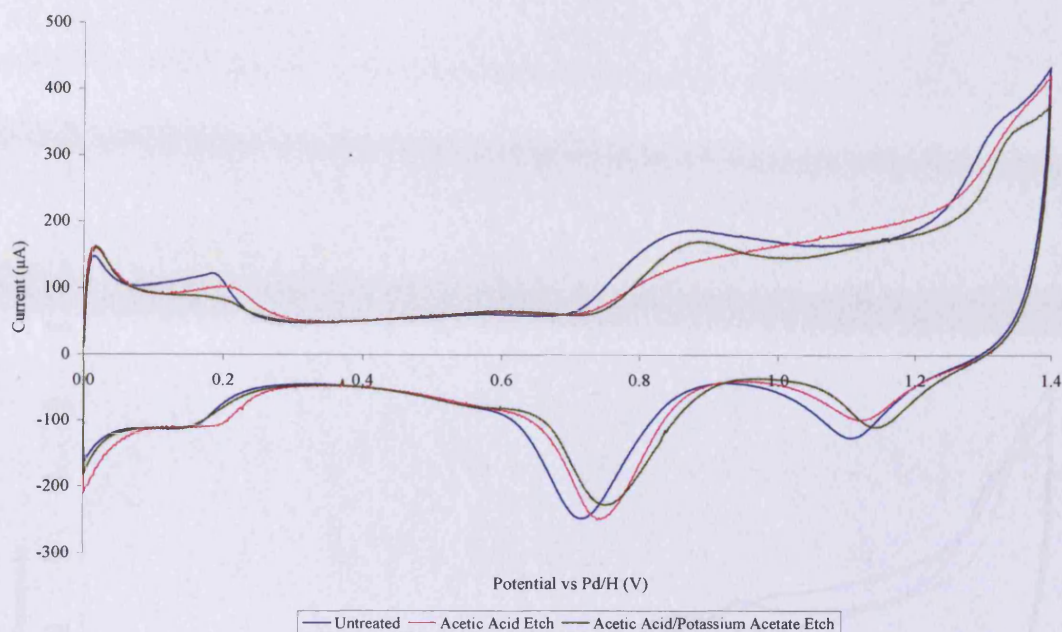

Figure 4.16 – CVs for untreated and etched catalyst 4268, (0.5% Pd, 1.8% Au)[0.6]/G{2}
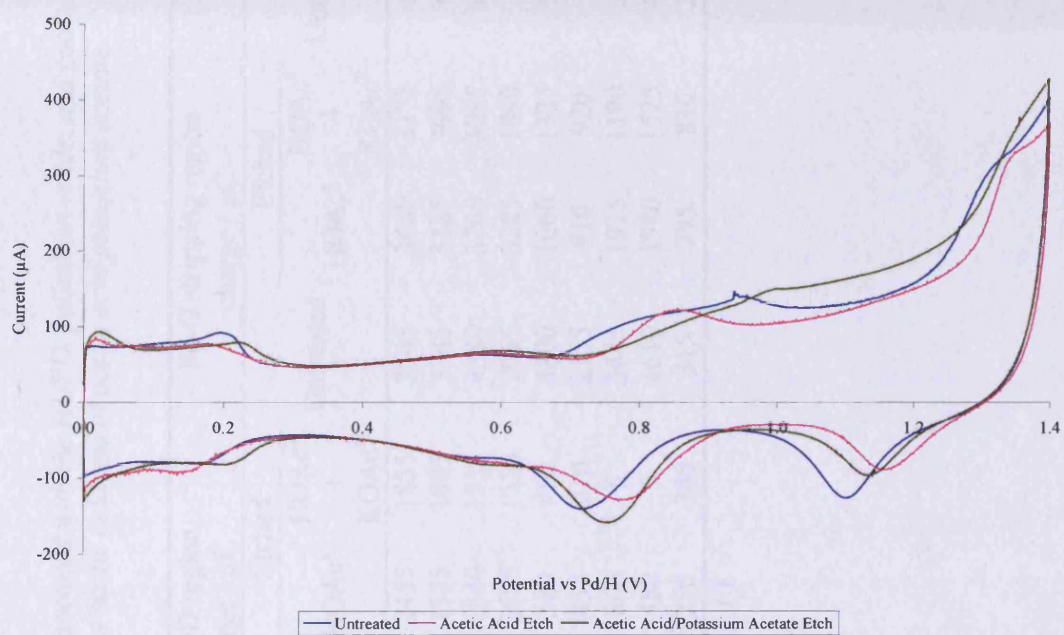
Figure 4.17 – CVs for untreated and etched catalyst 4267, (0.2% Pd, 1.8% Au)[0.2]/G{2}

Table 4.2 – Batch 2 catalysts: charges (normalised^z) associated with the HUPD, palladium-oxide, and gold-oxide regions before and after exposure to solutions of acetic acid and of acetic acid/potassium acetate

Catalyst		HUPD region charge / μC			Pd-O stripping region charge / μC			Au-O stripping region charge / μC		
			Etched			Etched			Etched	
ref no	description	Untreated	HOAc^a	HOAc^a + KOAc^b	Untreated	HOAc^a	HOAc^a + KOAc^b	Untreated	HOAc^a	HOAc^a + KOAc^b
3329	(1.0% Pd, 0.0% Au)[∞]/G{2}	2190	1840	1895	3130	3160	3440	n/o	n/o	n/o
3331	(1.0% Pd, 0.4% Au)[4.8]/G{2}	2200	1380	560	3455	2655	2420	n/o	n/o	n/o
3332	(1.7% Pd, 0.6% Au)[4.8]/G{2}	3910	2040	1620	5075	3920	4380	n/o	n/o	n/o
3333	(1.0% Pd, 1.0% Au)[1.9]/G{2}	2135	1335	680	3570	3395	1855	75	185	325
3334	(1.0% Pd, 1.8% Au)[1.0]/G{2}	2035	1485	1185	2475	2660	2805	110	105	165
3335	(1.0% Pd, 2.7% Au)[0.7]/G{2}	1495	895	505	1840	2010	1870	410	370	525
4268	(0.5% Pd, 1.8% Au)[0.6]/G{2}	670	20	360	1235	1655	1430	540	410	440
4267	(0.2% Pd, 1.8% Au)[0.2]/G{2}	130	200	185	475	560	600	495	335	385

^{a}acetic acid ^{z}for procedure see Section 2.2.10

^{b}potassium acetate

n/o = not observed

144

Figures 4.18 – 4.25 show CVs for untreated and etched Batch 3 catalysts. Similar trends in terms of reductions in the charges associated with the HUPD and palladium-oxide stripping regions were observed after exposure as well as shifts in the potentials required to strip to oxides of palladium and of gold. The charges associated with the hydrogen under-potential deposition region, palladium-oxide stripping region, and gold-oxide stripping region are shown in Table 4.3.
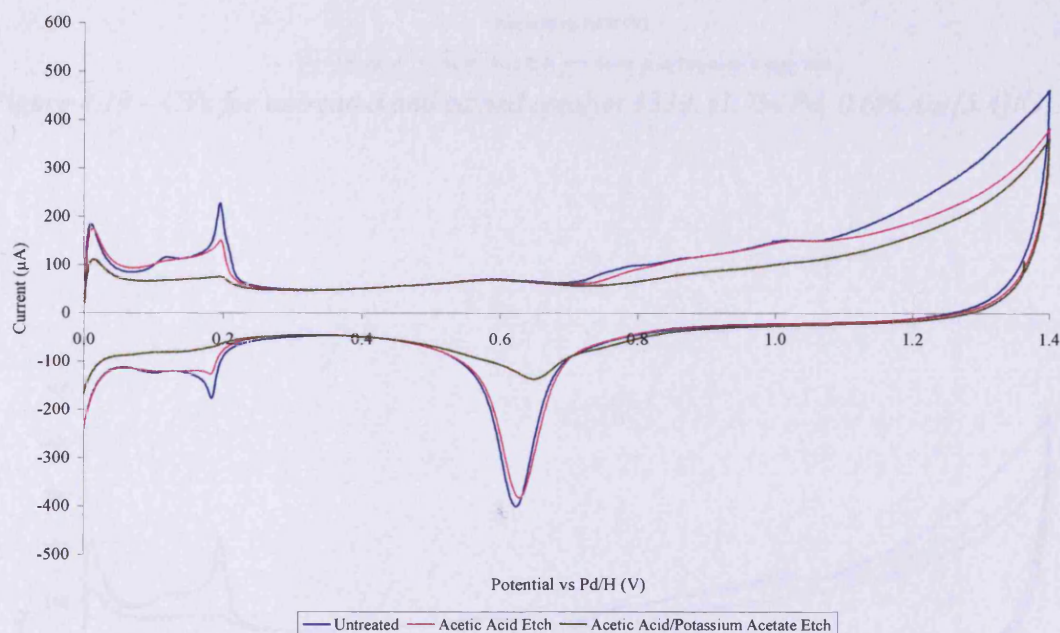
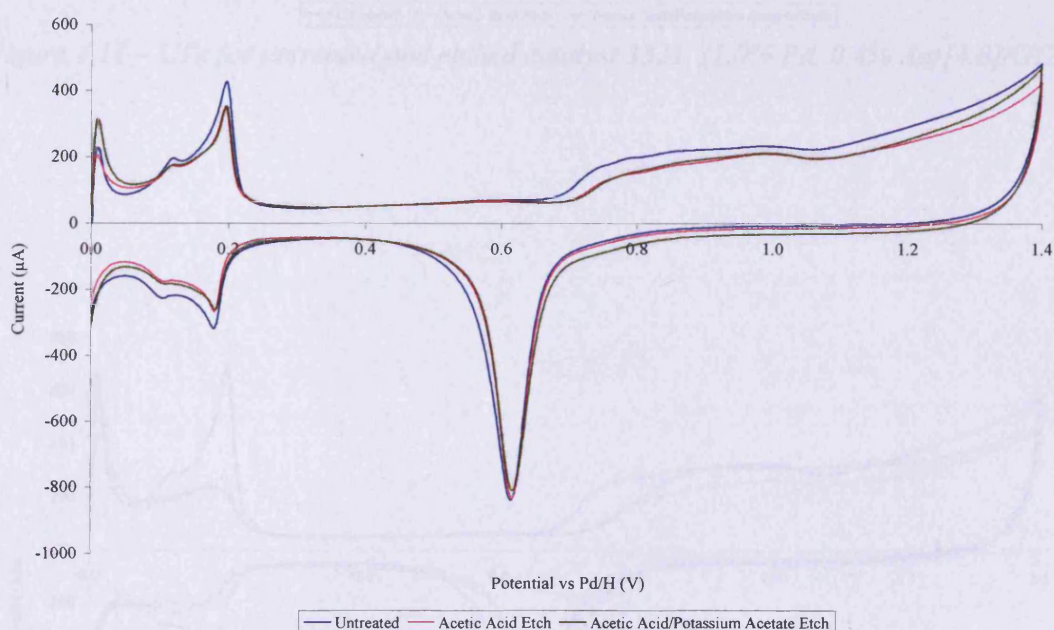*Figure 4.18 – CVs for untreated and etched catalyst, (1.0% Pd, 0.0% Au)[∞]/G{3}*
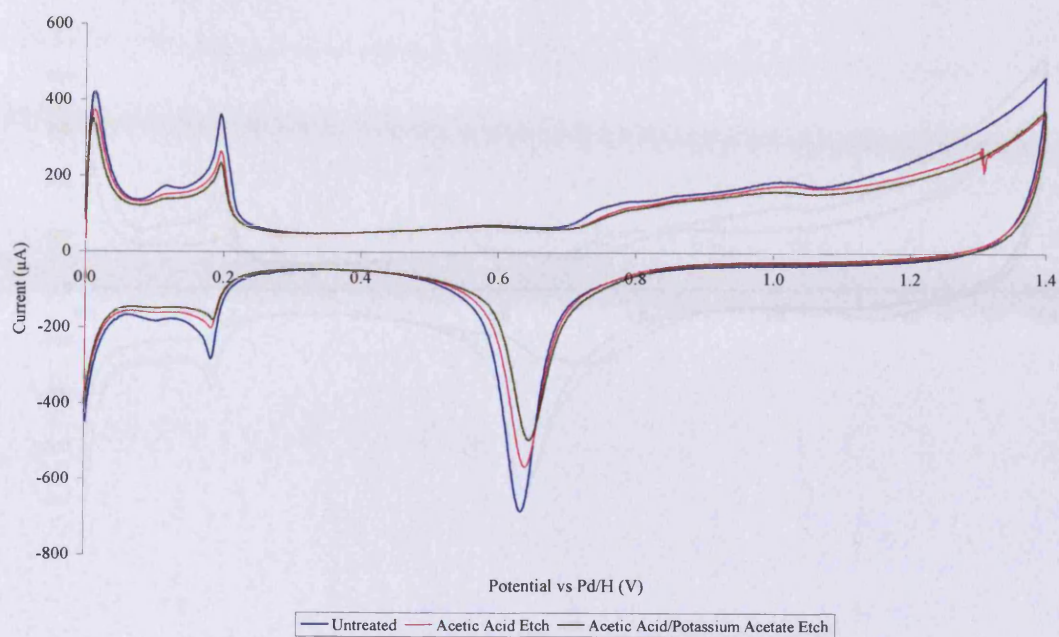
Figure 4.19 – CVs for untreated and etched catalyst 3339, (1.7% Pd, 0.6% Au)[5.4]/G{3}
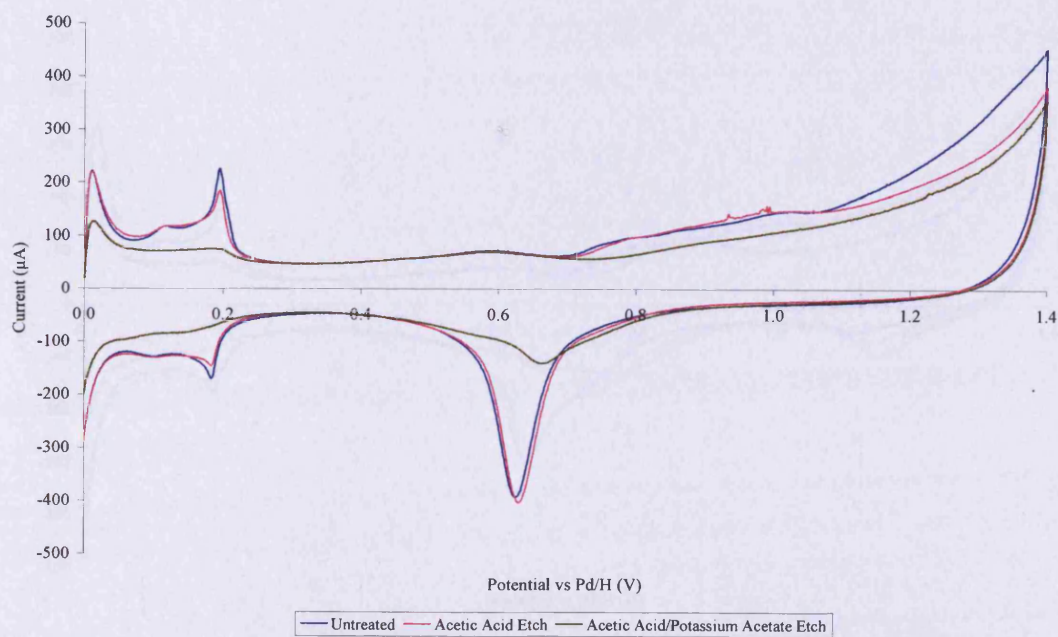
Figure 4.20 – CVs for untreated and etched catalyst 3338, (1.0% Pd, 0.4% Au)[4.9]/G{3}
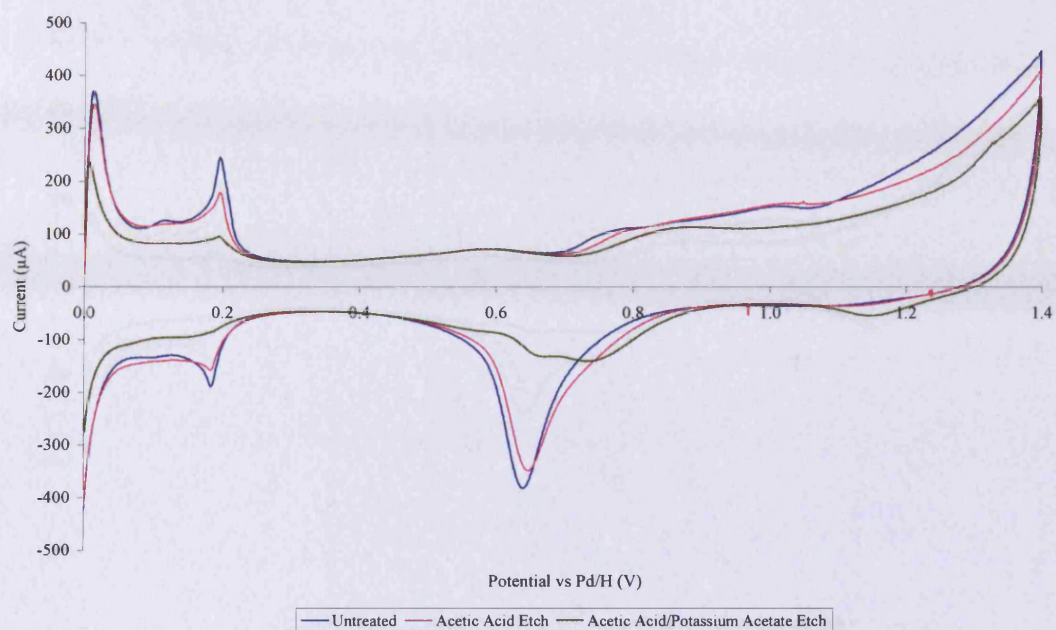
Figure 4.21 – CVs for untreated and etched catalyst 3340, (1.0% Pd, 0.9% Au)[2.1]/G{3}
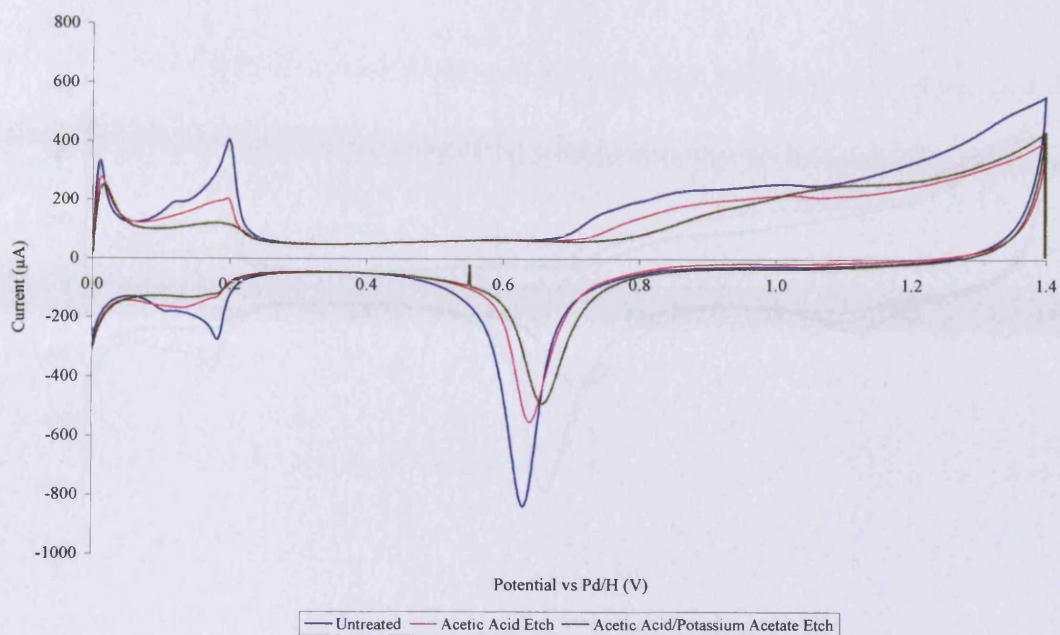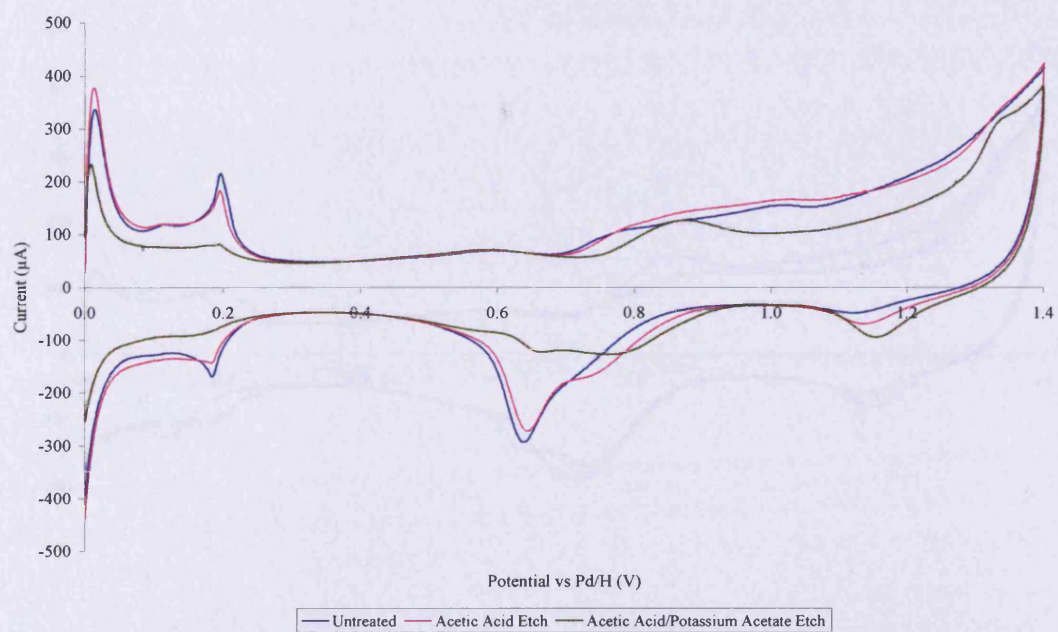

Figure 4.22 – CVs for untreated and etched catalyst 3341, (1.0% Pd, 1.7% Au)[1.1]/G{3}
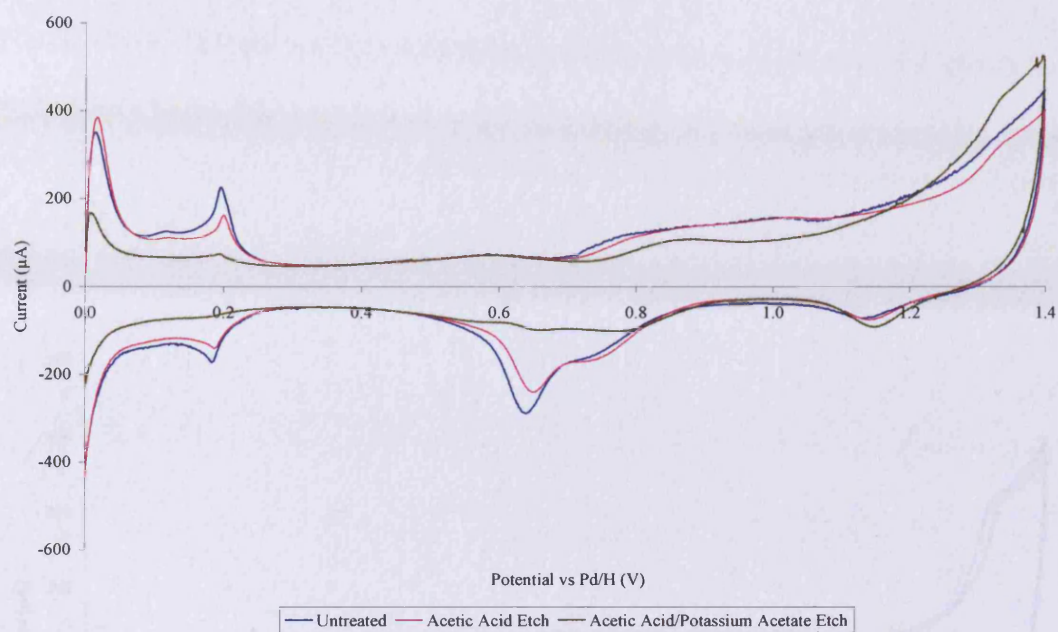
Figure 4.23 – CVs for untreated and etched catalyst 3342, (1.0% Pd, 2.6% Au)[0.7]/G{3}
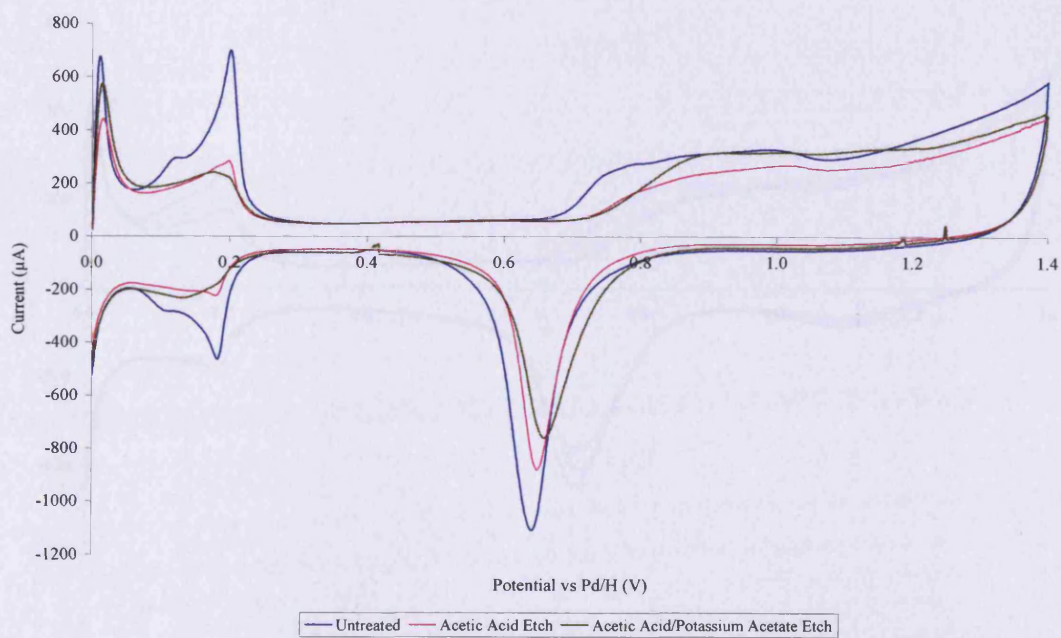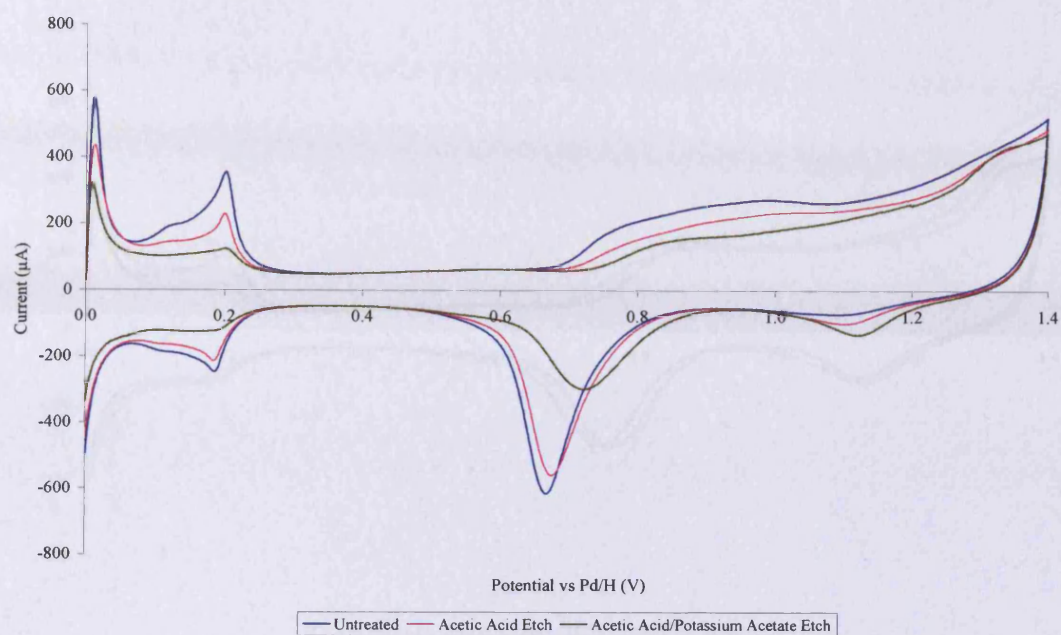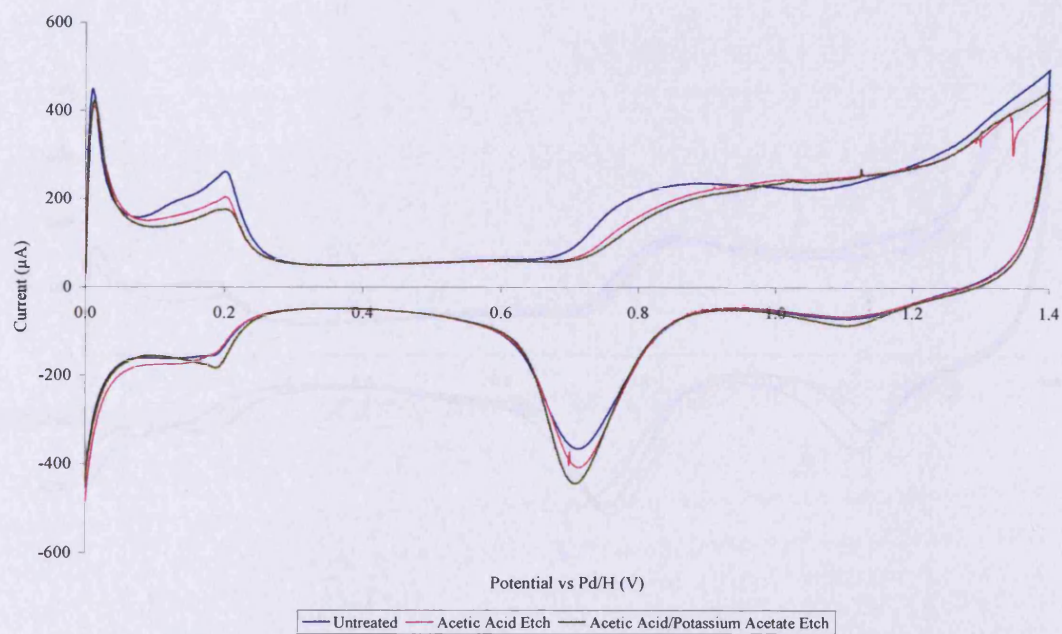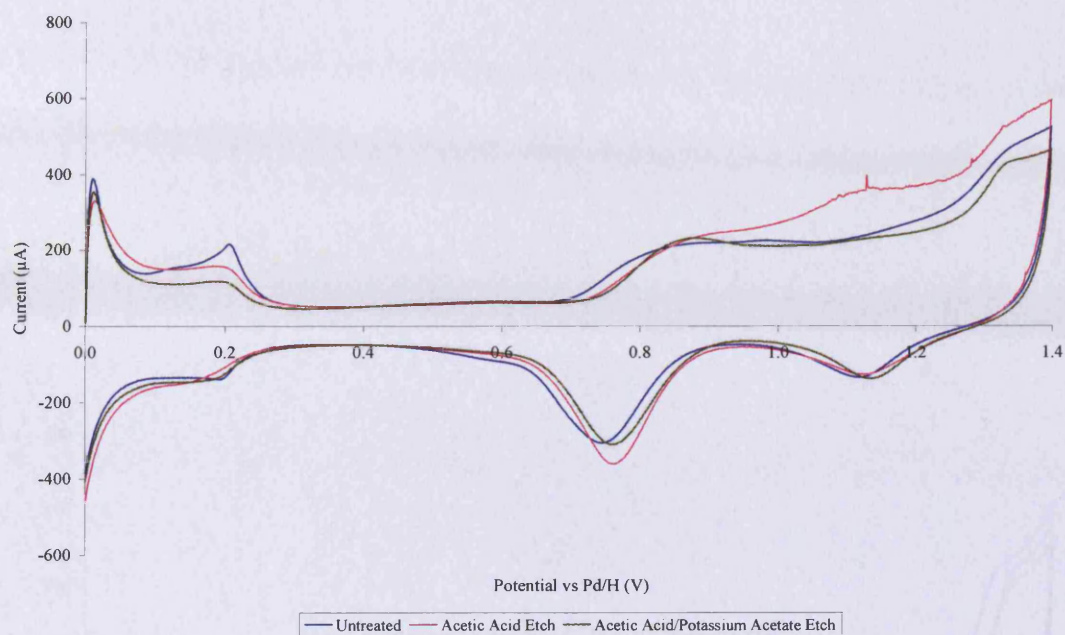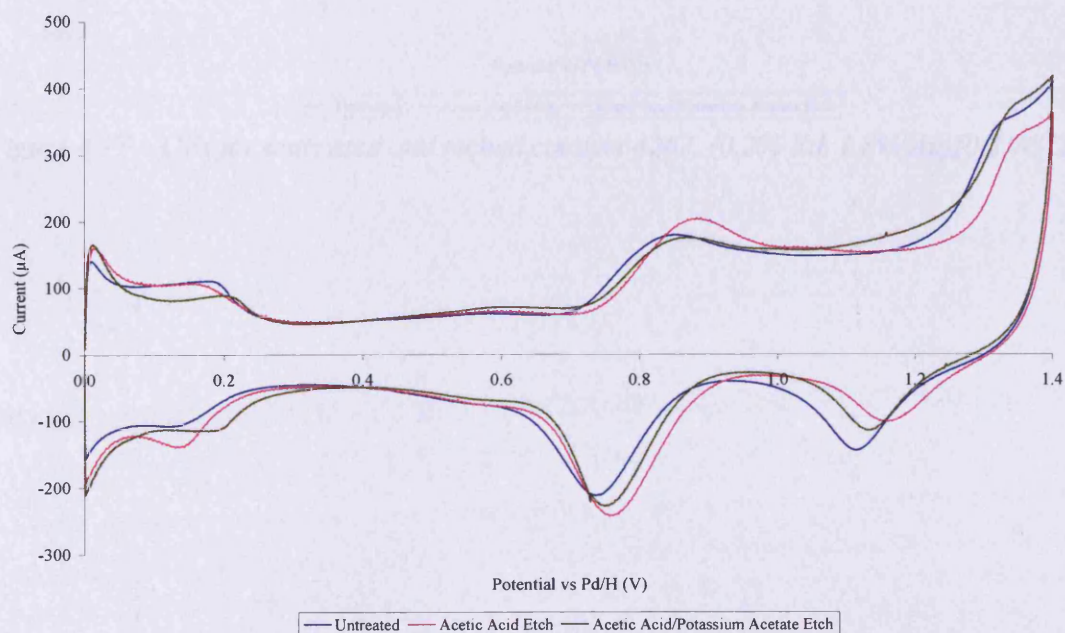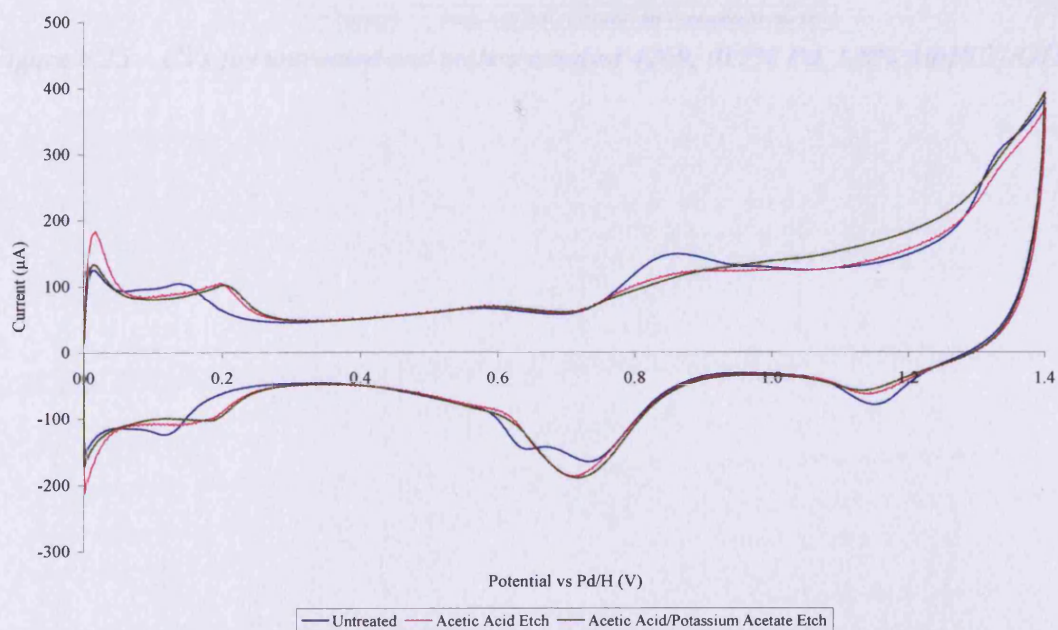

Figure 4.24 – CVs for untreated and etched catalyst 4270, (0.5% Pd, 1.8% Au)[0.5]/G{3}
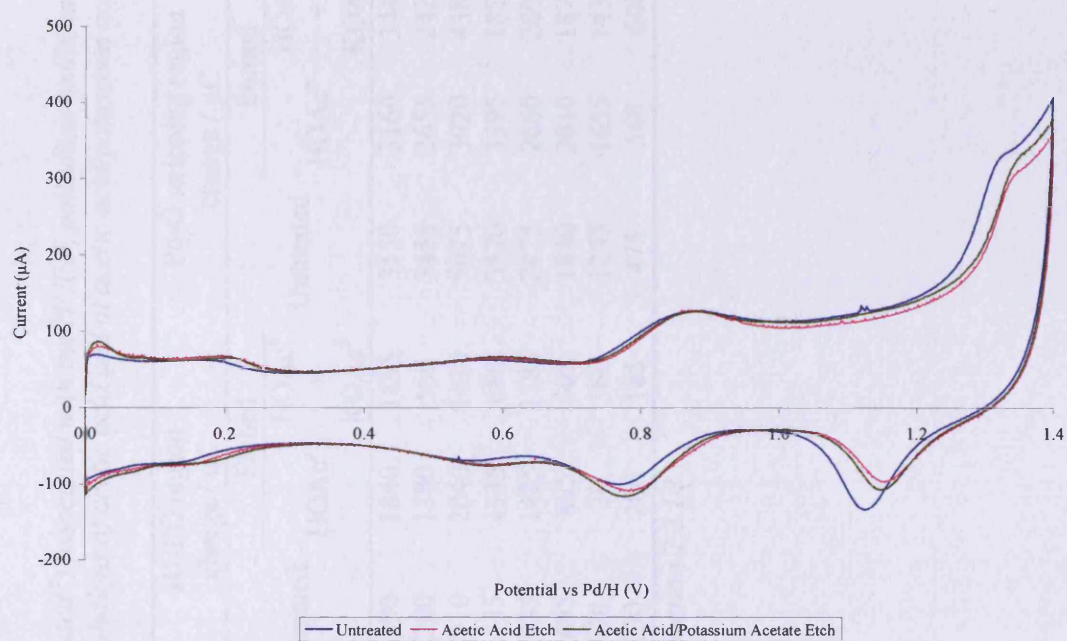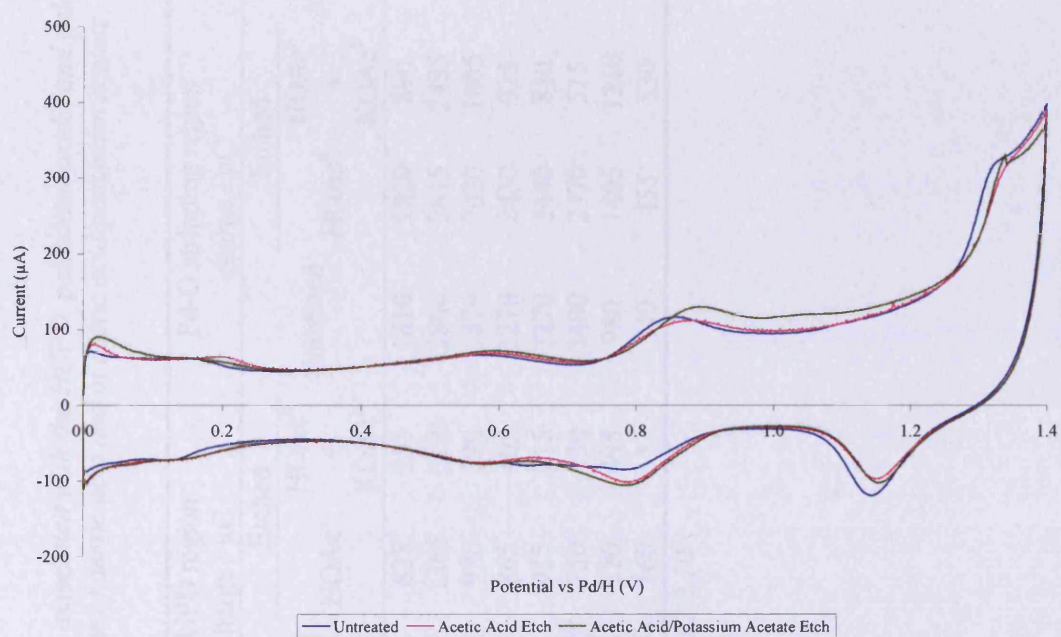
Figure 4.25 – CVs for untreated and etched catalyst 4269, (0.2% Pd, 1.8% Au)[0.2]/G{3}

Table 4.3 – Batch 3 catalysts: charges (normalised ^{z}) associated with the HUPD, palladium-oxide, and gold-oxide regions before and after exposure to solutions of acetic acid and of acetic acid/potassium acetate

Catalyst		HUPD region charge / μC			Pd-O stripping region charge / μC			Au-O stripping region charge / μC		
			Etched			Etched			Etched	
ref no	description	Untreated	HOAc^a	HOAc^a + KOAc^b	Untreated	HOAc^a	HOAc^a + KOAc^b	Untreated	HOAc^a	HOAc^a + KOAc^b
3336	(1.0% Pd, 0.0% Au)[∞]/G{3}	880	835	255	1810	1820	890	n/o	n/o	n/o
3339	(1.7% Pd, 0.6% Au)[5.4]/G{3}	1705	1365	1230	2860	2615	2435	n/o	n/o	n/o
3338	(1.0% Pd, 0.4% Au)[4.9]/G{3}	930	930	290	1870	2020	1005	n/o	n/o	n/o
3340	(1.0% Pd, 0.9% Au)[2.1]/G{3}	1100	865	405	2270	2430	925	n/o	15	95
3341	(1.0% Pd, 1.7% Au)[1.1]/G{3}	955	915	315	2270	2440	810	50	150	285
3342	(1.0% Pd, 2.6% Au)[0.7]/G{3}	1045	750	230	2400	2370	515	120	185	275
4270	(0.5% Pd, 1.8% Au)[0.5]/G{3}	420	520	495	980	1405	1310	190	125	100
4269	(0.2% Pd, 1.8% Au)[0.2]/G{3}	140	160	5	340	455	530	410	345	370

^{a}*acetic acid* 　　　^{z}*for procedure see Section 2.2.10*
^{b}*potassium acetate*
n/o = not observed

4.1.1.1 Conclusions

When palladium-gold/graphite catalysts were heated and allowed to react with solutions containing acetate anions, reductions in the surface areas of palladium occurred in almost every case. The surfaces thus generated were enriched with gold indicating that the changes in palladium surface area were due to the loss, via dissolution or etching of palladium from the catalysts, and not by the sintering of palladium particles. The promoting effect of potassium acetate was evident in most, but not all cases.

4.1.2 Catalyst Exposure to Acetic Acid and Potassium Acetate under Oxidising Conditions

Palladium-gold catalysts were exposed to acetic acid solutions containing potassium acetate in an electrochemical cell. This experiment was intended to mimic reaction conditions during vinyl acetate synthesis, and involved mounting a catalyst onto a working electrode and immersing it in an electrolyte solution containing acetic acid and potassium acetate (0.5 mol dm^{-3} potassium acetate dissolved in acetic acid). The potential of the electrode was then swept from 0.00 V to 1.40 V and back to 0.00 V twice. The working electrode was then transferred to an electrochemical cell containing 0.5 mol dm^{-3} sulphuric acid and the state of the catalyst was characterised by cyclic voltammetry. This was carried out using catalysts from Batch 1, Batch 2, and Batch 3 and the CVs recorded were compared to CVs obtained for the catalysts in their untreated states. Figures 4.26 – 4.29 show CVs for selected catalysts.

Figure 4.26 shows CVs before and after catalyst 3336, (1.0% Pd, 0.0% Au)[∞]/G{3}, was exposed to acetic acid and potassium acetate under oxidising conditions. After exposure, a small reduction in the charge associated with the hydrogen under-potential deposition region was observed. Also notable was the reduction in the extent of surface oxidation i.e. the charge associated with palladium-oxide formation (in the forward sweep) was smaller after exposure. This was reproduced in the reverse sweep, where the charge associated with palladium-oxide stripping was less than that for the process occurring over the untreated catalyst. The reduction in the charge associated with palladium-oxide formation was greater than the reduction in charge associated with palladium-oxide stripping; this indicates that the original palladium surface may have

contained contaminants which were oxidised during the first forward sweep thereby contributing to the observed charge.
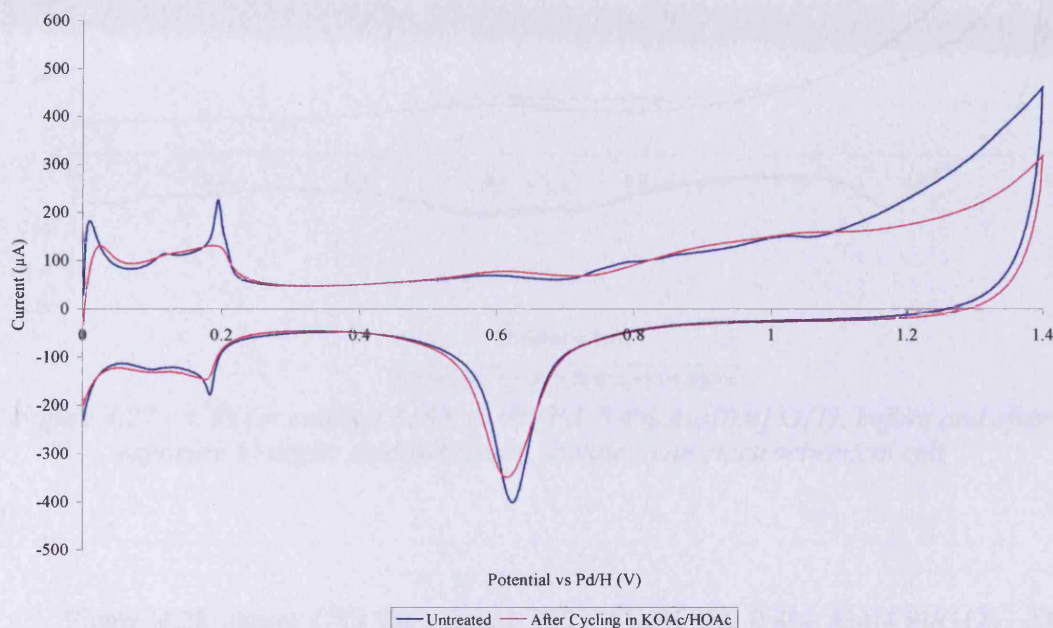
Figure 4.26 – CVs for catalyst 3336, (1.0% Pd, 0.0% Au)[∞]/G{3}, before and after exposure to acetic acid/potassium acetate in an electrochemical cell

Figure 4.27 shows CVs for catalyst 3183, (0.0% Pd, 0.4% Au)[0.0]/G{1}, before and after exposure to acetic acid and potassium acetate. As expected the CV for the gold catalyst did not contain a hydrogen under-potential deposition region, but gold-oxide formation was observed on the forward sweep. Gold-oxide stripping was observed at ~ 1.15 V on the reverse sweep and the charges associated with it did not change after exposure. This result indicates that the surface area of gold did not change when the catalyst was exposed to acetic acid and potassium acetate under oxidising conditions. The untreated catalyst was again found to have a greater charge associated with its forward sweep, presumably due to the oxidation of adsorbed contaminants on the catalyst surface.
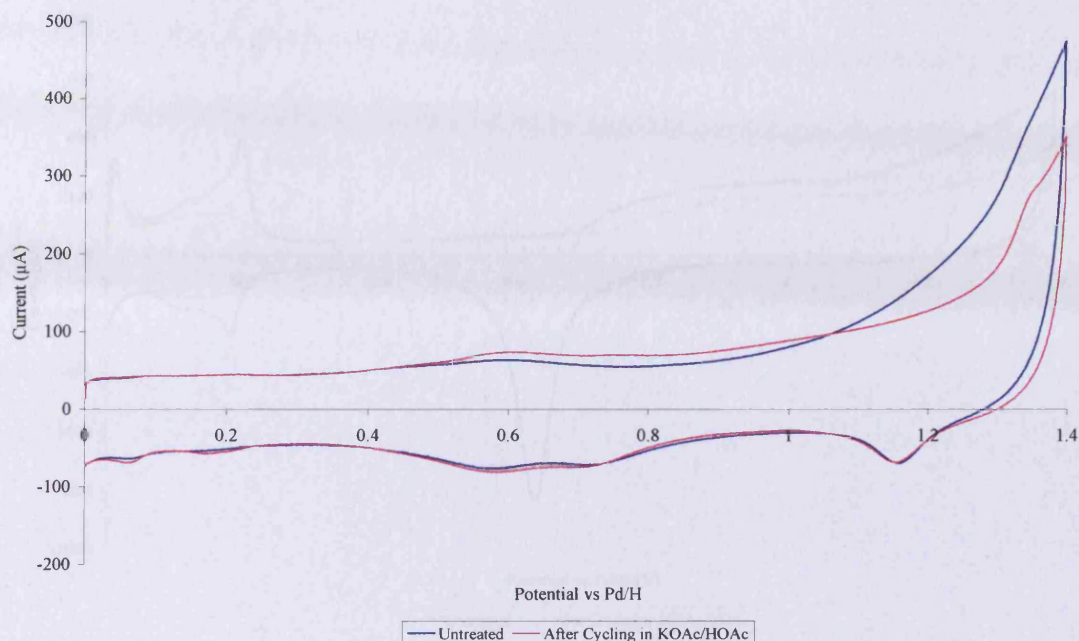
Figure 4.27 – CVs for catalyst 3183, (0.0% Pd, 0.4% Au)[0.0]/G{1}, before and after exposure to acetic acid/potassium acetate in an electrochemical cell

Figure 4.28 shows CVs for catalyst 3331, (1.0% Pd, 0.4% Au)[4.8]/G{2}. After exposure to acetic acid and potassium acetate, not only was the charge associated with the hydrogen under-potential deposition region reduced but the region had undergone extensive attenuation. In parallel, the charge associated with the stripping of palladium-oxide was also reduced and the potential required for palladium-oxide stripping tended towards that of gold-oxide. There was no direct evidence for the presence gold at the surface (the gold-oxide stripping region was absent) but the reduction in the charge associated with the hydrogen under-potential deposition region and the movement of the palladium-oxide stripping peak potential both suggest that the gold concentration at the surface increased as a result of the acetic acid/potassium acetate treatment.
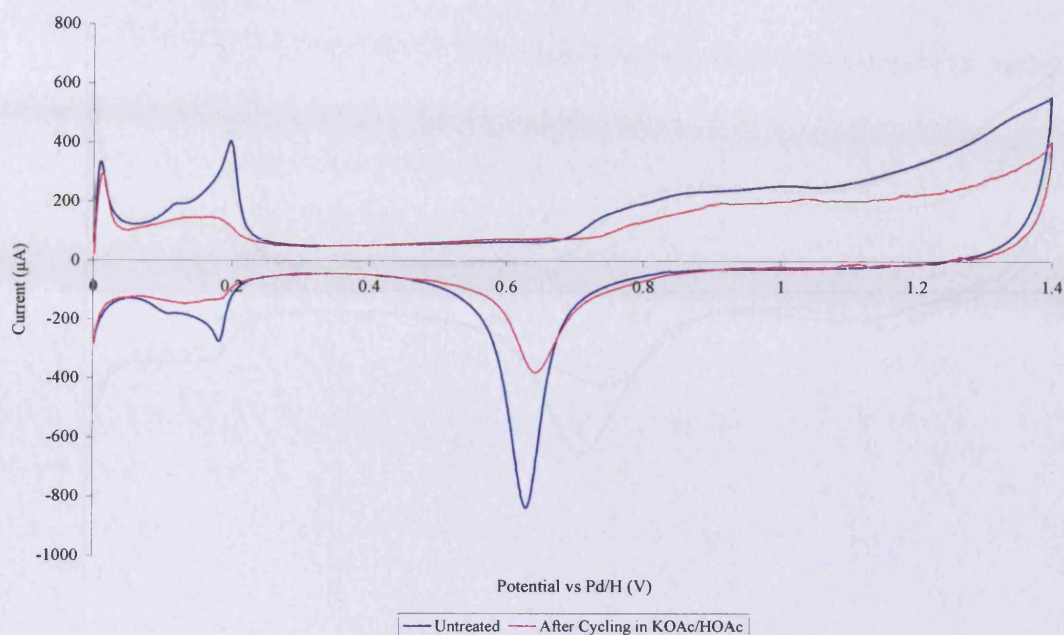
Figure 4.28 – CVs for catalyst 3331, (1.0% Pd, 0.4% Au)[4.8]/G{2}, before and after exposure to acetic acid/potassium acetate in an electrochemical cell

CVs for catalyst 3334, (1.0% Pd, 1.8% Au)[1.0]/G{2}, are shown in Figure 4.29. After exposure, the charges associated with the HUPD and palladium-oxide regions were once again reduced and there was evidence for surface gold. Furthermore, after treatment with acetic acid/potassium acetate there appeared to be both a palladium-rich alloy (~ 0.64 V) and a gold-rich alloy (~ 0.74 V) at the surface. In addition, the very gold-rich phase (~ 1.09 V) appeared to be depleted of palladium (movement of peak to ~ 1.15 V) after exposure to these conditions.
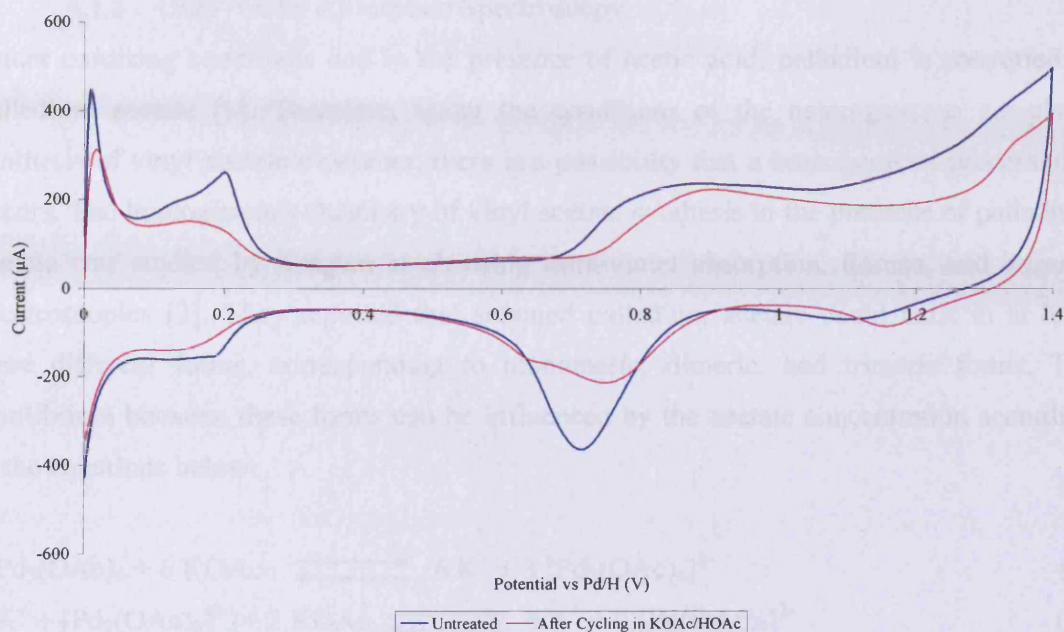
Figure 4.29 – CVs for catalyst 3334, (1.0% Pd, 1.8% Au)[1.0]/G{2}, before and after exposure to acetic acid/potassium acetate in an electrochemical cell

Overall, these CVs show (i) reductions in charge associated with the HUPD and palladium-oxide stripping regions indicating losses in palladium surface area, and (ii) evidence that the acetic acid/potassium acetate treatment caused a gold enrichment of some alloy surfaces.

4.1.3 Ultra-Violet Absorption Spectroscopy

Under oxidising conditions and in the presence of acetic acid, palladium is converted to palladium acetate [1]. Therefore, under the conditions of the heterogeneous gas-phase synthesis of vinyl acetate monomer, there is a possibility that a homogeneous process also occurs. The homogeneous chemistry of vinyl acetate synthesis in the presence of palladium acetate was studied by Kragten et al. using ultra-violet absorption, Raman, and infrared spectroscopies [2]. They reported that solvated palladium acetate could exist in at least three different forms, corresponding to monomeric, dimeric, and trimeric forms. The equilibrium between these forms can be influenced by the acetate concentration according to the equations below.

$$2\ Pd_3(OAc)_6 + 6\ KOAc \rightleftharpoons 6\ K^+ + 3\ [Pd_2(OAc)_6]^{2-} \tag{1}$$

$$2\ K^+ + [Pd_2(OAc)_6]^{2-} + 2\ KOAc \rightleftharpoons 4\ K^+ + 2\ [Pd(OAc)_4]^{2-} \tag{2}$$
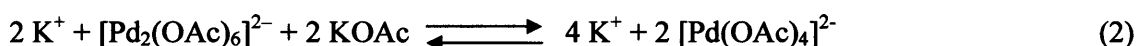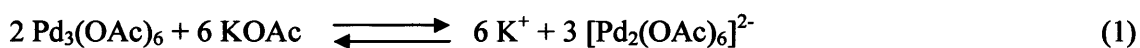
The various palladium acetate species have different catalytic activities for vinyl acetate formation [2]. Catalytic activity increases in proportion to the palladium acetate and potassium acetate concentrations, up to concentrations of the latter for which all the trimers are converted to dimers [3, 4] (1). At higher concentrations, the rate of vinyl acetate formation is inversely proportional to the potassium acetate concentration [3]. Thus, adding potassium acetate first creates a catalytically active species, but at high concentrations, the acetate ions function as inhibitors. These results can be interpreted as follows. At low potassium acetate concentrations, the relatively inactive palladium trimers are partially converted to active dimers. At high concentrations, however, less active species also form. The less active species could be either palladium acetate monomers or palladium acetate dimers that are fully coordinated by acetate ligands. Since ethylene molecules are expected to coordinate to terminal positions on the dimer [5], coordination of ethylene to palladium acetate complex followed by reaction to form vinyl acetate requires the presence of vacant terminal sites on the dimers. The maximum activity would then be expected to occur when the concentration of coordinatively unsaturated palladium acetate dimers is highest. It is also possible that the coordination of ethylene could convert palladium acetate dimers to monomers, but this reaction is expected to be significantly slower than that of the competing ethylene acetoxylation reaction. Kragten et al. also showed that dimeric and

trimeric palladium acetates could be detected by ultra-violet absorption spectroscopy via transitions at ~ 350 nm and ~ 400 nm respectively.

4.1.3.1 Spectra of palladium acetate solutions derived from Batch 1, Batch 2, and Batch 3 catalysts

Palladium acetate solutions were derived from Batch 1, Batch 2, and Batch 3 catalysts according to the procedure described in Section 2.5.4. Ultra-violet absorption spectra of these solutions were then recorded using a procedure also described in Section 2.5.4.

Solutions obtained using acetic acid

Figure 4.30 shows ultra-violet absorption spectra for solutions obtained from Batch 1 catalysts. Each spectrum contained a peak occurring at ~ 400 nm which is diagnostic of the presence of trimeric palladium acetate. The spectrum for the solution derived from catalyst 3183, (0.0% Pd, 0.4% Au)[0.0]/G{1}, showed the lowest absorption while the spectra for the solutions derived from palladium-containing catalysts showed that the intensity of this peak and hence the concentration of trimeric palladium acetate increased in the following order: catalyst 4266, catalyst 4265, catalyst 3182, catalyst 3186, catalyst 3187, catalyst 3185, catalyst 3188, and catalyst 3200. The spectra for solutions derived from catalyst 4266 and catalyst 4265 also contained the hint of a peak at ~ 350 nm. This is diagnostic of the presence of dimeric palladium acetate.

Generally, the extent of palladium dissolution from each catalyst was proportional to the intensity of the peak at ~ 400 nm.

Figure 4.30 – Ultra-violet absorption spectra for palladium acetate solutions derived from reaction of Batch 1 catalysts with acetic acid

3182 = (1.0% Pd, 0.0% Au)[∞]/G{1}	*3187 = (1.0% Pd, 1.7% Au)[1.1]/G{1}*
3185 = (1.6% Pd, 0.6% Au)[4.8]/G{1}	*3188 = (1.0% Pd, 2.5% Au)[0.7]/G{1}*
3184 = (1.0% Pd, 1.4% Au)[4.7]/G{1}	*4266 = (0.5% Pd, 1.8% Au)[0.5]/G{1}*
3186 = (1.0% Pd, 1.0% Au)[2.0]/G{1}	*4265 = (0.2% Pd, 1.7% Au)[0.2]/G{1}*
3200 = (1.0% Pd, 0.9% Au)[1.9]/G{1}	*3183 = (0.0% Pd, 0.4% Au)[0.0]/G{1}*

Ultra-violet absorption spectra for solutions obtained from Batch 2 catalysts are shown in Figure 4.31. Generally, each spectrum contained two peaks; the first, at ~ 350 nm, indicated the presence of dimeric palladium acetate. The second, at ~ 400 nm, indicated the existence of trimeric palladium acetate. At ~ 400 nm, the spectrum for the solution derived from catalyst 3330, (0.0% Pd, 0.4% Au)[0.0]/G{2}, showed an intensity comparable with that of solutions from certain palladium-containing catalysts. The spectra derived from the palladium-containing catalysts of Batch 2 indicated that the concentration of trimeric palladium acetate increased in the following order: catalyst 4268, catalyst 4267, catalyst 3335, catalyst 3334, catalyst 3331, catalyst 3329, catalyst 3332, and catalyst 3333. Due to the co-existence of two palladium acetate species, the extent of palladium dissolution from these catalysts was difficult to assess.

Figure 4.31 – Ultra-violet absorption spectra for palladium acetate solutions derived from reaction of Batch 2 catalysts with acetic acid

3329 = (1.0% Pd, 0.0% Au)[∞]/G{2}	3334 = (1.0% Pd, 1.8% Au)[1.0]/G{2}
3331 = (1.0% Pd, 0.4% Au)[4.8]/G{2}	3335 = (1.0% Pd, 2.7% Au)[0.7]/G{2}
3332 = (1.7% Pd, 0.6% Au)[4.8]/G{2}	4268 = (0.5% Pd, 1.8% Au)[0.6]/G{2}
3333 = (1.0% Pd, 1.0% Au)[1.9]/G{2}	4267 = (0.2% Pd, 1.8% Au)[0.2]/G{2}
3330 = (0.0% Pd, 0.4% Au)[0.0]/G{2}	

Figure 4.32 shows ultra-violet absorption spectra for solutions obtained from Batch 3 catalysts. These spectra also contained peaks at ~ 350 nm and ~ 400 nm diagnostic of the co-existence of palladium acetate dimers and trimers. Spectral intensity at ~ 400 nm increased in the following order: catalyst 4270, catalyst 4269, catalyst 3337, (0.0% Pd, 0.4% Au)[0.0]/G{3}, catalyst 3338, catalyst 3339, catalyst 3342, catalyst 3340, catalyst 3336, and catalyst 3341. Again, the extent of palladium dissolution was difficult to assess based on the intensity of the peak occurring at ~ 400 nm.

Figure 4.32 – Ultra-violet absorption spectra for palladium acetate solutions derived from reaction of Batch 3 catalysts with acetic acid

3336 = (1.0% Pd, 0.0% Au)[∞]/G{3}	*3341 = (1.0% Pd, 1.7% Au)[1.1]/G{3}*
3339 = (1.7% Pd, 0.6% Au)[5.4]/G{3}	*3342 = (1.0% Pd, 2.6% Au)[0.7]/G{3}*
3338 = (1.0% Pd, 0.4% Au)[4.9]/G{3}	*4270 = (0.5% Pd, 1.8% Au)[0.5]/G{3}*
3340 = (1.0% Pd, 0.9% Au)[2.1]/G{3}	*4269 = (0.2% Pd, 1.8% Au)[0.2]/G{3}*
3337 = (0.0% Pd, 0.4% Au)[0.0]/G{3}	

Solutions obtained using 0.5 mol dm^{-3} potassium acetate in acetic acid

Figure 4.33 shows spectra for solutions derived from Batch 1 catalysts. Each spectrum contained a peak at ~ 350 nm diagnostic of the presence of palladium acetate in its dimeric form. Thus, the effect of higher acetate concentrations used in the modification stage was to shift the position of the equilibrium between palladium acetate trimers and dimers significantly towards that of the dimers. The spectrum for the solution derived from catalyst 3183, (0.0% Pd, 0.4% Au)[0.0]/G{1}, showed the lowest absorption, while the spectra for the solutions obtained from palladium-containing catalysts showed that the concentration of the dimeric palladium acetate (and hence the extent of palladium dissolution) increased in the order: catalyst 3182, catalyst 4265, catalyst 4266, catalyst 3184, catalyst 3188, catalyst 3187, catalyst 3185, and catalyst 3200.
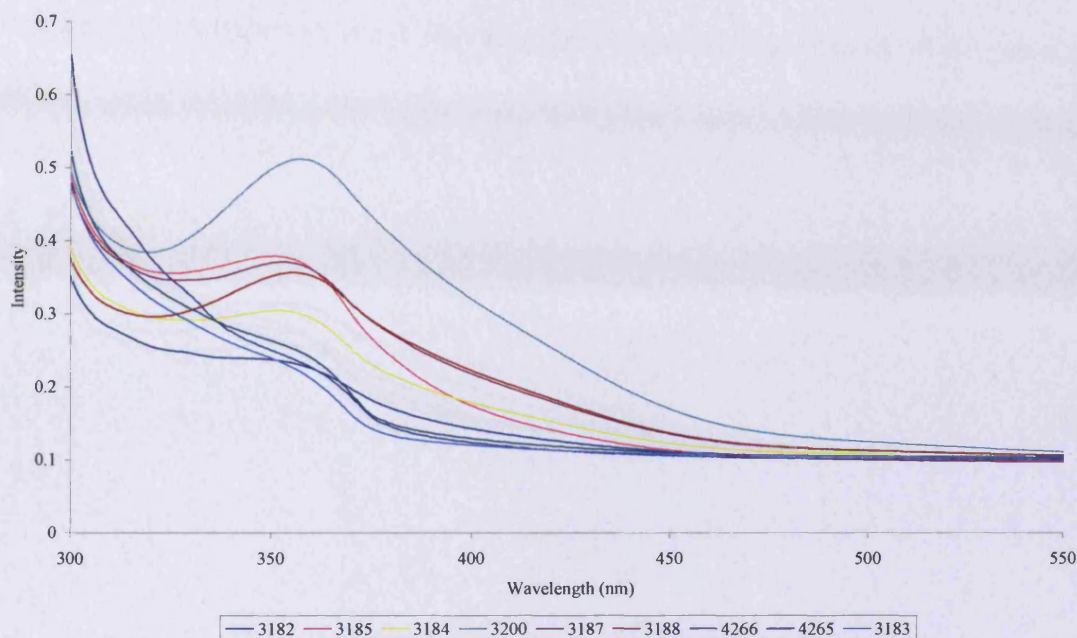
Figure 4.33 – Ultra-violet absorption spectra for palladium acetate solutions derived from reaction of Batch 1 catalysts with 0.5 mol dm^{-3} potassium acetate in acetic acid

3182 = (1.0% Pd, 0.0% Au)[∞]/G{1}	3187 = (1.0% Pd, 1.7% Au)[1.1]/G{1}
3185 = (1.6% Pd, 0.6% Au)[4.8]/G{1}	3188 = (1.0% Pd, 2.5% Au)[0.7]/G{1}
3184 = (1.0% Pd, 1.4% Au)[4.7]/G{1}	4266 = (0.5% Pd, 1.8% Au)[0.5]/G{1}
3186 = (1.0% Pd, 1.0% Au)[2.0]/G{1}	4265 = (0.2% Pd, 1.7% Au)[0.2]/G{1}
3200 = (1.0% Pd, 0.9% Au)[1.9]/G{1}	3183 = (0.0% Pd, 0.4% Au)[0.0]/G{1}

Spectra for the solutions derived from Batch 2 catalysts are shown in Figure 4.34. These spectra contained two peaks, indicating the presence of dimers and trimers. The spectrum for the solution obtained from catalyst 3330, (0.0% Pd, 0.4% Au)[0.0]/G{2}, showed an intensity comparable with that of solutions from certain palladium-containing catalysts and the spectra for solutions derived from palladium-containing catalysts showed that the absorption (and hence concentration of dimeric palladium acetate) increased in the following order: catalyst 4267, catalyst 4268, catalyst 3329, catalyst 3334, catalyst 3335, catalyst 3333, catalyst 3331, and catalyst 3332. Due to the co-existence of the two palladium acetate species, the extent of palladium dissolution was difficult to assess based on the intensity of the peak occurring at ~ 350 nm.
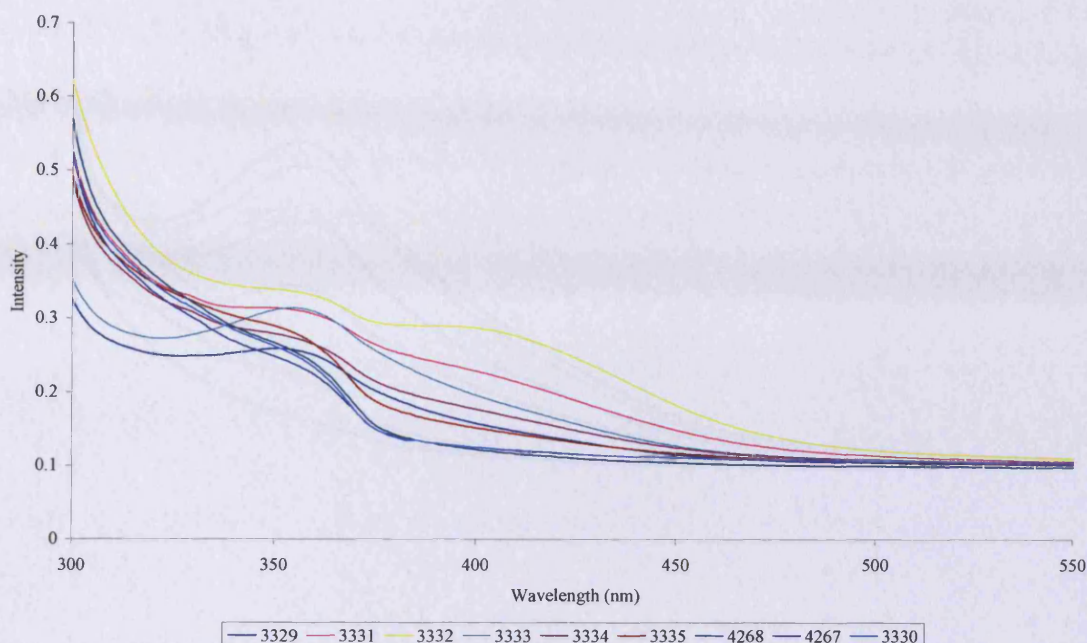
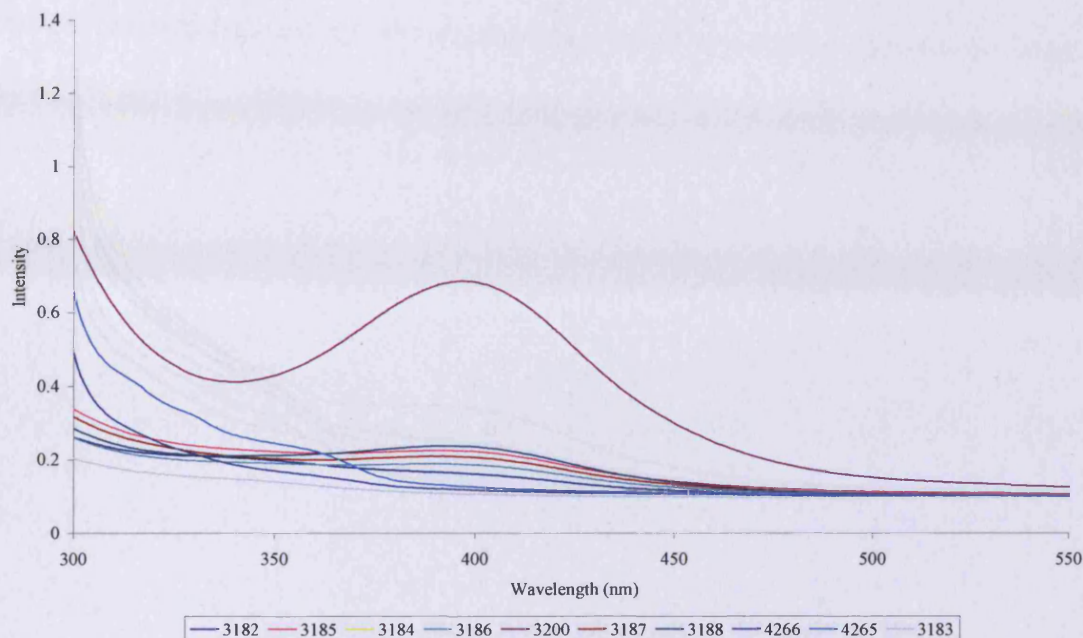*Figure 4.34 – Ultra-violet absorption spectra for palladium acetate solutions derived from reaction of Batch 2 catalysts with 0.5 mol dm^{-3} potassium acetate in acetic acid*

3329 = (1.0% Pd, 0.0% Au)[∞]/G{2}	3334 = (1.0% Pd, 1.8% Au)[1.0]/G{2}
3331 = (1.0% Pd, 0.4% Au)[4.8]/G{2}	3335 = (1.0% Pd, 2.7% Au)[0.7]/G{2}
3332 = (1.7% Pd, 0.6% Au)[4.8]/G{2}	4268 = (0.5% Pd, 1.8% Au)[0.6]/G{2}
3333 = (1.0% Pd, 1.0% Au)[1.9]/G{2}	4267 = (0.2% Pd, 1.8% Au)[0.2]/G{2}
	3330 = (0.0% Pd, 0.4% Au)[0.0]/G{2}

Spectra for the solutions obtained from Batch 3 catalysts are shown in Figure 4.35. These spectra (like those shown in Figure 4.33) contained a single peak at ~ 350 nm, due to the presence of dimeric palladium acetate. The spectrum for the solution obtained from catalyst 3337, (0.0% Pd, 0.4% Au)[0.0]/G{3}, showed an intensity comparable with that of solutions from certain palladium-containing catalysts and the intensity of the solutions derived from palladium-containing catalysts increased in the order: catalyst 4269, catalyst 4270, catalyst 3336, catalyst 3341, catalyst 3339, catalyst 3340, catalyst 3342, and catalyst 3338.
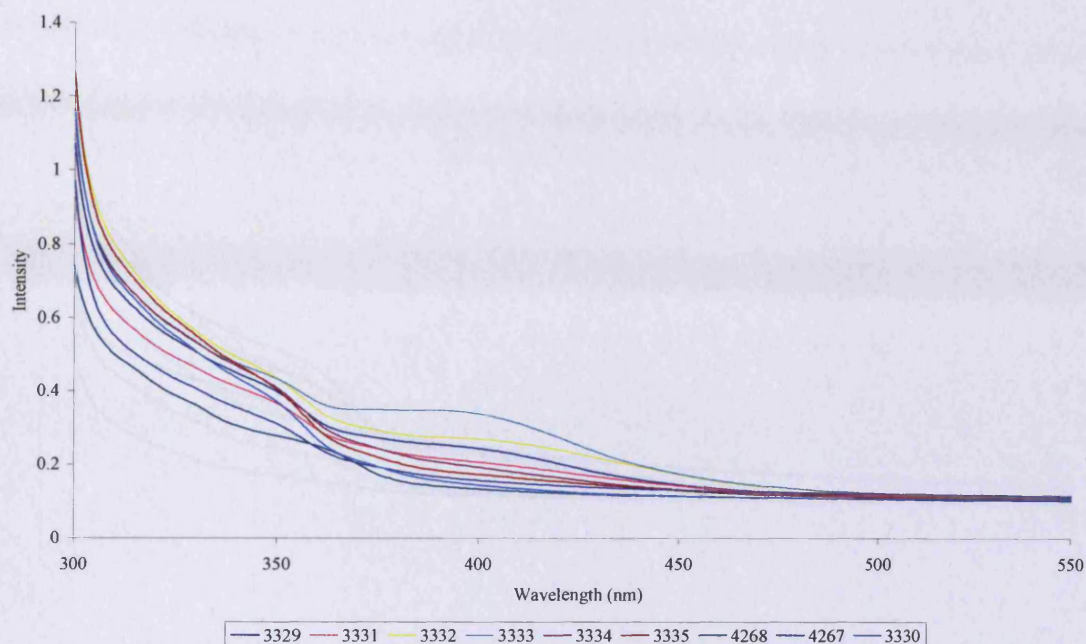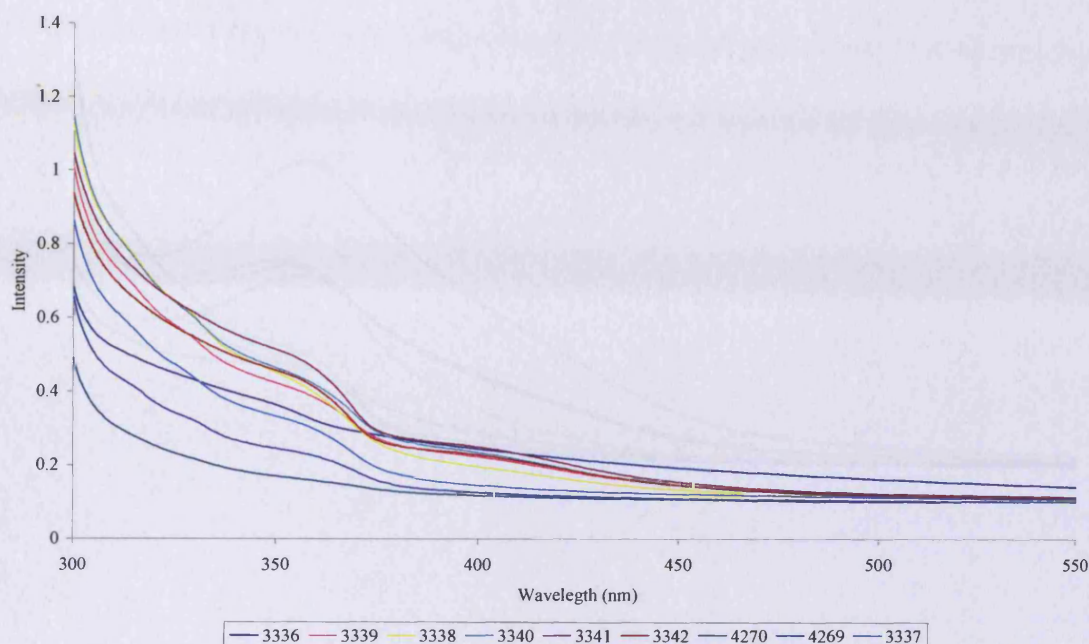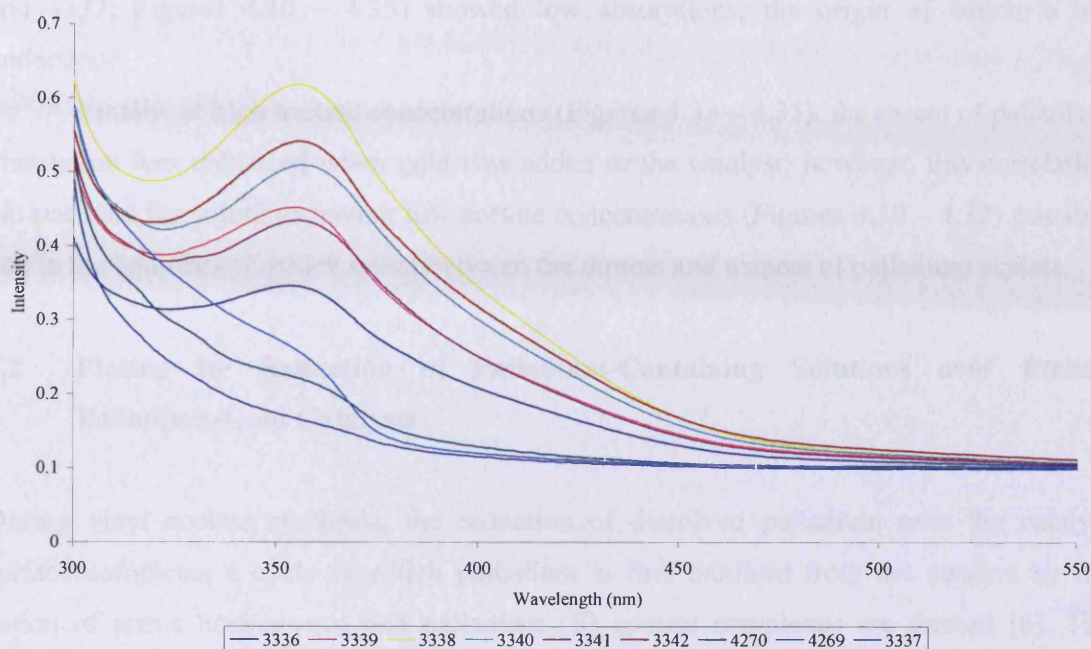
Figure 4.35 – Ultra-violet absorption spectra for palladium acetate solutions derived from reaction of Batch 3 catalysts with 0.5 mol dm^{-3} potassium acetate in acetic acid

3336 = (1.0% Pd, 0.0% Au)[∞]/G{3}	3341 = (1.0% Pd, 1.7% Au)[1.1]/G{3}
3339 = (1.7% Pd, 0.6% Au)[5.4]/G{3}	3342 = (1.0% Pd, 2.6% Au)[0.7]/G{3}
3338 = (1.0% Pd, 0.4% Au)[4.9]/G{3}	4270 = (0.5% Pd, 1.8% Au)[0.5]/G{3}
3340 = (1.0% Pd, 0.9% Au)[2.1]/G{3}	4269 = (0.2% Pd, 1.8% Au)[0.2]/G{3}
3337 = (0.0% Pd, 0.4% Au)[0.0]/G{3}	

4.1.3.2 Conclusions

Figures 4.30 – 4.35 show that dimers and trimers of palladium acetate were formed when palladium and palladium-gold catalysts were exposed to solutions containing acetic acid and acetic acid/potassium acetate.

At low acetate concentrations (Figures 4.30 – 4.32), palladium acetate trimers were predominant but dimers were also detected in solutions derived from Batch 2 and Batch 3 catalysts (Figures 4.31 and 4.32). At higher acetate concentrations the spectra for solutions derived from Batch 1 and Batch 3 catalysts (Figures 4.33 and 4.35) indicated the presence (almost exclusively) of palladium acetate in its dimeric state (via peak maxima at ~ 350 nm) whilst the spectra for the solutions derived from Batch 2 catalysts (Figure 4.34) indicated the co-existence of the palladium acetate dimers and trimers. At both acetate concentrations, the spectra for solutions derived from gold/graphite catalysts (3183, 3330,

and 3337; Figures 4.30 – 4.35) showed low absorptions, the origin of which is not understood.

Finally, at high acetate concentrations (Figures 4.33 – 4.35), the extent of palladium dissolution was enhanced when gold was added to the catalyst; however, this correlation did not hold for solutions having low acetate concentrations (Figures 4.30 – 4.32) possibly due to the equilibrium which exists between the dimers and trimers of palladium acetate.

4.2 Plating by Reduction of Palladium-Containing Solutions over Etched Palladium-Gold Catalysts

During vinyl acetate synthesis, the reduction of dissolved palladium over the catalyst surface completes a cycle in which palladium is first oxidised from the catalyst by the action of acetic acid/oxygen and palladium (II) acetate complexes are formed [6]. The reduction of palladium (II) complexes plays an important role in the mechanism as this reduction is likely to be one of the redox processes which ultimately leads to the oxidation of ethylene and the formation of vinyl acetate.

To investigate this matter, palladium-containing solutions obtained by treating catalysts of Batch 1, Batch 2, and Batch 3 with solutions of acetic acid and of 0.5 mol dm^{-3} potassium acetate in acetic acid were reduced over etched catalyst surfaces to create new catalysts which had palladium plated (deposited from solution) over the etched catalyst surfaces. The plating procedure is described in Section 2.2.9.

4.2.1 Reduction by Hydrogen

Catalysts etched in acetic acid

Figures 4.36 – 4.38 show the CVs for etched and subsequently-plated Batch 2 catalysts 3329, and 3331 – 3335, 4268, and 4267. The following trends were observed: (i) in all cases the charge associated with the hydrogen under-potential deposition region increased on plating the etched catalyst, (ii) the charge associated with the palladium-oxide stripping region also increased. The charges are recorded in Table 4.4. These charge enhancements show that the palladium surface area of each catalyst increased as a result of the plating procedure.

Table 4.4 – Batch 2 catalysts: charges (normalised^z) associated with the hydrogen under-potential deposition region, the palladium-oxide stripping region, and the gold-oxide stripping region for catalysts etched in acetic acid and subsequently plated with palladium from palladium acetate solution

Catalyst		Region charge / μC					
ref no	description	HUPD		Pd-O stripping		Au-O stripping	
		Etched	Plated	Etched	Plated	Etched	Plated
3329	(1.0% Pd, 0.0% Au)[∞]/G{2}	1840	2290	3160	3715	–	–
3331	(1.0% Pd, 0.4% Au)[4.8]/G{2}	1380	1855	2655	3220	n/o	n/o
3332	(1.7% Pd, 0.6% Au)[4.8]/G{2}	2040	2615	3920	4485	n/o	n/o
3333	(1.0% Pd, 1.0% Au)[1.9]/G{2}	1335	2205	3395	4390	185	45
3334	(1.0% Pd, 1.8% Au)[1.0]/G{2}	1485	1880	2660	2880	105	95
3335	(1.0% Pd, 2.7% Au)[0.7]/G{2}	895	1360	2010	2380	370	335
4268	(0.5% Pd, 1.8% Au)[0.6]/G{2}	20	650	1655	1270	410	405
4267	(0.2% Pd, 1.8% Au)[0.2]/G{2}	200	170	560	595	335	305

n/o = not observed ^{z}*for procedure see Section 2.2.10*

In the case of the palladium-gold catalysts (i.e. with the exception of catalyst 3329, (1.0% Pd, 0.0% Au)[∞]/G{2}) the potential required to remove palladium-oxide from the surface of the plated catalyst was more negative than the potential required to remove it from the etched catalyst, indicating an enhanced palladium concentration at the surface. However, the potential was always greater then 0.62 V (Table 4.5), the value for palladium-oxide stripping from the pure palladium surface, showing that gold atoms migrated to the fresh surface created by the plating process.

Commencing with catalyst 3333, (1.0% Pd, 1.0% Au)[1.9]/G{2}, a gold-oxide stripping region was present for both the etched and plated catalysts. The charge associated with the gold-oxide stripping region was reduced by the palladium plating process, although the effect was not marked except for catalyst 3333 (Table 4.4). Moreover, in all cases, the peak minima moved to more negative potentials (Table 4.5). Both observations are consistent with palladium enrichment of the surface on plating.

Thus, the effects of palladium plating of these etched catalysts are that the process increased the palladium surface area and increased the palladium concentration in the surface.

The potentials required to remove palladium-oxide and gold-oxide from the surfaces of etched and plated Batch 2 catalysts are shown in Table 4.5. In nearly all cases, the potential required to strip palladium-oxide from plated catalyst was more negative than that

required to remove palladium-oxide from the corresponding etched catalyst. This is diagnostic of palladium enrichment of the surface particles. When detected, the potentials required to remove gold-oxide were also found to vary between the etched and plated catalysts, with the plated catalyst having the most negative potential in each case. This result is also diagnostic of palladium enrichment after plating.

Table 4.5 – Batch 2 catalysts: potentials required for palladium-oxide stripping and gold-oxide stripping for catalysts etched in acetic acid and subsequently plated with palladium from palladium acetate solution

Catalyst		Potential / V			
		Pd-O stripping		Au-O stripping	
ref no	description	Etched	Plated	Etched	Plated
3329	(1.0% Pd, 0.0% Au)[∞]/G{2}	0.62	0.62	–	–
3331	(1.0% Pd, 0.4% Au)[4.8]/G{2}	0.64	0.63	n/o	n/o
3332	(1.7% Pd, 0.6% Au)[4.8]/G{2}	0.65	0.64	n/o	n/o
3333	(1.0% Pd, 1.0% Au)[1.9]/G{2}	0.67	0.66	1.09	n/o
3334	(1.0% Pd, 1.8% Au)[1.0]/G{2}	0.71	0.70	1.09	1.08
3335	(1.0% Pd, 2.7% Au)[0.7]/G{2}	0.76	0.73	1.12	1.11
4268	(0.5% Pd, 1.8% Au)[0.6]/G{2}	0.76[a]	0.74[a]	1.16	1.11
4267	(0.2% Pd, 1.8% Au)[0.2]/G{2}	0.79[a]	0.72[a]	1.15	1.13

[a] *potential of most significant stripping feature*
n/o = not observed

Figure 4.36 – CVs for etched (acetic acid) and subsequently palladium-plated (a) catalyst 3329, (1.0% Pd, 0.0% Au)[∞]/G{2}, (b) catalyst 3331, (1.0% Pd, 0.4% Au)[4.8]/G{2}, and (c) catalyst 3332, (1.7% Pd, 0.6% Au)[4.8]/G{2}

Figure 4.37 – CVs for etched (acetic acid) and subsequently palladium-plated (a) catalyst 3333, (1.0% Pd, 1.0% Au)[1.9]/G{2}, (b) catalyst 3334, (1.0% Pd, 1.8% Au)[1.0]/G{2}, and (c) catalyst 3335, (1.0% Pd, 2.7% Au)[0.7]/G{2}

Catalysts etched in acetic acid, subsequently plated

The CVs for etched and plated catalyst analyses are shown in Figures 4.38 and 4.39. The shape is almost identical to those reported for the catalysts etched in oxalic acid. Values for the charges associated with the Pd(PH) palladium-oxide stripping, and gold-oxide stripping regions are given in Table 4.x. The potentials required for palladium-oxide and gold-oxide stripping from the etched and plated catalysts are also tabulated (Table 4.x).

Table 4.21 – Pd-catalysed catalyst charges associated with the Pd(PH) peak, the potential associated with the palladium-oxide stripping region, and the gold-oxide stripping region for catalysts etched in concentrated acetic acid and subsequently plated with palladium, using a nitrate-acetate solution

Figure 4.38 – CVs for etched (acetic acid) and subsequently palladium-plated (a) catalyst 4268, (0.5% Pd, 1.8% Au)[0.6]/G{2} and (b) catalyst 4267, (0.2% Pd, 1.8% Au)[0.2]/G{2}

The plated catalyst analyses indicate palladium species formed from hydrogen evolution from the palladium-containing metal particles as bulk palladium hydride undergoes stripping from...

Catalysts etched in acetic acid/potassium acetate

The CVs for etched and plated Batch 2 catalysts are shown in Figures 4.39 – 4.41. The general behaviour follows that reported for the catalysts etched in acetic acid. Values for the charges associated with the HUPD, palladium-oxide stripping, and gold-oxide stripping regions are shown in Table 4.6. The potentials required for palladium-oxide and gold-oxide stripping from etched and plated catalysts are also tabulated (Table 4.7).

Table 4.6 – Batch 2 catalysts: charges (normalised^z) associated with the hydrogen under-potential deposition region, the palladium-oxide stripping region, and the gold-oxide stripping region for catalysts etched in acetic acid/potassium acetate and subsequently plated with palladium from palladium acetate solution

Catalyst		Region charge / μC					
ref no	description	HUPD		Pd-O stripping		Au-O stripping	
		Etched	Plated	Etched	Plated	Etched	Plated
3329	(1.0% Pd, 0.0% Au)[∞]/G{2}	1895	2195	3440	3670	n/o	n/o
3331	(1.0% Pd, 0.4% Au)[4.8]/G{2}	560	1260	2420	2580	n/o	n/o
3332	(1.7% Pd, 0.6% Au)[4.8]/G{2}	1620	2295	4380	4195	n/o	n/o
3333	(1.0% Pd, 1.0% Au)[1.9]/G{2}	680	2690	1855	3620	325	n/o
3334	(1.0% Pd, 1.8% Au)[1.0]/G{2}	1185	1970	2805	3400	165	40
3335	(1.0% Pd, 2.7% Au)[0.7]/G{2}	505	1800	1870	2905	525	275
4268	(0.5% Pd, 1.8% Au)[0.6]/G{2}	360	845	1435	1560	440	360
4267	(0.2% Pd, 1.8% Au)[0.2]/G{2}	185	195	600	695	385	390

n/o = not observed   *^{z}for procedure see Section 2.2.10*

The plated catalysts show a substantial peak at 0.02 V associated with hydrogen evolution from the palladium-containing metal particles as bulk palladium hydride undergoes decomposition. The charge associated with hydrogen evolution is subtracted from that for the whole region (extending to ~ 0.25 V, in order to obtain the values of the charge for the hydrogen under-potential deposition region quoted in Table 4.6).

There are some unexpected aspects of catalyst behaviour as shown by these CVs. First, there is almost no movement of the palladium-oxide stripping peak potential on plating for catalyst 3332, (1.7% Pd, 0.6% Au)[4.8]/G{2}, and only a marginal increase in the charge associated with this region. Furthermore, there is very little loss of charge or movement of potential with plating, in respect of the gold-oxide stripping regions for

catalyst 4268, (0.5% Pd, 1.8% Au)[0.6]/G{2}, and catalyst 4267, (0.2% Pd, 1.8% Au)[0.2]/G{2}, suggesting that some gold surfaces in these catalysts may be resistant to plating by palladium.

Nevertheless, the overall behaviour revealed in these CVs indicate that palladium plating of these etched catalysts again gives rise to an increase in palladium surface area and an increased surface concentration of palladium.

Table 4.7 – Batch 2 catalysts: potentials required for palladium-oxide stripping and gold-oxide stripping for catalysts etched in acetic acid/potassium acetate and subsequently plated with palladium from palladium acetate solution

Catalyst		Potential / V			
		Pd-O stripping		Au-O stripping	
ref no	description	Etched	Plated	Etched	Plated
3329	(1.0% Pd, 0.0% Au)[∞]/G{2}	0.62	0.62	–	–
3331	(1.0% Pd, 0.4% Au)[4.8]/G{2}	0.66	0.64	n/o	n/o
3332	(1.7% Pd, 0.6% Au)[4.8]/G{2}	0.66	0.66	n/o	n/o
3333	(1.0% Pd, 1.0% Au)[1.9]/G{2}	0.72	0.65	1.11	n/o
3334	(1.0% Pd, 1.8% Au)[1.0]/G{2}	0.71	0.69	1.09	n/o
3335	(1.0% Pd, 2.7% Au)[0.7]/G{2}	0.76	0.73	1.13	1.11
4268	(0.5% Pd, 1.8% Au)[0.6]/G{2}	0.75[a]	0.74[a]	1.13	1.11
4267	(0.2% Pd, 1.8% Au)[0.2]/G{2}	0.78[a]	0.76[a]	1.14	1.13

[a]*potential of most significant stripping feature*
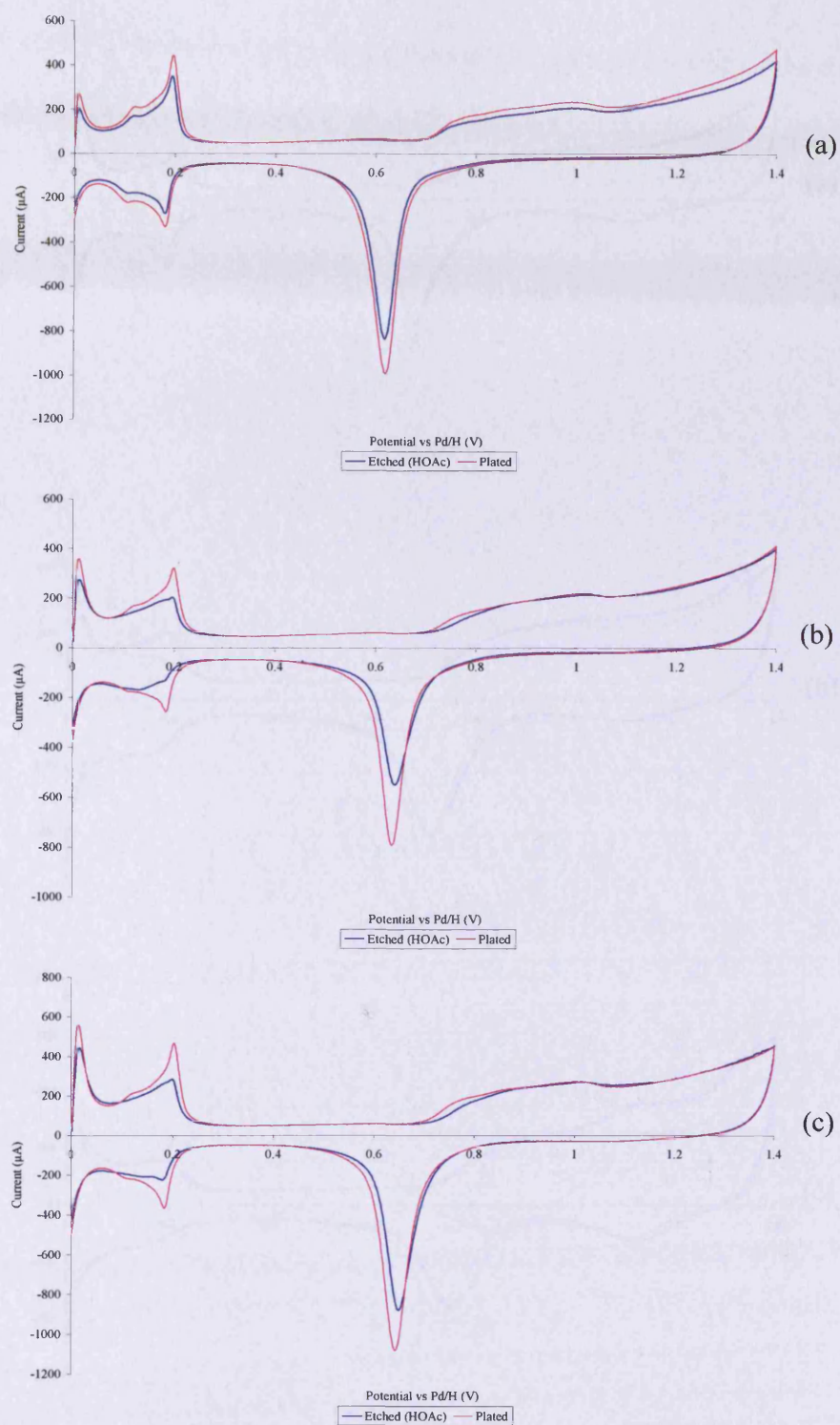*n/o = not observed*

Figure 4.39 – CVs for etched (acetic acid/potassium acetate) and subsequently palladium-plated (a) catalyst 3329, (1.0% Pd, 0.0% Au)[∞]/G{2}, (b) catalyst 3331, (1.0% Pd, 0.4% Au)[4.8]/G{2}, and (c) catalyst 3332, (1.7% Pd, 0.6% Au)[4.8]/G{2}
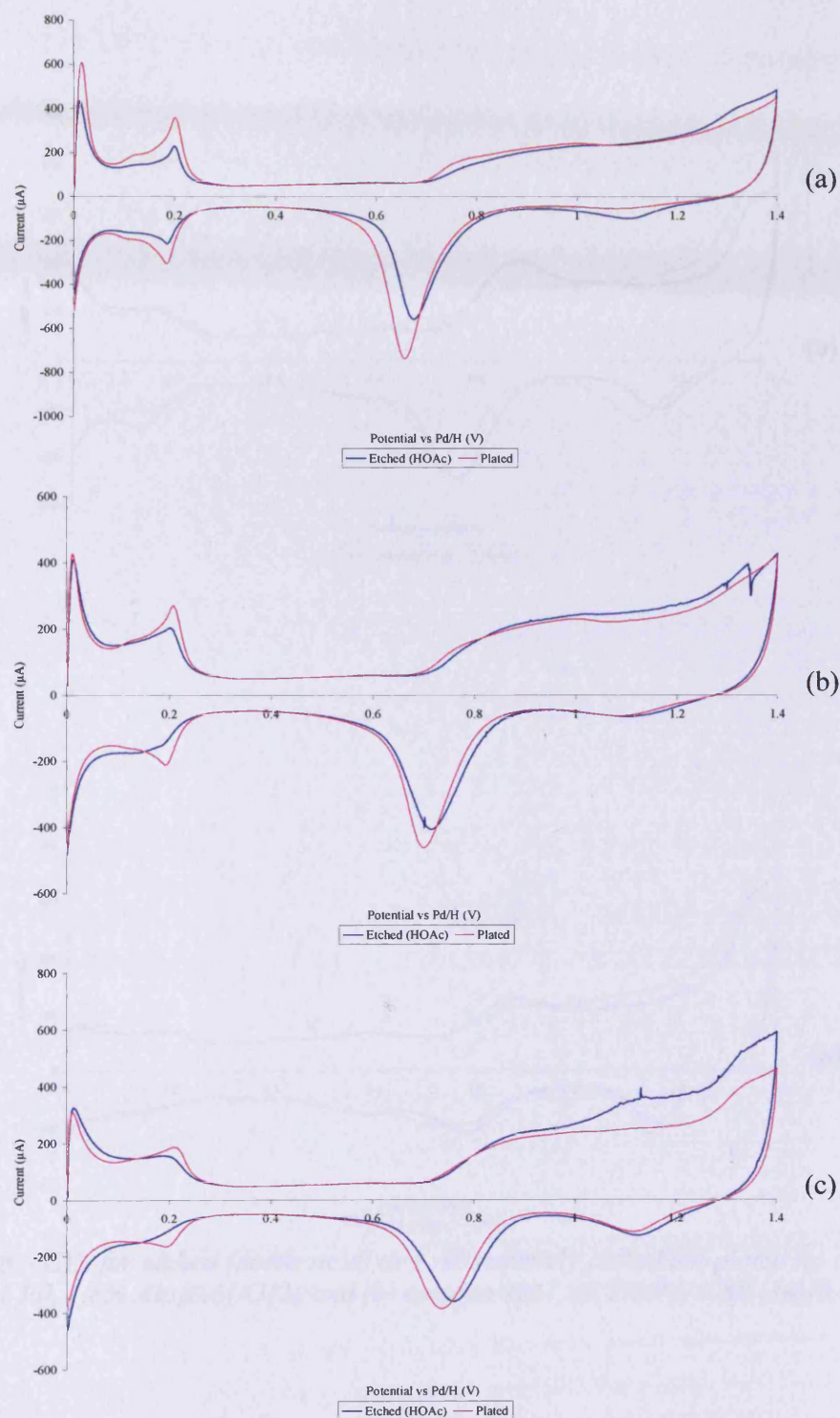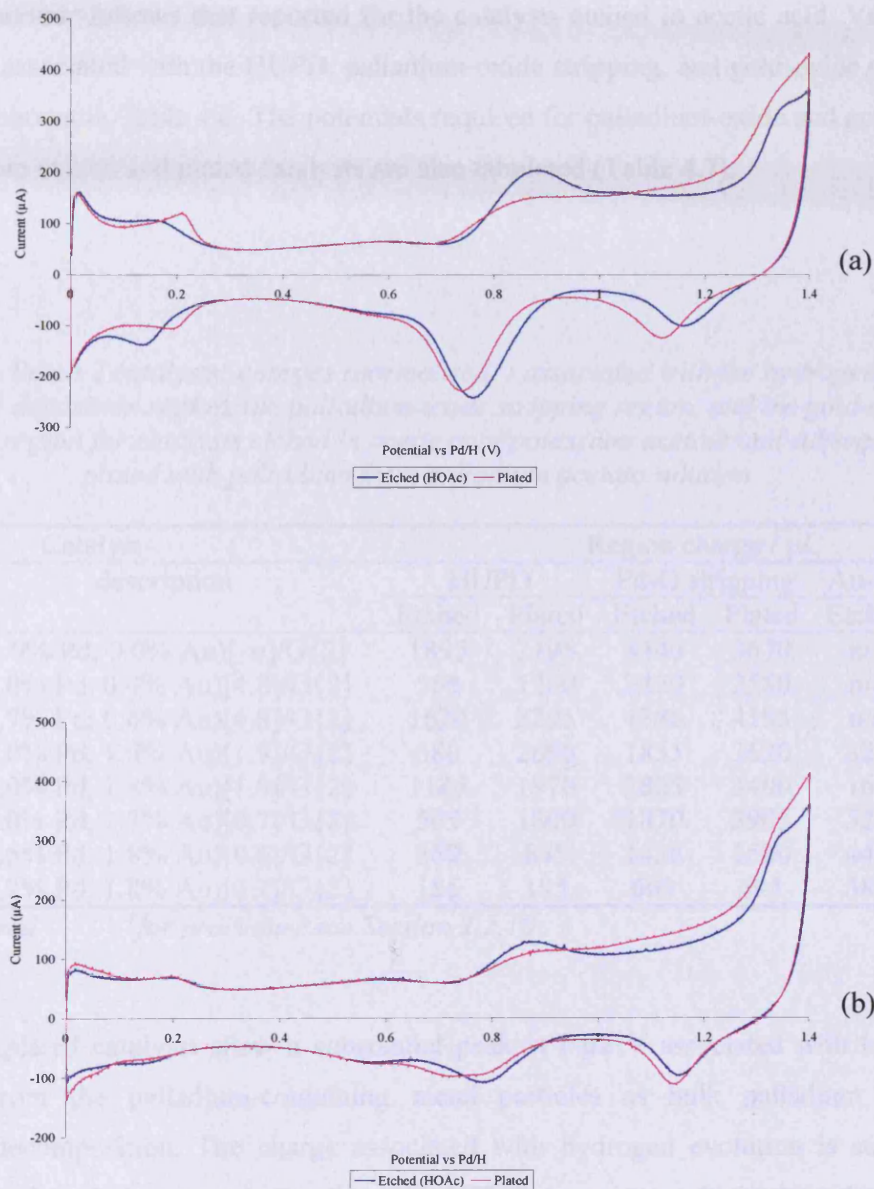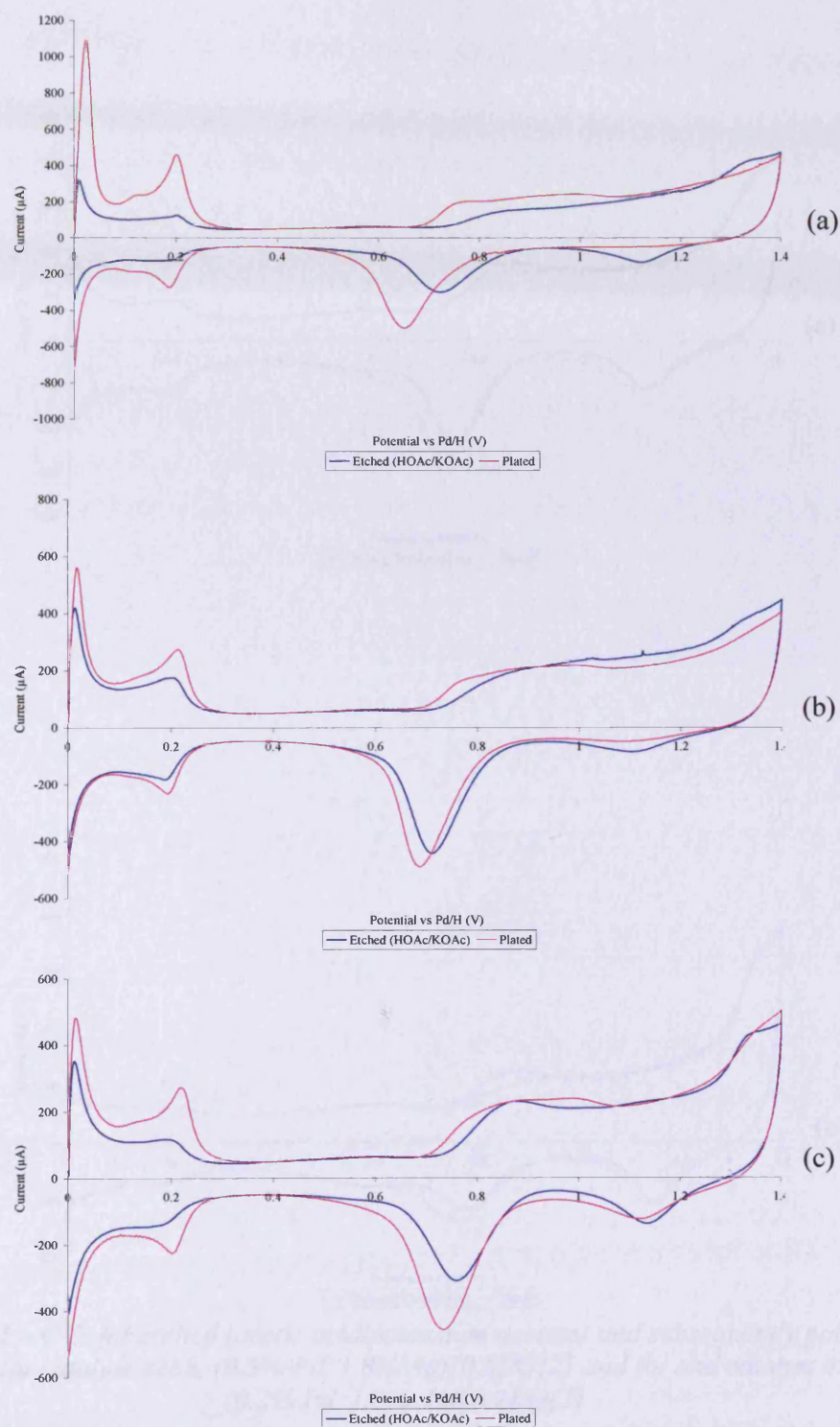
Figure 4.40 – CVs for etched (acetic acid/potassium acetate) and subsequently palladium-plated (a) catalyst 3333, (1.0% Pd, 1.0% Au)[1.9]/G{2}, (b) catalyst 3334, (1.0% Pd, 1.8% Au)[1.0]/G{2}, and (c) catalyst 3335, (1.0% Pd, 2.7% Au)[0.7]/G{2}

4.2.2   Reduction by Ethylene

Both 1 catalysts etched in acetic acid and in acetic acid/potassium acetate (Section 2.2.8) were plated by the reduction of palladium-containing solutions using ethylene (Section 2.2.9). The chemistry of the reduction may be formally expressed as follows:

$$Pd(OAc)_2 + C_2H_4 + H_2O \rightarrow Pd + 2HOAc + CH_3CHO$$

It was found that, for the two catalysts studied, it would provide information about the role of ethylene during the gas-phase synthesis of vinyl acetate monomer.

For the catalysts reduced with hydrogen (Section 4.2.1), relevant information was obtained from the first CVs recorded after catalyst reduction (Figures 4.39 – 4.41). However, when reduction was effected with ethylene, the situation was more complex because of the presence of adsorbed ethylene and to ethylene oxidation during the first cycle. It was, however, found that these effects were almost absent when a second cycle was conducted immediately after the first. Thus, Figures 4.41 – 4.33 each show (i) a CV for the etched catalyst and (ii) the comparative CV for the plated material.

Catalyst etched in acetic acid

Figures 4.42 – 4.43 show the CVs for etched and subsequently plated (by ethylene) catalysts 4136 and 4135 ....(s).

For catalysts, the charge associated with the hydrogen underpotential region was obtained by subtracting the baseline associated with hydrogen evolution; these residual charges were ... .

[Figure (a) — current (µA) vs Potential vs Pd/H (V); legend: Etched (HOAc/KOAc), Plated]

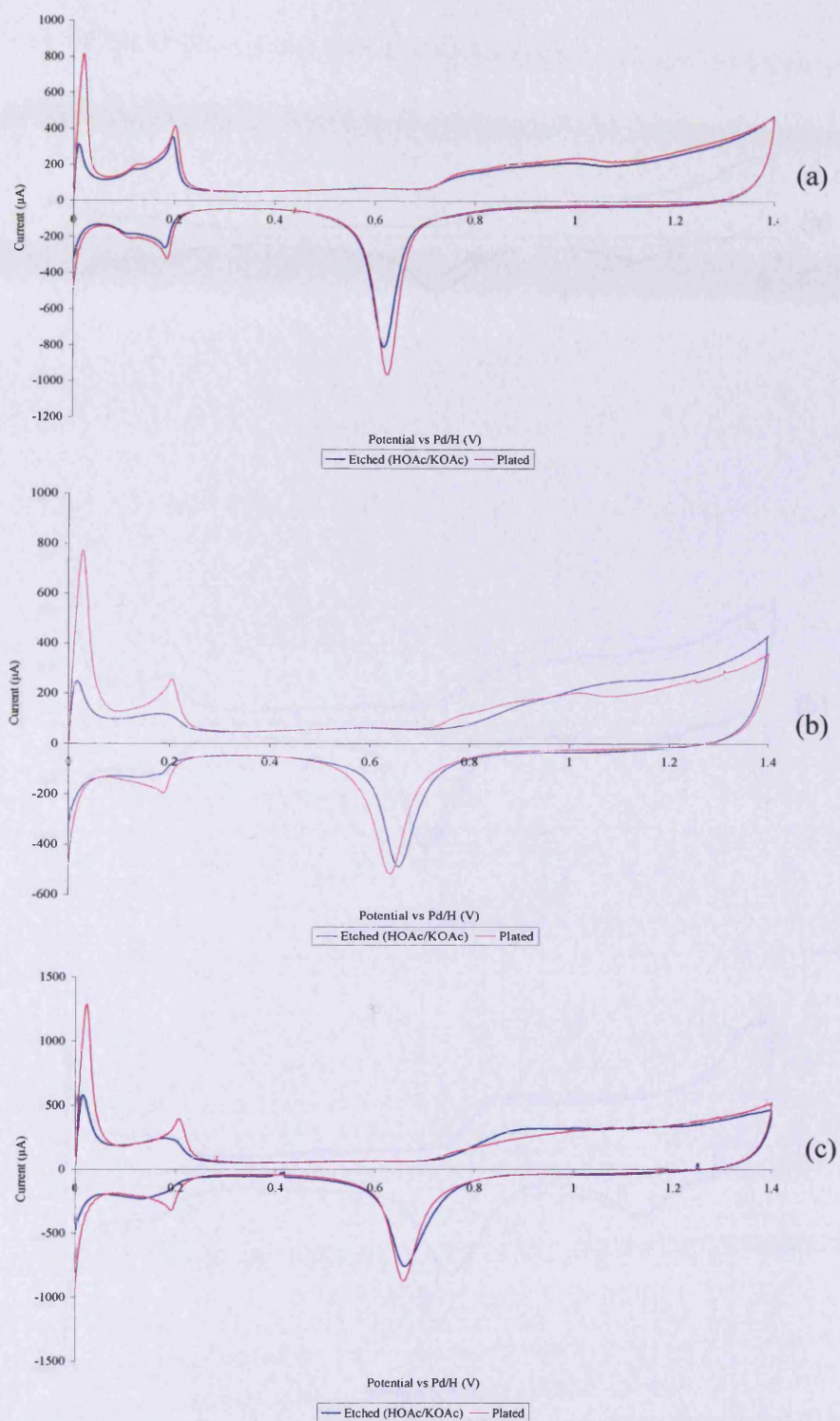[Figure (b) — current (µA) vs Potential vs Pd/H (V); legend: Etched (HOAc/KOAc), Plated]

Figure 4.41 – CVs for etched (acetic acid/potassium acetate) and subsequently palladium-plated (a) catalyst 4268, (0.5% Pd, 1.8% Au)[0.6]/G{2} and (b) and catalyst 4267, (0.2% Pd, 1.8% Au)[0.2]/G{2}

4.2.2   Reduction by Ethylene

Batch 3 catalysts etched in acetic acid and in acetic acid/potassium acetate (Section 2.2.8) were plated by the reduction of palladium-containing solutions using ethylene (Section 2.2.9). The chemistry of the reduction may be formally expressed as follows:

$$6\ Pd(OAc)_2 + CH_2{=}CH_2 + 4\ H_2O \longrightarrow 6\ Pd + 2\ CO_2 + 12\ HOAc \tag{3}$$
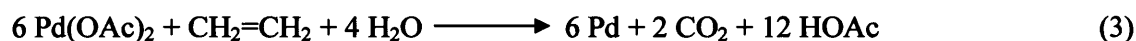
It was hoped that the CVs for the catalysts so reduced would provide information about the role of ethylene during the gas-phase synthesis of vinyl acetate monomer.

For the catalysts reduced with hydrogen (Section 4.2.1), relevant information was obtained from the first CV recorded after catalyst reduction (Figures 4.36 – 4.41). However, when reduction was effected by ethylene the situation was more complex due to the presence of adsorbed ethylene and to ethylene oxidation during the first cycle. It was, however, found that these effects were almost absent when a second cycle was conducted immediately after the first. Thus, Figures 4.42 – 4.53 each show (i) a CV for the etched catalyst and (ii) two consecutive CVs for the plated catalyst.

Catalysts etched in acetic acid

Figures 4.42 – 4.47 show the CVs for etched and subsequently-plated Batch 3 catalysts 3336 and 3338 – 3342.

For each CV, the charge associated with the hydrogen under-potential deposition region was calculated by subtracting the charge associated with hydrogen evolution from the total charge associated with the CV from 0.00 V to ~ 0.25 V in the forward sweep.
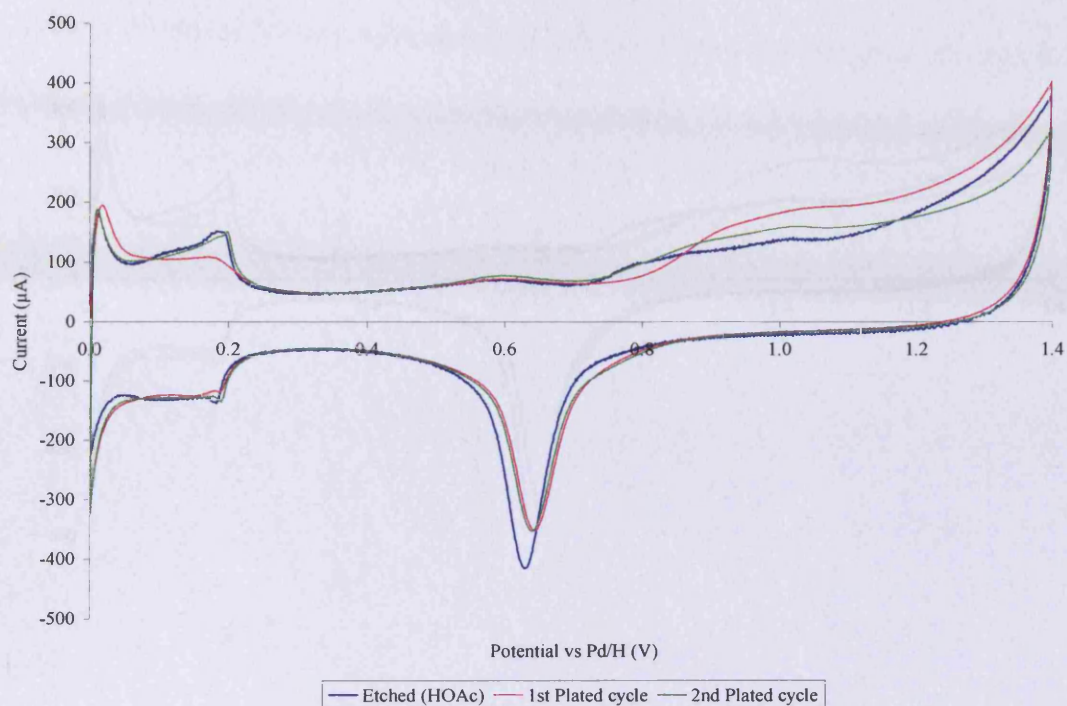
Figure 4.42 – CVs for etched (acetic acid) and subsequently palladium-plated catalyst 3336, (1.0% Pd, 0.0% Au)[∞]/G{3}
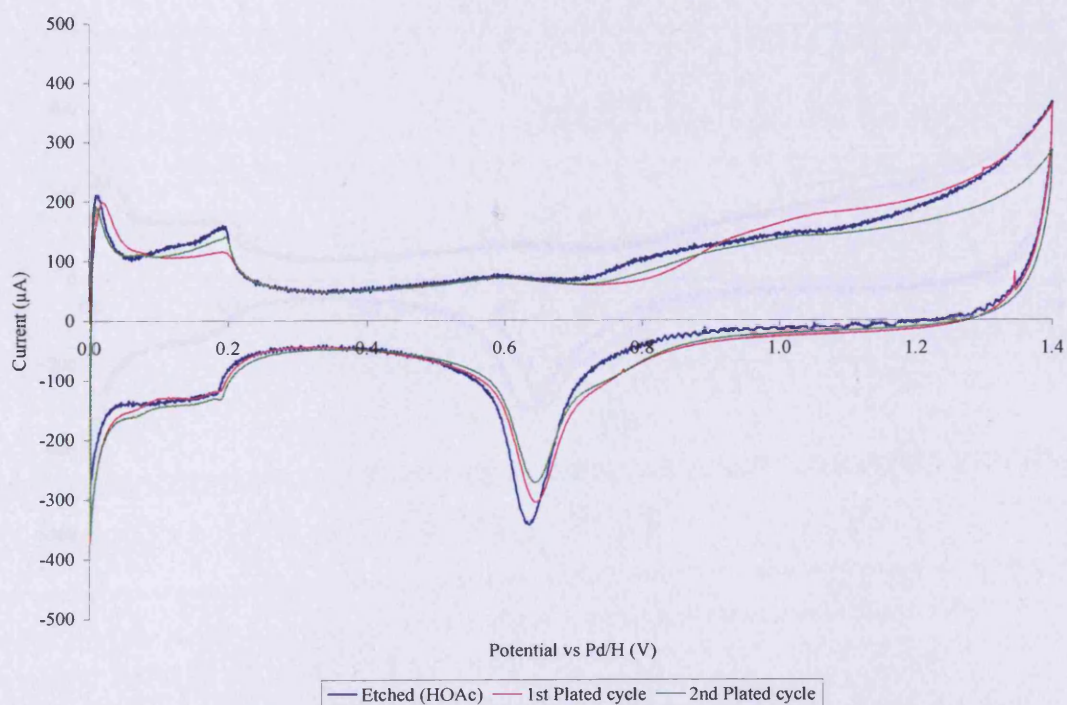
Figure 4.43 – CVs for etched (acetic acid) and subsequently palladium-plated catalyst 3338, (1.0% Pd, 0.4% Au)[4.9]/G{3}
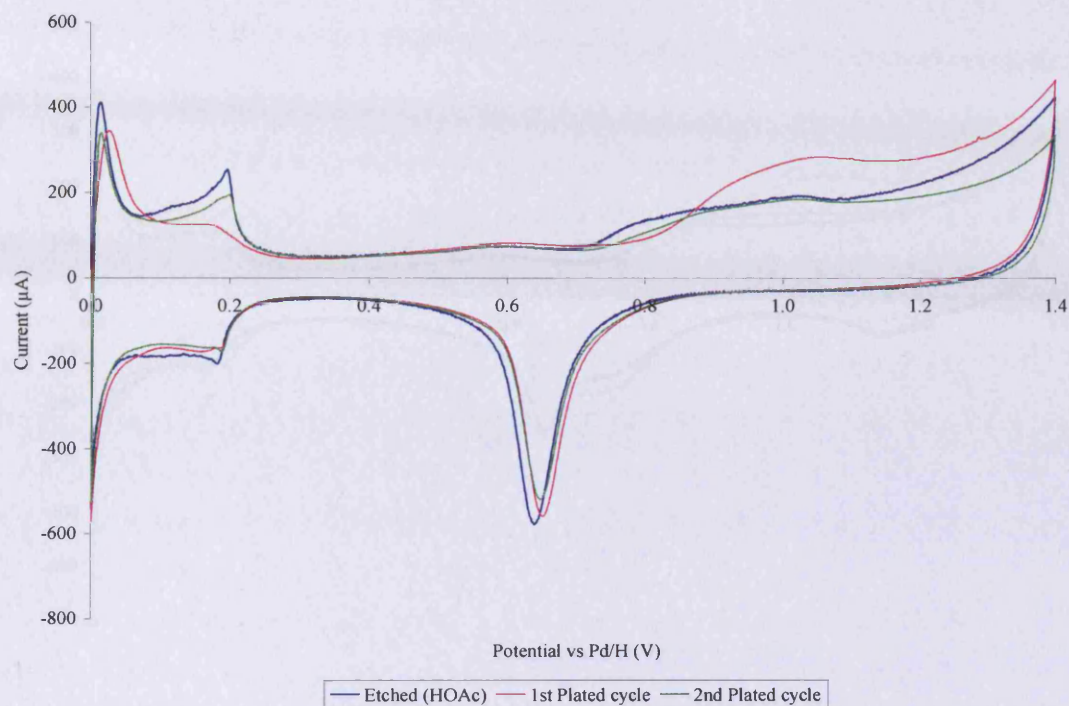
*Figure 4.44 – CVs for etched (acetic acid) and subsequently palladium-plated catalyst
3339, (1.7% Pd, 0.6% Au)[5.4]/G{3}*
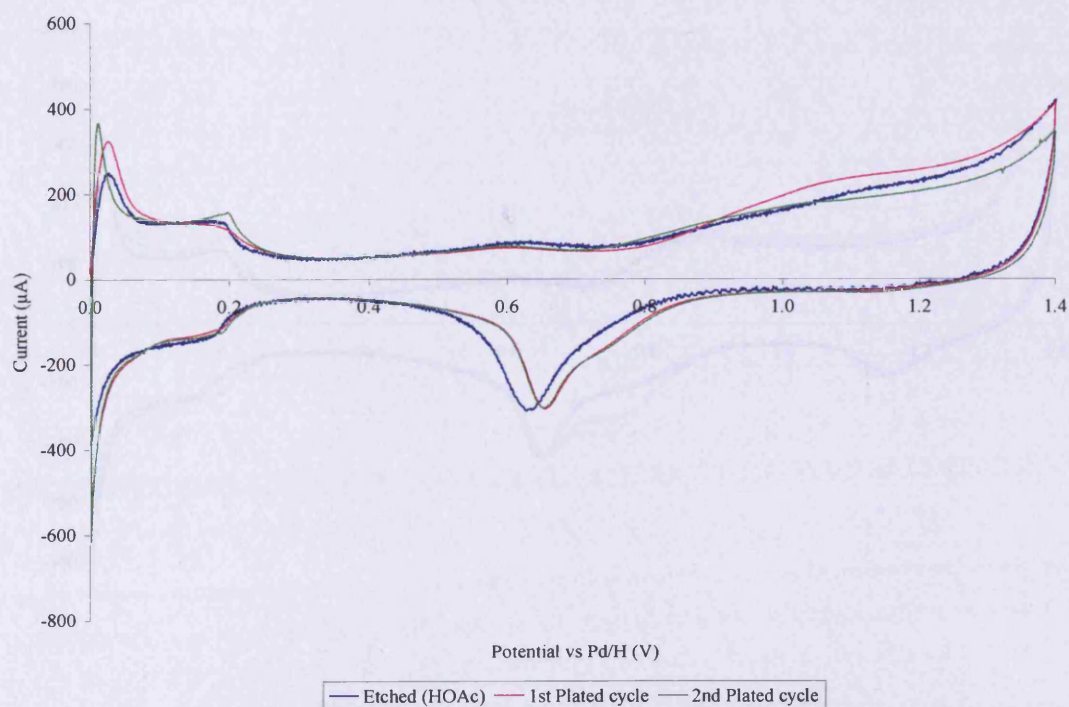
*Figure 4.45 – CVs for etched (acetic acid) and subsequently palladium-plated catalyst
3340, (1.0% Pd, 0.9% Au)[2.1]/G{3}*
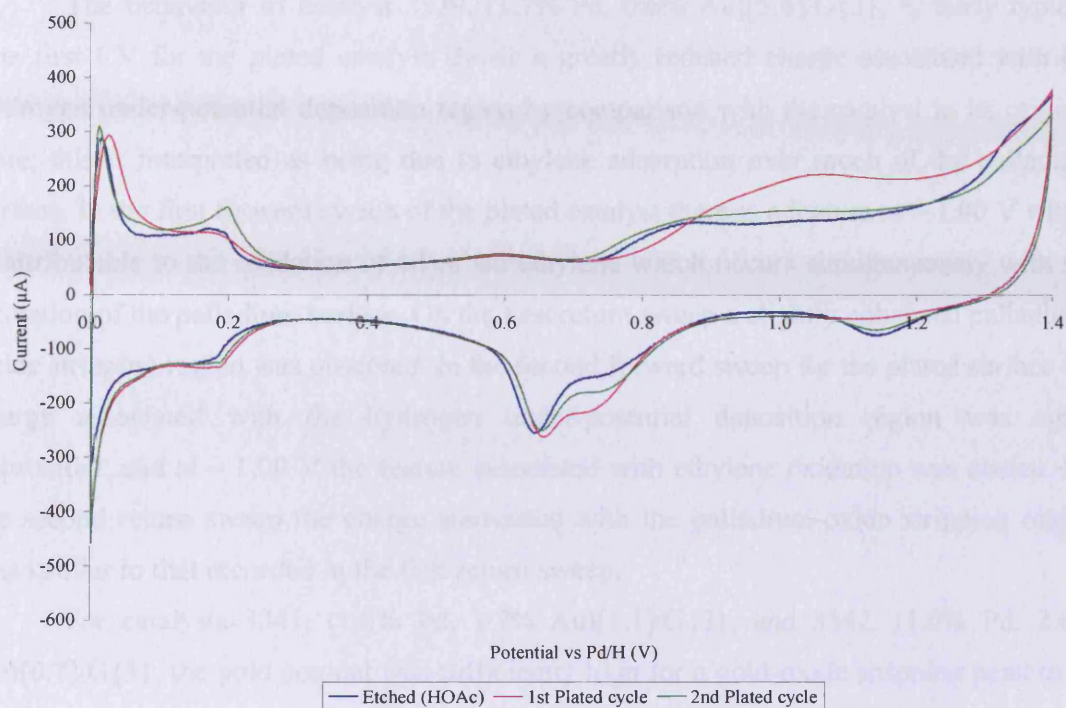
Figure 4.46 – CVs for etched (acetic acid) and subsequently palladium-plated catalyst 3341, (1.0% Pd, 1.7% Au)[1.1]/G{3}
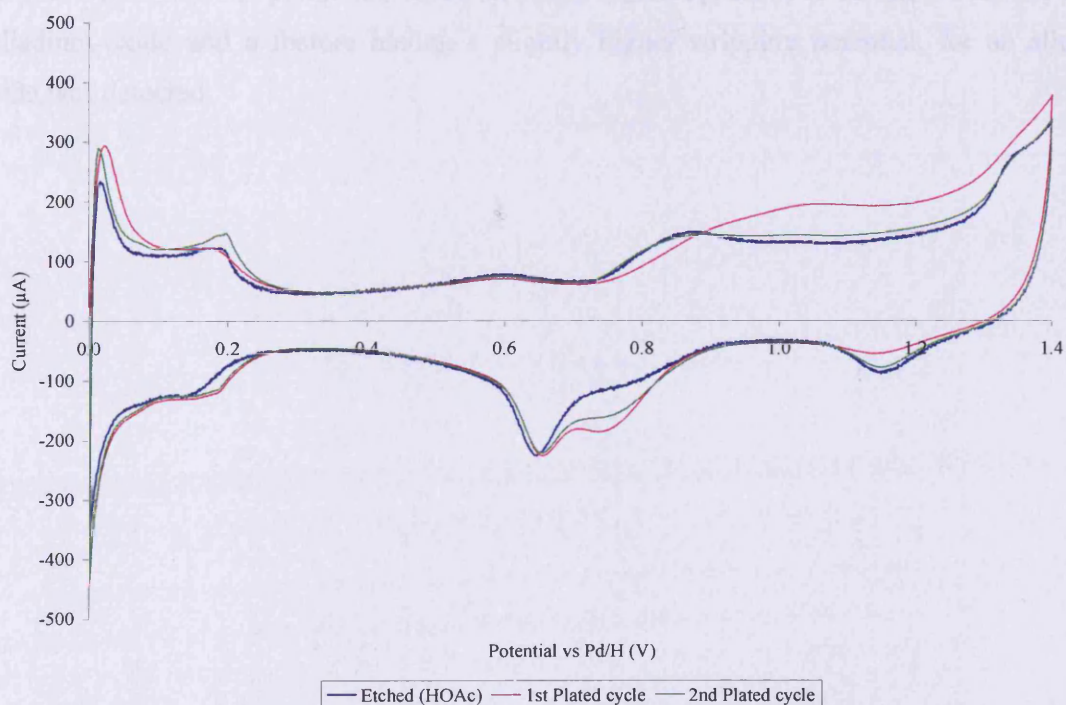
Figure 4.47 – CVs for etched (acetic acid) and subsequently palladium-plated catalyst 3342, (1.0% Pd, 2.6% Au)[0.7]/G{3}

The behaviour of catalyst 3339, (1.7% Pd, 0.6% Au)[5.4]/G{3}, is fairly typical. The first CV for the plated catalyst shows a greatly reduced charge associated with the hydrogen under-potential deposition region by comparison with the catalyst in its original state; this is interpreted as being due to ethylene adsorption over much of the palladium surface. In the first forward sweep of the plated catalyst there is a feature at ~ 1.00 V which is attributable to the oxidation of adsorbed ethylene which occurs simultaneously with the oxidation of the palladium surface. On the first return sweep a slightly enhanced palladium-oxide stripping region was observed. In the second forward sweep for the plated surface the charge associated with the hydrogen under-potential deposition region was again substantial, and at ~ 1.00 V the feature associated with ethylene oxidation was absent. On the second return sweep the charge associated with the palladium-oxide stripping region was similar to that recorded in the first return sweep.

For catalysts 3341, (1.0% Pd, 1.7% Au)[1.1]/G{3}, and 3342, (1.0% Pd, 2.6% Au)[0.7]/G{3}, the gold content was sufficiently high for a gold-oxide stripping peak to be observed in the return sweeps. The values for the plated catalyst were smaller than that for the original etched catalyst due to palladium deposition on the gold surface during plating. For these catalysts, the palladium-oxide stripping region appeared to be split; a feature for palladium-oxide and a feature having a slightly higher stripping potential, for an alloy-oxide was detected.

Table 4.8 – Batch 3 catalysts: charges (normalised ^{z}) associated with the hydrogen under-potential deposition region, the palladium-oxide stripping region, and the gold-oxide stripping region for catalysts etched in acetic acid and subsequently plated with palladium from palladium acetate solution

Catalyst		Region charge / μC								
		HUPD			Pd-O			Au-O		
ref no	description	Etched	Plated 1st cycle	Plated 2nd cycle	Etched	Plated 1st cycle	Plated 2nd cycle	Etched	Plated 1st cycle	Plated 2nd cycle
3336	(1.0% Pd, 0.0% Au)[∞]/G{3}	910	535	945	1990	1885	1910	n/o	n/o	n/o
3339	(1.7% Pd, 0.6% Au)[5.4]/G{3}	1615	15	1410	2855	2940	3000	n/o	n/o	n/o
3338	(1.0% Pd, 0.4% Au)[4.9]/G{3}	1025	635	1045	1850	2005	2045	n/o	n/o	n/o
3340	(1.0% Pd, 0.9% Au)[2.1]/G{3}	785	10	1250	2450	2500	2490	n/o	n/o	n/o
3341	(1.0% Pd, 1.7% Au)[1.1]/G{3}	530	10	1200	2390	2605	2375	195	n/o	90
3342	(1.0% Pd, 2.6% Au)[0.7]/G{3}	625	15	1120	2155	2565	2350	225	75	90

n/o = not observed ^{z}for procedure see Section 2.2.10

The potentials required to remove palladium-oxide and gold-oxide from the surfaces of etched and plated Batch 3 catalysts are shown in Table 4.9. In contrast to the catalysts plated by hydrogen (Section 4.2.1), the potential required to remove palladium-oxide from the surface of a plated catalyst was found to be equal or slightly more positive than that required for the removal of palladium-oxide from the corresponding etched catalyst. This is due to absorbed ethylene restricting the extent of oxide formation and hence the potential required for palladium-oxide/gold-oxide removal regardless of any enhancement in the palladium compositions of the catalyst surfaces.

Table 4.9 – Batch 3 catalysts: potentials required for palladium-oxide stripping and gold-oxide stripping for catalysts etched in acetic acid and subsequently plated with palladium from palladium acetate solution

Catalyst		Potential / V					
		Pd-O stripping			Au-O stripping		
ref no	description	Etched	Plated 1st cycle	Plated 2nd cycle	Etched	Plated 1st cycle	Plated 2nd cycle
3336	(1.0% Pd, 0.0% Au)[∞]/G{3}	0.63	0.64	0.64	–	–	–
3339	(1.7% Pd, 0.6% Au)[5.4]/G{3}	0.64	0.65	0.65	n/o	n/o	n/o
3338	(1.0% Pd, 0.4% Au)[4.9]/G{3}	0.64	0.64	0.64	n/o	n/o	n/o
3340	(1.0% Pd, 0.9% Au)[2.1]/G{3}	0.63	0.65	0.65	n/o	n/o	n/o
3341	(1.0% Pd, 1.7% Au)[1.1]/G{3}	0.64	0.66	0.65	1.13	n/o	1.13
3342	(1.0% Pd, 2.6% Au)[0.7]/G{3}	0.65	0.66	0.66	1.14	1.14	1.14

n/o = not observed

Acetic acid/potassium acetate etched catalysts

Figures 4.48 – 4.53 show CVs for etched and subsequently-plated Batch 3 catalysts 3336 and 3338 – 3342.

For each CV the charge associated with the hydrogen under-potential deposition region was calculated by subtracting the charge associated with hydrogen evolution from the total charge associated with the CV from 0.00 V to ~ 0.25 V in the forward sweep.

Figure 4.48 – CVs for etched (acetic acid/potassium acetate) and subsequently palladium-plated catalyst 3336, (1.0% Pd, 0.0% Au)[∞]/G{3}

Figure 4.49 – CVs for etched (acetic acid/potassium acetate) and subsequently palladium-plated catalyst 3338, (1.0% Pd, 0.4% Au)[4.9]/G{3}

Figure 4.50 – CVs for etched (acetic acid/potassium acetate) and subsequently palladium-plated catalyst 3339, (1.7% Pd, 0.6% Au)[5.4]/G{3}
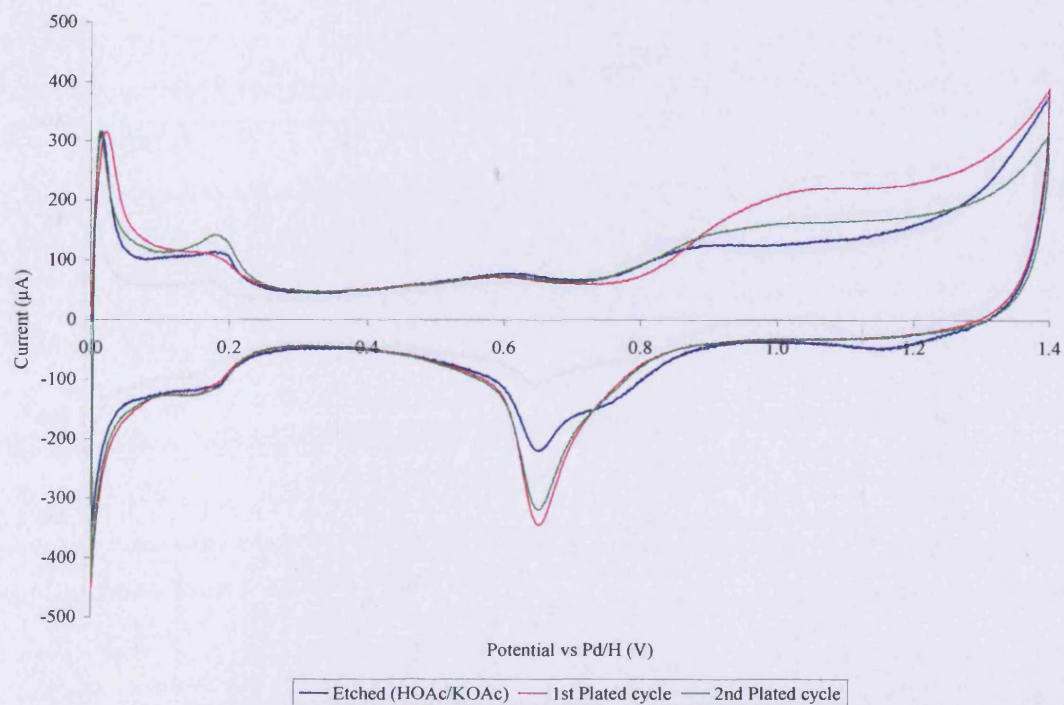
Figure 4.51 – CVs for etched (acetic acid/potassium acetate) and subsequently palladium-plated catalyst 3340, (1.0% Pd, 0.9% Au)[2.1]/G{3}
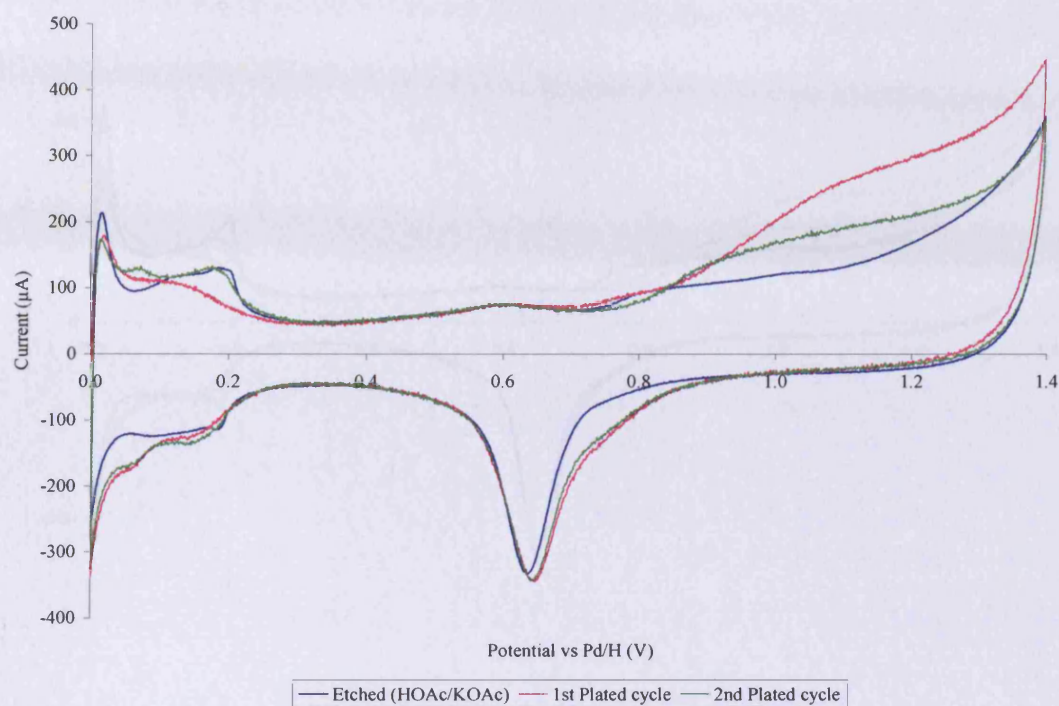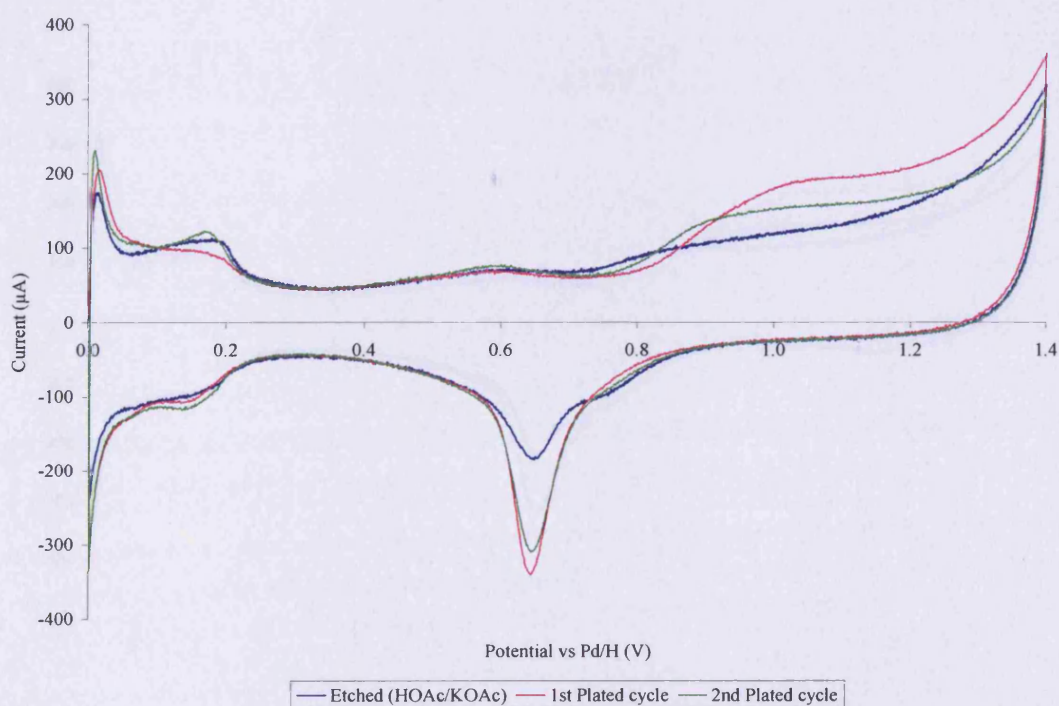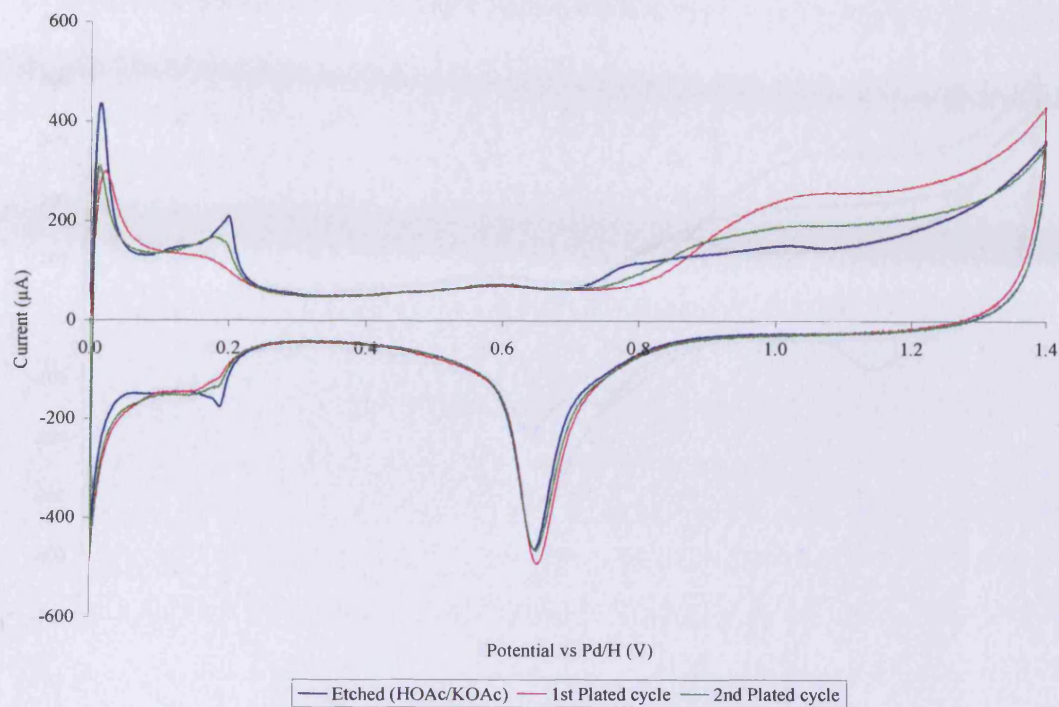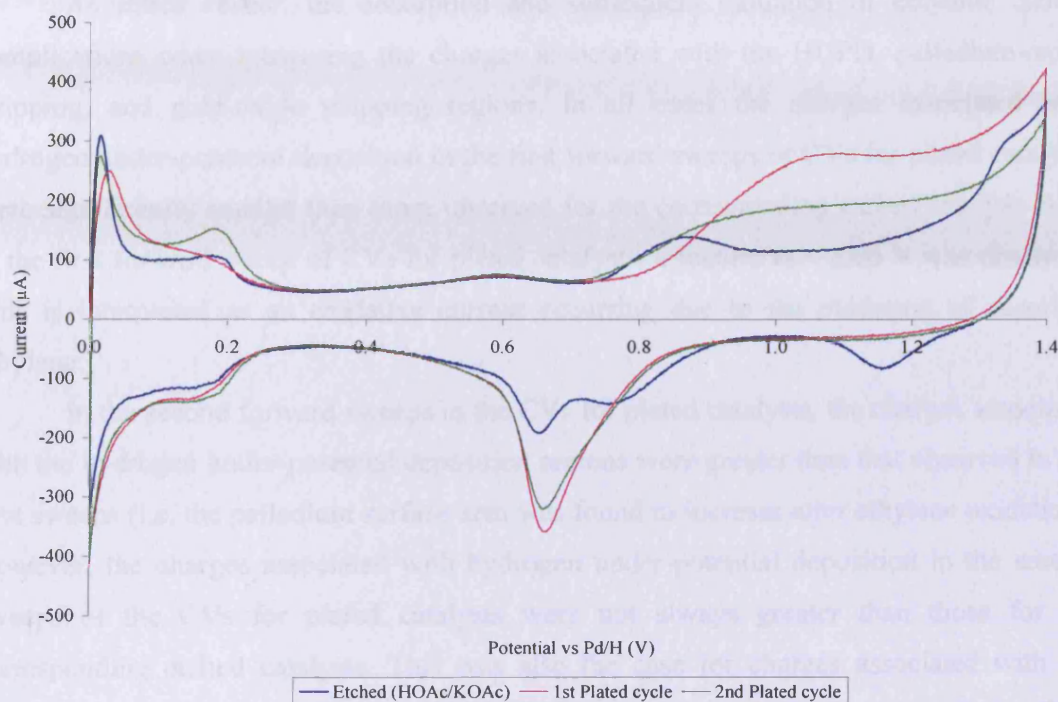
Figure 4.52 – CVs for etched (acetic acid/potassium acetate) and subsequently palladium-plated catalyst 3341, (1.0% Pd, 1.7% Au)[1.1]/G{3}
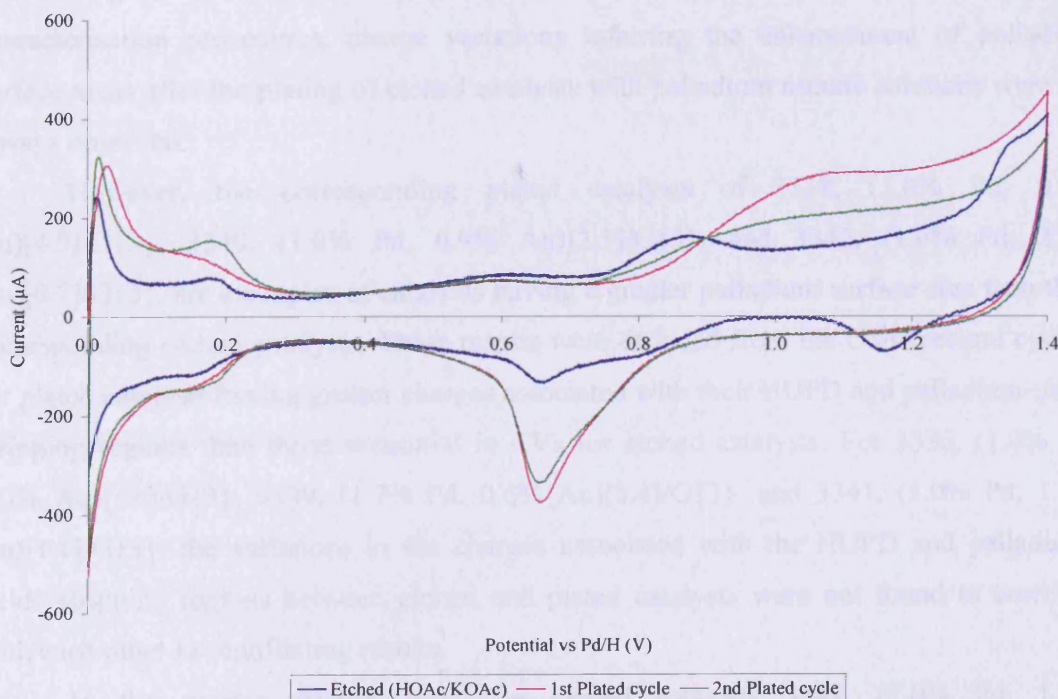
Figure 4.53 – CVs for etched (acetic acid/potassium acetate) and subsequently palladium-plated catalyst 3342, (1.0% Pd, 2.6% Au)[0.7]/G{3}

As stated earlier, the adsorption and subsequent oxidation of ethylene caused complications when measuring the charges associated with the HUPD, palladium-oxide stripping, and gold-oxide stripping regions. In all cases the charges associated with hydrogen under-potential deposition in the first forward sweeps of CVs for plated catalysts were significantly smaller than those observed for the corresponding etched catalyst. Also in the first forward sweep of CVs for plated catalysts, a feature at ~ 1.00 V was observed. This is interpreted as an oxidative current occurring due to the oxidation of adsorbed ethylene.

In the second forward sweeps in the CVs for plated catalysts, the charges associated with the hydrogen under-potential deposition regions were greater than that observed in the first sweeps (i.e. the palladium surface area was found to increase after ethylene oxidation). However, the charges associated with hydrogen under-potential deposition in the second sweeps of the CVs for plated catalysts were not always greater than those for the corresponding etched catalysts. This was also the case for charges associated with the palladium-oxide stripping regions in the first and second reverse sweeps of the CVs. Therefore, due to the choice of the reductant, and the processes which occur when palladium-gold catalysts are exposed to the positive potentials inherent in catalyst characterisation procedures, charge variations inferring the enhancement of palladium surface areas after the plating of etched catalysts with palladium acetate solutions were not always observed.

However, the corresponding plated catalysts of 3338, (1.0% Pd, 0.4% Au)[4.9]/G{3}, 3340, (1.0% Pd, 0.9% Au)[2.1]/G{3}, and 3342, (1.0% Pd, 2.6% Au)[0.7]/G{3}, are examples of catalysts having a greater palladium surface area than their corresponding etched catalysts. These results were deduced from the CVs (second cycles) for plated catalysts having greater charges associated with their HUPD and palladium-oxide stripping regions than those measured in CVs for etched catalysts. For 3336, (1.0% Pd, 0.0% Au)[∞]/G{3}, 3339, (1.7% Pd, 0.6% Au)[5.4]/G{3}, and 3341, (1.0% Pd, 1.7% Au)[1.1]/G{3}, the variations in the charges associated with the HUPD and palladium-oxide stripping regions between etched and plated catalysts were not found to correlate with each other i.e. conflicting results.

In the reverse sweeps, CVs for etched catalysts 3341, (1.0% Pd, 1.7% Au)[1.1]/G{3}, and 3342, (1.0% Pd, 2.6% Au)[0.7]/G{3}, gold-oxide stripping regions (as

well as palladium-oxide stripping regions) were detected. In the first cycle of the CVs for the corresponding plated catalysts, no gold-oxide stripping regions were detected. Therefore, it is likely that gold particles were plated with palladium during the plating process. The charges associated with the hydrogen under-potential deposition, palladium-oxide stripping (first and second cycles), and gold-oxide stripping regions for etched and plated Batch 3 catalysts are shown in Table 4.10. The potentials required to strip palladium-oxide (first and second cycles) and gold-oxide are shown in Table 4.11.

Table 4.10 – Batch 3 catalysts: charges (normalised[z]) associated with the hydrogen under-potential deposition region, the palladium-oxide stripping region, and the gold-oxide stripping region for catalysts etched in acetic acid/potassium acetate and subsequently plated with palladium from palladium acetate solution

Catalyst		Region charge / μC								
		HUPD			Pd-O			Au-O		
ref no	description	Etched	Plated 1st cycle	Plated 2nd cycle	Etched	Plated 1st cycle	Plated 2nd cycle	Etched	Plated 1st cycle	Plated 2nd cycle
3336	(1.0% Pd, 0.0% Au)[∞]/G{3}	795	20	945	1725	2545	2525	n/o	n/o	n/o
3339	(1.7% Pd, 0.6% Au)[5.4]/G{3}	1330	10	1120	2520	2765	2560	n/o	n/o	n/o
3338	(1.0% Pd, 0.4% Au)[4.9]/G{3}	670	10	645	1450	1920	1775	n/o	n/o	n/o
3340	(1.0% Pd, 0.9% Au)[2.1]/G{3}	630	10	835	2000	2305	2255	40	n/o	n/o
3341	(1.0% Pd, 1.7% Au)[1.1]/G{3}	535	10	855	2135	2605	2515	250	n/o	n/o
3342	(1.0% Pd, 2.6% Au)[0.7]/G{3}	315	10	915	1515	3030	2935	315	n/o	n/o

n/o = not observed   [z]for procedure see Section 2.2.10

Table 4.11 – Batch 3 catalysts: potentials required for palladium-oxide stripping and gold-oxide stripping for catalysts etched in acetic acid/potassium acetate and subsequently plated with palladium from palladium acetate solution

Catalyst		Potential / V					
		Pd-O stripping			Au-O stripping		
ref no	description	Etched	Plated 1st cycle	Plated 2nd cycle	Etched	Plated 1st cycle	Plated 2nd cycle
3336	(1.0% Pd, 0.0% Au)[∞]/G{3}	0.64	0.65	0.64	–	–	–
3339	(1.7% Pd, 0.6% Au)[5.4]/G{3}	0.65	0.65	0.65	n/o	n/o	n/o
3338	(1.0% Pd, 0.4% Au)[4.9]/G{3}	0.65	0.64	0.64	n/o	n/o	n/o
3340	(1.0% Pd, 0.9% Au)[2.1]/G{3}	0.65	0.65	0.65	1.14	n/o	n/o
3341	(1.0% Pd, 1.7% Au)[1.1]/G{3}	0.65	0.66	0.66	1.15	n/o	n/o
3342	(1.0% Pd, 2.6% Au)[0.7]/G{3}	0.66	0.66	0.65	1.15	n/o	n/o

n/o = not observed

4.2.3 Conclusions

The effect of reducing palladium acetate over etched Batch 2 and Batch 3 catalysts is shown in Sections 4.2.1 and 4.2.2 respectively.

For catalysts reduced using hydrogen; Figures 4.36 – 4.38 and 4.39 – 4.41 the CVs for plated catalysts revealed greater charges associated with the HUPD and palladium-oxide stripping regions than those in the CVs for the corresponding etched catalysts. These results indicated that the plated catalysts had greater palladium surface areas than their corresponding etched catalysts. In addition, it was found that surface composition could be monitored by the potential required to remove palladium-oxide from the surface of the catalyst. i.e. the potential required to remove palladium-oxide varied as a function of palladium-gold composition (Section 3.2).

The presence of ethylene (Figures 4.42 – 4.47 and 4.48 – 4.53) gave rise to more complicated CVs than those recorded for the catalysts reduced using hydrogen. This was due to ethylene adsorption and its subsequent oxidation. However, adsorbed ethylene was found to undergo oxidation at ~ 1.00 V in the first cycle (forward sweeps) in the CVs for the plated catalysts. The second cycles for the plated catalysts showed an increase (from that of the first cycle) in the charges associated with the hydrogen under-potential deposition regions. The charges associated with the HUPD and palladium-oxide stripping regions were not always found to be greater than those observed for the etched catalyst and therefore CV did not imply the enhancement of the palladium surface area for every catalyst. The presence of ethylene also provided implications for judging palladium/gold compositions via the *potential* (i.e. peak minima) of the palladium-oxide stripping peak. Thus, ethylene adsorption altered the extent of surface oxidation and hence the potential required for palladium-oxide stripping.

However, regardless of the reductant used the results were essentially the same. Greater charges were observed for the HUPD and palladium-oxide stripping regions in the CVs for the plated catalysts. This indicates that palladium was reduced or plated over etched catalyst surfaces and catalysts exhibiting greater palladium surface areas were generated. The loss of features inferring the presence of gold particles at etched catalyst surfaces were also observed after plating, suggesting that gold had been plated with palladium in these instances.

4.3   Examples of Untreated, Etched, and Plated Palladium-Gold Catalysts

In Section 4.1 CVs for untreated and etched Batch 1, Batch 2, and Batch 3 catalysts were presented and used to show the effect of etching on surface composition and in Section 4.2 the effects of palladium-plating the etched catalysts were examined. CVs for etched and plated catalysts were shown for Batch 2 materials, where the reduction was carried out by hydrogen (Section 4.2.1) and for Batch 3, where the reductant was ethylene (Section 4.2.2). Here CVs for untreated, etched, and plated catalysts are directly compared. The Figures which follow show CVs for untreated, etched, and plated catalysts along with the charges associated with the HUPD region, palladium-oxide, and gold-oxide stripping regions, for catalysts etched using (i) acetic acid and (ii) acetic acid/potassium acetate.

Figures 4.54 – 4.57 provide information for plated catalysts in which the palladium acetate was plated or reduced using hydrogen. Corresponding CVs for catalysts plated using ethylene as the reductant were complicated by the processes of ethylene adsorption and oxidation, and are not shown here.

Catalysts etched in acetic acid

Figure 4.54 shows CVs for untreated, etched, and plated Batch 1 catalyst 3187, (1.0% Pd, 1.7% Au)[1.1]/G{1}. The charge associated with the hydrogen under-potential deposition region decreased on etching and increased on plating which reflected changes in palladium surface area after each treatment. The charges associated with the palladium-oxide stripping region varied similarly supporting this interpretation (Table 4.12). Thus, the plated catalyst had the highest and the etched catalyst had the lowest palladium surface areas.
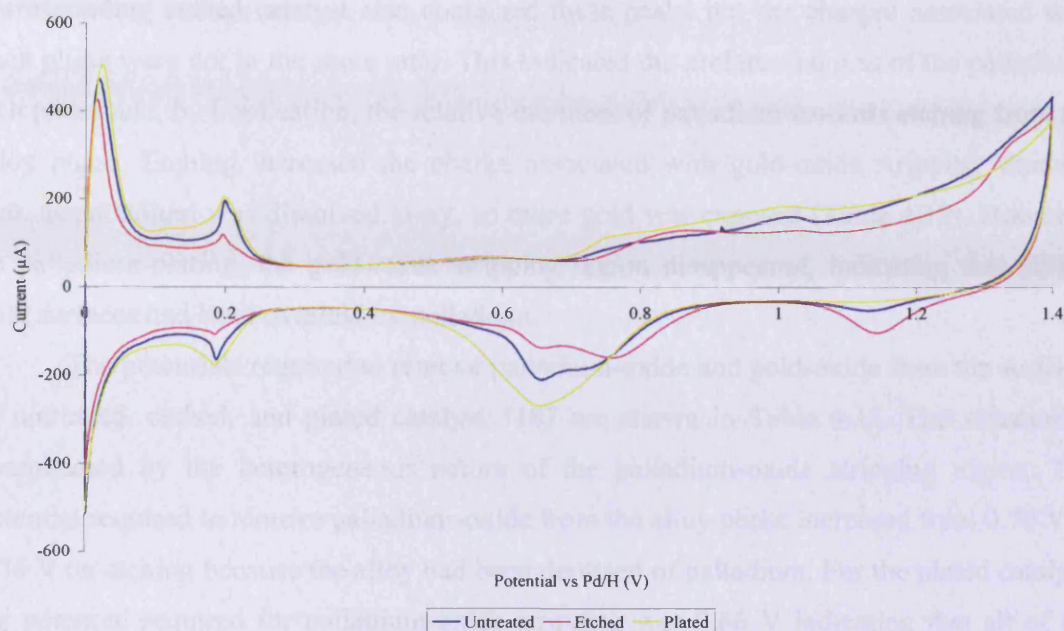
Figure 4.54 – CVs for untreated, etched (acetic acid), and plated catalyst 3187,
(1.0% Pd, 1.7% Au)[1.1]/G{1}

Table 4.12 – Untreated, etched (acetic acid), and plated catalysts: charges (normalised ^{z})
associated with the hydrogen under-potential deposition region and with the palladium-
oxide and gold-oxide stripping regions

| Catalyst | | Region charge / µC | | |
ref no	description	HUPD	Pd-O stripping	Au-O stripping
3200 untreated	(1.0% Pd, 0.9% Au)[1.9]/G{1}	2185	4755	140
3200 etched[a]	n/a	615	1065	385
3200 plated	(1.0% Pd, 0.9% Au)[1.9]/G{1}	2550	5225	n/o
3187 untreated	(1.0% Pd, 1.7% Au)[1.1]/G{1}	745	2100	100
3187 etched[a]	n/a	460	910	315
3187 plated	(1.0% Pd, 1.7% Au)[1.1]/G{1}	1080	2575	n/o

[a]*composition unknown* ^{z}*for procedure see Section 2.2.10*
n/o = not observed

The reverse sweep in the CV for untreated catalyst 3187, shows that the palladium-
oxide stripping region contained two peaks, one occurring at the potential expected for the
stripping of palladium-oxide from a palladium-rich phase (probably palladium-rich
particles) and the other occurring at a more positive potential, expected for palladium-oxide
stripping from a phase in which palladium co-existed with gold (alloy particles). The

corresponding etched catalyst also contained these peaks but the charges associated with each phase were not in the same ratio. This indicated the preferential loss of the palladium-rich phase and, by implication, the relative inertness of palladium towards etching from the alloy phase. Etching increased the charge associated with gold-oxide stripping showing that, as palladium was dissolved away, so more gold was exposed (Table 4.12). However, on palladium-plating, the gold-oxide stripping region disappeared, indicating that all the gold surfaces had been overlaid by palladium.

The potentials required to remove palladium-oxide and gold-oxide from the surfaces of untreated, etched, and plated catalyst 3187 are shown in Table 4.13. The situation is complicated by the heterogeneous nature of the palladium-oxide stripping region. The potential required to remove palladium-oxide from the alloy phase increased from 0.70 V to 0.76 V on etching because the alloy had been depleted of palladium. For the plated catalyst, the potential required for palladium-oxide stripping was 0.66 V indicating that all of the palladium in the surface behaved as if it was in a palladium-rich phase. The potential required to remove gold-oxide increased marginally from 1.13 V to 1.14 V on etching and this region was not observed after plating. Thus, etching provided gold enrichment via palladium loss whereas plating provided palladium enrichment by deposition on the gold surface.

Table 4.13 – Untreated, etched (acetic acid), and plated catalysts: potentials required to strip palladium-oxide and gold-oxide

Catalyst		Stripping potential / V		
ref no	description	Pd-O		Au-O
3200 untreated	(1.0% Pd, 0.9% Au)[1.9]/G{1}	0.65		1.13
3200 etched[a]	n/a		0.76	1.14
3200 plated	(1.0% Pd, 0.9% Au)[1.9]/G{1}	0.63		n/o
3187 untreated	(1.0% Pd, 1.7% Au)[1.1]/G{1}	0.66	0.70	1.13
3187 etched[a]	n/a	0.66	0.76	1.14
3187 plated	(1.0% Pd, 1.7% Au)[1.1]/G{1}	0.66		n/o

[a]composition unknown
n/o = not observed

CVs for untreated, etched, and plated Batch 1 catalyst 3200, (1.0% Pd, 0.9% Au)[1.9]/G{1}, are shown in Figure 4.55 and the charges and potentials associated with the various regions are given in Tables 4.12 and 4.13. The charges associated with the

hydrogen under-potential deposition region for each variant changed in the manner reported for catalyst 3187. In general, the behaviour of catalyst 3200 resembled that of catalyst 3187 and the interpretations given for catalyst 3187 carry over for catalyst 3200. There are, however, differences in detail. The loss of palladium area on etching was greater for catalyst 3200 and the surface area gain on plating was also greater. Untreated catalyst 3200 appeared (from the palladium-oxide stripping region) to contain palladium-rich surfaces, but etching was so severe that the etched catalyst showed only the remaining gold-rich alloy surface. On plating, the palladium-rich surface was, of course, restored.

Indeed, for plated catalyst 3200, the palladium-oxide stripping potential appeared to be more negative (at 0.63 V) than that for the untreated catalyst (at 0.66 V), indicating less mobility of gold into the plated surface than occurred with catalyst 3187.
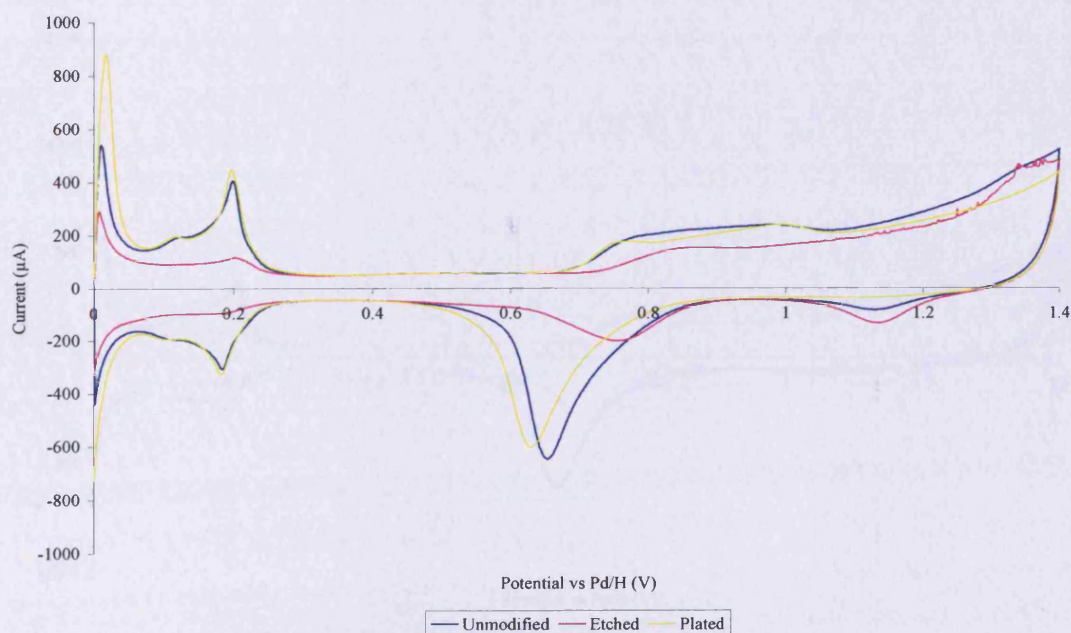
Figure 4.55 – CVs for untreated, etched (acetic acid), and plated catalyst 3200, (1.0% Pd, 0.9% Au)[1.9]/G{1}

Catalysts etched in acetic acid/potassium acetate

CVs for untreated, etched, and plated Batch 2 catalyst 3333, (1.0% Pd, 1.0% Au)[1.9]/G{2}, and catalyst 3335, (1.0% Pd, 2.7% Au)[0.7]/G{2}, are shown in Figures 4.56 and 4.57 and the charges and potentials associated with the various regions are shown in Tables 4.14 and 4.15. The general trends for catalyst 3333 are similar to those discussed for catalysts etched using acetic acid. These include a loss of palladium surface area on etching and a more than compensating gain on plating.
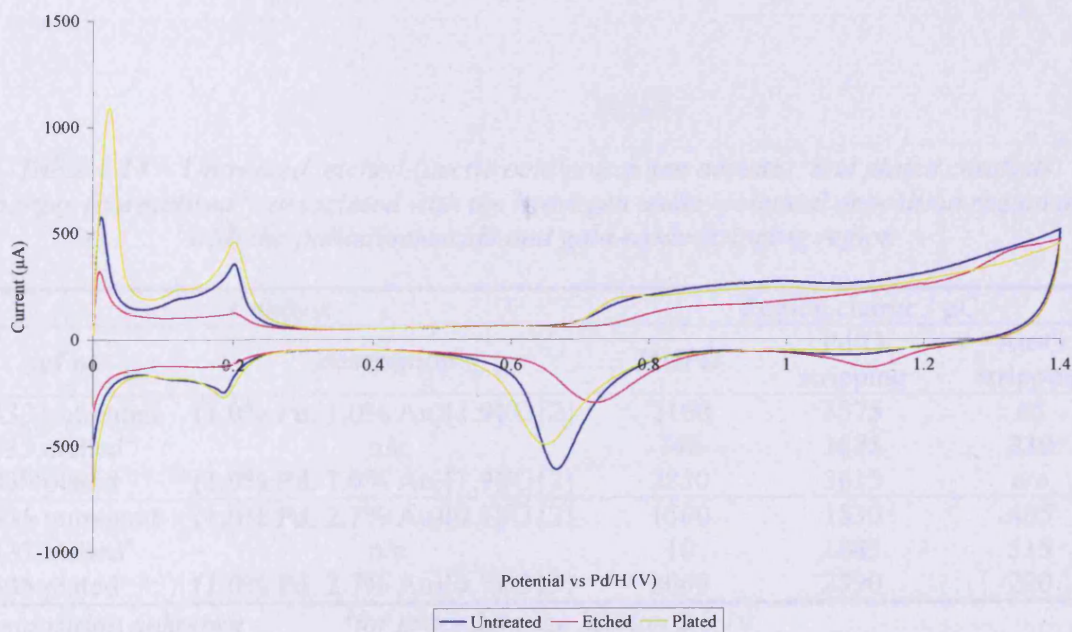
Figure 4.56 – CVs for untreated, etched (acetic acid/potassium acetate), and plated catalyst 3333, (1.0% Pd, 1.0% Au)[1.9]/G{2}
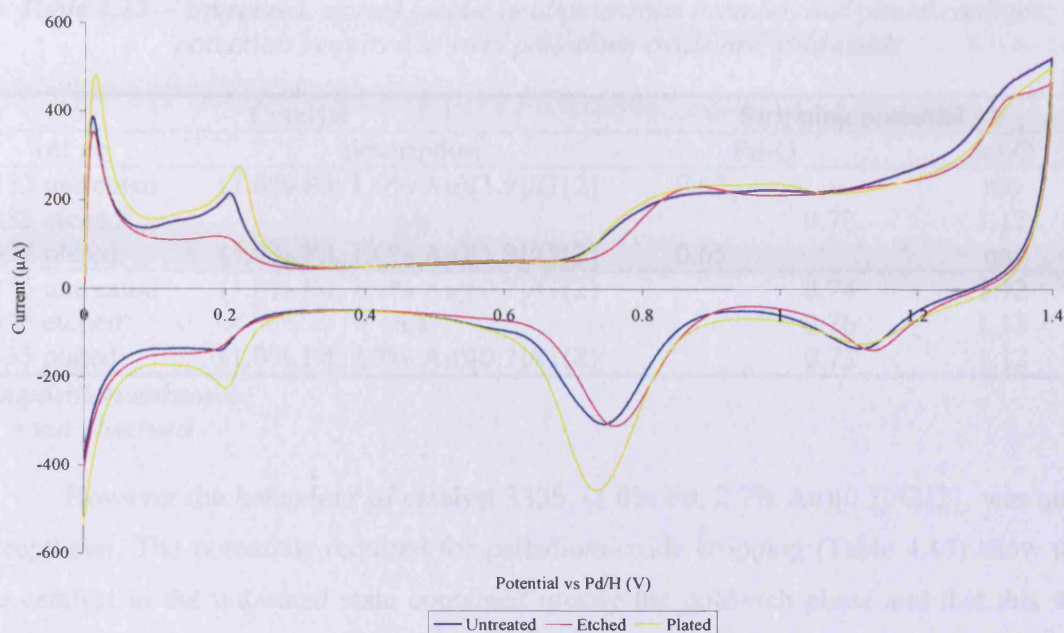
Figure 4.57 – CVs for untreated, etched (acetic acid/potassium acetate), and plated catalyst 3335, (1.0% Pd, 2.7% Au)[0.7]/G{2}

Table 4.14 – Untreated, etched (acetic acid/potassium acetate), and plated catalysts: charges (normalised ^{z}) associated with the hydrogen under-potential deposition region and with the palladium-oxide and gold-oxide stripping region

Catalyst		Region charge / μC		
ref no	description	HUPD	Pd-O stripping	Au-O stripping
3333 untreated	(1.0% Pd, 1.0% Au)[1.9]/G{2}	2160	3575	65
3333 etched[a]	n/a	740	1875	330
3333 plated	(1.0% Pd, 1.0% Au)[1.9]/G{2}	2850	3615	n/o
3335 untreated	(1.0% Pd, 2.7% Au)[0.7]/G{2}	1500	1830	405
3335 etched[a]	n/a	10	1885	515
3335 plated	(1.0% Pd, 2.7% Au)[0.7]/G{2}	2060	2890	290

^{a}composition unknown ^{z}for procedure see Section 2.2.10

n/o = not observed

Table 4.15 – Untreated, etched (acetic acid/potassium acetate), and plated catalysts:
potentials required to strip palladium-oxide and gold-oxide

Catalyst		Stripping potential / V	
ref no	description	Pd-O	Au-O
3333 untreated	(1.0% Pd, 1.0% Au)[1.9]/G{2}	0.67	n/o
3333 etched[a]	n/a	0.72	1.12
3333 plated	(1.0% Pd, 1.0% Au)[1.9]/G{2}	0.65	n/o
3335 untreated	(1.0% Pd, 2.7% Au)[0.7]/G{2}	0.74	1.12
3335 etched[a]	n/a	0.76	1.13
3335 plated	(1.0% Pd, 2.7% Au)[0.7]/G{2}	0.73	1.12

[a]*composition unknown*
n/o = *not observed*

However the behaviour of catalyst 3335, (1.0% Pd, 2.7% Au)[0.7]/G{2}, was quite exceptional. The potentials required for palladium-oxide stripping (Table 4.15) show that the catalyst in the untreated state contained mostly the gold-rich phase and that this was retained on etching. Remarkably, although the palladium plating increased the palladium surface area (Table 4.14) the surface phase present continued to be (according to the palladium-oxide stripping potential) the gold-rich alloy. This indicates again the rapid diffusion of gold into the plated palladium layer.

4.4   Characterisation of Untreated, Etched, and Plated Palladium-Gold Catalysts by use of Physical Methods

Etched catalysts were prepared by exposure of (untreated) catalysts to solutions of acetic acid and 0.5 mol dm^{-3} potassium acetate in acetic acid (Section 2.2.8). The palladium-containing solutions so obtained were then reduced, using hydrogen, over the etched catalysts to prepare a series of plated catalysts (Section 2.2.9). Surface characterisation of these etched and plated catalysts was described in Sections 4.1 – 4.3; this Section is concerned with bulk characterisation of these catalysts.

4.4.1   X-Ray Diffraction

Three untreated, etched, and plated catalysts from each Batch were characterised using X-ray diffraction according to the procedure described in Section 2.5.1. The reference

numbers and descriptions of the catalysts selected are re-iterated in Table 4.16 for convenience.

Table 4.16 – Reference numbers and descriptions for catalysts characterised by X-ray diffraction

Catalyst	
ref no	description
3185	(1.6% Pd, 0.6% Au)[4.8]/G{1}
3184	(1.0% Pd, 0.4% Au)[4.7]/G{1}
3186	(1.0% Pd, 1.0% Au)[2.0]/G{1}
3331	(1.0% Pd, 0.4% Au)[4.8]/G{2}
3332	(1.7% Pd, 0.6% Au)[4.8]/G{2}
3333	(1.0% Pd, 1.0% Au)[1.9]/G{2}
3339	(1.7% Pd, 0.6% Au)[5.4]/G{3}
3338	(1.0% Pd, 0.4% Au)[4.9]/G{3}
3340	(1.0% Pd, 0.9% Au)[2.1]/G{3}

Figure 4.58 shows the diffractograms obtained for Batch 1 untreated, etched, and plated catalysts. Each is characterised by the presence of two peaks, one occurring at the position expected for pure gold and one at the position expected for pure palladium. The diffractograms fall into three series corresponding to the treatment they had received. In addition, diffractograms for catalyst 3184, (1.0% Pd, 0.4% Au)[4.7]/G{1}, and catalyst 3186, (1.0% Pd, 1.0% Au)[2.0]/G{1}, also showed the presence of a third peak having a value of 2θ intermediate between that of pure gold and pure palladium. Such a peak is particularly evident for the untreated, etched, and plated versions of catalyst 3186, (1.0% Pd, 1.0% Au)[2.0]/G{1}. Diffractograms for untreated, etched, and plated versions of catalyst 3185, (1.6% Pd, 0.6% Au)[4.8]/G{1}, did not contain this peak.

Catalysts
3184 u   (1.0% Pd, 0.4% Au)[4.7]/G{1}
3184 e   (1.0% Pd, 0.4% Au)[4.7]/G{1}
3184 p   (1.0% Pd, 0.4% Au)[4.7]/G{1}
3185 u   (1.6% Pd, 0.6% Au)[4.8]/G{1}
3185 e   (1.6% Pd, 0.6% Au)[4.8]/G{1}
3185 p   (1.6% Pd, 0.6% Au)[4.8]/G{1}
3186 u   (1.0% Pd, 1.0% Au)[2.0]/G{1}
3186 e   (1.0% Pd, 1.0% Au)[2.0]/G{1}
3186 p   (1.0% Pd, 1.0% Au)[2.0]/G{1}
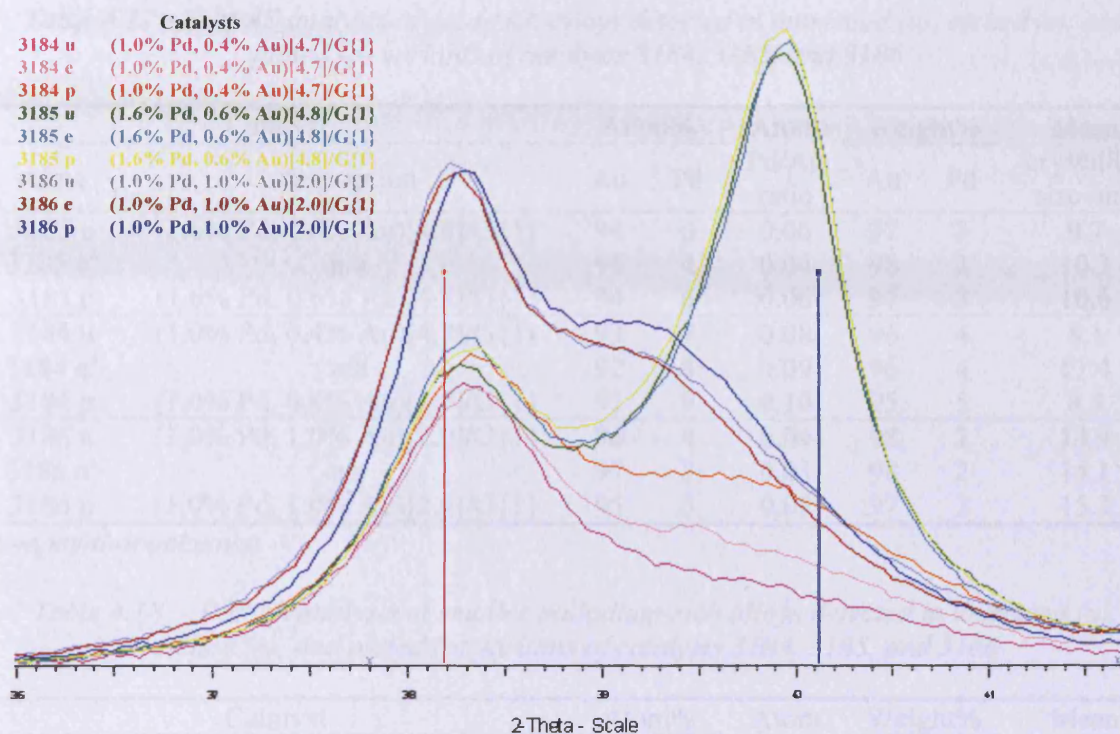
Figure 4.58 – Diffractograms for untreated (u), etched (e), and plated (p) variants of Batch 1 catalysts 3184, 3185, and 3186

TOPAS analysis showed that Batch 1 untreated, etched, and plated catalysts contained gold-rich phases and palladium-rich phases. The gold-rich particles had mean crystallite sizes ranging from 8.1 – 15.2 nm and contained 91 – 97 atom% gold (Table 4.17). Two sets of palladium-rich alloys were detected, i.e. small palladium-rich particles (sizes ranging from 2.1 – 10.6 nm) containing 54 – 92 atom% palladium (Table 4.18) and larger palladium-rich particles (sizes ranging from 11.3 – 14.7 nm) containing 93 atom% palladium (Table 4.19). The existence of larger palladium-rich particles were only detected for variants of catalyst 3185.

Table 4.17 – TOPAS analysis of gold-rich alloys detected in untreated (u), etched (e), and plated (p) variants of catalysts 3184, 3185, and 3186

Catalyst		Atom%		Atom Pd/Au ratio	Weight%		Mean crystallite size /nm
ref no	description	Au	Pd		Au	Pd	
3185 u	(1.6% Pd, 0.6% Au)[4.8]/G{1}	94	6	0.06	97	3	9.7
3185 e[a]	n/a	96	4	0.04	98	2	10.3
3185 p	(1.6% Pd, 0.6% Au)[4.8]/G{1}	94	6	0.06	97	3	10.6
3184 u	(1.0% Pd, 0.4% Au)[4.7]/G{1}	93	7	0.08	96	4	8.1
3184 e[a]	n/a	92	8	0.09	96	4	11.4
3184 p	(1.0% Pd, 0.4% Au)[4.7]/G{1}	91	9	0.10	95	5	8.3
3186 u	(1.0% Pd, 1.0% Au)[2.0]/G{1}	96	4	0.04	98	2	14.4
3186 e[a]	n/a	97	3	0.03	98	2	14.1
3186 p	(1.0% Pd, 1.0% Au)[2.0]/G{1}	95	5	0.05	97	3	15.2

[a]*composition unknown*

Table 4.18 – TOPAS analysis of smaller palladium-rich alloys detected in untreated (u), etched (e), and plated (p) variants of catalysts 3184, 3185, and 3186

Catalyst		Atom%		Atom Pd/Au ratio	Weight%		Mean crystallite size /nm
ref no	description	Au	Pd		Au	Pd	
3185 u	(1.6% Pd, 0.6% Au)[4.8]/G{1}	45	55	1.22	60	40	10.6
3185 e[a]	n/a	28	72	2.57	42	58	5.3
3185 p	(1.6% Pd, 0.6% Au)[4.8]/G{1}	30	70	2.33	44	56	4.9
3184 u	(1.0% Pd, 0.4% Au)[4.7]/G{1}	8	92	11.50	14	86	3.2
3184 e[a]	n/a	32	68	2.13	47	53	2.1
3184 p	(1.0% Pd, 0.4% Au)[4.7]/G{1}	14	86	6.14	23	77	3.8
3186 u	(1.0% Pd, 1.0% Au)[2.0]/G{1}	43	57	1.33	59	41	3.5
3186 e[a]	n/a	46	54	1.17	61	39	3.9
3186 p	(1.0% Pd, 1.0% Au)[2.0]/G{1}	43	57	1.33	58	42	3.8

[a]*composition unknown*

Table 4.19 – TOPAS analysis of larger palladium-rich alloys detected in untreated (u), etched (e), and plated (p) variants of catalysts 3184, 3185, and 3186

Catalyst		Atom%		Atom Pd/Au ratio	Weight%		Mean crystallite size /nm
ref no	description	Au	Pd		Au	Pd	
3185 u	(1.6% Pd, 0.6% Au)[4.8]/G{1}	7	93	13.29	13	87	11.3
3185 e[a]	n/a	7	93	13.29	12	88	14.7
3185 p	(1.6% Pd, 0.6% Au)[4.8]/G{1}	7	93	13.29	12	88	14.2

[a]*composition unknown*

Diffractograms for untreated, etched, and plated versions of Batch 2 catalysts are shown in Figure 4.59. Each diffractogram contained two peaks, one occurring near the 2θ value for pure gold and another near the 2θ value for pure palladium. For some catalysts, intensity appeared between the value expected for pure gold and the value expected for pure palladium. Like Batch 1 catalysts, Batch 2 catalysts also clearly fell into three groups corresponding to untreated, etched, and plated variants of catalysts 3331, (1.0% Pd, 0.4% Au)[4.8]/G{2}, 3332, (1.7% Pd, 0.6% Au)[4.8]/G{2}, and 3333, (1.0% Pd, 1.0% Au)[1.9]/G{2}.

Catalysts

3331 u (1.0% Pd, 0.4% Au)[4.8]/G{2}
3331 e (1.0% Pd, 0.4% Au)[4.8]/G{2}
3331 p (1.0% Pd, 0.4% Au)[4.8]/G{2}
3332 u (1.7% Pd, 0.6% Au)[4.8]/G{2}
3332 e (1.7% Pd, 0.6% Au)[4.8]/G{2}
3332 p (1.7% Pd, 0.6% Au)[4.8]/G{2}
3333 u (1.0% Pd, 1.0% Au)[1.9]/G{2}
3333 e (1.0% Pd, 1.0% Au)[1.9]/G{2}
3333 p (1.0% Pd, 1.0% Au)[1.9]/G{2}

2-Theta - Scale
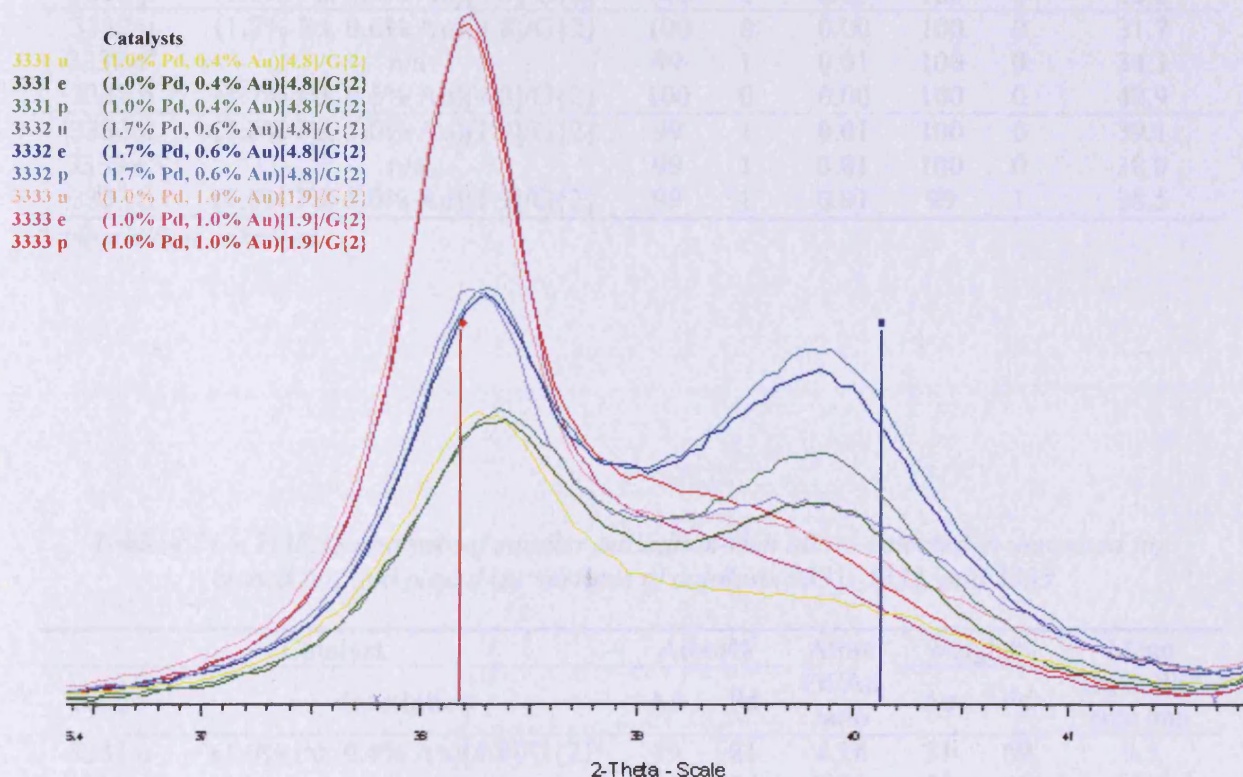
Figure 4.59 – Diffractograms for untreated (u), etched (e), and plated (p) variants of Batch 2 catalysts 3331, 3332, and 3333

Analysis of these diffractograms showed that, as for the Batch 1 catalysts, three types of palladium-gold phase co-existed: gold-rich particles (sizes ranging from 29.7 – 42.9 nm) containing 99 – 100 atom% gold (Table 4.20); small palladium-rich particles (sizes ranging from 2.1 – 15.3 nm) containing 59 – 81 atom% palladium (Table 4.21), and

199

larger palladium-rich particles (sizes ranging from 11.5 – 20.6 nm) containing 97 – 100 atom% palladium (Table 4.22).

Table 4.20 – TOPAS analysis of gold-rich alloys detected in untreated (u), etched (e), and plated (p) variants of catalysts 3331, 3332, and 3333

Catalyst		Atom%		Atom Pd/Au ratio	Weight%		Mean crystallite size /nm
ref no	description	Au	Pd		Au	Pd	
3331 u	(1.0% Pd, 0.4% Au)[4.8]/G{2}	100	0	0.00	100	0	29.7
3331 e[a]	n/a	99	1	0.01	100	0	30.9
3331 p	(1.0% Pd, 0.4% Au)[4.8]/G{2}	100	0	0.00	100	0	28.2
3332 u	(1.7% Pd, 0.6% Au)[4.8]/G{2}	100	0	0.00	100	0	31.7
3332 e[a]	n/a	99	1	0.01	100	0	34.3
3332 p	(1.7% Pd, 0.6% Au)[4.8]/G{2}	100	0	0.00	100	0	42.9
3333 u	(1.0% Pd, 1.0% Au)[1.9]/G{2}	99	1	0.01	100	0	39.1
3333 e[a]	n/a	99	1	0.01	100	0	38.0
3333 p	(1.0% Pd, 1.0% Au)[1.9]/G{2}	99	1	0.01	99	1	38.5

[a]*composition unknown*

Table 4.21 – TOPAS analysis of smaller palladium-rich alloys detected in untreated (u), etched (e), and plated (p) variants of catalysts 3331, 3332, and 3333

Catalyst		Atom%		Atom Pd/Au ratio	Weight%		Mean crystallite size /nm
ref no	description	Au	Pd		Au	Pd	
3331 u	(1.0% Pd, 0.4% Au)[4.8]/G{2}	19	81	4.26	31	69	9.5
3331 e[a]	n/a	26	74	2.85	39	61	11.7
3331 p	(1.0% Pd, 0.4% Au)[4.8]/G{2}	41	59	1.44	56	44	15.3
3332 u	(1.7% Pd, 0.6% Au)[4.8]/G{2}	34	66	1.94	49	51	7.2
3332 e[a]	n/a	27	73	2.70	40	60	7.0
3332 p	(1.7% Pd, 0.6% Au)[4.8]/G{2}	32	68	2.13	47	53	2.1
3333 u	(1.0% Pd, 1.0% Au)[1.9]/G{2}	41	59	1.44	57	43	3.0
3333 e[a]	n/a	56	44	0.79	70	30	4.1
3333 p	(1.0% Pd, 1.0% Au)[1.9]/G{2}	37	63	1.70	52	48	3.3

[a]*composition unknown*

Table 4.22 – TOPAS analysis of larger palladium-rich alloys detected in untreated (u), etched (e), and plated (p) variants of catalysts 3331, 3332, and 3333

Catalyst		Atom%		Atom Pd/Au ratio	Weight%		Mean crystallite size /nm
ref no	description	Au	Pd		Au	Pd	
3331 u	(1.0% Pd, 0.4% Au)[4.8]/G{2}	0	100	∞	0	100	13.8
3331 e[a]	n/a	0	100	∞	1	99	16.0
3331 p	(1.0% Pd, 0.4% Au)[4.8]/G{2}	3	97	32.33	6	94	11.5
3332 u	(1.7% Pd, 0.6% Au)[4.8]/G{2}	1	99	99.00	2	98	12.2
3332 e[a]	n/a	0	100	∞	0	100	14.2
3332 p	(1.7% Pd, 0.6% Au)[4.8]/G{2}	2	98	49.00	3	97	12.5
3333 u	(1.0% Pd, 1.0% Au)[1.9]/G{2}	2	98	49.00	4	96	12.1
3333 e[a]	n/a	1	99	99.00	2	98	12.2
3333 p	(1.0% Pd, 1.0% Au)[1.9]/G{2}	1	99	99.00	2	98	20.6

[a]composition unknown

Diffractograms for untreated, etched, and plated Batch 3 catalysts are shown in Figure 4.60. Again, each diffractogram is comprised of two peaks and clearly the diffractograms fall into three groups corresponding to the untreated, etched, and plated versions of each catalyst. Two types of palladium-gold phase were detected: gold-rich particles (sizes ranging from 9.1 – 16.4 nm) which contained 89 – 98 atom% gold (Table 4.23) and palladium-rich particles (sizes ranging from 2.9 – 6.2 nm) containing 64 – 89 atom% palladium (Table 4.24).
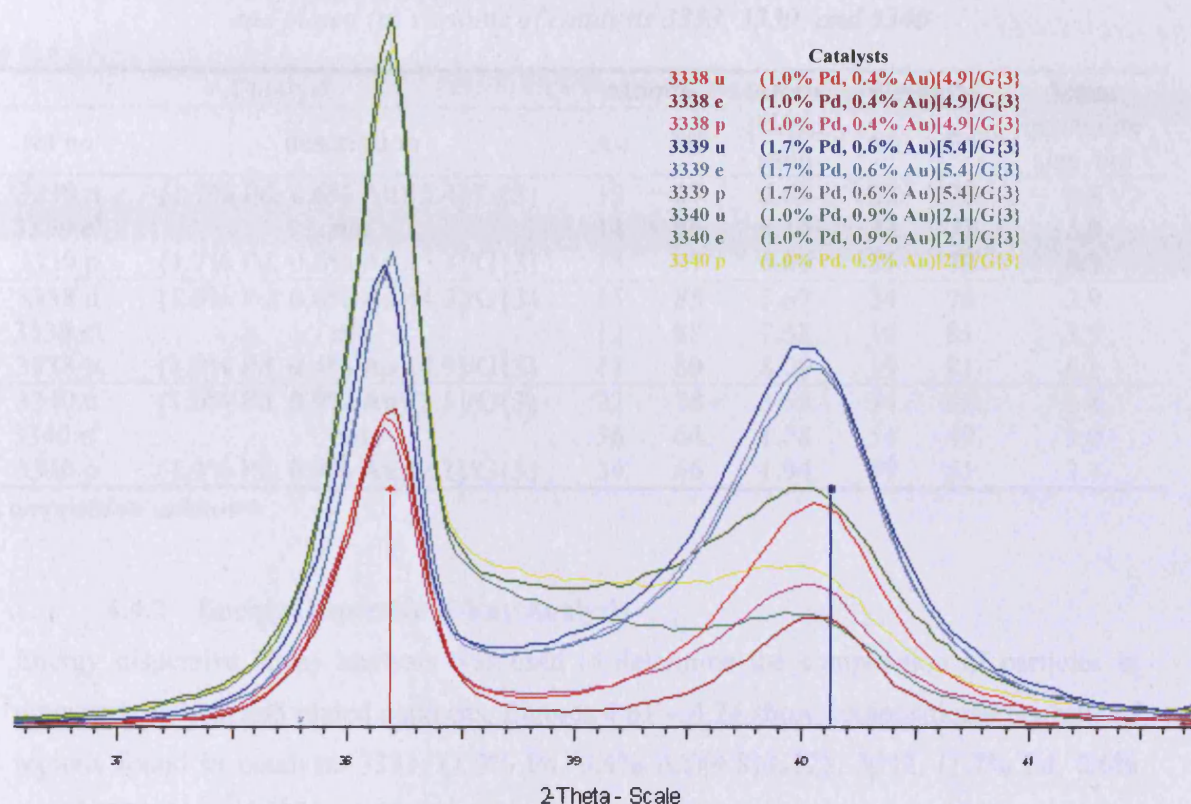
	Catalysts
3338 u	**(1.0% Pd, 0.4% Au)[4.9]/G{3}**
3338 e	**(1.0% Pd, 0.4% Au)[4.9]/G{3}**
3338 p	**(1.0% Pd, 0.4% Au)[4.9]/G{3}**
3339 u	**(1.7% Pd, 0.6% Au)[5.4]/G{3}**
3339 e	(1.7% Pd, 0.6% Au)[5.4]/G{3}
3339 p	(1.7% Pd, 0.6% Au)[5.4]/G{3}
3340 u	(1.0% Pd, 0.9% Au)[2.1]/G{3}
3340 e	(1.0% Pd, 0.9% Au)[2.1]/G{3}
3340 p	(1.0% Pd, 0.9% Au)[2.1]/G{3}

2-Theta - Scale

Figure 4.60 – Diffractograms for untreated (u), etched (e), and plated (p) variants of Batch 3 catalysts 3338, 3339, and 3340

Table 4.23 – TOPAS analysis of gold-rich alloys detected in untreated (u), etched (e), and plated (p) variants of catalysts 3338, 3339, and 3340

Catalyst		Atom%		Atom Pd/Au ratio	Weight%		Mean crystallite size /nm
ref no	description	Au	Pd		Au	Pd	
3339 u	(1.7% Pd, 0.6% Au)[5.4]/G{3}	1	99	99.00	2	98	12.2
3339 e[a]	n/a	0	100	∞	0	100	14.2
3339 p	(1.7% Pd, 0.6% Au)[5.4]/G{3}	2	98	49.00	3	97	12.5
3338 u	(1.0% Pd, 0.4% Au)[4.9]/G{3}	0	100	∞	0	100	13.8
3338 e[a]	n/a	0	100	∞	1	99	16.0
3338 p	(1.0% Pd, 0.4% Au)[4.9]/G{3}	3	97	32.33	6	94	11.5
3340 u	(1.0% Pd, 0.9% Au)[2.1]/G{3}	2	98	49.00	4	96	12.1
3340 e[a]	n/a	1	99	99.00	2	98	12.2
3340 p	(1.0% Pd, 0.9% Au)[2.1]/G{3}	1	99	99.00	2	98	20.6

[a]*composition unknown*

Table 4.24 – TOPAS analysis of palladium-rich alloys detected in untreated (u), etched (e), and plated (p) variants of catalysts 3338, 3339, and 3340

	Catalyst	Atom%		Atom	Weight%		Mean
ref no	description	Au	Pd	Pd/Au ratio	Au	Pd	crystallite size /nm
3339 u	(1.7% Pd, 0.6% Au)[5.4]/G{3}	13	87	6.69	22	78	3.8
3339 e[a]	n/a	14	86	6.14	23	77	5.9
3339 p	(1.7% Pd, 0.6% Au)[5.4]/G{3}	13	87	6.69	21	79	6.2
3338 u	(1.0% Pd, 0.4% Au)[4.9]/G{3}	15	85	5.67	24	76	2.9
3338 e[a]	n/a	12	88	7.33	19	81	5.9
3338 p	(1.0% Pd, 0.4% Au)[4.9]/G{3}	11	89	8.09	19	81	6.1
3340 u	(1.0% Pd, 0.9% Au)[2.1]/G{3}	22	78	3.55	34	66	3.4
3340 e[a]	n/a	36	64	1.78	51	49	3.0
3340 p	(1.0% Pd, 0.9% Au)[2.1]/G{3}	34	66	1.94	49	51	3.4

[a]*composition unknown*

4.4.2 Energy Dispersive X-Ray Analysis

Energy dispersive X-ray analysis was used to determine the composition of particles in untreated, etched, and plated catalysts. Figures 4.61 – 4.74 show compositional analysis of regions found in catalysts 3331, (1.0% Pd, 0.4% Au)[4.8]/G{2}, 3332, (1.7% Pd, 0.6% Au)[4.8]/G{2}, and 3333, (1.0% Pd, 1.0% Au)[1.9]/G{2}.

Figure 4.61 shows compositional analysis of a cluster of metal particles found in untreated catalyst 3331, (1.0% Pd, 0.4% Au)[4.8]/G{2}. The region under analysis had an area of approximately 2500 nm^2 (50 nm x 50 nm) and it was found to contain a predominance of palladium with a trace of gold. Compositional analysis of a single metal particle (found in untreated catalyst 3331, (1.0% Pd, 0.4% Au)[4.8]/G{2}) having an approximate area of 2500 nm^2 (50 nm x 50 nm) is shown in Figure 4.62. This particle was in close proximity to the large metallic cluster already analysed (Figure 4.61). The particle contained significant amounts of gold and a small amount of palladium. Analysis along a linear element of approximately 40 nm in length in untreated catalyst 3331, (1.0% Pd, 0.4% Au)[4.8]/G{2}, is shown in Figure 4.63. The linear element crossed a cluster of metal particles in close proximity. The line analysis revealed a substantial predominance of palladium over gold. In some regions the palladium intensities detected were an order of magnitude greater than those detected for gold.

Figures 4.64 – 4.66 show compositional analysis and particle gradient analysis of regions which contain predominance's of palladium and of gold found in etched catalyst

3331, (composition unknown). Figure 4.64 shows a region having an area of approximately 2500 nm^2 (50 nm x 50 nm). The particle examined was almost pure palladium. The micrograph and corresponding energy dispersive X-ray analysis shown in Figure 4.65 shows compositional analysis of a region having an approximate area of 625 nm^2 (25 nm x 25 nm). The particle thus analysed was comprised of gold with a small amount of palladium. Figure 4.66 shows particle gradient analysis along a linear element approximately 70 nm in length. This linear element crossed what appeared to be a metal particle and a cluster of metallic particles having an irregular appearance which might have been caused by the etching process. The line analysis showed that the region mainly consisted of palladium with small amounts of gold. The analysis crossed a region of the graphite support where no signals characteristic of metallic transitions were detected.
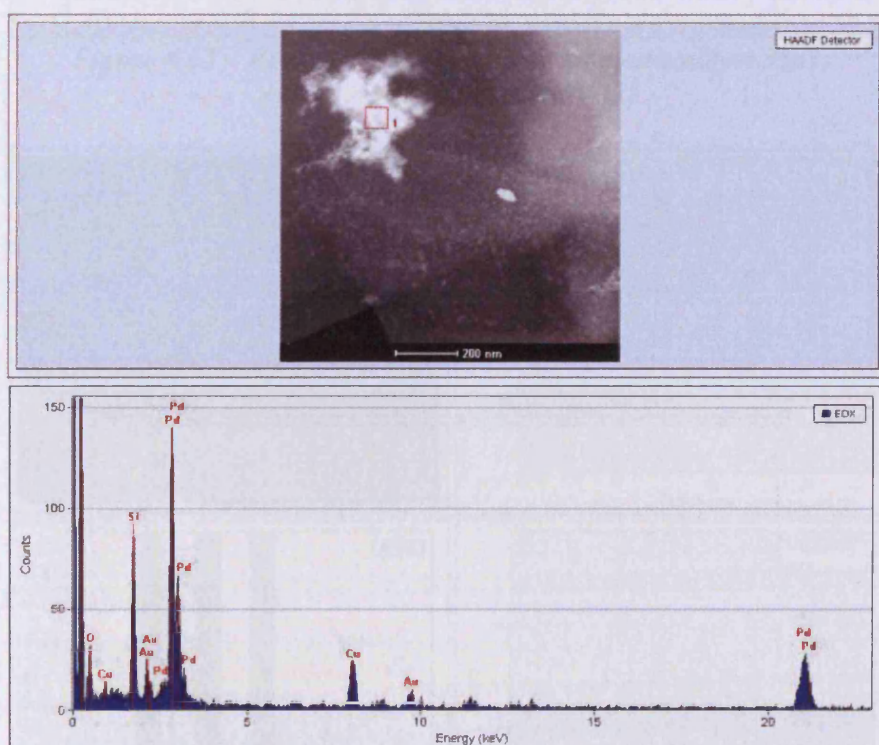

*Figure 4.61 – Particle analysis (1) in untreated catalyst 3331,
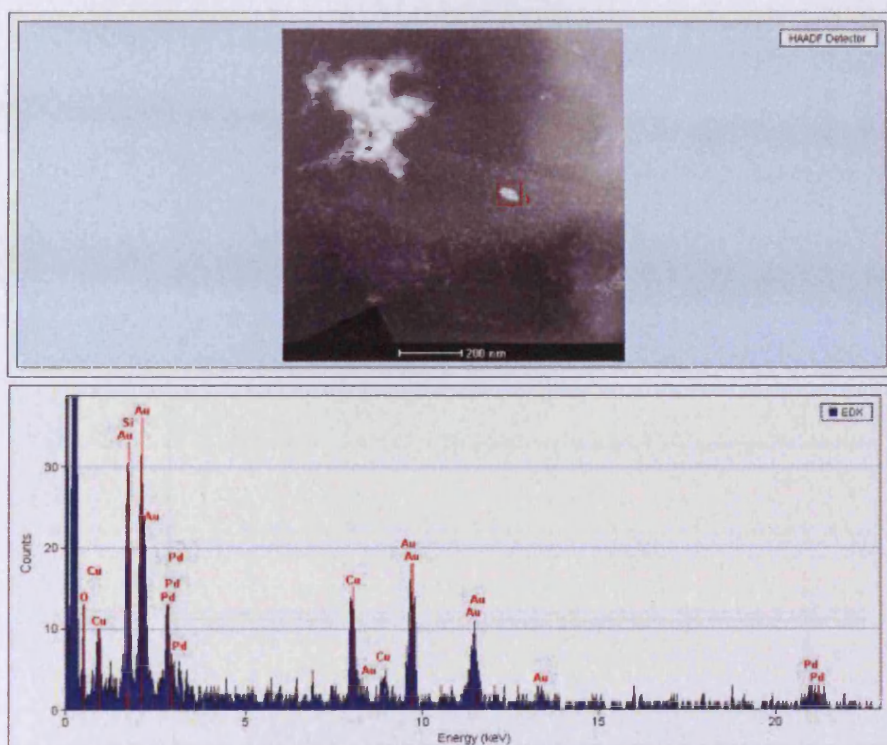(1.0% Pd, 0.4% Au)[4.8]/G{2}*

Figure 4.62 – Particle analysis (2) in untreated catalyst 3331,
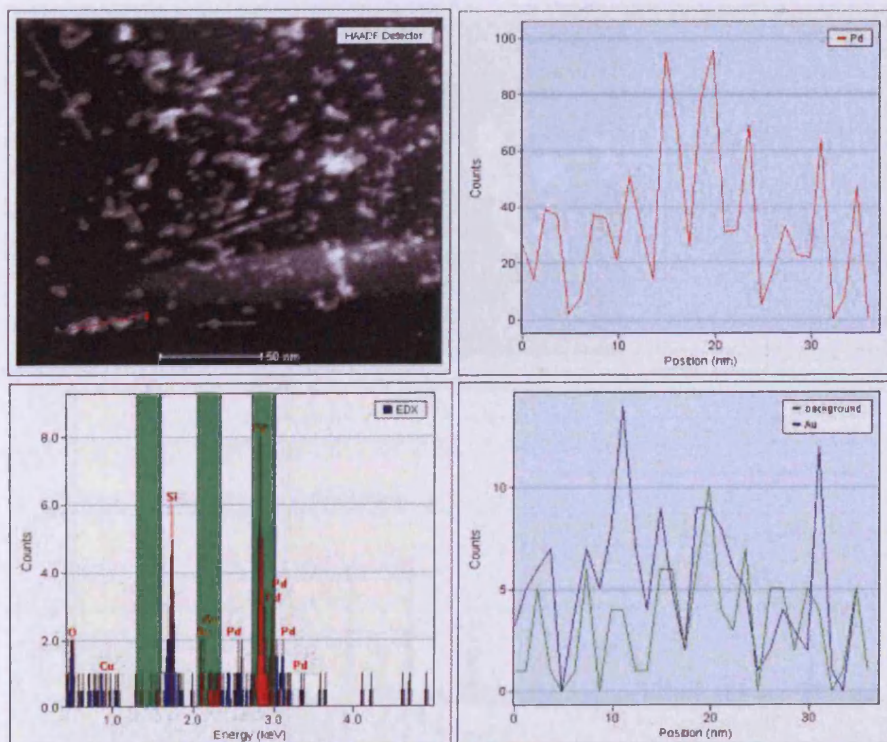*(1.0% Pd, 0.4% Au)[4.8]/G{2}*

Figure 4.63 – Particle gradient analysis in untreated catalyst 3331,
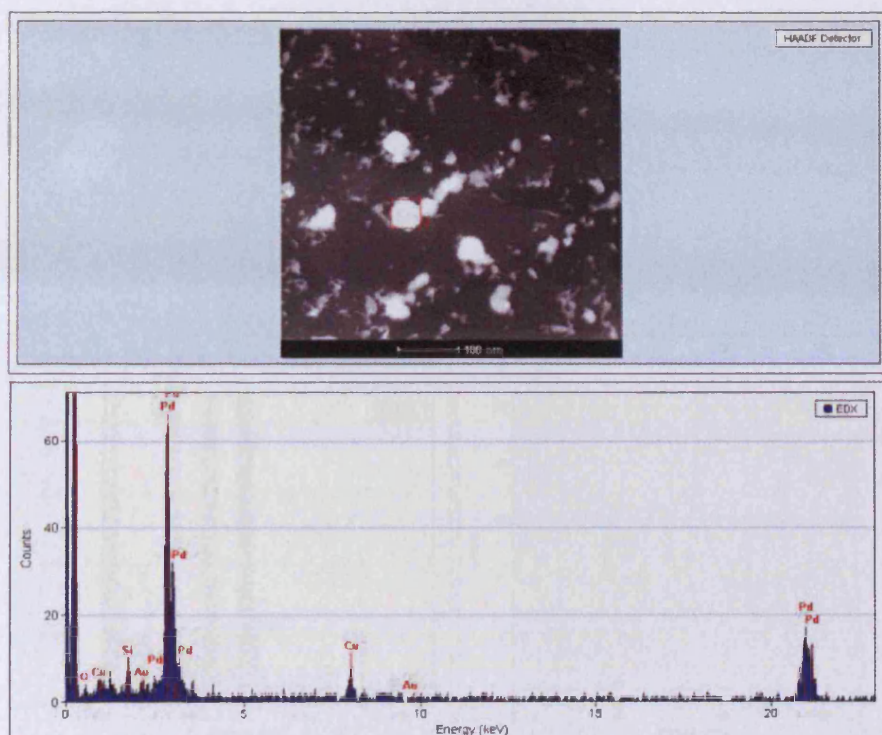*(1.0% Pd, 0.4% Au)[4.8]/G{2}*

Figure 4.64 – Particle analysis (1) in etched catalyst 3331,
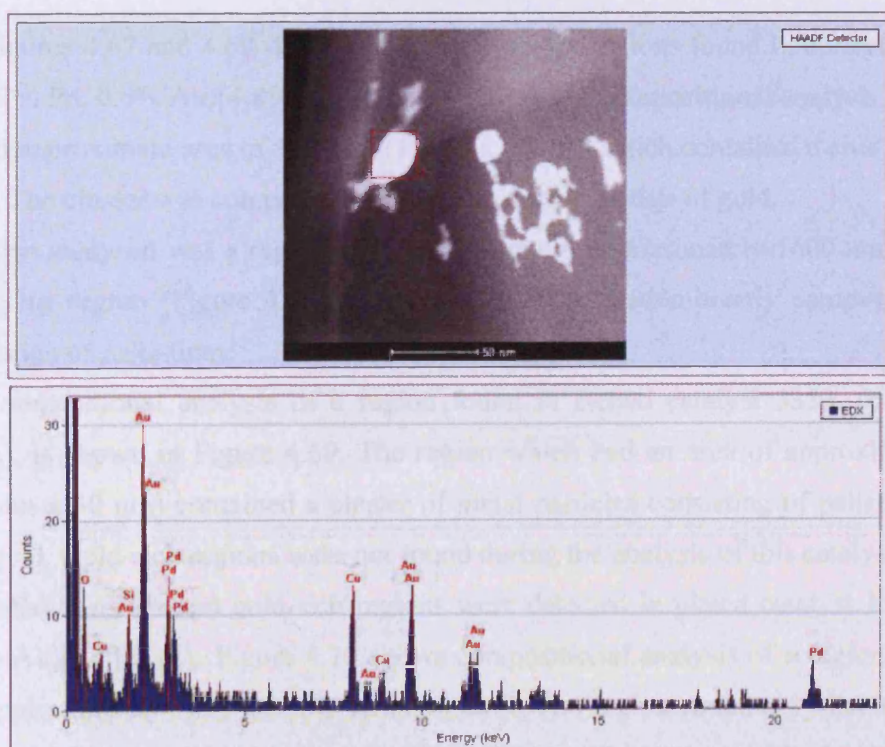*(composition unknown)*

Figure 4.65 – Particle analysis (2) in etched catalyst 3331,
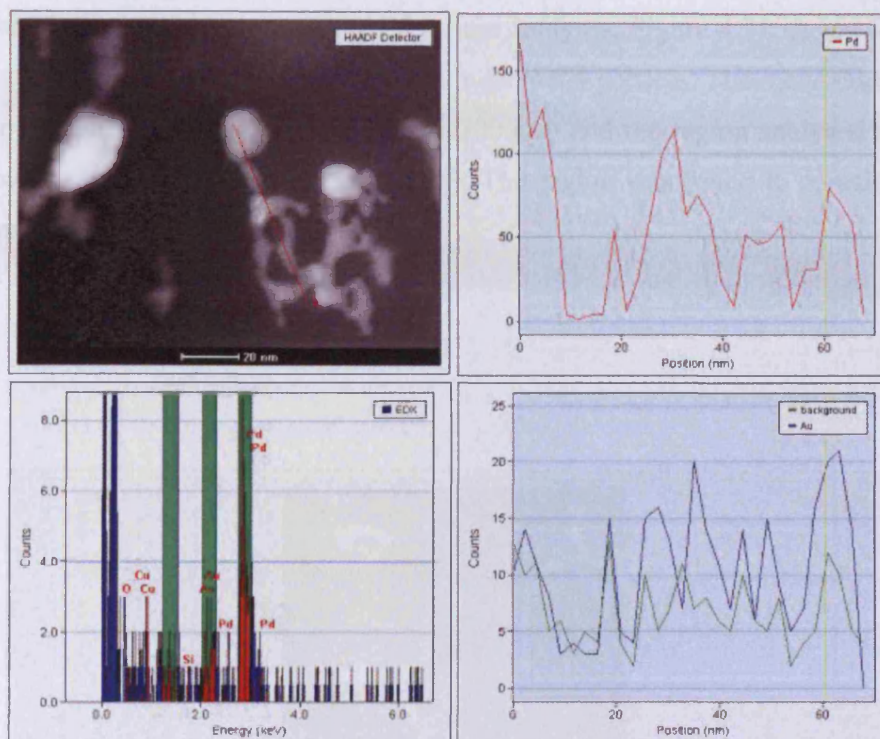*(composition unknown)*

Figure 4.66 – Particle gradient analysis in etched catalyst 3331,
(composition unknown)

Figures 4.67 and 4.68 show particle analysis for regions found in untreated catalyst 3332, (1.7% Pd, 0.6% Au)[4.8]/G{2}. Figure 4.67 shows compositional analysis of a region having an approximate area of 100 nm² (10 nm x 10 nm) which contained a cluster of metal particles. The cluster was composed of palladium with a vestige of gold.

Also analysed was a region covering an area of approximately 1600 nm² (40 nm x 40 nm). This region (Figure 4.68) contained a particle predominantly composed of gold with a vestige of palladium.

Compositional analysis of a region found in etched catalyst 3332, (composition unknown), is shown in Figure 4.69. The region which had an area of approximately 900 nm² (30 nm x 30 nm) contained a cluster of metal particles consisting of palladium and a trace of gold. Gold-rich regions were not found during the analysis of this catalyst.

Palladium-rich and gold-rich regions were detected in plated catalyst 3332, (1.7% Pd, 0.6% Au)[4.8]/G{2}. Figure 4.70 shows compositional analysis of a region having an area of approximately 1600 nm² (40 nm x 40 nm). The region contained what appeared to be a small metal particle and a cluster of metallic particles and analysis showed that this region contained both palladium and gold. The large copper signal can be attributed to the

207

grid on which the catalyst was mounted for these analyses. Figure 4.71 shows composition analysis of a region containing a portion of a huge metal particle. The metal particle had an area of approximately 40000 nm^2 (200 nm x 200 nm) and the region analysed had an area of approximately 2500 nm^2 (50 nm x 50 nm). The region was found to contain gold with similar amounts of palladium.

Figure 4.67 – Particle analysis (1) in untreated catalyst 3332,
(1.7% Pd, 0.6% Au)[4.8]/G{2}

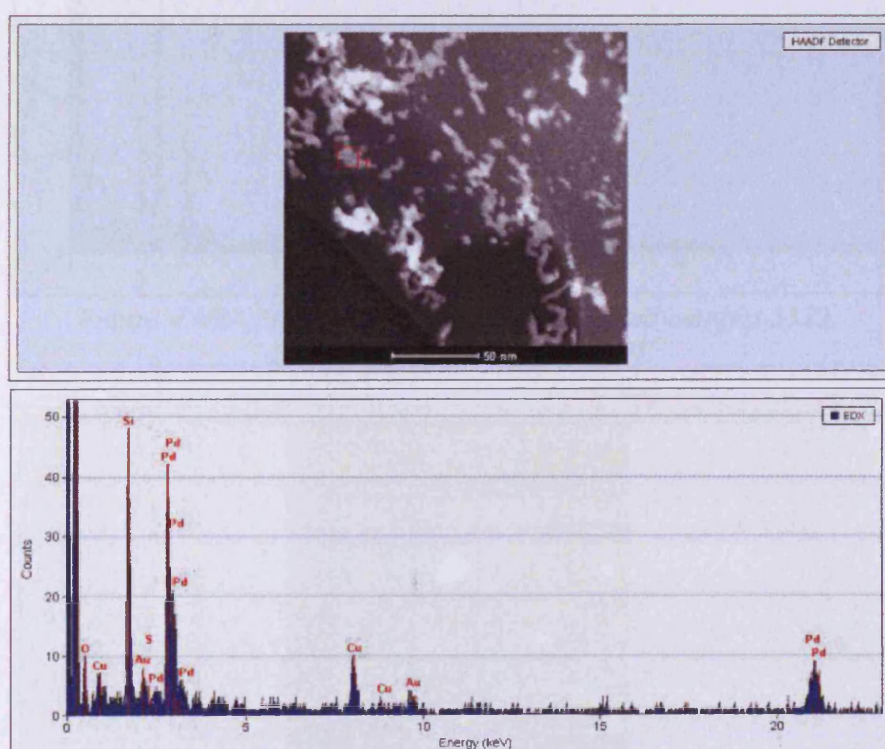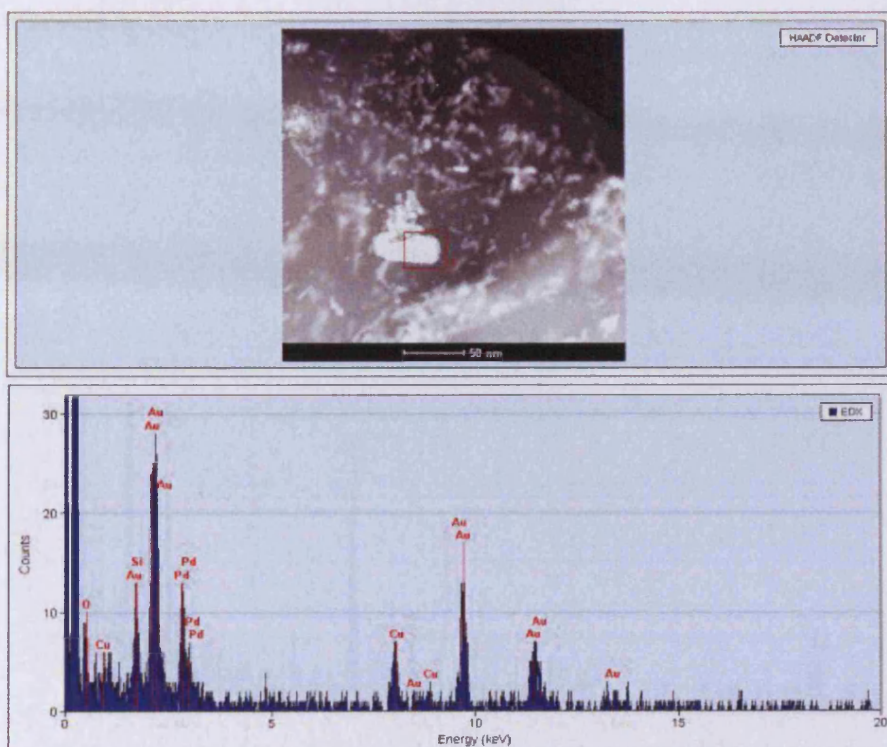*Figure 4.68 – Particle analysis (2) in untreated catalyst 3332,*
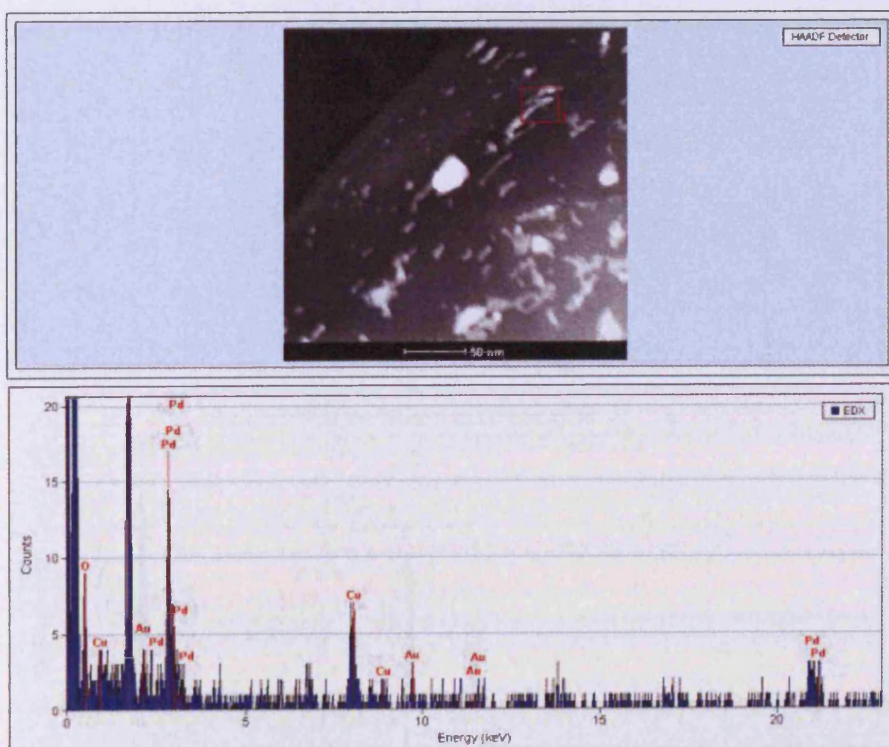*(1.7% Pd, 0.6% Au)[4.8]/G{2}*

Figure 4.69 – Particle analysis in etched catalyst 3332,
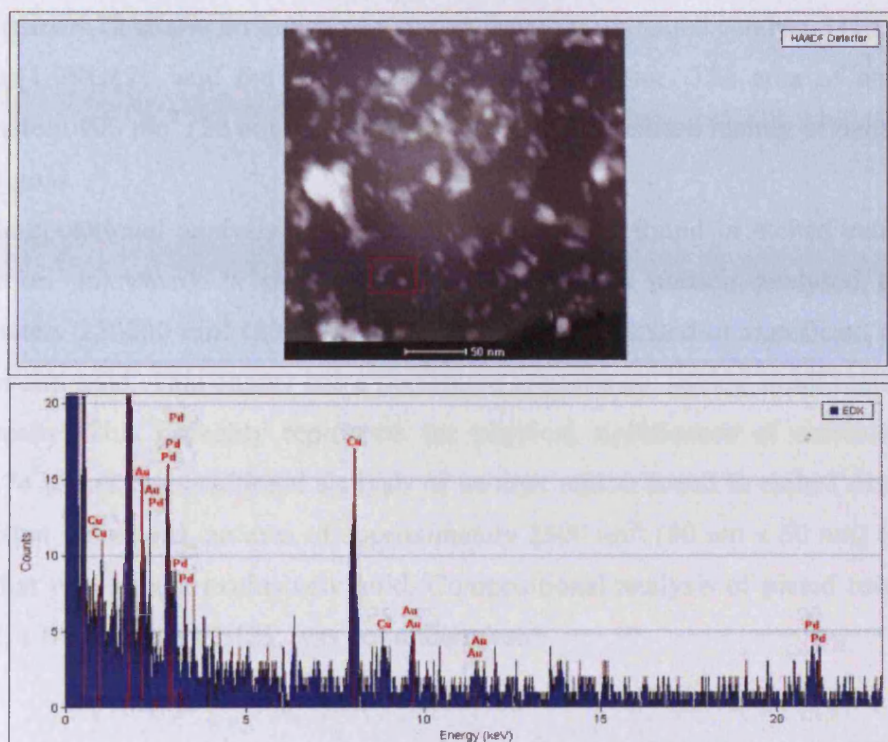*(composition unknown)*

*Figure 4.70 – Particle analysis (1) in plated catalyst 3332,
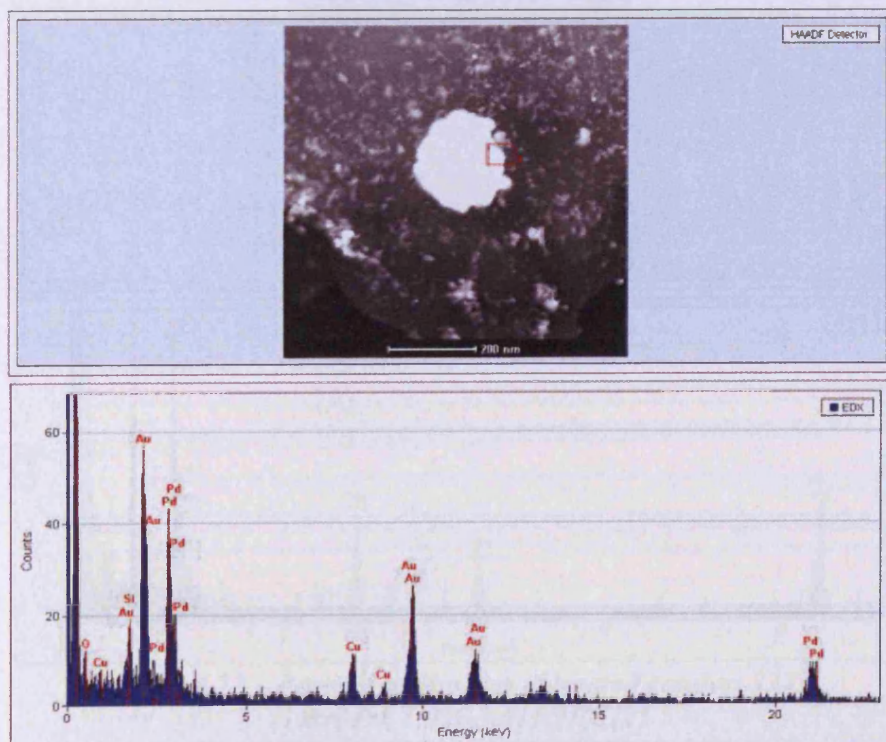(1.7% Pd, 0.6% Au)[4.8]/G{2}*

*Figure 4.71 – Particle analysis (2) in plated catalyst 3332,
(1.7% Pd, 0.6% Au)[4.8]/G{2}*

Figure 4.72 shows an image of a region found in untreated catalyst 3333, (1.0% Pd, 1.0% Au)[1.9]/G{2}, and the analysis of a metallic cluster. The area of analysis was approximately 400 nm^2 (20 nm x 20 nm) and the cluster consisted mainly of palladium with a trace of gold.

Compositional analysis of a large metallic cluster found in etched catalyst 3333, (composition unknown), is shown in Figure 4.73. This portion analysed an area of approximately 250000 nm^2 (500 nm x 500 nm) which consisted of significant amounts of palladium and gold. This cluster has a perforated appearance, having small regions of zero metal density. This probably represents the physical significance of corrosive etching. Figure 4.74 shows compositional analysis of another region found in etched catalyst 3333, (composition unknown), an area of approximately 2500 nm^2 (50 nm x 50 nm) contained a particle that was almost exclusively gold. Compositional analysis of plated catalyst 3333, (1.0% Pd, 1.0% Au)[1.9]/G{2}, was not undertaken.
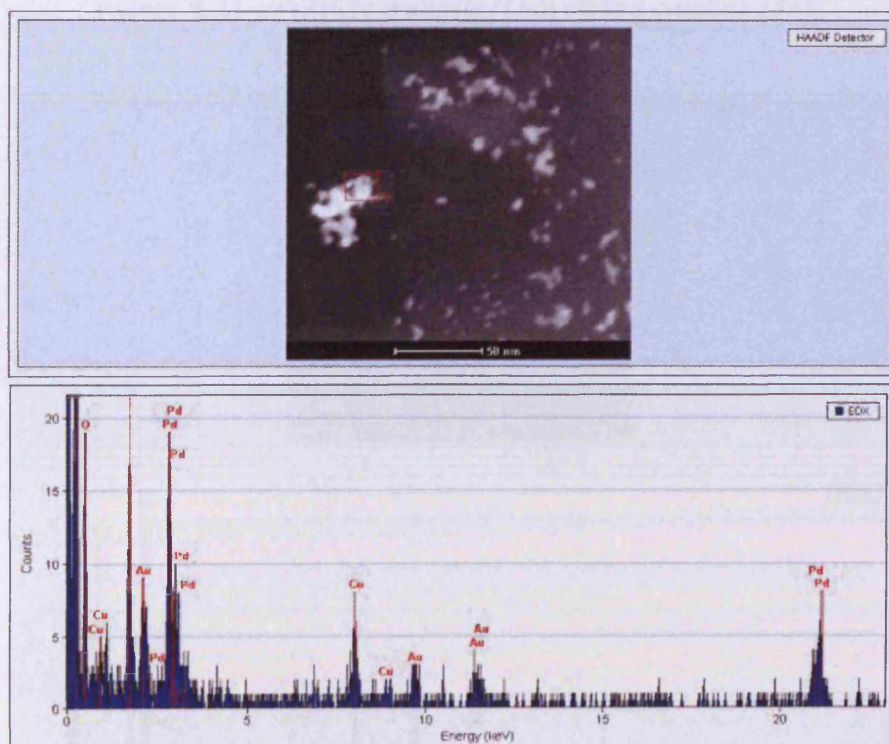

Figure 4.72 – Particle analysis in untreated catalyst 3333,
(1.0% Pd, 1.0% Au)[1.9]/G{2}
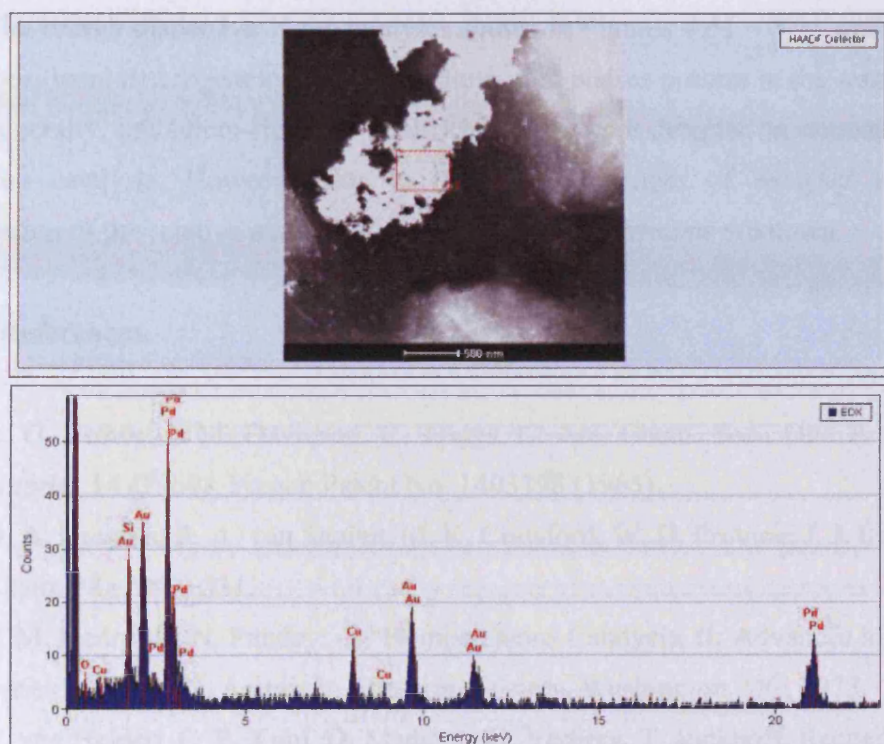
Figure 4.73 – Particle analysis (1) in etched catalyst 3333,
(composition unknown)
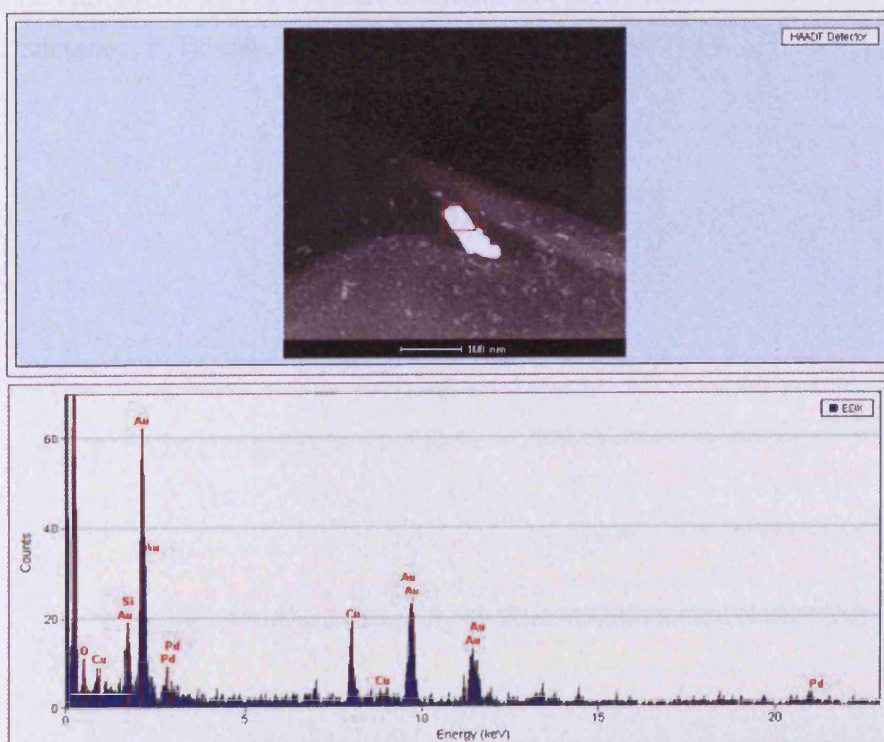
Figure 4.74 – Particle analysis (2) in etched catalyst 3333,
(composition unknown)

The energy dispersive X-ray analyses shown in Figures 4.61 – 4.74 again highlight the compositional heterogeneity of the palladium-gold phases present in the catalysts under study. Generally, palladium-rich and gold-rich phases were detected in untreated, etched, and plated catalysts. However, due to the limited number of analyses undertaken, quantification of the relative amount of each phase present remains unknown.

4.5 References

[1] R. G. Brown, J. M. Davidson, C. Triggs, C. Am. Chem. Soc., Div. Petrol. Chem. Preprint 14 (1969); French Patent No. 1403398 (1965).

[2] D. A. Kragten, R. A. van Santen, M. K. Crawford, W. D. Provine, J. J. Lerou, Inorg. Chem. 38 (1999) 331.

[3] P. M. Henry, R. N. Pandey, *in* "Homogeneous Catalysis, II; Advances in Chemistry Series 132", p. 33, American Chemical Society, Washington, DC, 1973.

[4] R. van Helden, C. F. Kohl, D. Medema, G. Verberg, T. Jonkhoff, Recueil 87 (1968) 961.

[5] R. N. Pandey, P. M. Henry, Can. J. Chem. 53 (1975) 1833.

[6] B. Samanos, P. Boutry, R. Montarnal, J. Catal. 23 (1971) 19.

CHAPTER 5
REACTIVITY OF
GRAPHITE-SUPPORTED
PALLADIUM-GOLD
CATALYSTS

5.1 Nitrobenzene Hydrogenation over Palladium-Gold Catalysts

The hydrogenation of nitrobenzene was used to measure the activities of Batch 1, Batch 2, and Batch 3 catalysts according to the procedure described in Section 2.1.5.1.

5.1.1 Rates of Nitrobenzene Hydrogenation over Batch 1, Batch 2, and Batch 3 Catalysts

Rates observed for nitrobenzene hydrogenation over Batch 1 catalysts are shown in Table 5.1. Values varied from $46 - 201$ μmol s^{-1} g$_{cat}$$^{-1}$. The rate did not increase linearly with palladium loading (Figure 5.1) suggesting that the hydrogenation rate may be influenced by a parameter such as palladium particle-size, which is known not to vary linearly with palladium loading (Section 3.3). For catalyst 3183, (0.0% Pd, 0.4% Au)[0.0]/G{1}, activity was zero.

Table 5.1 – Hydrogenation activities of Batch 1 catalysts

Catalyst		Nitrobenzene hydrogenation rate
ref no	description	/ μmol s^{-1} g$_{cat}$$^{-1}$
3182	(1.0% Pd, 0.0% Au)[∞]/G{1}	113
3185	(1.6% Pd, 0.6% Au)[4.8]/G{1}	148
3184	(1.0% Pd, 0.4% Au)[4.7]/G{1}	115
3186	(1.0% Pd, 1.0% Au)[2.0]/G{1}	116
3200	(1.0% Pd, 0.9% Au)[1.9]/G{1}	201
3187	(1.0% Pd, 1.7% Au)[1.1]/G{1}	80
3188	(1.0% Pd, 2.5% Au)[0.7]/G{1}	132
4266	(0.5% Pd, 1.8% Au)[0.5]/G{1}	70
4265	(0.2% Pd, 1.7% Au)[0.2]/G{1}	46
3183	(0.0% Pd, 0.4% Au)[0.0]/G{1}	0
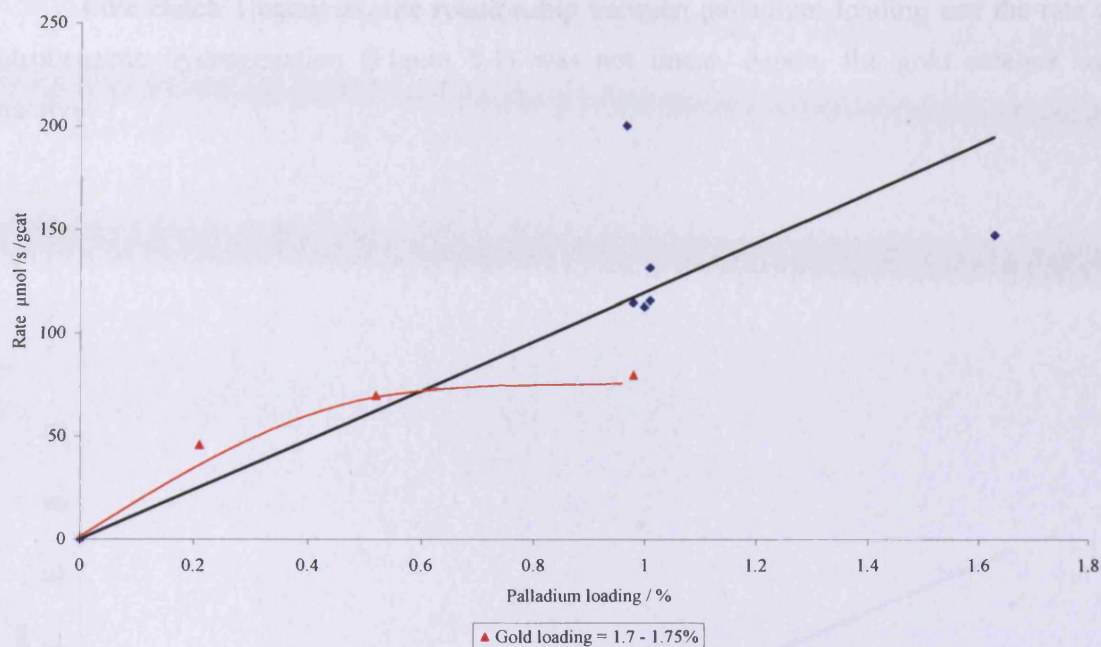
Figure 5.1 – Batch 1 catalysts: variation of activity with palladium loading

Activities of Batch 2 catalysts for nitrobenzene hydrogenation are shown in Table 5.2. Values varied from 47 – 286 μmol s^{-1} g$_{cat}$$^{-1}$, and their dependence on palladium loading is shown in Figure 5.2.

Table 5.2 – Hydrogenation activities of Batch 2 catalysts

Catalyst		Nitrobenzene hydrogenation rate / μmol s^{-1} g$_{cat}$$^{-1}$
ref no	description	
3329	(1.0% Pd, 0.0% Au)[∞]/G{2}	106
3331	(1.0% Pd, 0.4% Au)[4.8]/G{2}	159
3332	(1.7% Pd, 0.6% Au)[4.8]/G{2}	231
3333	(1.0% Pd, 1.0% Au)[1.9]/G{2}	162
3334	(1.0% Pd, 1.8% Au)[1.0]/G{2}	232
3335	(1.0% Pd, 2.7% Au)[0.7]/G{2}	286
4268	(0.5% Pd, 1.8% Au)[0.6]/G{2}	65
4267	(0.2% Pd, 1.8% Au)[0.2]/G{2}	47
3330	(0.0% Pd, 0.4% Au)[0.0]/G{2}	0

Like Batch 1 catalysts, the relationship between palladium loading and the rate of nitrobenzene hydrogenation (Figure 5.1) was not linear. Again, the gold catalyst was inactive.
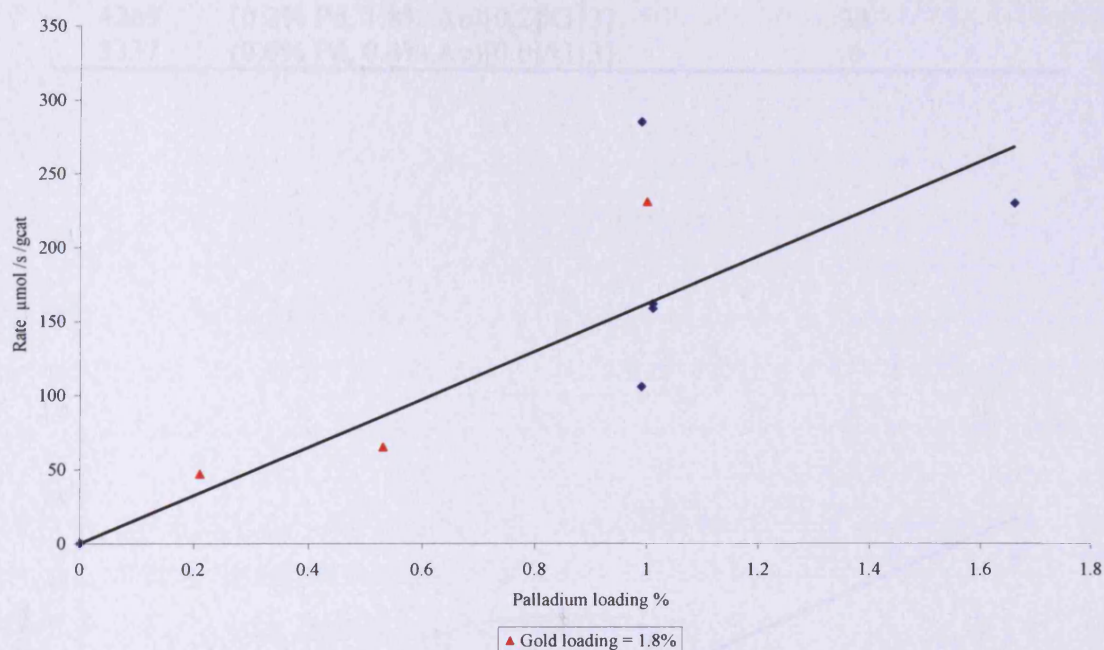
Figure 5.2 – Batch 2 catalysts: variation of activity with palladium loading

Rates of nitrobenzene hydrogenation over Batch 3 catalysts are shown in Table 5.3. Values ranged from 33 – 86 μmol s^{-1} g$_{cat}^{-1}$. Hydrogenation rates were lower than those obtained over catalysts of similar composition from Batches 1 and 2, they did not exhibit a linear relationship with palladium loading (Figure 5.3), and the gold catalyst was again inactive.

Table 5.3 – Hydrogenation activities of Batch 3 catalysts

Catalyst		Nitrobenzene hydrogenation rate / μmol s^{-1} g$_{cat}^{-1}$
ref no	description	
3336	(1.0% Pd, 0.0% Au)[∞]/G{3}	51
3339	(1.7% Pd, 0.6% Au)[5.4]/G{3}	86
3338	(1.0% Pd, 0.4% Au)[4.9]/G{3}	58
3340	(1.0% Pd, 0.9% Au)[2.1]/G{3}	67
3341	(1.0% Pd, 1.7% Au)[1.1]/G{3}	74
3342	(1.0% Pd, 2.6% Au)[0.7]/G{3}	70
4270	(0.5% Pd, 1.8% Au)[0.5]/G{3}	57
4269	(0.2% Pd, 1.8% Au)[0.2]/G{3}	33
3337	(0.0% Pd, 0.4% Au)[0.0]/G{3}	0
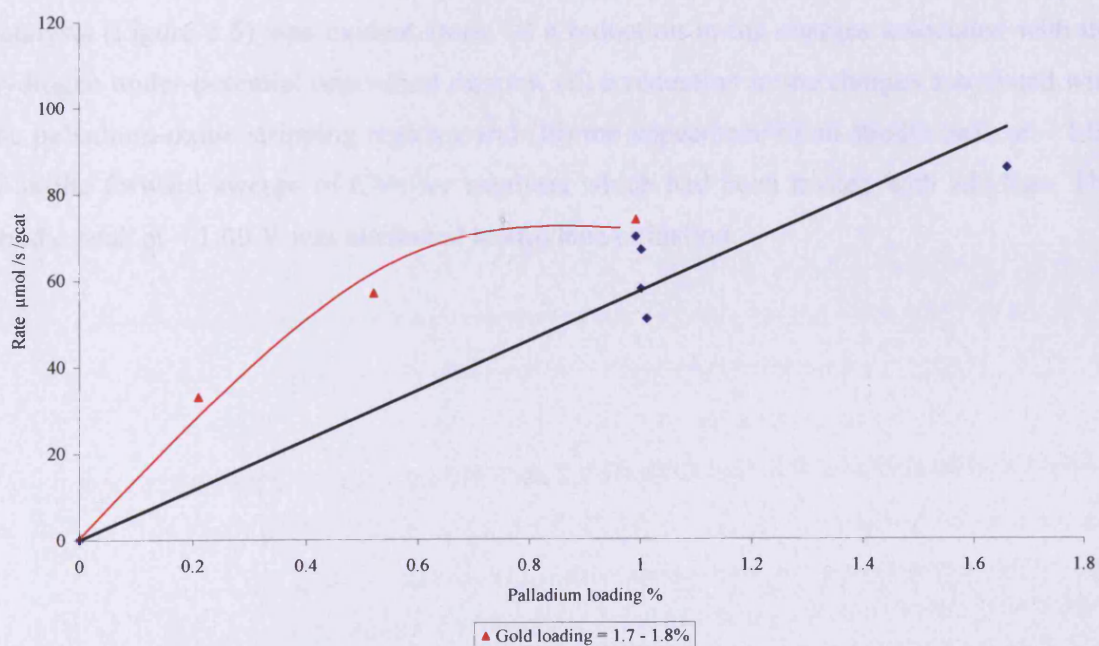
Figure 5.3 – Batch 3 catalysts: variation of activity with palladium loading

217

5.2   Ethylene Adsorption, Oxidation, and Reduction over Palladium-Gold Catalysts

Catalysts from Batch 1, Batch 2, and Batch 3 were examined by cyclic voltammetry, exposed to ethylene, and re-examined by cyclic voltammetry according to the procedure described in Section 2.3. Due to ethylene adsorption the procedure used for the collection of the CVs was slightly different to that normally used. A preliminary sweep was conducted from 0.30 V to 0.00 V. At 0.00 V the sweep polarity was changed and the potential was swept positively until an upper limit of 1.40 V was attained. This permitted the collection of important information regarding ethylene adsorption and its subsequent reduction.

5.2.1   Exposure of Palladium-Gold Catalysts from Batch 1, Batch 2, and Batch 3 to Ethylene and their Subsequent Examination

CVs for catalysts 3182, (1.0% Pd, 0.0% Au)[∞]/G{1}, and 3188, (1.0% Pd, 2.5% Au)[0.7]/G{1}, before and after exposure to ethylene are shown in Figures 5.4 and 5.5. The adsorption of ethylene on palladium/graphite (Figure 5.4) and palladium-gold/graphite catalysts (Figure 5.5) was evident from: (i) a reduction in the charges associated with the hydrogen under-potential deposition regions, (ii) a reduction in the charges associated with the palladium-oxide stripping regions, and (iii) the appearance of an anodic peak at ~ 1.00 V in the forward sweeps of CVs for catalysts which had been treated with ethylene. The anodic peak at ~ 1.00 V was attributed to ethylene oxidation.
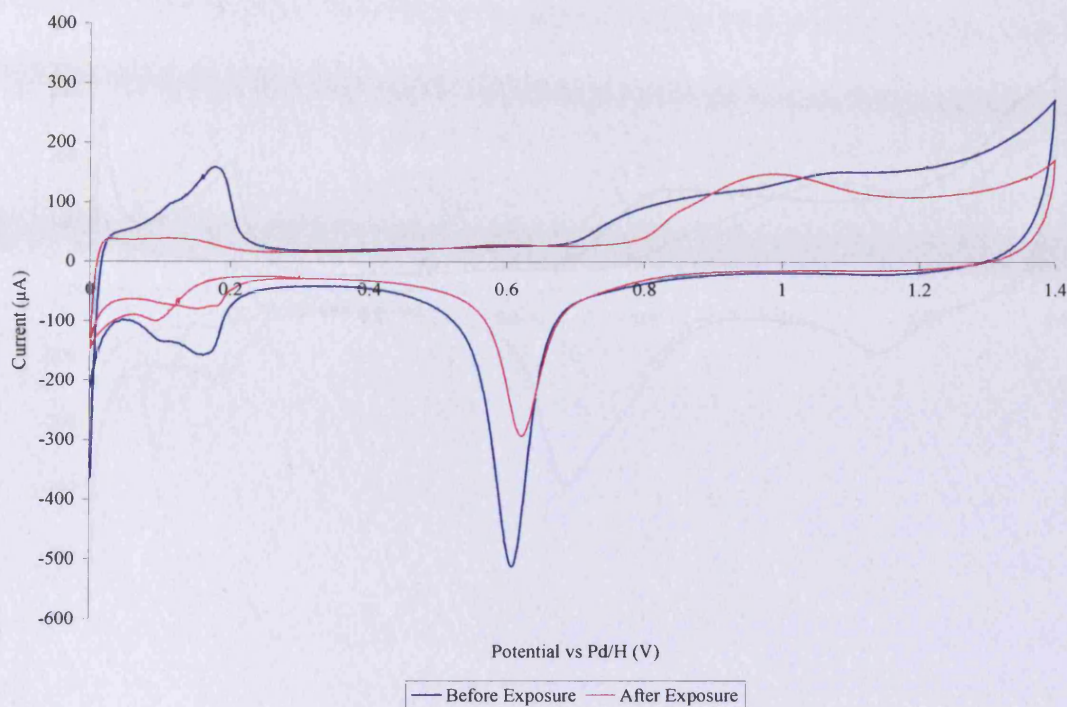
Figure 5.4 – Batch 1: CVs of catalyst 3182, (1.0% Pd, 0.0% Au)[∞]/G{1}, before and after exposure to ethylene

In Figure 5.5 the charge associated with the stripping of gold-oxide was identical before and after exposure to ethylene showing that ethylene was not adsorbed by the gold component of this palladium-gold/graphite catalyst. The appearance of a cathodic peak at ~ 0.10 V in the reverse sweep for the treated catalyst CV shows that a small degree of ethylene reduction occurred. The palladium-oxide stripping region for untreated catalyst 3188, (1.0% Pd, 2.5% Au)[0.7]/G{1}, indicated that the palladium existed in palladium-rich and gold-rich phases. After exposure to ethylene the palladium appeared to exist only in gold-rich phases.
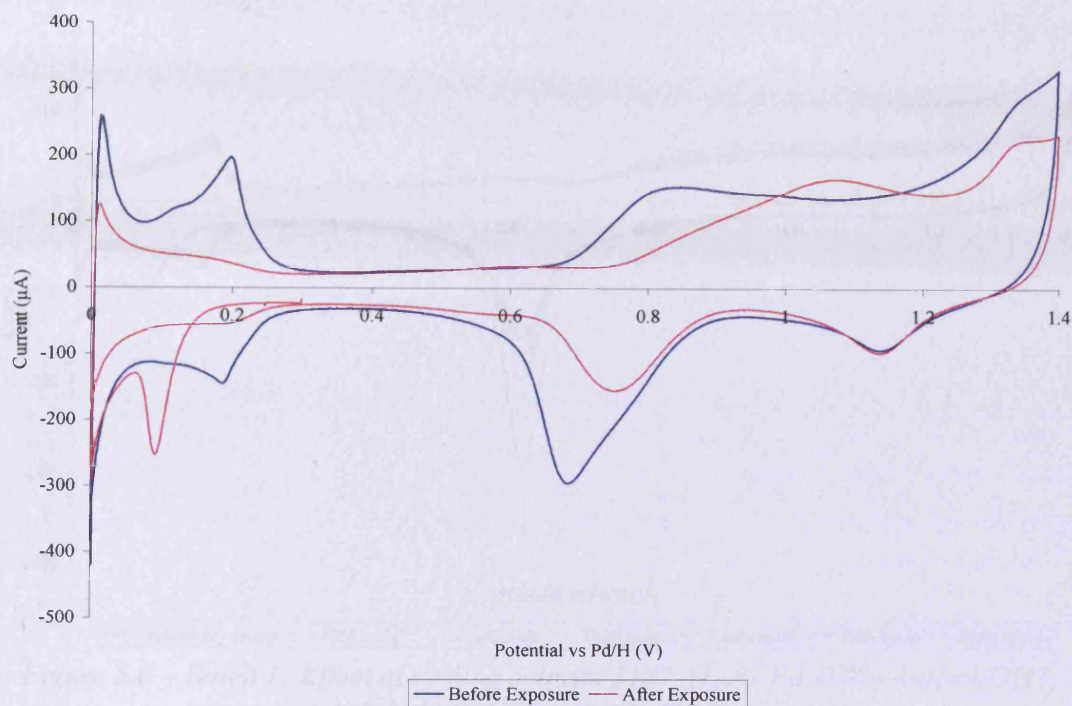
Figure 5.5 – Batch 1: CVs of catalyst 3188, (1.0% Pd, 2.5% Au)[0.7]/G{1}, before and after exposure to ethylene

Figures 5.6 and 5.7 show the effect of conducting successive cycles after the same two catalysts had been exposed to ethylene. The first cycle in each Figure shows the state of the catalyst surface after ethylene exposure. The forward sweep of the first cycle contains an anodic peak at ~ 1.00 V and the charge associated with the hydrogen under-potential deposition region in the second cycle increased from its value in the first cycle. Further cycling showed that the charge associated with the hydrogen under-potential deposition region decreased. The charge associated with the palladium-oxide stripping region also decreased on cycling. This is attributed to the electrochemical etching of palladium.

220
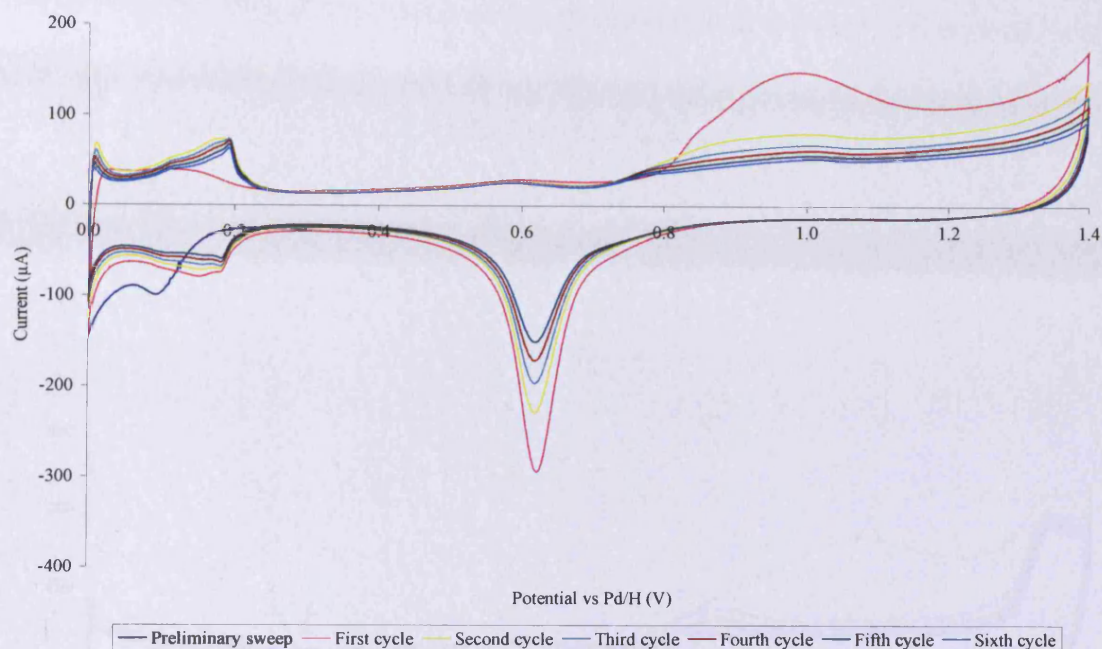
Figure 5.6 – Batch 1: Effect of cycling catalyst 3182, (1.0% Pd, 0.0% Au)[∞]/G{1}, catalyst after exposure to ethylene

Figure 5.7 shows that the charge associated with the stripping of gold-oxide increased with cycle number. This indicates that the surface area of gold increased on cycling, whereas that of palladium decreased. The appearance of a cathodic peak (~ 0.10 V) in the preliminary sweep shows ethylene reduction. The charges associated with the HUPD and oxide stripping regions of Batch 1 catalysts, before and after ethylene exposure are shown in Table 5.4. The extent of ethylene adsorption is also shown; it approached 100% with the introduction of gold to the catalyst.
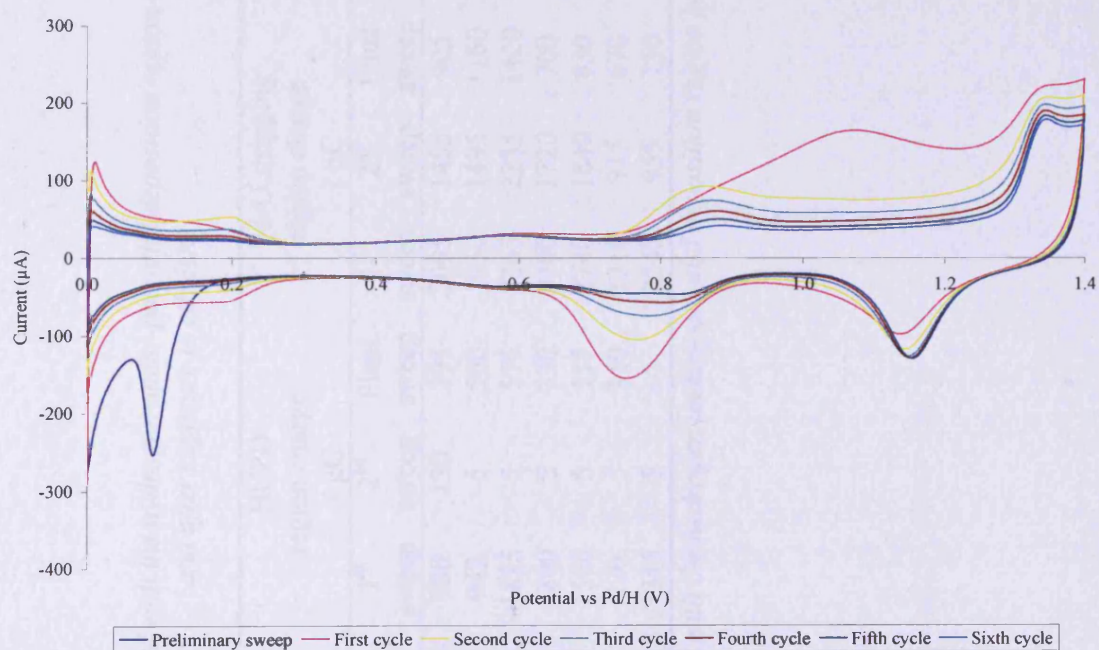
Figure 5.7 – Batch 1: Effect of cycling catalyst 3188, (1.0% Pd, 2.5% Au)[0.7]/G{1}, after exposure to ethylene

Table 5.4 – Batch 1 catalysts: charges associated with the hydrogen under-potential deposition region and oxide stripping regions before and after exposure to ethylene

Catalyst		HUPD region charge / μC			Pd-O stripping region charge / μC			Au-O stripping region charge / μC		Extent of ethylene adsorption (%)[a]
ref no	description	1st sweep	2nd sweep	Final sweep	1st sweep	2nd sweep	Final sweep	1st sweep	Final sweep	
3182	(1.0% Pd, 0.0% Au)[∞]/G{1}	980	130	395	2095	1455	905	n/o	n/o	87
3185	(1.6% Pd, 0.6% Au)[4.8]/G{1}	945	5	500	1950	1495	1160	n/o	100	99
3184	(1.0% Pd, 0.4% Au)[4.7]/G{1}	1835	5	575	3265	2235	1420	n/o	n/o	100
3186	(1.0% Pd, 1.0% Au)[2.0]/G{1}	1800	5	330	3100	1720	700	185	365	100
3200	(1.0% Pd, 0.9% Au)[1.9]/G{1}	1500	5	115	2740	1840	630	110	270	100
3187	(1.0% Pd, 1.7% Au)[1.1]/G{1}	470	5	110	1210	915	670	80	235	99
3188	(1.0% Pd, 2.5% Au)[0.7]/G{1}	1345	5	5	2545	955	150	210	515	100

[a]*calculated based on the charges associated with the hydrogen under-potential deposition region before and after ethylene exposure*

n/o = not observed

223

Figures 5.8 and 5.9 show the effect of ethylene adsorption by catalysts 3333, (1.0% Pd, 1.0% Au)[1.9]/G{2}, and 3335, (1.0% Pd, 2.7% Au)[0.7]/G{2}. After ethylene exposure, blocking of palladium sites in the hydrogen under-potential deposition region was observed, and this was accompanied by a smaller charge associated with the palladium-oxide striping region.
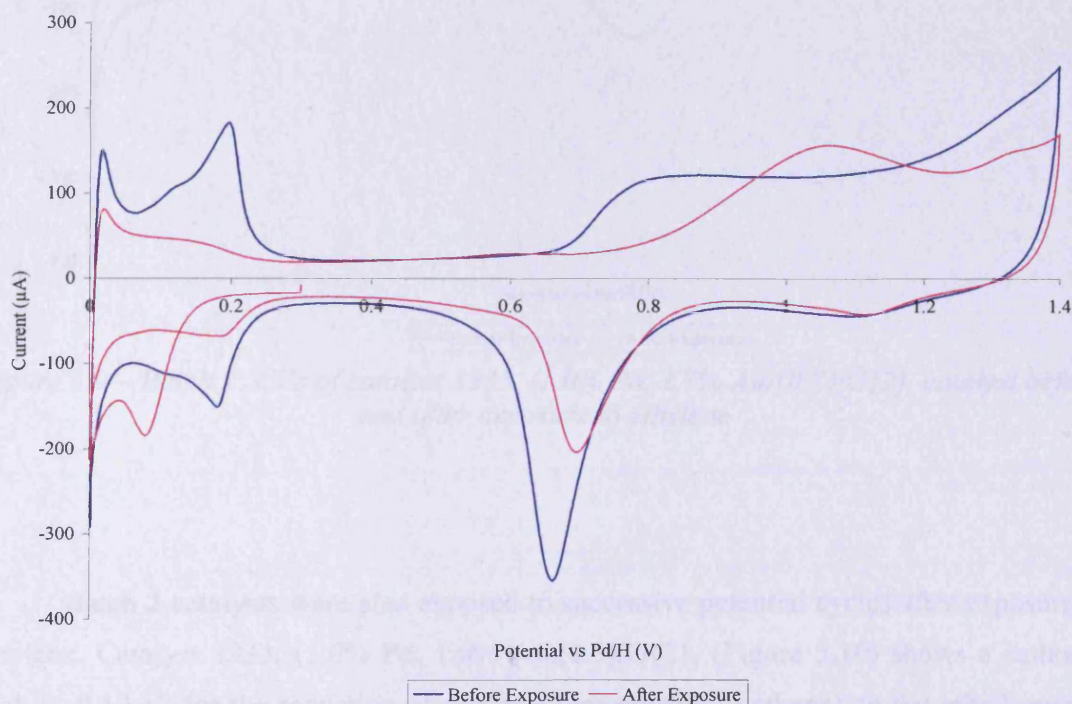
Figure 5.8 – Batch 2: CVs of catalyst 3333, (1.0% Pd, 1.0% Au)[1.9]/G{2}, catalyst before and after exposure to ethylene

Figure 5.9 shows CVs for catalyst 3335, (1.0% Pd, 2.7% Au)[0.7]/G{2}, before and after exposure to ethylene. Again, a decrease in charge was associated each feature providing a measure of palladium surface area, and an increase in the charge associated with gold-oxide stripping region was observed, indicating an increase in gold surface area.
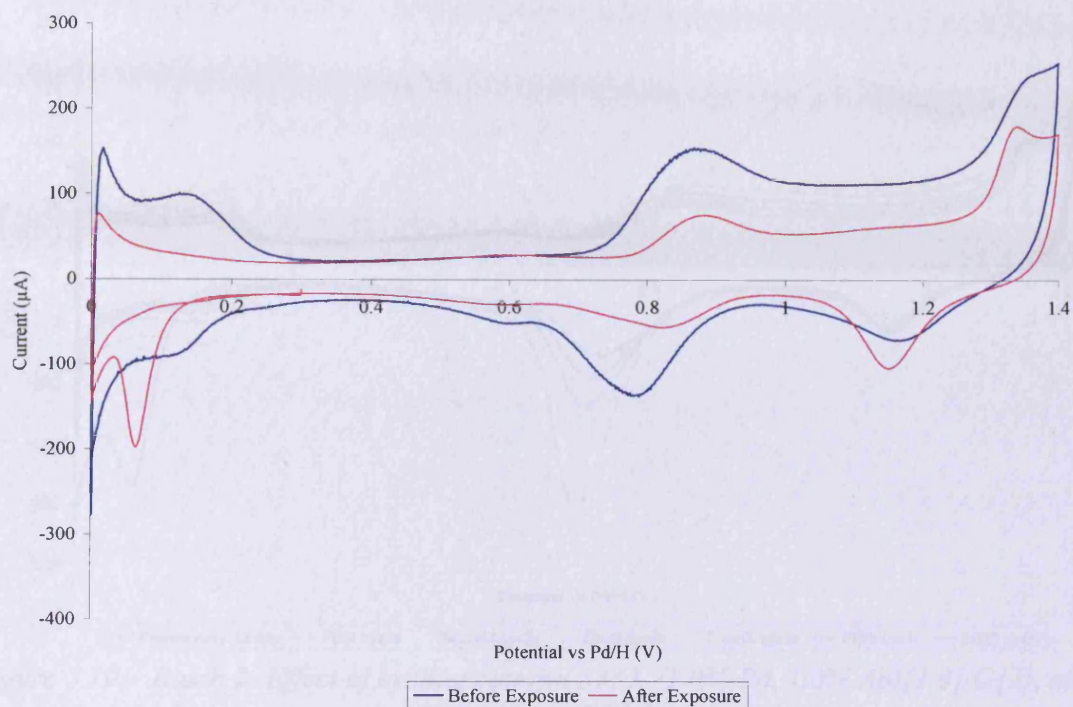
Figure 5.9 – Batch 2: CVs of catalyst 3335, (1.0% Pd, 2.7% Au)[0.7]/G{2}, catalyst before and after exposure to ethylene

Batch 2 catalysts were also exposed to successive potential cycles after exposure to ethylene. Catalyst 3333, (1.0% Pd, 1.0% Au)[1.9]/G{2}, (Figure 5.10) shows a cathodic peak (~ 0.10 V) for the reduction of ethylene (presumably to ethane) on the initial reverse sweep (labelled preliminary sweep). The first and second cycles show the regeneration of the hydrogen under-potential deposition region, interpreted as the oxidation of ethylene and desorption of the products from these surfaces. Further cycles show decreasing charges associated with the HUPD and palladium-oxide stripping regions and this is attributed to the electrochemical etching of palladium from the catalyst surface. For catalyst 3335, (1.0% Pd, 2.7% Au)[0.7]/G{2}, (Figure 5.11) after ethylene exposure, the hydrogen under-potential deposition region was not regenerated. For this catalyst, the charge associated with the palladium-oxide stripping region decreased rapidly, leaving a catalyst enriched with gold at its surface.

Figure 5.10 – Batch 2: Effect of cycling catalyst 3333, (1.0% Pd, 1.0% Au)[1.9]/G{2}, after exposure to ethylene

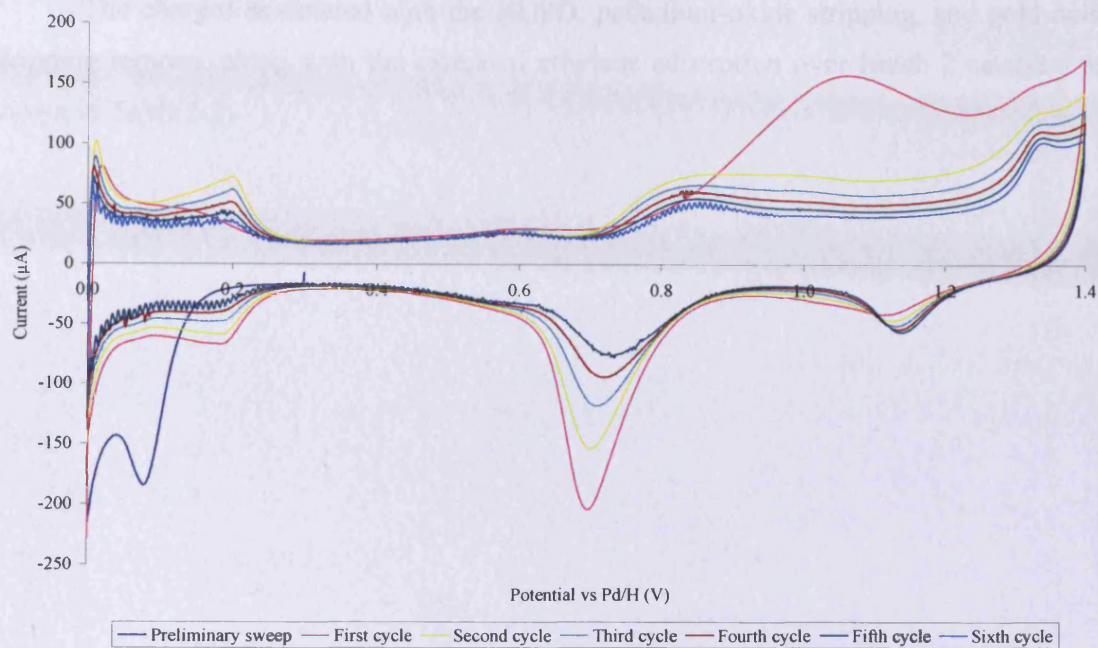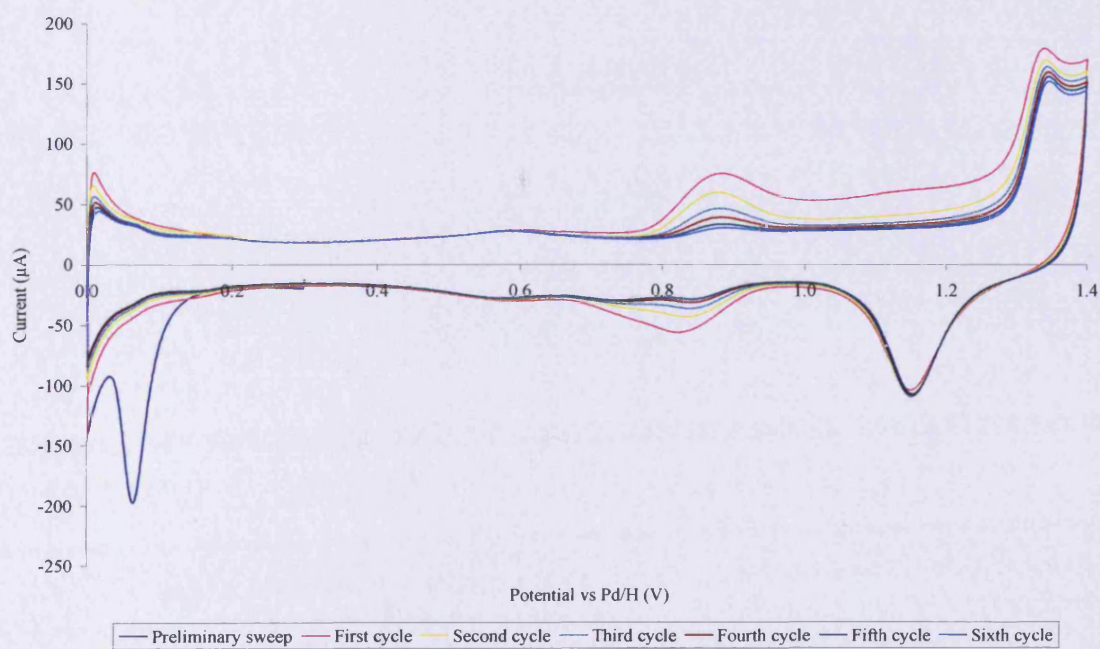*Figure 5.11 – Batch 2: Effect of cycling catalyst 3335, (1.0% Pd, 2.7% Au)[0.7]/G{2}, after exposure to ethylene*

The charges associated with the HUPD, palladium-oxide stripping, and gold-oxide stripping regions, along with the extent of ethylene adsorption over Batch 2 catalysts are shown in Table 5.5.

Table 5.5 – Batch 2 catalysts: charges associated with the hydrogen under-potential deposition region and oxide stripping regions before and after exposure to ethylene

	Catalyst	HUPD region charge / μC			Pd-O stripping region charge / μC			Au-O stripping region charge / μC		Extent of ethylene adsorption (%)[a]
ref no	description	1st sweep	2nd sweep	Final sweep	1st sweep	2nd sweep	Final sweep	1st sweep	Final sweep	
3329	(1.0% Pd, 0.0% Au)[∞]/G{2}	2035	95	545	2565	2080	1180	n/o	n/o	95
3331	(1.0% Pd, 0.4% Au)[4.8]/G{2}	1055	5	345	2205	1210	860	n/o	n/o	100
3332	(1.7% Pd, 0.6% Au)[4.8]/G{2}	1175	5	505	3075	1470	1030	n/o	n/o	100
3333	(1.0% Pd, 1.0% Au)[1.9]/G{2}	1300	5	165	2135	1250	470	60	175	100
3334	(1.0% Pd, 1.8% Au)[1.0]/G{2}	1115	5	35	1410	565	285	130	410	100
3335	(1.0% Pd, 2.7% Au)[0.7]/G{2}	410	0	0	690	260	215	215	455	100

[a]calculated based on the charges associated with the hydrogen under-potential deposition region before and after ethylene exposure
n/o = not observed

Table 5.6 – Batch 3 catalysts: charges associated with the hydrogen under-potential deposition region and oxide stripping regions before and after exposure to ethylene

	Catalyst	HUPD region charge / μC			Pd-O stripping region charge / μC			Au-O stripping region charge / μC		Extent of ethylene adsorption (%)[a]
ref no	description	1st sweep	2nd sweep	Final sweep	1st sweep	2nd sweep	Final sweep	1st sweep	Final sweep	
3336	(1.0% Pd, 0.0% Au)[∞]/G{3}	600	145	465	1140	950	894	n/o	n/o	76
3339	(1.7% Pd, 0.6% Au)[5.4]/G{3}	600	5	435	1075	870	794	n/o	n/o	99
3338	(1.0% Pd, 0.4% Au)[4.9]/G{3}	525	90	385	940	825	762	n/o	n/o	83
3340	(1.0% Pd, 0.9% Au)[2.1]/G{3}	360	0	230	730	655	572	n/o	n/o	100
3341	(1.0% Pd, 1.7% Au)[1.1]/G{3}	655	0	175	1270	795	580	48	116	100
3342	(1.0% Pd, 2.6% Au)[0.7]/G{3}	570	5	185	1260	910	706	79	145	99

[a]calculated based on the charges associated with the hydrogen under-potential deposition region before and after ethylene exposure
n/o = not observed

Batch 3 catalysts provided similar CVs (not shown). The charges associated with the HUPD and oxide regions along with the extent of ethylene adsorption are shown in Table 5.6. The surface chemistry for Batch 3 catalysts followed that described for Batch 1 and Batch 2 catalysts.

5.2.2 Conclusions

Figures 5.4 – 5.11 show the effect of ethylene on palladium and palladium-gold catalysts. The CVs show that ethylene adsorption occurs over palladium but that limited or no adsorption occurs over gold. Following ethylene adsorption, reductions in the charges associated with the HUPD and palladium-oxide stripping regions were observed and their regeneration were observed after ethylene oxidation. For catalyst 3335, (1.0% Pd, 2.7% Au)[0.7]/G{2}, (Figure 5.11) the regeneration of the HUPD region was not observed. Possibly due to the rate of electrochemical etching being as fast or faster than that of ethylene oxidation.

Finally, the extent of ethylene adsorption was enhanced by the introduction of gold to the catalyst i.e. palladium-gold catalysts adsorbed ethylene to a greater extent than palladium catalysts.

5.3 High Throughput Experimentation

Modern catalyst development, in its early stages, involves a process known as high throughput experimentation (HTE). This approach is very effective for the discovery of new materials which exhibit catalytic activity in many chemical applications. HTE accelerates catalyst development programmes within a very short timeframe. In this investigation, certain untreated, etched, and plated catalysts from Batch 2 were tested on a high throughput testing rig (HTTR) at BP's Hull Research & Technology Centre (HRTC). The procedure followed in this HTE programme (e.g. catalyst preparation, experimental conditions etc) is described in Section 2.1.5.2.

Nine sets of untreated, etched, and plated catalysts (i.e. twenty seven catalysts in total) were sent to HRTC of which three were selected for HTE. Catalyst reference numbers and catalyst descriptions are re-iterated in Table 5.7 for convenience.

Table 5.7 – Reference numbers and descriptions for catalysts used in the HTE programme

Catalyst	
ref no	description
3331	(1.0% Pd, 0.4% Au)[4.8]/G{2}
3332	(1.7% Pd, 0.6% Au)[4.8]/G{2}

5.3.1 Space-Time Yield

During the HTE programme, catalyst activity was measured after approximately 14, 24, 29, 35, and 39 h (Table 5.8). Activity was measured using online gas chromatography (GC) and the space-time yields (STY) were calculated in the units of g_{VA} kg_{cat}^{-1} h^{-1} where g_{VA} = grams vinyl acetate produced.

Regardless of metal loadings clear differences in the initial catalytic activities of untreated (3331 u), etched (3332 e), and plated (3332 p) catalysts were observed. The untreated catalyst had the highest activity, and the activity of the plated catalyst exceeded that of the etched catalyst. This is consistent with the notions (i) that the initial deposition of palladium and gold formed a catalytically active alloy and (ii) the etched catalyst contained gold-rich particles (formed as a result of palladium etching) and was thus least active for vinyl acetate formation. The plated catalyst had an activity intermediate between that of the untreated and etched catalysts, probably due to it having a higher palladium content than that of the etched catalyst but, it not being alloyed. This palladium was likely to be in a less active form than that in the untreated catalyst.
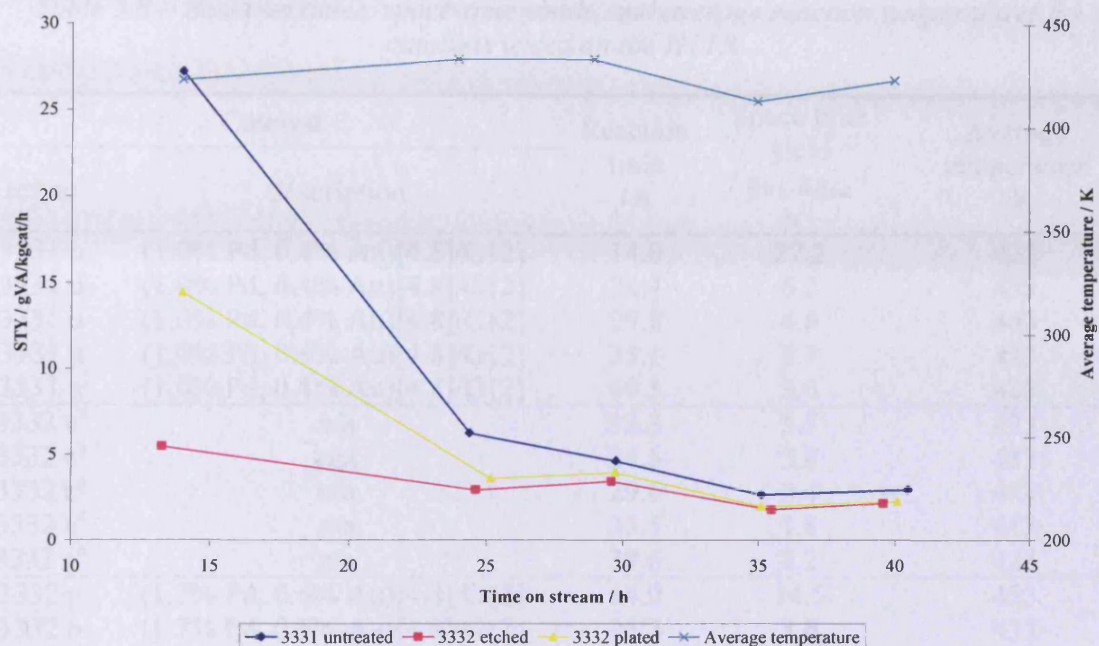
Figure 5.12 – Variation of the space-time yield with time and temperature for untreated catalyst 3331, etched catalyst 3332, and plated catalyst 3332 (see Table 5.7 for descriptions)

The initial catalyst activities (STY at ~ 14 h) were 27.2, 5.5, and 14.5 g_{VA} kg_{cat}^{-1} h^{-1} for untreated 3331 (3331 u), etched 3332 (3332 e), and plated 3332 (3332 p) respectively. After ~ 20 h, the activities of each catalyst fell to a low level. It was therefore difficult to draw meaningful conclusions regarding the effect of temperature on catalyst activity.

The final measurements revealed that the catalytic activities were 3.0, 2.2, and 2.3 g_{VA} kg_{cat}^{-1} h^{-1} for 3331 u, 3332 e, and 3332 p respectively and after ~ 40 h; the catalysts had clearly undergone deactivation. The rates of catalyst deactivation probably followed the initial order of catalyst activity (i.e. 3331 u > 3332 p > 3332 e).

Table 5.8 – Reaction times, space-time yields, and average reaction temperatures for catalysts tested on the HTTR

Catalyst		Reaction time / h	Space time yield / g_{VA} kg_{cat}^{-1} h^{-1}	Average temperature / K
ref no	description			
3331 u	(1.0% Pd, 0.4% Au)[4.8]/G{2}	14.0	27.2	423
3331 u	(1.0% Pd, 0.4% Au)[4.8]/G{2}	24.4	6.2	433
3331 u	(1.0% Pd, 0.4% Au)[4.8]/G{2}	29.8	4.6	443
3331 u	(1.0% Pd, 0.4% Au)[4.8]/G{2}	35.1	2.7	413
3331 u	(1.0% Pd, 0.4% Au)[4.8]/G{2}	40.5	3.0	423
3332 e[a]	n/a	13.3	5.5	423
3332 e[a]	n/a	24.6	3.0	433
3332 e[a]	n/a	29.6	3.4	443
3332 e[a]	n/a	35.5	1.8	413
3332 e[a]	n/a	39.6	2.2	423
3332 p	(1.7% Pd, 0.6% Au)[4.8]/G{2}	14.0	14.5	423
3332 p	(1.7% Pd, 0.6% Au)[4.8]/G{2}	25.2	3.6	433
3332 p	(1.7% Pd, 0.6% Au)[4.8]/G{2}	29.7	4.0	443
3332 p	(1.7% Pd, 0.6% Au)[4.8]/G{2}	35.1	2.0	413
3332 p	(1.7% Pd, 0.6% Au)[4.8]/G{2}	40.1	2.3	423

[a]*composition unknown*

5.3.2 Selectivity

In the same experiment the selectivity, S (based on the amounts of vinyl acetate and carbon dioxide formed) was measured. Similar trends to those found for catalyst activity (Section 5.3.1) were observed (Table 5.9). Initially, 3331 u (S = 59.8 %) was the most selective catalyst whereas 3332 e was the least selective (S = 25.6 %). The plated catalyst provided a selectivity intermediate between these extremes (S = 37.2 %). After approximately 24 h the order of catalyst selectivity changed, the most selective catalyst was still 3331 u but 3332 e had become slightly more selective than 3332 p. For each catalyst, the deactivation was accompanied by a loss of selectivity. However, the temperature was not maintained constant by the instrumentation, and there is clear evidence for each catalyst that the selectivity varied inversely with temperature (Figure 5.13).

Table 5.9 – Reaction times, selectivity's, and average reaction temperatures for catalysts tested on the HTTR

Catalyst		Reaction time / h	Selectivity[a] / %	Average temperature / K
ref no	description			
3331 u	(1.0% Pd, 0.4% Au)[4.8]/G{2}	14.0	59.8	423
3331 u	(1.0% Pd, 0.4% Au)[4.8]/G{2}	24.4	24.2	433
3331 u	(1.0% Pd, 0.4% Au)[4.8]/G{2}	29.8	19.9	443
3331 u	(1.0% Pd, 0.4% Au)[4.8]/G{2}	35.1	30.7	413
3331 u	(1.0% Pd, 0.4% Au)[4.8]/G{2}	40.5	27.0	423
3332 e[b]	n/a	13.3	25.6	423
3332 e[b]	n/a	24.6	20.4	433
3332 e[b]	n/a	29.6	17.4	443
3332 e[b]	n/a	35.5	25.7	413
3332 e[b]	n/a	39.6	22.9	423
3332 p	(1.7% Pd, 0.6% Au)[4.8]/G{2}	14.0	37.2	423
3332 p	(1.7% Pd, 0.6% Au)[4.8]/G{2}	25.2	18.7	433
3332 p	(1.7% Pd, 0.6% Au)[4.8]/G{2}	29.7	16.4	443
3332 p	(1.7% Pd, 0.6% Au)[4.8]/G{2}	35.1	22.6	413
3332 p	(1.7% Pd, 0.6% Au)[4.8]/G{2}	40.1	20.5	423

[a]based on the amounts of vinyl acetate and carbon dioxide formed
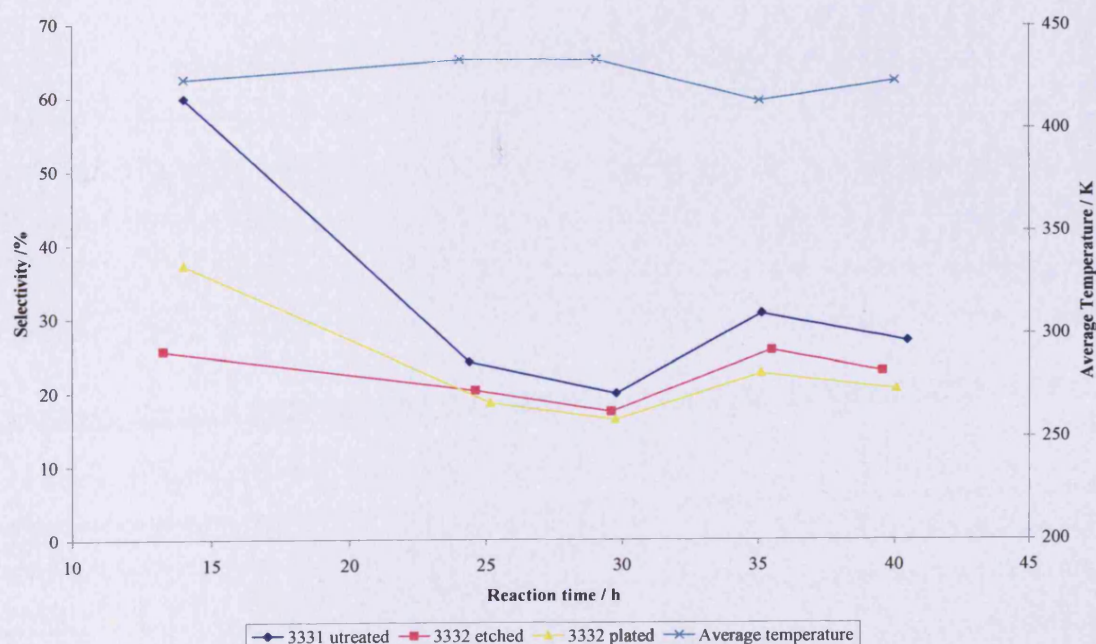[b]composition unknown

Figure 5.13 – Variation of the selectivity to VAM with time and temperature for untreated catalyst 3331, etched catalyst 3332, and plated catalyst 3332 (see Table 5.9 for descriptions)

CHAPTER 6
DISCUSSION

6.1 Characterisation: Bulk Properties of Palladium-Gold Catalysts

Catalysts used commercially for vinyl acetate synthesis consist of palladium-gold particles supported on a microsperiodal silica support [1 – 5]. Due to the low conductivity of silica, these catalysts were not suitable for use in the present investigation, so palladium-gold catalysts were prepared using low surface area graphite as support material. Three Batches of catalysts were prepared using a variety of methods (Tables 2.1 – 2.4). Each Batch consisted of a palladium/graphite catalyst, various palladium-gold/graphite catalysts, and a gold/graphite catalyst.

The bulk properties of the catalysts were assessed using: X-ray fluorescence to determine metal loadings, atom compositions, and palladium/gold atom ratios, X-ray diffraction to determine particle-composition and mean particle-size, high resolution transmission electron microscopy to determine particle-size distribution and morphology, and energy dispersive X-ray analysis to determine the composition of individual metal particles. These techniques allowed bulk properties such as particle-size and particle composition (i.e. the extent of alloying) to be monitored as a function of preparation method and overall catalyst composition.

6.1.1 Measurement of Palladium and Gold Loadings: X-Ray Fluorescence

For Batch 1 catalysts, actual and intended palladium and gold loadings were in close agreement (Table 3.1). Palladium loadings were correct to ± 0.02% and gold loadings were correct to ± 0.06% [exceptions: catalyst 3187, (1.0% Pd, 1.7% Au)[1.1]/G{1}, and catalyst 3200, (1.0% Pd, 0.9% Au)[1.9]/G{1}]. Catalyst 3187 contained 0.07% less gold than intended, which was consistent with a yellow colouration of the solution after reduction. However, catalyst 3200 contained 0.86% less gold than expected and the reasons for this major discrepancy remain unknown. The properties of catalyst 3200 were of particular interest as it was the only catalyst prepared in this study to give a diffractogram which resembled that of a commercial LEAP catalyst (Figure 6.1). Thus, this catalyst had bulk alloy properties similar to that of the commercial LEAP catalyst. Its behaviour is discussed in greater detail in Section 6.6.

For Batch 2 catalysts, the actual and intended metal loadings were again in close agreement (Table 3.2). The palladium loadings were correct to ± 0.01% [exception: catalyst

4268, (0.5% Pd, 1.8% Au)[0.6]/G{2}, + 0.03%] and the gold loadings were correct to ± 0.02% [exception: catalyst 3335, (1.0% Pd, 2.7% Au)[0.7]/G{2}, + 0.09%].

For Batch 3 catalysts, all palladium loadings were correct to ± 0.02% and all gold loadings were correct ± 0.10% (Table 3.3).

Thus, the preparative methods employed provided catalysts having the required metal loadings.

6.1.2 Particle Composition and Particle-Size Measurements

6.1.2.1 X-ray diffraction

Using Vergard's law and by applying the Scherrer equation to the X-ray diffratograms (Section 3.1.2) the compositions of the palladium-gold phases present in Batch 1, Batch 2, and Batch 3 catalysts were determined together with estimates of mean particle-size for each phase. The metallic phases consisted of large gold-rich particles and smaller palladium-rich particles (i.e. two types of alloy particle were present); however, there were differences in detail.

Batch 1 and Batch 2 catalysts (which were prepared by slurry precipitation and reduction with formaldehyde and hydrazine respectively) contained large gold-rich particles and smaller palladium-rich particles. Between Batches there were no significant differences in the particle-size or composition for catalysts having similar overall compositions and hence the reductant used was not significant. However, there were exceptions: catalyst 3200, (1.0% Pd, 0.9% Au)[1.9]/G{1}, contained smaller gold-rich particles than expected by comparison with the mean properties of Batch 1 catalysts and catalyst 3185, (1.6% Pd, 0.6% Au)[4.8]/G{1}, contained larger palladium-rich particles than expected. The reasons for these variations lie in the composition of the other particles, showing the degree of variability in the phases formed when palladium-gold catalysts are prepared using graphite supports. Thus, gold-rich particles in catalyst 3200 contained on average approximately four times more palladium than the comparable gold-rich particles in the other Batch 1 catalysts, and the palladium-rich particles in 3185 contained much less gold than the palladium-rich particles of other Batch 1 catalysts. Batch 3 catalysts (which were prepared by incipient wetness impregnation and reduction with hydrazine) contained

large gold-rich particles, smaller palladium-rich particles, and an additional phase consisting of large, almost pure, gold particles.

In general, gold-rich particles were larger than palladium-rich particles. However, the particles which gave rise to diffraction and provided the diffractograms on which these analyses are based were particles having diameters greater than a threshold value of ~ 2 nm. Particles having diameters less than this threshold value are X-ray invisible and would not have contributed to the information obtained.

6.1.2.2 High resolution transmission electron microscopy

High resolution transmission electron microscopy was used to investigate particle-size and particle morphology in Batch 1, Batch 2, and Batch 3 catalysts (Section 3.1.3). Micrographs of the metallic regions in certain Batch 1 catalysts show that, at high palladium/gold atom ratios, the catalysts contained small, well dispersed metal particles and as the palladium/gold atom ratio decreased (the gold composition increased) the catalysts contained larger metal particles which often appeared as aggregates or clusters. This is consistent with gold tending to exist as large particles on graphitic surfaces. Particle-size distributions which excluded aggregates (Figure 3.4) were consistent with the findings of X-ray diffraction; each technique revealed the tendency of gold to exist as large particles, and palladium to exist as smaller particles, with gold-rich and palladium-rich particles showing intermediate behaviour.

6.1.2.3 Energy dispersive X-ray analysis

Energy dispersive X-ray analysis provided the compositions of regions and sometimes of individual particles in Batch 1, Batch 2, and Batch 3 catalysts (Section 3.1.4). Figures 3.5 – 3.9 show palladium-rich and gold-rich particles existing in close proximity and particles which contained both palladium-rich and gold-rich regions (i.e. compositional gradients occurred within given particles). These results are also consistent with those of X-ray diffraction, each highlighting the compositional heterogeneity of palladium-gold phases existing in these catalysts.

To summarise. Chapter 3 shows that the prepared catalysts contain metal particles of various sizes and palladium-gold compositions. In Chapter 4 this variability was used to

advantage to investigate etching effects which, as will be seen in Section 6.6, played a role in clarifying the mechanism of vinyl acetate synthesis.
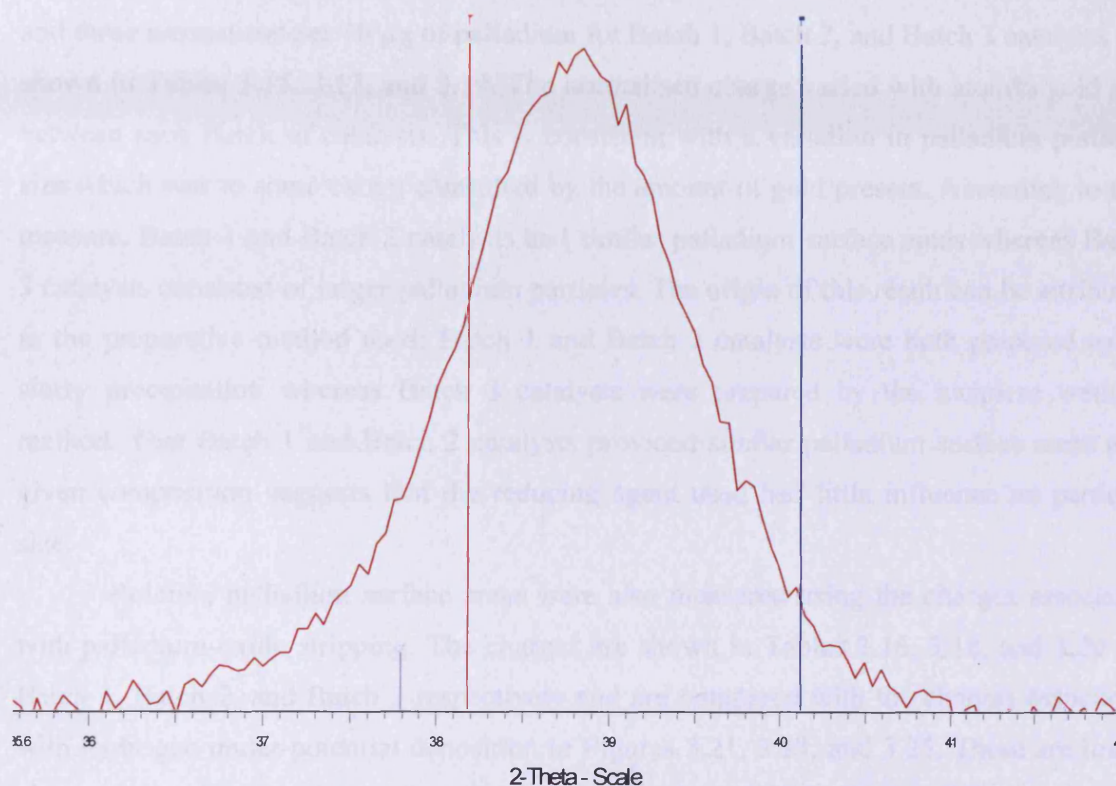
Figure 6.1 – An X-ray diffractogram for a commercial LEAP catalyst

6.2   Characterisation: Surface Properties of Palladium-Gold Catalysts

Because, the surface properties of catalyst particles are of paramount importance, Batch 1, Batch 2, and Batch 3 catalysts were characterised by cyclic voltammetry (Section 3.2). Relative palladium surface areas were determined from the charges associated with the hydrogen under-potential deposition and palladium-oxide stripping regions in the CVs whereas relative gold surface areas were determined from the charges associated with the gold-oxide stripping regions. Palladium surface areas were also measured by use of CO chemisorption. The extent of surface alloy formation was estimated from (i) the potentials required for oxide stripping from catalyst surfaces, (ii) X-ray photoelectron spectroscopy, and (iii) propan-2-ol electrooxidation.

6.2.1 Palladium and Gold Surface Areas

The charge associated with hydrogen under-potential deposition over palladium-based catalysts provided estimates of the relative palladium surface areas. The measured values and those normalised per 10 μg of palladium for Batch 1, Batch 2, and Batch 3 catalysts are shown in Tables 3.15, 3.17, and 3.19. The normalised charge varied with atom% gold and between each Batch of catalysts. This is consistent with a variation in palladium particle-size which was to some extent controlled by the amount of gold present. According to this measure, Batch 1 and Batch 2 catalysts had similar palladium surface areas whereas Batch 3 catalysts consisted of larger palladium particles. The origin of this result can be attributed to the preparative method used; Batch 1 and Batch 2 catalysts were both prepared using slurry precipitation whereas Batch 3 catalysts were prepared by the incipient wetness method. That Batch 1 and Batch 2 catalysts provided similar palladium surface areas at a given composition suggests that the reducing agent used had little influence on particle-size.

Relative palladium surface areas were also measured using the charges associated with palladium-oxide stripping. The charges are shown in Tables 3.16, 3.18, and 3.20 for Batch 1, Batch 2, and Batch 3 respectively and are compared with the charges associated with hydrogen under-potential deposition in Figures 3.21, 3.23, and 3.25. These are linear plots passing through the origin, as required if hydrogen under-potential deposition and palladium-oxide stripping each provide a genuine measure of palladium surface area. However, the gradient of the line was not equal to the expected value of 2 due to various associated uncertainties. These included (i) the deconvolution method (i.e. separation of charges associated with absorption and adsorption processes), (ii) the charge associated with the adsorption of anions at potentials similar to those required for hydrogen under-potential deposition, and (iii) the possibility of over-oxidation of palladium (bulk oxidation) at positive potentials. However, the linear nature of these graphs demonstrate that measurements of charge associated with hydrogen under-potential deposition and with palladium-oxide stripping are each valid measures of available palladium surface area in these catalysts.

At the outset, it was known that the upper (most positive) potential used in the voltammetric sweep would be insufficient to completely oxidise gold surfaces in these catalysts. The limit of 1.4 V (versus Pd/H) was chosen because, at higher potentials, oxygen

evolution occurs. However, regardless of the potential limit used, the charges associated with gold-oxide stripping can be used to measure the relative gold surface area of these catalysts. The charges were small, indicating that the gold surface area was small and suggesting that the gold particles might be large.

Absolute palladium surface areas were measured using CO chemisorption. The results obtained (Table 3.23) were consistent with findings of hydrogen under-potential deposition showing that the palladium surface areas of Batch 1 and Batch 2 catalysts were approximately equal and generally greater than those of Batch 3. Figure 6.2 shows a plot of charge associated with hydrogen under-potential deposition versus the palladium surface areas obtained by CO chemisorption. This plot should be linear, the line passing through the origin. Although the variation is approximately linear (there being substantial scatter) the line for Batch 1 and Batch 2 catalysts crosses the ordinate at ~ 0.5 m^2 g^{-1}. This indicates
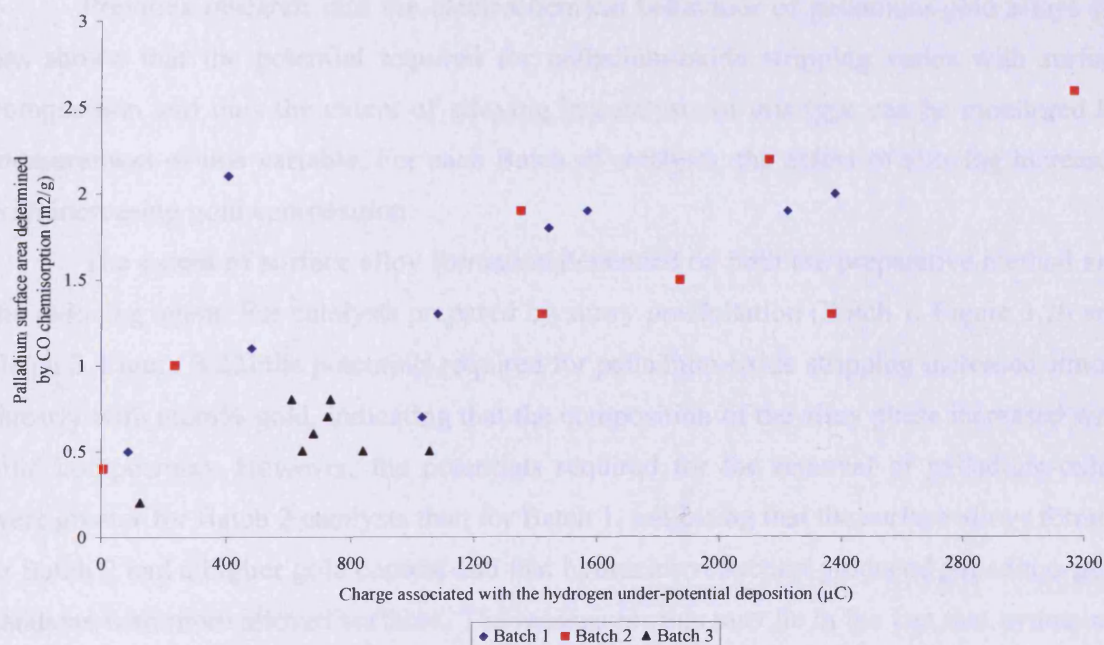
Figure 6.2 – Palladium surface area measurement: comparison of results obtained by CO chemisorption and hydrogen under-potential deposition

that a proportion of the surface palladium adsorbs CO but not hydrogen. Since CO is more strongly adsorbed than hydrogen on most catalytically active metals, and since the effect of gold is generally to weaken adsorption on palladium, this suggests that palladium surrounded by gold in a gold-rich alloy particle adsorbs CO but not hydrogen.

239

When catalysts were heated to 673 K and 923 K palladium area was reduced as the metal particles grew in size (sintered) (Section 3.2.2). The situation was complex, cyclic voltammetry suggesting that, at 673 K, particles having particular palladium/gold compositions underwent preferential sintering whereas, at higher temperatures, palladium particles sintered.

6.2.2 Surface Alloy Formation

The extent of surface alloy formation crucially depends upon the relative amounts and the specific locations of the constituent metals at the surface. Surface compositions were therefore investigated using cyclic voltammetry and the extent of surface alloying determined. The effects of (i) the preparative method (slurry precipitation versus incipient wetness) and (ii) the reducing agent (formaldehyde versus hydrazine) on the extent of alloying were both investigated.

Previous research into the electrochemical behaviour of palladium-gold alloys [6] has shown that the potential required for palladium-oxide stripping varies with surface composition and thus the extent of alloying in catalysts of this type can be monitored by measurement of this variable. For each Batch of catalysts, the extent of alloying increased with increasing gold composition.

The extent of surface alloy formation depended on both the preparative method and the reducing agent. For catalysts prepared by slurry precipitation (Batch 1, Figure 3.20 and Batch 2, Figure 3.22) the potentials required for palladium-oxide stripping increased almost linearly with atom% gold, indicating that the composition of the alloy phase increased with gold composition. However, the potentials required for the removal of palladium-oxide were greater for Batch 2 catalysts than for Batch 1, indicating that the surface alloys formed in Batch 2 had a higher gold content and that hydrazine reduction produced palladium-gold catalysts with more alloyed surfaces. The reasons for this may lie in the fact that hydrazine, being a more powerful reducing agent, is less selective in terms of which species it reduces first. Batch 3 catalysts were prepared using an incipient wetness method and for catalysts having bulk compositions < 50 atom% gold the potentials required for palladium-oxide stripping varied only very slightly. These potentials were only slightly more positive than the potential required to remove palladium-oxide from a pure palladium catalyst and it is thus clear that the surfaces of these catalysts (at this composition) consisted of a palladium-

rich alloy and that this was consistent for catalysts in this range of compositions. However, in the range 50 – 80 atom% gold the potentials required to strip palladium-oxide were comparable to those required for Batches 1 and 2 (at comparable compositions) suggesting that the compositions of these alloy phases were much richer in gold.

The potentials required to remove palladium-oxide from the surfaces of Batch 1, Batch 2, and Batch 3 catalysts are plotted as a function of bulk composition (atom% gold) in Figure 6.3 (re-iterated from Figure 3.26). The Figure summarises the extent of surface alloying as described.
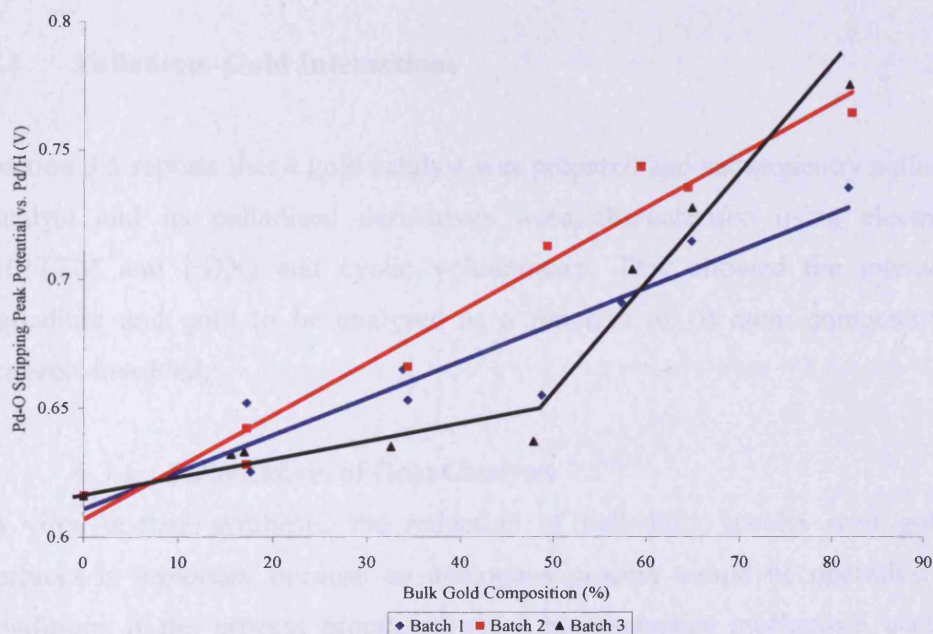
Figure 6.3 – Variation of palladium-oxide stripping potential with atom% gold

Surface composition in Batch 1, Batch 2, and Batch 3 catalysts was also investigated using X-ray photoelectron spectroscopy. This is not as surface sensitive a technique as cyclic voltammetry; however, because the electron escape depths for palladium and gold are small, the results obtained (Section 3.1.5) are interpreted ignoring the effects of electrons escaping from subsurface regions. Thus, X-ray photoelectron spectroscopy diagnosed the existence of palladium, gold, and palladium-gold phases at the surfaces of Batch 1, Batch 2, and Batch 3 catalysts and showed that these surfaces were

enriched with palladium with respect to the nominal bulk composition, in agreement with the findings of cyclic voltammetry.

After catalysts had been heated to 673 K or 923 K the palladium-oxide stripping potential moved to more positive values (Section 3.2.2), indicating enhanced alloy formation. Similarly, the profiles for propan-2-ol electrooxidation developed a feature attributable to reaction at an alloy surface after catalysts had been heated (Section 3.4.2). Enhanced alloying at elevated temperatures is to be expected; it would have been interesting to see if the extent of alloying was dependant on the period of time for which the catalysts were maintained at these high temperatures.

6.3   Palladium-Gold Interactions

Section 3.5 reports that a gold catalyst was prepared and subsequently palladised. The gold catalyst and its palladised derivatives were characterised using electron microscopy (HRTEM and EDX) and cyclic voltammetry. This allowed the interactions between palladium and gold to be analysed as a function of (i) atom composition and (ii) the reagents involved.

6.3.1   Palladisation of Gold Catalysts

In vinyl acetate synthesis, the reduction of palladium species over gold-rich catalyst surfaces is important because an analogous process would be operative under reaction conditions if the process proceeded via a homogeneous mechanism occurring within a liquid-layer of acetic acid and acetate adducts. Therefore, a 20% gold/graphite having a high gold surface area was prepared and various amounts of palladium were deposited and immobilised over it.

The tendency of gold to exist as large particles was once again exposed by high resolution transmission electron microscopy. However, cyclic voltammetry showed that the surface area of gold in this catalyst was sufficient such that palladium deposition could be monitored by (i) the reduction in the intensity of gold features in the CVs and (ii) an increase in the intensities of the features which provide a measure of palladium surface area (hydrogen under-potential deposition and palladium-oxide stripping).

Results obtained (Section 3.5) show that, following palladisation, the metallic phases formed were strongly dependant upon the agent used to reduce the palladium. Using hydrazine at low palladium compositions, palladium reduction occurred preferentially over the surface of the gold particles. This was diagnosed from the cathodic charge at potentials more positive than that expected for palladium-oxide stripping (i.e. alloy-oxide stripping). A small amount of pure palladium was detected, presumably due to palladium deposition onto the graphite support. Where larger amounts of palladium were reduced over the gold surface, the charge associated with alloy-oxide stripping increased with increasing palladium composition until it reached a maximum. This showed that alloy formation had reached a maximum. At higher palladium compositions palladium nucleated on the catalyst support. At very high palladium compositions the catalyst provided features diagnostic of a palladium-only catalyst due to the gold particles being covered with a layer of palladium. By contrast, reduction in hydrogen provided simultaneous deposition of palladium onto the surfaces of the gold particles and onto the graphite support; neither location was initially preferred.

Thus, the phases formed when palladium is reduced over gold surfaces are strongly dependant on the reducing agent chosen and the choice of the reducing agent can be used to advantage when preparing palladium-gold catalysts because it influences the location of the second metal.

The findings of Section 3.5 strongly support the designation of a stripping peak occurring at potentials intermediate of that required for palladium-oxide stripping and that required for gold-oxide stripping as that representing oxide stripping from a palladium-gold alloy phase.

6.4   Catalyst Characterisation: An Overview

In Chapters 3, 4, and 5, catalysts from Batches 1, 2, and 3 were extensively characterised using a range of methods. These provided information on the bulk and surface properties of each catalyst and related them to bulk composition and the preparative method used. In practice, these techniques provided detailed and complementary information concerning the bulk and surface phases present. There were clear differences, particularly in metal particle-

size and the extent of alloying, between catalysts prepared using the slurry precipitation and incipient wetness methods.

X-ray fluorescence confirmed that, in general, the combination of preparative method and reducing agent chosen (Table 2.1) caused immobilisation of the desired amounts of palladium and gold onto the catalyst support, and thus provided catalysts with a range of palladium/gold atom ratios suitable for an investigation based on composition.

X-ray diffraction is commonly used for the characterisation of LEAP catalysts [7] and was used again here (Figures 3.1 – 3.3, Tables 3.5 – 3.11). The metallic particles in these graphite-supported catalysts were far more heterogeneous both in composition and size than those present in the commercial LEAP catalyst. This was evident from the diffractograms, which consisted of two peaks, and which were analysed to provide an estimate of mean particle-size and the atom% composition of each phase present. The results allowed the following conclusions to be drawn; (i) the preparative methods provided metallic particles which were heterogeneous in composition and variable in size, (ii) the largest particles were gold-rich, and (iii) the smallest particles were palladium-rich. By contrast LEAP catalysts consist of palladium-gold alloy particles of uniform size (4 – 5 nm) and composition together with a highly dispersed palladium phase [8].

High resolution electron micrographs showed that, as the palladium/gold atom ratio decreased, the particle-size tended to increase (Figure 3.4, Table 3.12). Energy dispersive X-ray analysis provided individual particle compositions and particle-sizes. Figures 3.5 – 3.9 showed that selected regions contained particles of various sizes and palladium-gold compositions.

Surface characterisation was preformed using X-ray photoelectron spectroscopy, and cyclic voltammetry. Independently, each method enabled the conclusion to be drawn that the surfaces of these particles consisted of palladium, gold, and palladium-gold phases. X-ray photoelectron spectroscopy showed that the palladium/gold ratio at the surface exceeded that of the bulk; this follows from the observation that palladium-containing particles were, on average, smaller than gold-containing particles and hence the palladium surface area was greater than that of gold per unit mass of metal present. Catalyst CVs confirmed this trait. More highly alloyed catalysts showed smaller charges associated with their palladium-oxide stripping regions than less extensively alloyed catalysts, i.e. gold-rich palladium particles were larger (smaller areas per unit mass) than palladium-rich particles.

6.5   Hydrogenation Activity of Prepared Catalysts

In this investigation it was necessary, at an early stage, to be confident that the catalysts that had been prepared contained palladium in an active state. Since a reactor for vinyl acetate synthesis was not available, it was decided to examine the hydrogenation activities of the prepared materials. The hydrogenation of nitrobenzene to aniline and water at room temperature is an activity test widely used in industrial laboratories, and the equipment was readily available at Johnson Matthey. It was in this context that the measurements recorded in Section 5.1 were obtained.

Figures 5.1 – 5.3 show that activity rose as palladium loading was increased. All three pure gold catalysts showed immeasurably small or zero activity. This is as expected, pure gold having a diminishingly small hydrogenation activity by comparison with pure palladium unless it is in an extremely finely divided state [9, 10]. There is a suggestion, in two of the three Figures, that the rise of activity was of fractional order in palladium loading at constant gold loading (red curves) but the data points are too few for this to be claimed with confidence. In general, the scatter of the points in each Figure is greater than would have been expected for a series of pure palladium catalysts of differing areas, suggesting that alloying and alloy-particle-size effects may have influenced activity. However, any interpretation along these lines would have required a more extensive study and was beyond the scope of the present investigation.

The activities of Batch 1 and Batch 2 catalysts were significantly higher, at any given palladium loading, than that of Batch 3 catalysts, indicating that the slurry precipitation method was more effective than the incipient wetness method (for the production of hydrogenation catalysts).

6.6 Reactivity at Palladium-Gold Surfaces under VA Synthesis Conditions

6.6.1 Palladium Etching in Palladium-Gold Catalysts: Effects of Bulk Properties

The bulk properties of Batch 1, Batch 2, and Batch 3 catalysts were examined before and after they were exposed to components of the VAM synthesis reaction. X-ray diffraction allowed the quantification of properties such as particle composition and particle-size. For all catalysts used in the study, palladium existing in gold-rich alloy phases appeared to be resistant to dissolution (etching) under the conditions employed in the model dissolution experiments. This conclusion is based on measurements of the palladium content of the gold-rich particles examined in untreated, etched, and plated Batch 1, (Table 4.17), Batch 2 (Table 4.20), and Batch 3 (Table 4.23) catalysts. In contrast, palladium-rich particles, which were also detected in untreated, etched, and plated catalysts of Batch 1 (Table 4.18), Batch 2 (Table 4.21), and Batch 3 (Table 4.24) appeared to undergo dissolution. These particles were consistently smaller than the gold-rich particles and the palladium content of these particles in untreated, etched, and plated variants of each catalyst was reduced after exposure to potassium acetate in acetic acid solutions. This suggests that palladium in palladium-rich particles (of these sizes) is not resistant to dissolution. Batch 1 (Table 4.19) and Batch 2 (Table 4.22) untreated, etched, and plated catalysts also contained larger palladium-rich alloy particles ($\sim 11 - 20$ nm) and, like the large gold-rich particles, the palladium present in these particles appeared to resist dissolution. This remarkable result shows that palladium existing in larger particles (> 10 nm and depending upon particle composition) was resistant to dissolution. The etch-resistant particles all contained gold, which provides a strong indication that the role of gold in commercial LEAP catalysts is to control particle-size and to stabilise the palladium phase against dissolution.

That particle composition and particle-size controls palladium dissolution has implications for the synthesis mechanism. In this connection, Lambert and co-workers [8] have reported that commercial LEAP catalysts contain palladium in two forms, (i) palladium-gold alloy particles of $4 - 5$ nm in size, and (ii) highly dispersed palladium particles. The alloy compositions varied between catalysts with compositions between $15 - 59$ atom% gold being reported. Based on the palladium and gold loadings of commercial LEAP catalysts, an alloy composition of 59 atom% gold implies that a very large proportion of the palladium is present in a highly dispersed, non-alloyed form (and may,

indeed be X-ray invisible). The behaviour of the present palladium-gold/graphite catalysts leads to a conclusion that palladium existing in such a well dispersed, non-alloyed state would be susceptible to dissolution. An ultra-violet absorption measurement of a solution obtained by subjecting a commercial LEAP catalyst to the standard palladium dissolution conditions used in this work is shown in Figure 6.4. The spectrum is compared to solutions obtained from certain Batch 1 catalysts; it is clear that the palladium dissolution from the commercial catalyst was *greater* than that from graphite-supported catalysts 3182, 3185, 3184, 3186, 3187, 3188, and 3183. In this investigation, the only catalyst to have greater palladium dissolution than the commercial catalyst was 3200 – the one and only catalyst to have a diffractogram like that of a LEAP catalyst (Figures 3.1 – 3.3).

Such palladium dissolution from LEAP catalysts would provide palladium complexes [11] at the catalyst surface and therefore conditions might be generated in the gas-phase LEAP process for a homogeneous catalytic reaction as described by Samanos et al. [12].
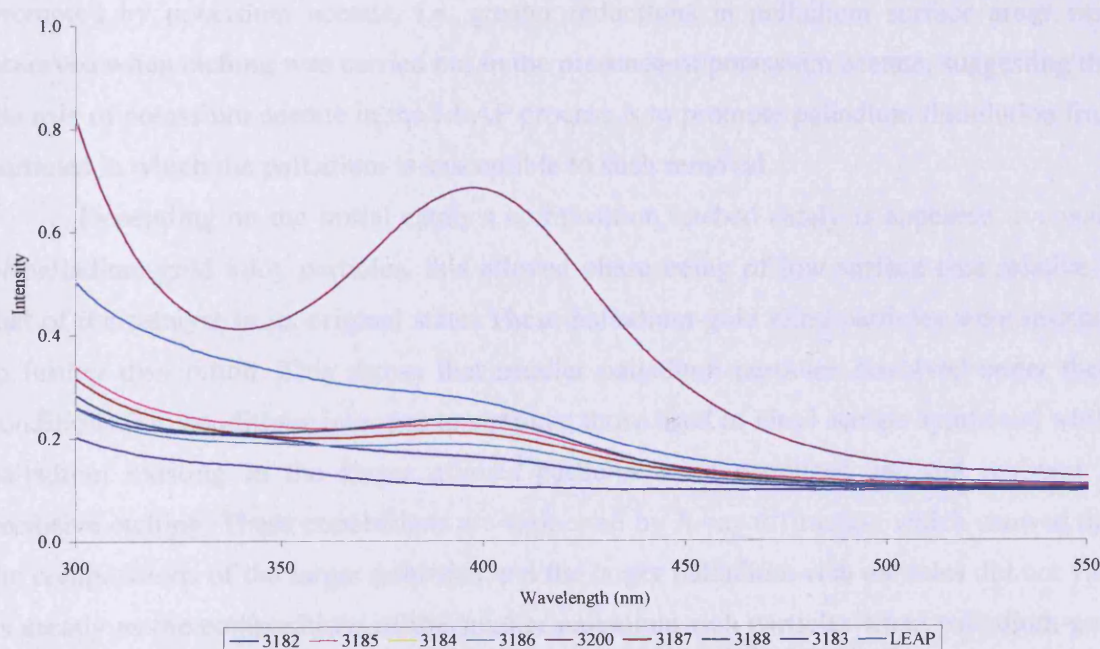

Figure 6.4 – Ultra-violet absorption spectrum of the solution obtained by etching a LEAP catalyst in a potassium acetate/acetic acid mixture and spectra obtained after similar treatments of certain Batch 1 catalysts

6.6.2   Palladium   Etching   in   Palladium-Gold   Catalysts: Effects   of   Surface
          Properties

Cyclic voltammograms of Batch 1, Batch 2, and Batch 3 catalysts in their untreated and etched states are shown in Section 4.1. Measurement of the charges associated with the hydrogen under-potential deposition regions and the palladium-oxide stripping regions of untreated and etched catalysts showed that the effect of palladium dissolution was to reduce the amount and surface area of palladium in the catalyst and thus enhance the gold composition. Palladium-oxide and gold-oxide stripping in etched catalysts required more positive potentials, which is again diagnostic of an enhancement in the composition of gold at the etched surfaces. The appearance of cathodic charge at potentials slightly positive of the potential required for palladium-oxide stripping was observed, indicating that cyclic voltammetry distinguishes between palladium and palladium-gold phases i.e. different surface phases/surface alloying. It was common for an etched catalyst either (i) to show the first appearance of gold at the surface (i.e. the untreated catalyst had no detectable gold at the surface) or (ii) to show an increased surface area of gold. Palladium dissolution was promoted by potassium acetate, i.e. greater reductions in palladium surface areas were observed when etching was carried out in the presence of potassium acetate, suggesting that the role of potassium acetate in the LEAP process is to promote palladium dissolution from particles in which the palladium is susceptible to such removal.

Depending on the initial catalyst composition, etched catalysts appeared to consist of palladium-gold alloy particles, this alloyed phase being of low surface area relative to that of the catalyst in its original state. These palladium-gold alloy particles were resistant to further dissolution. This shows that smaller palladium particles dissolved under these conditions (i.e. conditions intended to simulate those used in vinyl acetate synthesis) whilst palladium existing in the larger *alloyed* particles were stabilised and are resistant to corrosive etching. These conclusions are supported by X-ray diffraction which showed that the compositions of the larger gold-rich and the larger palladium-rich particles did not vary as greatly as the compositions of the smaller palladium-rich particles when palladium-gold catalysts underwent etching. This result was mirrored in the reverse process, plating.

Similar results were obtained when palladium etching was carried out in an electrochemical cell (Section 4.1.2) where certain palladium-gold catalysts were exposed to acetic acid/potassium acetate at oxidising potentials. These experiments, which again

mimic reaction conditions, showed gold particles to be resistant to etching (Figure 4.27) and hence supported the proposal that it is the palladium particles which are dissolved under such conditions. Thus, the role of gold in a *homogeneous alloy catalyst* may be to stabilise the palladium phase from dissolution and hence promote the *heterogeneous* catalytic pathway for vinyl acetate formation.

Ultra-violet absorption studies of the solutions obtained after palladium etching showed that these solutions contained palladium acetate dimers and trimers. Such complexes have been used as homogeneous catalysts for the conversion of ethylene to vinyl acetate [11]. The type of palladium acetate complex formed was dependant on the acetate concentration [11] showing that an equilibrium exists between the palladium acetate dimers and trimers and it is controlled by the concentration of potassium acetate.

To summarise, the results obtained by X-ray diffraction, cyclic voltammetry, and ultra-violet absorption spectroscopy show that small palladium particles undergo dissolution when palladium-gold catalysts are exposed to solutions of acetic acid and acetic acid/potassium acetate i.e. under conditions which simulate VA synthesis, whereas palladium existing in alloyed phases are largely stabilised in this respect. That palladium acetate complexes, like those which are used in the liquid-phase synthesis of vinyl acetate, can be derived from *heterogeneous* palladium-gold catalysts under these conditions demonstrates that vinyl acetate synthesis could proceed via a homogeneous catalytic pathway within a film of acetate adducts which surround the catalyst particles under gas-phase process conditions [13]. The practice of adding potassium acetate to the LEAP reactor to maintain activity and selectivity strongly supports a model in which the overall reaction involves both heterogeneous and homogeneous components.

6.6.3 Palladium Plating

Hydrogen reduction. When etched catalysts were reduced in hydrogen in the presence of the solutions used in their preparation, palladium was plated over the etched catalyst surface – the plating results are described in Section 4.2.1.

Cyclic voltammetry showed that plated catalysts had higher palladium surface areas than the corresponding etched catalysts. Plated catalysts also showed more negative palladium-oxide and gold-oxide stripping potentials than etched catalysts. For some catalysts, gold-oxide stripping regions which appeared after etching disappeared on plating,

suggesting that they had became covered by palladium. Remarkably, the potentials required to remove palladium-oxide from the surfaces of plated catalysts were almost always more positive than those required to remove palladium-oxide from a pure palladium catalyst; this showed clearly that gold rapidly diffused into the freshly deposited palladium surfaces. Gold was therefore highly mobile under these conditions.

Ethylene reduction. Etched catalysts were also reduced by ethylene in the presence of solutions generated in their preparation; this again resulted in plating. This was a very significant result because ethylene is a reactant in vinyl acetate synthesis. However, the presence of ethylene complicated the measurement of stripping potentials and charges associated with the hydrogen under-potential deposition and palladium-oxide stripping regions. However, the results indicated that plated catalysts had become enriched with palladium and hence the conclusions follow those set out for reduction in hydrogen.

6.6.4   The Catalytic Cycle

Palladium-etching and palladium-plating acting together under reaction-like conditions provide a catalytic cycle which may facilitate homogeneously-catalysed vinyl acetate formation under the conditions of the heterogeneous gas-phase process. Palladium dissolution provides a pathway by which a homogeneous palladium acetate catalyst may be generated from the graphite-supported (or silica-supported) palladium-gold catalyst and then becomes coordinated by additional acetate and olefinic ligands. The presence of coordinated ethylene, in a redox process, then reduces the palladium acetate complex to metallic palladium and undergoes oxidation to give vinyl acetate.

Such oxidation/reduction cycles would cause the catalyst particles to undergo constant change in both surface and bulk composition and these changes, if not in balance, would be expected, to lead to catalyst deactivation.
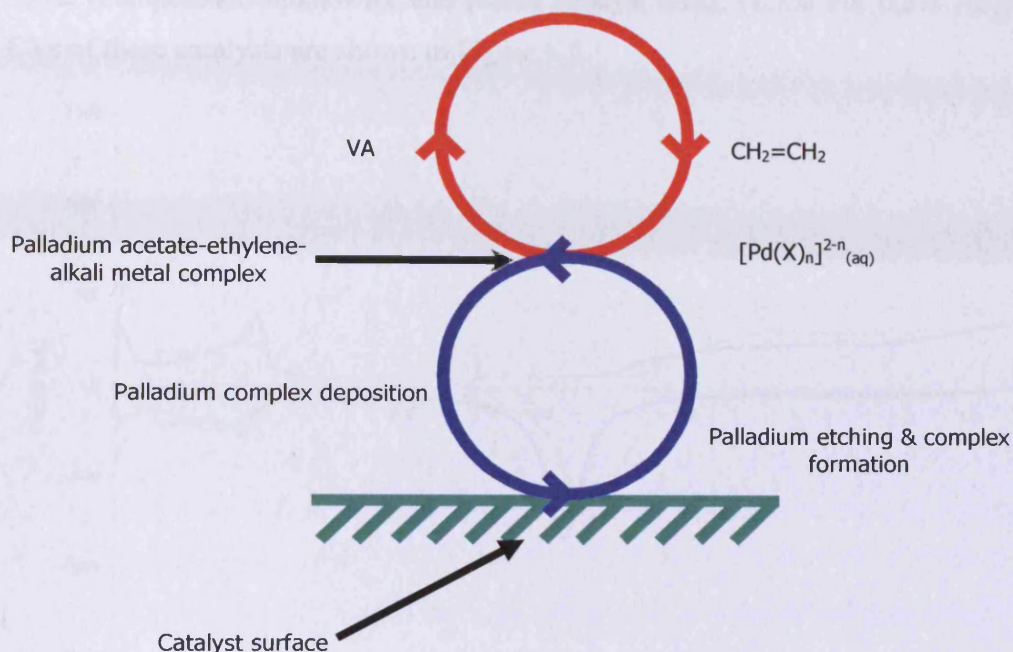
Figure 6.5 – Illustration of how the homogeneous catalytic synthesis of vinyl acetate may proceed in a liquid-layer of acetic acid/acetate adducts at a heterogeneous catalyst surface

6.7   Vinyl Acetate Synthesis

Characterisation of Batch 1, Batch 2, and Batch 3 catalysts allowed properties such as particle-size, surface and bulk composition, and the extent of alloying to be determined (Chapter 3). These defined catalysts were then treated with acetic acid, potassium acetate, and ethylene (and combinations of these reagents) and the catalysts were then re-characterised (Chapters 4 and 5) to determine how these properties had been influenced by the reagents involved in vinyl acetate synthesis.

Certain catalysts were tested for vinyl acetate synthesis activity in an industrial reactor. This test concentrated on the measurement of (i) the space-time yield (STY) with respect to vinyl acetate formation, (ii) the selectivity to vinyl acetate (based on the amounts of vinyl acetate and carbon dioxide formed), and (iii) the dependence of catalyst history on these parameters. Rate constants, orders of reaction, and activation energies were not investigated as they have been studied elsewhere [14 – 16]. Results were presented in Section 5.3 for untreated catalyst 3331, (1.0% Pd, 0.4% Au)[4.8]/G{2}, etched catalyst

3332, (composition unknown), and plated catalyst 3332, (1.7% Pd, 0.6% Au)[4.8]/G{2}.
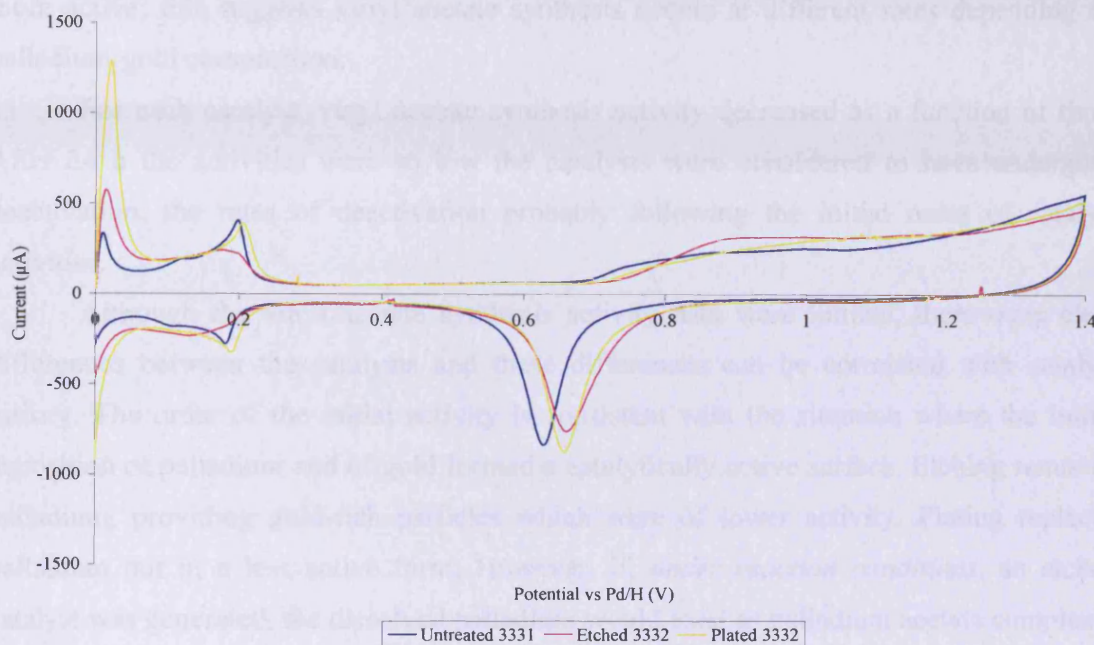CVs of these catalysts are shown in Figure 6.5.

*Figure 6.6 – CVs for untreated catalyst 3331, (1.0% Pd, 0.4% Au)[4.8]/G{2}, etched
catalyst 3332, (composition unknown), and plated catalyst 3332, (1.7% Pd, 0.6%
Au)[4.8]/G{2}*

6.7.1 Space-Time Yield

The rate of vinyl acetate formation was quantified using the space-time yield, a parameter
used to express the rate of a catalytic reaction in terms of the mass of catalyst used per unit
time.

First, the STYs for vinyl acetate formation over all three catalysts were two orders
of magnitude below the level expected for materials likely to be used as commercial
catalysts. This result can be explained in part by the fact that these catalysts had lower
palladium surface areas than commercial LEAP catalysts. Initially, untreated catalyst 3331
showed the highest activity, followed by plated catalyst 3332. Etched catalyst 3332 showed
the lowest activity. The order of initial catalyst activities was proportional to palladium
surface areas as determined using the charges associated with the hydrogen under-potential
deposition and palladium-oxide stripping regions (Figure 6.6). The catalysts having the
highest palladium surface areas (untreated and plated catalysts) were most active, whilst the
catalyst with the lowest palladium surface area (etched catalyst) was the least active.

Although having similar palladium areas (Figure 6.6), plated catalyst 3332 contained a higher alloy component than untreated catalyst 3331 and the untreated catalyst was the more active; this suggests vinyl acetate synthesis occurs at different rates depending on palladium-gold composition.

For each catalyst, vinyl acetate synthesis activity decreased as a function of time. After 24 h the activities were so low the catalysts were considered to have undergone deactivation, the rates of deactivation probably following the initial order of catalyst activities.

Although the vinyl acetate synthesis activity data were limited, there were clear differences between the catalysts and these differences can be correlated with catalyst history. The order of the initial activity is consistent with the situation where the initial deposition of palladium and of gold formed a catalytically active surface. Etching removed palladium, providing gold-rich particles which were of lower activity. Plating replaced palladium but in a less active form. However, if, *under reaction conditions*, an etched catalyst was generated, the dissolved palladium would exist as palladium acetate complexes in the liquid-layer of acetic acid and acetate adducts which has been proposed to exist around the catalyst particles [13]. The palladium acetate complexes would then catalyse the homogeneous conversion of ethylene to vinyl acetate, and therefore contribute to the STY.

6.7.2 Selectivity to Vinyl Acetate

Catalyst selectivity was measured at the same intervals as those used for the catalyst activity measurements. Initially, the order of catalyst selectivities followed the order of the initial space-time yields and during the temperature programme which was designed to investigate the extent of catalyst deactivation, the selectivity responded inversely to changes in temperature within the range studied. The major by-product was carbon dioxide.

6.8   Gas-Phase Vinyl Acetate Synthesis: Mechanistic Implications

The mechanism by which vinyl acetate is formed in the gas-phase over supported palladium-gold catalysts remains a topic of much debate (Chapter 1). The main aim of this study was to investigate the effect of the chemical components involved in vinyl acetate synthesis on the bulk and surface properties of palladium-gold catalysts and to gain insights which might advance our understanding of the mechanism by which vinyl acetate is formed in BP's LEAP process. Palladium-gold particles were prepared on graphite to enable electrochemical characterisation, and the catalysts characterised. The active phases consisted of particles having a variety of palladium-gold compositions and particle-sizes. These findings were ideal in that the fate of these different types of particle could be monitored as catalysts were treated with acetate-based solutions and ethylene.

The results, presented in Chapter 4, show that the mechanism of the gas-phase synthesis of vinyl acetate is strongly dependant upon the composition and size of the particles contained in the catalyst. The key feature of the surface chemistry of these catalysts is the extent to which palladium resists dissolution from the bimetallic catalyst particles. An optimised heterogeneous catalyst would be one in which no palladium underwent dissolution. Whenever dissolution takes place the possibility exists that concurrent homogeneous catalysis can occur. The mechanisms associated with these two routes are presented in the next sub-sections.

6.8.1   Heterogeneous Catalysis of VA Formation over Palladium-Gold Particles

Nakamura and Yasui [17, 18] proposed that, in the gas-phase, vinyl acetate is formed by the combination of activated acetic acid and activated ethylene intermediates, species which are co-adsorbed at the palladium catalyst surface. Goodman and co-workers [14 –16], using supported and unsupported palladium and palladium-gold catalysts, confirmed the findings of Nakamura and Yasui, proposing that vinyl acetate is formed by a Langmuir-Hinshelwood mechanism. These authors conceived of the catalysis as being wholely heterogeneous. However, in view of the results presented here in Chapter 4, there is the possibility that, depending on particle-size, dissolution of palladium may have occurred to some extent which may have facilitated the formation of vinyl acetate homogeneously.

However, the results presented in Chapter 4 are fully consistent with the concept that vinyl acetate is formed over palladium-gold surfaces in a heterogeneously catalysed process. Etched palladium-gold catalysts had lost palladium by dissolution, but still contained palladium-gold alloy particles. This was confirmed by the potentials required for palladium-oxide stripping from the surfaces of the etched catalysts. The smaller charges associated with the palladium-oxide stripping regions of etched catalysts (relative to those associated with palladium-oxide from untreated catalysts) demonstrated the lower palladium surface areas associated with these particles, and showed that the particles resistant to dissolution are larger palladium-gold alloy particles. The palladium components of alloy particles appeared to be resistant to dissolution (X-ray methods showed that the composition of the palladium-rich particles varied whereas that of gold-rich particles was constant). Such particles are therefore the most suitable for the heterogeneous catalytic synthesis of vinyl acetate.

The extent of ethylene adsorption increased when palladium was alloyed with gold particles, indicating preferential ethylene adsorption over larger particles. This concurs with Goodman who suggested that vinyl acetate synthesis is a structure sensitive reaction occurring over small rather than large ensembles [16].

In conclusion, provided a palladium-gold catalyst consists of palladium-gold alloy particles of a specific composition and size, the palladium component of these particles will be resistant to dissolution and vinyl acetate formation will occur via a heterogeneous catalytic pathway.

6.8.2 Homogeneous Catalysis of VA Formation Resulting from the Presence of Palladium Particles

A mechanism for the homogeneous liquid-phase synthesis of vinyl acetate was proposed by van Helden et al. [19]. Later, Samanos et al. [12] and Zaidi et al. [20] suggested that the gas-phase synthesis occurs by a mechanism similar to that which occurs in the liquid-phase, palladium acetate being formed via dissolution of surface palladium. They also suggested that there were significant interactions between the catalyst and acetic acid. Later, Crathorne et al. [13] established that, under reaction conditions, gas-phase vinyl acetate catalysts are covered by a liquid-layer of potassium acetate, acetic acid, and water.

Table 6.1 – Melting points of various acetic acid/potassium acetate/water adducts [21]

Adduct	Melting point (K)
KOAc	565
KOAc.H₂O	428
KOAc.AcOH	414 – 423
KOAc.2AcOH	346 – 406
KOAc.3AcOH	337 – 372
KOAc. H₂O.AcOH	388 – 403
KOAc. H₂O.2AcOH	318 – 363
KOAc. 2H₂O.AcOH	392 – 413
KOAc. 2H₂O.2AcOH	345 – 393

The information in Table 6.1 shows that the melting point of potassium acetate is significantly reduced when it forms adducts with acetic acid and/or water. Thus, at temperatures typically used in the gas-phase synthesis of vinyl acetate (423 K) it is very likely that the products of palladium dissolution are present as a liquid-layer [13, 21].

Characterisation of etched catalyst surfaces suggested that palladium dissolution from palladium- and palladium-gold catalysts was facile and that the loss was predominantly from small palladium- or palladium-containing particles (This was diagnosed from a preferential reduction in the charges associated with palladium-oxide stripping from palladium particles as opposed to palladium-oxide stripping from palladium-gold alloy particles which occurs at a more positive potential in the CVs of etched catalysts). Ultra-violet absorption spectroscopy confirmed that palladium dissolution occurred from all catalysts studied.

It is therefore proposed that, under the conditions of the gas-phase synthesis of vinyl acetate, palladium complexes are formed from palladium particles via dissolution and this provides the conditions for homogeneous synthesis within the liquid-layer of acetic acid and potassium acetate which surrounds the catalyst particles. The results presented in Chapter 4 are thus consistent with the mechanism proposed by Samanos et al. [12].

6.8.3   The LEAP Process: Proposed Mechanism

Sections 6.8.1 and 6.8.2 suggest that the mechanism by which vinyl acetate is formed in the gas-phase is dependent upon the sizes of the metallic particles present in the catalyst. The morphology of the particles in the commercial catalyst is of crucial importance as it will influence the mechanism by which vinyl acetate is formed in the LEAP process.

As mentioned earlier, Lambert and co-workers [8] reported that LEAP catalysts were comprised of a single type of alloy particle (4 – 5 nm in size, 59 atom% gold) together with highly dispersed pure palladium. Consequently, although LEAP catalysts do not contain the range of palladium-gold particles that were present in the catalysts used in this investigation, predictions concerning the behaviour of LEAP catalysts when treated with acetic acid and potassium acetate may be made. Thus, small palladium particles in LEAP catalysts should undergo dissolution (promoted by potassium acetate) providing palladium complexes which facilitate a homogenously catalysed reaction. By contrast, palladium in the palladium-gold alloy phase is proposed to be resistant to dissolution therefore providing the surface required for heterogeneous vinyl acetate synthesis via a Langmuir-Hinshelwood mechanism.

Lambert's evidence supports this model in that (i) his used LEAP catalysts contained palladium acetate and (ii) the compositions of the alloy particles in used catalysts had undergone only a minor change (although they had sintered). This provides further evidence that the palladium phase is susceptible to dissolution whereas the alloy is resistant.

Palladium dissolution also has implications for catalyst selectivity, since as palladium in heterogeneously catalysed processes is expected to contribute to the formation of carbon dioxide whereas the homogeneous route is less likely to provide deep oxidation (via the adsorption of oxygen atoms at palladium surface sites [22, 23]). Thus, in the event of palladium dissolution, the extent of deep oxidation would be minimised thus promoting the catalyst selectivity.

Assuming the space-time yield for vinyl acetate formation is the sum of the space-time yield's of the processes by which vinyl acetate is formed heterogeneously and homogeneously the overall space-time yield is given by:

$$STY_{Overall} = STY_{Hetero} + STY_{Homo} \qquad (1)$$

As the method used to prepare LEAP catalysts (palladium/gold atom ratio = ~ 5) does not produce a catalyst having a completely alloyed surface [8], gold is required to stabilise as many of the palladium atoms as possible and thus promote the heterogeneous process for vinyl acetate formation. The residual palladium atoms form palladium particles, and potassium acetate (*which is always added in the LEAP process*) promotes palladium

dissolution from these particles. The presence of gold may have a second order effect as alloy formation influences the size of the palladium particles in the palladium phase, and may make them susceptible to dissolution. In this situation, the heterogeneous process for vinyl acetate formation over the palladium-gold particles is expected to be dominant ($STY_{Hetero} > STY_{Homo}$) and it is suggested that homogeneous vinyl acetate synthesis simply augments the overall space-time yield. Thus, the success of the LEAP process is largely due to a carefully formulated balance of two promoters, (i) gold, used to promote the heterogeneous catalytic process and (ii) potassium acetate, used to promote the homogeneous catalytic process, thereby maximising the total synthesis rate.

6.9   Conclusions

The Objectives of the Investigation set out in Section 1.5 were all achieved. Palladium-gold/graphite catalysts were prepared by two traditional methods and were extensively characterised (Objectives 1 and 2). The catalysts contained metallic particles having bimodal particle-size distributions and alloy compositions. The slurry method of preparation was superior to the incipient wetness method in giving catalysts of slightly higher activity, but catalysts prepared by both methods contributed comparable information to the investigation (Objective 3). Catalysts so prepared contained catalytically active palladium phases as judged by both nitrobenzene hydrogenation and by vinyl acetate synthesis (Objective 4).

Reactivity of surface palladium towards aqueous potassium acetate/acetic acid mixtures led to palladium etching and subsequent dissolution. This process was studied in detail as was the restorative process of palladium plating (Objective 5). The different responses of palladium-rich and gold-rich particles to etching led to the clear conclusion that the role of gold as a promoter is to render palladium resistant to dissolution (Objective 6). Since all catalysts, both those investigated here and those used commercially, contain palladium that is not stabilised by gold against dissolution, a clear route is available for the generation of palladium acetate complexes that may catalyse vinyl acetate synthesis in a parallel homogeneous process (Objective 7).

The conclusion that gold stabilises palladium and that palladium-gold alloy particles are a superior catalyst for vinyl acetate synthesis suggests that it is the heterogeneous

catalytic process that is most productive, and that the addition of potassium acetate in the LEAP process increases the space-time yield by utilising extracted palladium to provide a parallel homogeneous catalytic process. Therefore, a catalyst exclusively composed of stabilised palladium-gold alloy particles should be advantageous for the LEAP process. Not only would such a catalyst be optimised for heterogeneous catalytic operation, but the addition of potassium acetate would no longer be necessary. The synthesis would be expected to proceed with higher space-time yields though not, perhaps with quite as high a selectivity, because the presently-contributing homogeneous component of reaction may not contribute to carbon dioxide production.

6.10   References

[1]   European Patent No. 1175939.

[2]   US Patent No. 144544.

[3]   US Patent No. 6534438.

[4]   European Patent No. 1467814.

[5]   US Patent No. 032638.

[6]   M. Lukaszewski, A. Czerwinski, Electrochim. Acta, 48 (2003) 2435.

[7]   M. J. Cunnington, Personal Communication, BP Chemicals, 2002.

[8]   N. Macleod, J. M. Keel, R. M. Lambert, Appl. Catal., A 261 (2004) 37.

[9]   G. C. Bond, P. A. Sermon, G. Webb, D. A. Buchanan, P. B. Wells, J. Chem. Soc. Chem. Comm. (1973) 444.

[10]   P. A. Sermon, G. C. Bond, P. B. Wells, J. Chem. Soc. Faraday Trans. 1 75 (1979) 385.

[11]   D. A. Kragten, R. A. van Santen, M. K. Crawford, W. D. Provine, J. J. Lerou, Inorg. Chem. 38 (1999) 331.

[12]   B. Samanos, P. Boutry, R. Montarnal, J. Catal. 23 (1971) 19.

[13]   E. A. Crathorne, D. MacGowan, S. R. Morris, A. P. Rawlinson, J. Catal. 149 (1994) 254.

[14]   Y - F. Han, J - H. Wang, D. Kumar, Z. Yan, D. W. Goodman, J. Catal. 232 (2005) 467.

[15]   D. Kumar, Y - F. Han, M. S. Chen, D. W. Goodman, Catal. Lett. 106 (2006) 1.

[16]   Y - F. Han, D. Kumar, D. W. Goodman, J. Catal. 230 (2005) 362.

[17] S. Nakamura, T. Yasui, J. Catal. 17 (1970) 366.

[18] S. Nakamura, T. Yasui, J. Catal. 23 (1971) 315.

[19] R. van Helden, C. F. Kohll, D. Medema, G. Verberg, T. Jonkhoff, Recueil 87 (1968) 961.

[20] S. A. H. Zaidi, Appl. Catal. 38 (1988) 353.

[21] M. J. Cunnington, Personal Communication, BP Chemicals, 2006.

[22] R. Burch, F. J. Urbano, Appl. Catal., A 124 (1995) 121.

[23] S. C. Su, J. N. Carstens, A. T. Bell, J. Catal. 176 (1998) 125.